The influences of crustal extension, salt tectonics and gravity-driven deformation on the structural evolution of the Halten Terrace, offshore mid-Norway: new sights from 3D seismic data and fault analysis

Marsh, Nicola A

The influences of crustal extension, salt tectonics and gravity-driven deformation on the structural evolution of the Halten Terrace, offshore mid-Norway: new insights from 3D seismic data and fault analysis

Nicola A. Marsh

A thesis submitted in the requirements for the degree of Doctor of Philosophy at the Department of Earth Sciences, University of Durham

December 2008

The truth is that whoever touches this enticing subject...is bound to indulge freely in speculation. The problem is so broad, the factors involved are so numerous, and the work to be done with regard to salt structures is so great that we cannot...restrict our speculation to the narrow limits of exact knowledge.

- Everett DeGolyer, 1925

DECLARATION

No part of this thesis has previously been submitted for a degree at this or any other university. The work described in this thesis is entirely that of the author, except where reference is made to previously published or unpublished work.

Nicola A. Marsh

University of Durham

Department of Earth Sciences

December 2008

ACKNOWLEDGEMENTS

So many people have influenced my work over the last 3 years so I have a long list of people to thank, (so grab yourself a cup of tea and make sure you're sitting comfortably before you read on)…

I should start by thanking Paul Brockbank from StatoilHydro for initiating the project and Bob and Jonny for taking the project on board, for finding me funding and supporting my ideas over the past years. A big thank you goes to Jonny who has been my academic advisor/data loader/IT support during my PhD. I literally couldn't have finished my thesis without Jonny's support, particularly his patience when listening to my ideas and helping me to develop them into what is now my thesis.

A huge thank you goes to my wonderful friends in Durham who have made me laugh throughout the last 3 years – Professor Pugh for religiously drinking tea with me and for introducing 'the caterpillar' to the 21st century (!), 'My Boys' – Fabio and Cole – keeping me 'relaxed' and opening my eyes to the male obsession with 'ladies'…hilarious! And of course Steve, Bones and Ruth for making me laugh, stealing food and of course, the yummy cakes. Outside the 'dead zone' there are so many people that have made this experience an unforgettable one – Mike for being a fabulous friend and most importantly for introducing me to the world of adults that dress in baby clothes, Sarah B for being a great friend, completely mad as a broom but loads of fun, and to everyone else – Jen, Ginger Tom, Charlie for being fab too.

Special thanks go to Paul Brockbank for his ongoing support throughout my PhD and for helping to secure my summer placements in StatoilHydro (I owe you a beer!). Which takes me to Stjørdal – the list here is endless so I apologise if I miss anyone. A huge thank you goes to Philip Ringrose for believing in my project, for supporting my annual 'summer placements' in StatoilHydro and for integrating me into the team in Stjørdal, all of which has given me the drive to finish the thing! Another huge thanks goes to Susanne Kvarsvik for help in setting me up as a summer student – the apartment, the phone, the cash (!) – but also for being a great friend and for the introducing me to 'To rom og kjøkken'. Fem hundre tusen takk (!) to Rich for being a great friend, for introducing me to so many people and for drinking so many beers with me in Trondheim. Huge thank you to all my other friends in Norway – Simon and Helen, Susan, Kjell, Kristen and Jack to name a few - for making me so welcome, inviting me into their homes for cake, wine and bbq's and for making the experience so enjoyable. Another thank you has to go to all the people in StatoilHydro who made me so welcome, showed incredible interest in my work and provided me with fredags kake – something that should undoubtedly take place in every work place!

My biggest thank you's have to go to my Mum and Dad for supporting me through my decision to return to university (again!), for believing I could do it and for helping me move house about 20 times in the process! (Dad – you've always said education is really important if you're going to do well in life but I think I've had enough now! I'm hanging up my academic boots!) Without your continued love, support and encouragement I wouldn't have made it this far, so thank you.

Last, but by no means least, Steve. Thanks for being with me, for making me laugh, for explaining all things mathematical that go over my head, and for supporting my love of Norway and my decision to move over there. I can't wait to start our new adventure together – it makes all the hard work worth while.

CONTENTS

LIST OF FIGURES

Figure 2.3: Schematic block diagram illustrating the alternative model of fault growth (redrawn from Walsh et al, 2002) using sequential fault maps from the base of a syn-faulting sequence (b–d). (a) The location of pre-existing faults beneath the faulted horizon. (b) Faulting initiates on the horizon above the pre-existing fault system with nucleation close to the centre of each fault. Fault lengths increase rapidly while displacements accrue relatively slowly. (c) Propagation ceases when the faults begin to interact, while displacement continues to accumulate at near constant rates. Fault lengths are inherited from a pre-existing fault system (a). (d) Fault lengths remain fixed while displacements accrue.

Figure 2.4: The geometry of relay ramps. a) 3D block diagram of an intact relay ramp. b) As displacement increases faults grow and the relay ramp is breached by one or both fault tips or by newly formed faults

Figure 2.5: Existing models for the growth of faults and relay zones. (a) Present day fault geometry. (b) Conventional model for relay formation due to in plane propagation and coincidental overlap of originally kinematically isolated faults. (c) Alternative model of fault growth due to bifurcation of a kinematically coherent array of unconnected segments. (d) – (e) relationships between fault displacement and length for isolated and bifurcated faults (d and f redrawn from Walsh *et al*, 1996). (d) Horizon separation diagram for faults B and C. (e) Throw profiles for faults (solid lines) and aggregate throws (dotted lines) demonstrating the presence of a displacement minima in the overlap zone of B and C. Throw profile as expected for isolated faults such as Model 1. (f) Throw profiles (solid lines) and aggregate throws (dotted line) including the ramp rotation (dashed lines). The sum of fault throw plus ramp rotation produces a more regular profile than in (e) suggesting that faults are a kinematically coherent structure as in Model 2

Figure 2.6: The global distribution of basins containing salt structures (black areas). Basins containing undeformed salt are omitted. Note, HB = Haltenbanken, offshore mid-Norway, GC = Gulf of Mexico, CP = Campos, LC = Lower Congo and LP = La Popa (from Hudec & Jackson, 2007)

Figure 2.7: Block diagram showing the schematic shapes of salt structures. Structural maturity increases with increasing size and coalescence of salt structures. (a) Elongate structures rising from line sources, (b) structures rising from point sources. From Hudec & Jackson, 2007

Figure 2.8: Comparison of creep and frictional strengths of various rock types in both tension and compression (Redrawn from Jackson & Vendeville, 1994). Note that wet salt effectively falls on the axis of zero strength

Figure 2.9: Simple 3-layer model of the crust with a weak, constant-strength salt layer between two brittle layers whose strength increases with depth. The strength of the salt layer is independent of depth, but is instead dependent on, ε = Strain rate and η = viscosity (redrawn from Vendeville and Jackson, 1993)

Figure 2.10: Density vs. Depth curves for various lithologies (1 = salt, 2 = dry sand, 3 = wet sand, 4 = wet shale, 5 = dry shale). The density of salt remains approximately constant with depth, whereas sand and shale increase in density during burial so that buried salt is less dense than its overburden at a critical point (D), (Modified from Jackson and Vendeville, 1986)

Figure 2.11: Types of viscous flow of an undeformed viscous material (a): (b) Poiseuille flow in which overburden pressure drives lateral flow in an unconfined layer. Velocities are slower at the boundaries because of viscous drag; and (c) Viscous material is sheared due to lateral translation of the overburden during Couette flow (redrawn from Rowan, 2006)

Figure 2.12: Examples of hydraulic-head gradient analysis in salt tectonics (modified from Hudec & Jackson, 2007). (a) A uniform overburden thickness above a flat lying salt layer

produces no hydraulic head gradient, even though the salt thickness varies, thus salt remains at rest. (b) A laterally varying overburden thickness above a tabular salt layer produces a pressure gradient from point 1 to point 2 but no elevation head gradient. Salt will flow from left to right along the pressure gradient. (c) A uniform overburden thickness above an inclined, tabular salt layer produces an elevation head gradient from Point 1 to Point 2 but no pressure head gradient. Salt will flow from left to right down the elevation head gradient

Figure 2.13: The effects of displacement loading on pre-existing salt structures. (a) Salt is horizontally loaded during shortening, by inward movement of one or both walls. The horizontal displacement load overcomes the vertical gravitational load forcing the salt to rise. In a natural example the top of the salt structure would flow out over the sediment surface rather than form a vertical column. (b) During extension, the salt is unloaded horizontally by outward movement of one or both walls. The vertical gravitational load then exceeds the horizontal displacement load so the salt subsides

Figure 2.14: (a) Cross section in an experimental model illustrating the formation of a reactive diapir and primary peripheral sink in response to graben faulting. The overburden comprises one prekinematic layer (L1) and two synkinematic layers (L2 and L3), each made of several stratified sub-layers. The lowermost layer was flexed upwards as the shoulders of the graben and underlying reactive diaper rose. I indicates the location of the primary peripheral sink indicated by thinning of the basal layer toward the diapir (Redrawn from Vendeville, 2002). (b) Example of a reactive diapir in the Gulf of Mexico (from Hudec and Jackson, 2007). (c) Cross-section from the West African margin illustrating the geometry of salt rollers (from Rouby et al, 2002)

Figure 2.15: Vertical sections through an experimental model showing progressive fall of a diapir. Diapir subsidence increases with increasing extension. The diapir becomes wider and lower, the overlying graben deepens and the slip of the crestal faults increases. The overlying growth graben subsides into and indents the widening diapir (Modified from Vendeville et al, 1992b)

Figure 2.16: Schematic rise and fall of diapirs during sedimentation. Three types of extensional turtle structure successively form: turtle structure horst, turtle anticlines and mock turtle anticlines (from Vendeville *et al*, 1992b)

Figure 2.17: Schematic cartoon showing the deformation pattern of the viscous décollement and brittle overburden during gliding above a basement step (from Gaullier *et al*, 1993). The viscous source layer flows during gliding causing the overburden located above the step to flex, partly mimicking the topography of the underlying basement. A graben bounded by two normal faults formed in the upper hinge of the flexure trending parallel to the basement step. A ridge of salt rose reactively below the graben eventually piercing the graben floor diapirically

Figure 2.18: Examples of extensional fault-propagation folds. (a) Fault-propagation fold associated with warping beyond the fault tip-line (Modified from Walsh & Watterson, 1987); and (b) Idealised cross-sections illustrating the evolution of folds in the Gulf of Suez as a result of vertical fault propagation (Modified from Withjack et al, 1990). (c) Sketch of a fault-propagation fold above a master normal fault. Crossed area represents an evaporitic package. Hydrocarbons are trapped within the secondary supra-salt structures produced by folding and within the sub-salt basement block (redrawn from Withjack & Callaway, 2000)

Figure 2.19: Examples of fault-propagation folds from seismic and field data. (a) Line-drawing of a seismic section from the Suez rift (from Patton *et al*, 1994), (b) Detailed

Figure 2.29: Dextral strike-slip movement on a sinuous fault producing a pull-apart basin (Halten Terrace) close to compressional uplift (Nordland Ridge). (Modified from Caselli, 1987)

Figure 3.1: (a) Sampling the vertical time thickness of an interval leads to an overestimation of the 'true' thickness of beds in the hangingwall of a tilted fault block, the same occurs in the footwall. Across fault measurement errors occur if the footwall and hangingwall beds dip at different angles; (b) An overestimation of 'true' thickness also occurs in synclines where beds dip at a higher angle towards the limbs of the syncline than near the axis where $T_{vert} = T_{true.}$ An interval of equal thickness will show apparent growth towards the limbs of the syncline (A to B). Similarly, an underestimation of the change in thickness across a syn-folding interval will occur due to an overestimation of thickness on its limbs (inset)

Figure 3.2: Present-day fault polygons mapped (a) in the basement (Base Salt horizon) and (b) in the cover strata (Åre Coal horizon) showing a clear upward decrease in the number and density of faults between basement and cover. S_F = Smørbukk Fault, S_{FW} = Smørbukk Footwall Graben, S_{HW} = Smørbukk Hangingwall Graben, S_{CF} = Smorbukk compressional fold, S_{South} = Smorbukk southerly trace, N_F = Northern Fault, T_F = Trestakk Fault, T_{FW} = Trestakk Footwall Graben, E_F = Eastern Fault, T_{syn} = Trestakk syncline, NE_{syn} = Northeast syncline. The Smørbukk fault polygon remains unshaded at basement level due to a lack of constraint on the hangingwall cut-off close to the edge of the survey

Figure 3.3: Fault orientation plots highlighting the mean vector (strike) azimuth and mean circular deviation (spread of data from the mean) of faults that intersect horizons moving progressively up sequence from (a) Base Salt (Permo-Triassic) to (b) Åre Coal (Early Jurassic) (c) Top Ile (Middle Jurassic) and (d) Top Lange Sandstone (Early Cretaceous). We represent the progressive rotation of mean strike azimuth and the increasing spread of fault orientations through time in (e), where the dashed line indicates an increase in the mean strike azimuth during Åre Coal (Early Jurassic) to Top Melke interval, the dotted line shows a shift in the mean strike azimuth to a decreasing trend after Top Melke deposition and the solid line highlights the onset of gravity-driven deformation and salt withdrawal synchronous with a shift in polarity of the trend

Figure 3.4: Uninterpreted and interpreted seismic profile across the footwall and hangingwall of the Smørbukk fault (Cross section A, Figure 1c). Faults that cut the Permo-Triassic and hangingwall layer-parallel reflector packages are highlighted. The pre-salt basement section shows no thickness changes across faults and no divergent reflectors in their hangingwalls. An Intra-Salt to Base Salt interval is folded around basement highs and reflectors onlap onto the Base Salt reflector (Inset)

Figure 3.5: Time-thickness maps for eleven stratigraphic intervals used to constrain the timing of fault and fold growth from the Upper Permian to Early Cretaceous (see Figure 2 for seismic stratigraphic intervals). Thickness changes across A, D & E are due to measurement errors associated with calculating the vertical thickness of intervals. B & C represent thickness changes within the salt layer which we suggest records the passive flow of evaporites in response to Jurassic rifting. F records the onset of fault growth during rift initiation. Faults remained active during the remaining intervals (G – K). Note, colour scales are different for each interval

Figure 3.6: Cross section D (see Figure 1c for location) across the south of the Trestakk fault, an area of complex interaction between basement-cover faulting, gravity sliding and salt diapirism. Pink shaded area highlights the period of salt withdrawal indicated by thickening above the footwall of S_{south}. See Figure 5 for fault annotations. Key to seismic marker horizons and intervals are shown in Figure 2

Figure 3.7: Cross section B (for location see Figure 1c) through the Smørbukk fault and Trestakk monocline illustrating the onset of fault activity across the area. The Smørbukk fault becomes active post-Intra Are deposition whereas the cover fault to the east remains inactive until post-Top Ile deposition, synchronous with the development of the cover monocline above a basement horst. See Figure 5 for fault and fold annotations, F = flexural fault. Key to seismic marker horizons and intervals are shown in Figure 2

Figure 3.8: Cross section C (for location see Figure 1c) through the Northern fault and adjacent northeast syncline. Growth across the northern fault initiates post-Åre Coal deposition continuing until Top Lange Sandstone deposition in the Early Cretaceous. Onlap and thinning onto the Base Cretaceous Unconformity in the east supports our interpretation of ongoing tectonic activity until at least Early Cretaceous Top Lange Sandstone deposition, with thinning of the subsequent succession suggesting activity continued synchronous with Near Top Lange Formation deposition. See Figure 5 for fault and fold annotations. Key to seismic marker horizons and intervals are shown in Figure 2

Figure 3.9: Cross section E (see Figure 1c for location) through the Smørbukk hangingwall graben illustrating the late onset of activity across the structure relative to other faults in the area. Thickening across faults is restricted to post-Top Ile formation deposition, with the maximum thickness changes during the Earliest Cretaceous. See Figure 5 for fault annotations. Key to seismic marker horizons and intervals are shown in Figure 2

Figure 3.10: (A) Layer parallel strata in a pre-rift setting, including the deposition of Triassic evaporites (highlighted with crosses). (B) The onset of faulting in the basement causes folding and flexure of cover strata where faults form and depocentres develop above basement lows. (C) The localisation of strain onto a few faults in the basement causes increased folding, flexure and faulting in the cover. Strain in the cover localises onto a few major faults and around areas of flexure e.g. hangingwall rollovers, synclines and anticlines. The most significant depocentres follow the axis of major faults and folds. (D) Fault growth in a low-strain rate syn-rift environment leads to salt withdrawal as sedimentation rate out paces salt supply rate. Sufficient dip on the underlying basement surface initiated gravity-driven deformation. The thickening of Early Cretaceous sediments in the footwall and hangingwall of faults records the onset of salt withdrawal. Salt evacuates up or down dip of the fault causing the collapse and rotation of overlying faults synchronous with withdrawal

Figure 3.11: Fault activity maps tracking the evolution of faults in the basement and cover sequence from the Early Jurassic to Early Cretaceous. The basement behaves as a pure brittle system in which strain becomes progressively localised through time, whereas in the cover sequence more faults develop as the basin evolves with the onset of gravity sliding and salt withdrawal in the Middle Jurassic. Depocentres that form above deforming basement blocks become more widespread as basement faults gain sufficient displacement to fold the cover

Figure 4.1: Basement-cover fault linkage scenarios in a system influenced by ductile evaporites, based on observations made in the Channel Basin by Stewart et al, 1997. Experimental models and observations from seismic data suggest the nature of linkage evolves as basement fault displacement relative to detachment layer thickness increases through time: (a) A coupled system in which a continuous fault links basement and cover strata by offsetting the entire evaporite sequence; (b) Partial coupling of the basement and cover via a detachment in the salt layer and (c) A decoupled system in which cover extension initiates due to gravity-sliding above an inclined basement surface. Large displacement basement faults and a thin salt layer favour coupled basement-cover fault growth whereas thick salt and low displacement basement faults favour decoupled faults

Figure 4.2: 3D block diagrams showing the development of a dipping surface during normal faulting. (a) The displacement along the strike of an isolated normal fault (redrawn from

Freeman *et al*, 1990). Note the variation in dip around the fault due to footwall uplift and hangingwall rollover. (b) During the evolution of a relay ramp between overlapping fault segments bedding is reoriented to accommodate displacement transfer between fault segments resulting in a dipping surface in the relay zone (redrawn from Peacock, 2003). Note, the evolution of dip on a basement surface which is separated from the cover by an intervening detachment layer, will initiate gravity-sliding when the surface gains sufficient dip

Figure 4.3: (a) Regional study area showing the location of the Halten Terrace with offshore platforms, terraces and basins. (b) Fault polygon map from the Halten Terrace with the location of hydrocarbon fields (purple = gas/condensate, green = oil/gas and red = gas) the Åsgard area (grey box) and regional seismic lines referred to in the text. (c) Time structure map from Middle Jurassic Top Garn interval (see Figure 4.4) across the Halten Terrace highlighting the distribution and nomenclature of structures across the region. For (b) and (c) co-ordinates are for UTM zone 32N

Figure 4.4: Fault population orientation data sub-divided into three systems: System 1 includes faults striking between N-S and NE-SW, System 2 includes those striking between NE-SW and E-W and System 3 is all other orientations. (a) Time structure map (Top Garn) illustrating fault orientation data across the Halten Terrace where the dashed box outlines the Åsgard area. Fault orientation data for the Åsgard area is divided into (b) basement faults and (c) cover faults. S_F = Smørbukk Fault, S_{FW} = Smørbukk Footwall Graben, S_{HW} = Smørbukk Hangingwall Graben, S_{CF} = Smorbukk compressional fold, T_F = Trestakk Fault, T_{FW} = Trestakk Footwall Graben, E_F = Eastern Fault, T_{syn} = Trestakk syncline, NE_{syn} = Northeast syncline. The Smørbukk fault polygon remains unshaded at basement level due to a lack of constraint on the hangingwall cut-off close to the edge of the survey

Figure 4.5: Common structural styles identified in the Åsgard area and regionally across the Halten Terrace. Structural styles are divided into two categories thick- and thin-skinned (see text for detail). A = Low-relief basement rift blocks, B = Coupled faults, C = Fault propagation folds, D = Breached folds, E = Simple rollers and grabens (dots represent salt weld), F = Reactive diapirism, G = Gravity-sliding, H = Raft tectonics, I = Compressional fold

Figure 4.6: The distribution of structural styles based on observations from 2D and 3D regional seismic data, (a) in the Åsgard area and (b) across the Halten Terrace. The dotted box in (b) outlines the Åsgard area in (a). Key refers to structural styles highlighted in Figure 4.6. Note, areas of insufficient data quality or where no data is available remain unshaded

Figure 4.7: Cross-sections from the Åsgard area highlighting different degrees of interaction between basement and cover faults formed due to thick-skinned deformation; (a) The Smørbukk fault (S_F) is rooted in sub-salt basement stratigraphy thus is an example of thick-skinned coupled deformation. T (Base Salt) is the throw at base salt level. (b) East of the Smørbukk fault, basement and cover deformation are partially coupled. Cover faults detach on the mechanically weak evaporites, e.g. simple rollers (E) in the cover only. The locations of figures with more detailed interpretation are outlined by dashed boxes

Figure 4.8: Regional cross sections through the main fields on the Halten Terrace. (a) Kristin, Lavrans, Trestakk, Tyrihans and Mikkel. (b) Morvin, Smørbukk and Midgard and (c) structural styles that form oblique to the main NE-SW trend. The structural complexity of individual fields varies greatly across the area. Each figure shows blank seismic data and interpreted lines (Base Salt (purple), Top salt (pink), Åre Coal (green) and BCU (blue)). The distribution of structural styles is highlighted in a series of sketches along the top of each figure, whilst hard-linked faults are also highlighted in bold on the cross sections. The locations of figures with more detailed interpretation are highlighted

Figure 4.9: (a) Low-relief, basement blocks (structural style A) west of the Morvin field. Permo-Triassic basement faults decoupled from the cover are draped by the BCU due to extensive erosion in the west. (b) Coupled fault (bold) west of the Midgard field (see Figure 4.9b for location) offsets the entire salt sequence, linking basement and cover strata. (c) The Smørbukk fault which offsets the entire salt layer, coupling basement and cover faults

Figure 4.10: (a) Fault-propagation fold (structural style C) north of the Trestakk fault, note the Smørbukk Sør field resides in the anticlinal flexure of the fold (see Figure 4.9b). (b) Structural style C is also observed in the north-east of the Åsgard area, in the west of the cross-section. Further east, the magnitude of basement and cover fault throw increases and the system becomes more coupled. The Grinda Graben is defined by complex rollers and grabens in the east. (c) The geometry of 'cover-only' faults which are planar up-dip, abruptly detaching on evaporites with a listric base. (d) Detailed interpretation of the geometry of a fault-propagation fold and a breached fold. (e) A breached fold (structural style D) from the Mikkel field and (f) from the Heidrun field (see Figure 4.3b for location of cross sections). Note, the location of the fields in (e) and (f) are highlighted by the dotted line

Figure 4.11: Examples of structural style E (a) A simple roller from the Gimsan Basin and (b) a series of complex rollers and graben through the Grinda Graben (see Figure 4.3b for the location of cross-sections. (c) Schematic diagram to illustrate the formation of a 'roller' due to differential loading in the hangingwall of a cover fault above mobile evaporites

Figure 4.12: Examples of structural style F; (a) a simple reactive diapir in the footwall of the Smørbukk fault, southern segment (see Figure 4.7a). (b) Cross-section through a salt spine in the Heidrun field, the only structure like it on the Halten Terrace. (c) Isochron illustrating the timing of diapir growth was Miocene in age (Post- Top Brygge), much later than other diapirs in the area which are Jurassic-Cretaceous in age. (d) Close up interpreted section through the diapir, highlighting the dimensions of the diapir and the main period of diapir growth. Note the stratigraphic age of the Kai formation is Upper Miocene – Lower Pliocene, and the Brygge formation is lower to middle Eocene (Eidvin *et al*, 1998)

Figure 4.13: Structural styles that form due to gravity-driven deformation above mobile evaporites; (a) A gravity-driven graben (structural style G) in the hangingwall of the Smørbukk fault forms perpendicular to the strike of the fault. (b) A series of rollers, graben and raft blocks trending NW-SE, oblique to the dominant fault trend and normal to the regional dip on the Halten Terrace. See Figure 4.3c for the location of cross-sections

Figure 4.14: (a) A cross-section through a compressional fold (structural style H) in the hangingwall of the Smørbukk fault. The fold, which forms due to gravity-sliding above an inclined basement surface, is defined by up-dip extension and down-dip compression against the Smørbukk fault. (b) A graph of fold amplitude vs. throw on the Smørbukk fault. The regression line shows a positive correlation between fold amplitude and throw supports our interpretation of gravity-sliding above a rotated hangingwall block, where the magnitude of displacement controls the magnitude fold development

Figure 4.15: Schematic diagram showing the relationship between the duration of extension and the degree of coupling between basement and cover faults from (A) a partially coupled system during the onset of rifting in the Early Jurassic to (B) an increasingly coupled system with coupled and partially coupled faults and the initiation of decoupled faults. (C) The system is dominated by decoupled and partially coupled faults due to gravity-driven deformation

Figure 4.16: D_{max}-length plots for thick-skinned basement and cover faults to illustrate (a) the positive correlation between the magnitude of displacement for both basement and cover faults, suggesting high displacement basement faults are balanced by higher displacement in the cover. (b) and (c) illustrate the relationship between the degree of coupling and the magnitude of displacement, which for both sub- and supra-salt faults increases as the degree of coupling increases, as we might expect. Note, C refers to coupled faults whereas PC refers to those that are partially coupled. Linear regression lines are included on each plot along with values of n (the number of points in the dataset) and R^2 (a statistical measure of how well a regression line approximates real data points, where 1 indicates a perfect fit)

Figure 4.17: The evolution of fault systems that form in the presence of a weak stratigraphy in map-view and cross-section, based on our observations from seismic data for (a) Coupled (structural styles B, E) (b) Partially coupled (structural styles A, C, E) and (c) Decoupled (structural styles G, H, I) basement and cover faults. Faults that initiate in the basement and cover progressively link in both map-view and cross-section as faults gain length and displacement

Figure 5.1: A comparison of existing conceptual models of fault growth (a) radial propagation, (b) segment linkage and (c) the alternative model, in both plan view, on a displacement against distance plot and a log maximum displacement versus log trace length plot. Each model follows contrasting pathways on the log L-log D plots, with the radially propagating model following a linear and predictable growth path whereas during segment linkage the model follows a step-wise, more unpredictable path. Individual segments may deviate from the idealised growth line as they begin to interact with neighbouring segments (stage ii, log-log plot in (b)) (Redrawn from Cartwright *et al*, 1995). (c) In the alternative model of fault growth, faults establish their length early in the growth history by rapid lateral propagation of fault tips (stage i and ii). Lateral growth is then retarded and the fault grows by accumulating displacement (stage iii).

Figure 5.2: (a) A coupled system in which a continuous fault links basement and cover strata by offsetting the entire evaporite sequence. (b) A decoupled system in which cover extension initiates due to gravity-sliding above an inclined basement surface.

Figure 5.3: (a) Fault polygon map for cover faults from the Åsgard area where S_F = Smørbukk Fault, S_{FW} = Smørbukk Footwall Graben, S_{HW} = Smørbukk Hangingwall Graben, T_F = Trestakk Fault, T_{FW} = Trestakk Footwall Graben, T_{TIP} = Trestakk tip, T_{SPLAY} = Trestakk splay and S_{MID} = Smørbukk Mid Fault. (c) Fault polygon map from the Halten Terrace with the location of hydrocarbon fields (purple = gas/condensate, green = oil/gas and red = gas) and the Åsgard area (grey box). The Smørbukk and Trestakk faults are highlighted.

Figure 5.4: Time difference maps illustrating the temporal evolution of faults in the Åsgard area. (a) Early Jurassic fault activity was restricted to a few NE-SW trending dominant faults. (b) Activity in the Early Cretaceous changed with the onset of gravity-driven fault activity oblique to the dominant NE-SW fault trend. S_F = Smørbukk fault and T_F = Trestakk fault.

Figure 5.5: (a) Schematic strike projection (i.e. view along normal to fault surface) of an idealised fault plane. Fault polygons, defined by the cut-offs of displaced horizons in the footwall and hangingwall of the mapped surface, are in white. Offset decreases towards the tip line. (b) A simple two-layer model used to depth convert fault polygons in the basement and cover. An average seismic velocity of 4000m/s is used for the cover sequence (layer 1). For the salt layer (layer 2) the seismic velocity was calculated taking into account the presence of a thick mud layer (see text for detail). (c) Displacement-length profile highlighting the uncertainty associated with constraining the length of faults mapped in

seismic data. Low magnitude scatter in displacement profiles quantifies the uncertainty in picking footwall and hangingwall cut-offs. (d) Schematic displacement contour diagram for a simple, isolated fault drawn normal to the fault surface (strike-view). Maximum displacement is in the fault centre (D_{max}).

Figure 5.6: (a) Fault polygon map for cover faults from the Åsgard area with the Trestakk fault, the Smørbukk fault and splays highlighted. T_F = Trestakk Fault, T_{FW} = Trestakk Footwall Graben, T_{TIP} = Trestakk tip, T_{SPLAY} = Trestakk splay and S_{MID} = Smørbukk Mid Fault, S_F = Smørbukk Fault, S_{SOUTH} = Smørbukk southern splay. Note, the locations of cross-sections in Figure 5.6 are highlighted. (b) Plan view of the Trestakk and Smørbukk faults interpreted from regional data, highlighting the portion of the fault covered by the Åsgard area dataset, the separation (S) and overlap (O) of the faults. Note, the length of the fault was measured from the regional data and D_{max} is interpreted from the Åsgard area.

Figure 5.7: Cross sections (a-e) through the Trestakk fault highlighting the change in geometry along strike of the fault from south (a) to north (f). T_F is the cover, and T_B is the basement portion of the fault. Note, the fault becomes increasingly shallow in dip towards the south in (a), where the hangingwall beds are rotated the most. As the Trestakk fault in the basement and cover lose displacement to the north the faults are steeper in dip and have less growth into their rotated hangingwalls (c, d). In (e) the displacement on T_B is insufficient to deform the cover, instead displacement is transferred onto M which folds and flexes the overlying cover forming fault S_{MID}.

Figure 5.8: The 3D geometry of the Trestakk fault. (a) A schematic block diagram illustrating the geometry of the Trestakk fault and associated footwall splays. (b) The geometry of the Trestakk fault surface which splays at its northern tip (T_{TIP}). Note, the locations of cross-sections in Fig.5.7 are highlighted on the fault surface. (c) A strike-view projection of the Trestakk fault surface contoured for dip, demonstrating the change in dip from relatively steeply dipping in the north (45°) to shallow in the south (15°).

Figure 5.9: 3D geometry of the Trestakk fault, (a) in map-view and (b) in strike view. The Trestakk fault and the location of: (c) the branchline, B, with the Trestakk splay and (d) the Trestakk footwall graben. Fault polygons are included for Intra Åre (light blue), Åre Coal (green), Top Åre (purple) and Top Ile (orange). (e) Displacement-length profile for the Trestakk fault and splays. Aggregate profile for C1 and C3 results in a more regular profile whereas the footwall graben (C2 and C4) cross-cut the Trestakk fault offsetting the profile.

Figure 5.10: Cross sections through the Smørbukk fault highlighting the geometry of the fault at D_{max} (a) and further south where the fault loses displacement (b). The basement and cover portions of the fault are highlighted. The geometry of the fault surface is similar along strike of the fault, with little variation dip compared to the Trestakk fault (see Figure 5.11).

Figure 5.11: The 3D geometry of the Smørbukk fault in map-view (a) and strike view (b). Note, the locations of the Smørbukk footwall and hangingwall grabens are highlighted in (a). (c) The branchline, B, between the Smørbukk Fault and Smørbukk south with the polygon for Åre Coal level highlighted on the fault. (d) Dip contours on the Smørbukk fault surface (e) Displacement-length profile for the Smørbukk fault, southern splay and the aggregate profile for S1 and S3 which results in a more regular profile.

Figure 5.12: Fault polygons in the basement (a) and cover (b) from the Åsgard area. Displacement-length profiles for faults highlighted in black have been plotted in Fig. 5.13. Cross-sections (c-e) illustrate the geometry of main faults used in displacement analyses.

Figure 5.13: Displacement-length profiles for basement (a) and cover faults (b) highlighted in Figure 5.12. D-L profiles for low displacement cover faults (inset in b) are highlighted in (d). (c) Irregular displacement profiles for basement faults B1, B2 and B8 have clear local displacement minima (D_{min}) and local displacement maxima defining segments (S) along each fault which suggests that faults were initially segmented along strike.

Figure 5.14: (a) Displacement maxima-length plots for basement and cover faults from the Åsgard area. (b) The Trestakk cover fault is much larger displacement than its basement continuation whereas the opposite is true for the Smørbukk fault. Individual plots of (c) cover and (d) basement faults highlighting R^2 and n values for each. In each case (a-d), a linear regression line is included for basement data, cover data or both.

Figure 5.15: (a) A log-log plot of displacement vs. length for basement and cover faults, the box in (a) outlines the area shown in (b). The dashed diagonal line represents the average scaling relation of faults documented in Schlische *et al* (1996) where $D_{max} = 0.03L^{1.06}$. Note Sb = Smørbukk basement fault, Tb = Trestakk basement fault, Sc = Smørbukk cover fault and Tc = Trestakk cover fault.

Figure 5.16: Displacement-length profiles for basement and cover portions of (a) the Smørbukk and (b) the Trestakk faults. (a) Displacement-length profiles for the Smørbukk fault show the basement fault displacement is larger than the cover displacement along the entire imaged and extrapolated length of the fault. The average displacement gradient in the basement is greater (0.05) than the cover (0.03). (b) The cover portion of the Trestakk fault has a much higher displacement gradient (0.06) and a larger D_{max} than the basement fault (0.014). The cover displacement profile crosses over becoming higher magnitude than the basement fault displacement profile at X. (c) The cumulative displacement profile for the Smørbukk and Trestakk faults has an irregular profile.

Figure 5.17: Faults that have undergone a component of gravity-driven deformation. (a) A zone of westerly-directed gravity-related deformation in the hangingwall of the Trestakk fault. The dominant direction of gravity-sliding is highlighted on the map, along with the location of cross-sections in (b) and (c) (dotted lines) and the critical point, C (red line), south of which gravity-sliding initiated. (b) Cross-section through the Smørbukk fault demonstrating the east-dipping basement surface beneath the footwall of the fault close to its displacement maximum. (c) Cross-section through the gravity-related faults taken approximately parallel to the direction of sliding. The faults shown in map-view in (a) are highlighted in bold. The average dip of the basement surface is towards the west, enabling westerly directed gravity-sliding to take place.

Figure 5.18: A new model of fault growth for cover faults that form due to (a) tectonic deformation and (b) tectonic and gravity-driven deformation. During tectonic deformation, segment linkage dominates the model which follows a step-wise growth path as predicted by Cartwright *et al*, 1995 (Modified from Cartwright *et al*, 1995). Note, in this model both basement and cover faults form due to segment linkage however basement faults have a larger D_{max} than in the cover. In (b) additional displacement due to gravity-driven deformation leads to cover faults, which have a larger D_{max} than the basement faults and higher displacement gradients. Faults follow the same step-wise pattern of linkage however due to a component of gravity-sliding faults gain more displacement and fall above the idealised growth line thus deflecting the trend to a steeper profile.

Figure 5.19: A model of fault growth for (A) extensional faults and (B) faults driven by extension and gravity-driven deformation, used to account for the differences in geometry between the two faults. In (A) the basement and cover faults initiate aligned with one another (stage 1), as the two faults gain displacement they link to one through-going fault (stage 2) which continues to gain displacement until the dip on the basement surface is sufficient to

initiate gravity-sliding and compressional folding in the hangingwall of the cover fault (stage 3). (B) In contrast the Trestakk basement and cover faults initiate with the cover fault offset slightly into the hangingwall of the basement fault (stage 1). As the faults gain displacement, the cover fault touches down on the footwall crest of the basement fault (stage 2), which is then utilised as a pivot point for ongoing displacement in the cover due to both extension and gravity-driven sliding (stage 3).

Figure 6.1: Table of fault characteristics and the mechanism of faulting summarised from chapter's 3, 4 and 5. A link exists between: the timing of fault activity; the orientation and geometry of structural styles; the degree of linkage through the salt layer; and the growth path of faults in salt-related systems. We can use the relationships established between characteristics to predict the mechanism of faulting, and thus the impact of faults on reservoir development (see section 6.1.2).

Figure 6.2: The original thickness of the evaporite layer on the Halten Terrace, (see Figure 4.7 for the full figure legend) based on regional knowledge, (see Chapter 4) and Stewart's (1999) model of detachment layer thickness and thin-skinned fault geometry. Cross-sections A-D highlight the change in structural geometry in the cover from north to south, which we relate to salt layer thickness and detachment dip (see Figure 6.3).

Figure 6.3: The impact of detachment layer thickness on thin-skinned extensional fault geometry, divided into low and high multilayer dip cases (modified from Stewart, 1999). (a) Low multilayer dip: (1) For a thin detachment layer, conjugate fault pairs intersect at the top detachment surface defining narrow graben and wide, relatively undeformed rafts. (2) For a thicker detachment, more complex symmetrical graben occur, underlain by a reactive diapir. Where no more detachment material is available to feed the diapir, the diapir collapses giving a new deep basin between the rafts (Vendeville & Jackson, 1992a, b). (3) For the thickest detachment layer, sufficient supply of detachment material delays diapir fall. (b) High multilayer dip, where high refers to sufficient regional dip to promote domino-faults that dip in the same direction as the dip of the detachment. (1) Domino faults of consistent, down-dip facing polarity and faults that are relatively closely spaced. (2) For a thicker detachment, back rotation of fault blocks is sufficient to allow a second, antithetic generation of faults to develop. Fault array characterised by thin, high horsts. (3) For the thickest detachment, keels of fault blocks, defined by first generation faults, never touch down.

Figure 6.4: Contrasting interpretations of the present-day thickness of a salt layer from the same seismic section (A). (B) A package of divergent reflectors are interpreted to indicate stratal thickening into the hangingwall of the fault during a period of fault activity synchronous with evaporite deposition. (C) A more holistic approach, in which basement and cover fault geometries are interpreted, interprets the evaporites as a pre-rift package.

ABSTRACT

Normal fault zones play a fundamental role in the development of sedimentary basins and in the migration and trapping of hydrocarbons. The idealised geometry of an isolated post-sedimentary normal fault (Barnett, 1987, Walsh & Watterson, 1989) and existing conceptual models that describe the process of fault growth and linkage in brittle systems (Childs *et al*, 1995; Cartwright *et al*, 1996; Childs *et al*, 1995, 1996b; Huggins et al, 1995), where fault planes composed of many overstepping segments are linked by areas of complex deformation called relay ramps, are generally well accepted. Relay zones can trap significant volumes of hydrocarbon or act as leakage points, thus understanding the style of fault linkage, which strongly influences the location of hydrocarbon traps and reservoir compartmentalisation, is vital for any petroleum system.

Existing models of fault growth may not be applicable to all structural settings. In particular the results presented suggest faults that form in brittle-ductile systems, require an alternative model of fault growth to account for the geometries that form in the presence of a weak mechanical stratigraphy, such as evaporites. Salt's fluid rheology and incompressibility make it inherently unstable under a range of geologic conditions resulting in often complex structural geometries.

Well data has been integrated with structural and stratigraphic interpretations of a high-quality 3D seismic dataset from the Åsgard area (see below) and regional knowledge derived from interpretations of 2D seismic lines. Crucially, these seismic datasets image faults and horizons within the sub-evaporite basement. These interpretations have allowed us to develop a new structural model which considers the relative contributions and impacts of basement faulting, gravity sliding and salt tectonics on the development of the Halten Terrace. The Halten Terrace, offshore Mid-Norway (**Figure 1.1a**) is the ideal location for such a study given the presence of both thick- and thin-skinned extensional tectonics in a system influenced by salt. Many parts of the Halten Terrace, which is the most prolific hydrocarbon province in offshore mid-Norway (Koch & Heum, 1995), are now considered mature (NPD, 2007). The decline in production (NPD, 2007) of significant volumes of hydrocarbons trapped within fault-bounded structural highs and the continuation of exploration activity has spurred on a drive to better understand the structure of the basin and the interplay between fault- and salt tectonics.

CHAPTER 1

1: INTRODUCTION

Normal fault zones play a fundamental role in the development of sedimentary basins and in the migration and trapping of hydrocarbons. There are now well-established idealised conceptual models for an isolated post-sedimentary normal fault (Barnett, 1987, Walsh & Watterson, 1989) and for the process of fault growth and linkage in brittle systems (Childs *et al*, 1995; Cartwright *et al*, 1996; Childs *et al*, 1995, 1996b; Huggins et al, 1995) where fault planes composed of many overstepping segments are linked by areas of complex deformation called relay ramps or zones. Such relay zones often host significant hydrocarbon traps, so that an understanding of the styles and evolution of fault linkages, which may strongly influence both trap location and reservoir compartmentalisation, is vital for any petroleum system hosted in an extensional basin.

The results of this study suggest that existing models of normal fault growth may not be applicable to all structural settings. In particular, faults formed in brittle-ductile systems exhibit specific geometric differences that require an alternative model of fault growth. Brittle-ductile systems develop when faulting occurs in the presence of weak mechanical layers in the stratigraphy, such as evaporites. The relatively weak, ductile rheology and incompressibility of salt make it inherently unstable under a range of geologic conditions resulting in often complex structural geometries. Given the relative abundance of significant salt deposits in many hydrocarbon-bearing basins, the structural geometries and evolution described in the present study are likely to be very widespread elsewhere in the world.

Well data has been integrated with structural and stratigraphic interpretations of a high-quality 3D seismic dataset from the Åsgard area of the Halten Terrace, offshore and west of Mid-Norway (**Figure 1.1a**) and linked to regional knowledge derived from interpretations of 2D seismic lines. Crucially, these seismic datasets are notable as they image faults and horizons within the sub-evaporite basement. These interpretations enable the development of a new structural model which considers the relative contributions and impacts of basement faulting, gravity sliding and salt tectonics on the development of the Halten Terrace. The Halten Terrace is the ideal location for such a study given the presence of both thick- and thin-skinned extensional tectonics in a system influenced by salt. The region lies in the most prolific hydrocarbon province in offshore mid-Norway (Koch & Heum,

1995) and is now considered mature (NPD, 2007). The decline in production of significant volumes of hydrocarbons trapped within fault-bounded structural highs (NPD, 2007) and the continuation of exploration activity has spurred a drive to better understand the structure of the basin and the interplay between fault- and salt tectonics.

1.1 THESIS SYNOPSIS

The thesis is presented as a series of key chapters (chapters 3, 4 & 5), introduced in chapter's 1 and 2 and summarised in the final chapter, where conclusions are presented, along with a discussion of the implications of the work.

Chapter 1 presents the main aims and objectives of the thesis, as well as a description of the dataset available for the study and the methodology applied.

Chapter 2 provides an overview of the background research relevant to the results and discussion in the thesis. It begins with a description of faulting patterns predicted by numerical and analogue models, followed by a more in-depth discussion of existing conceptual models of fault growth and linkage. The theory of extensional forced folding is supported by examples of analogue and experimental models, field studies and seismic data. Salt tectonics is then reviewed including the mechanics of salt deformation and a summary of salt mobility and fault growth. Finally, existing work on the structural and stratigraphic evolution of the Halten Terrace is summarised, including the regional geological setting, tectonostratigraphic evolution and a description of existing models for the structural evolution of the area.

In Chapter 3, a new structural model for the Permo-Triassic to Early Cretaceous evolution of the Åsgard area, derived from the interpretation of a 3D seismic dataset, is presented and discussed. The faults and folds are described and an interpretation of the timing of fault movement is presented. New findings on the role of basement fault growth, the presence of salt and the onset and duration of fault activity are presented in a conceptual model for the area. The implications for hydrocarbon prospectivity are discussed, with particular focus on the development of depocentres, sediment pathways and the relationship between reservoir thickness and quality.

In Chapter 4, it is suggested that the geometry of faults formed in the presence of a ductile layer will generally differ from fault patterns described in the literature typically from clastic sequences (e.g. Barnett, 1987). To test the hypothesis a

description of the geometry and distribution of structures in map view and cross-section, interpreted from regional seismic data across the Halten Terrace is presented. Observations are used to define nine structural styles that typify structures formed in the presence of regional-scale salt layers. The geometry of each structural style is described and an example of each is presented. The relationship between the geometry and temporal evolution of structural styles is discussed and an interpretation of the mechanisms that likely control the structural evolution presented.

In Chapter 5 existing conceptual models of fault growth and linkage, which may not apply to basins influenced by weak mechanical stratigraphic units, are discussed. This hypothesis is tested using displacement-length data from basement and cover fault surfaces in the Åsgard area. The along-strike evolution of the Trestakk fault is presented and used to develop a detailed conceptual model for fault growth and linkage in brittle-ductile systems.

Finally, Chapter 6 brings together the discussions from the previous chapters. Firstly, the results presented are used to rank the hydrocarbon prospectivity of structural styles interpreted from fields and prospects on the Halten Terrace.

1.2 DATA & METHODOLOGY

1.2.1 Dataset

The database used consists of a 3-D time-migrated seismic survey from the Åsgard area and a regional 3-D merged seismic dataset covering all the fields on the Halten Terrace, from which 14 seismic lines have been interpreted (**Figure 1.1b**). Data quality varies according to survey vintage, the area covered by the survey and the processing techniques applied to improve the imaging of reservoir intervals. As a result, sub-salt reflectors are more difficult to interpret in some datasets. Data from the Åsgard area is the best resolution, imaging the sub-salt basement stratigraphy, and provides optimal orientation and coverage with respect to the main fault trends. Horizons and faults were interpreted on this survey using the 3-D merged survey where necessary to quality check or extend the interpretation. In addition, the regional seismic data were used for individual line interpretations across areas of structural significance, i.e. across all the fields and prospects on the Halten Terrace, to define the geometry of faults and folds on a broader scale.

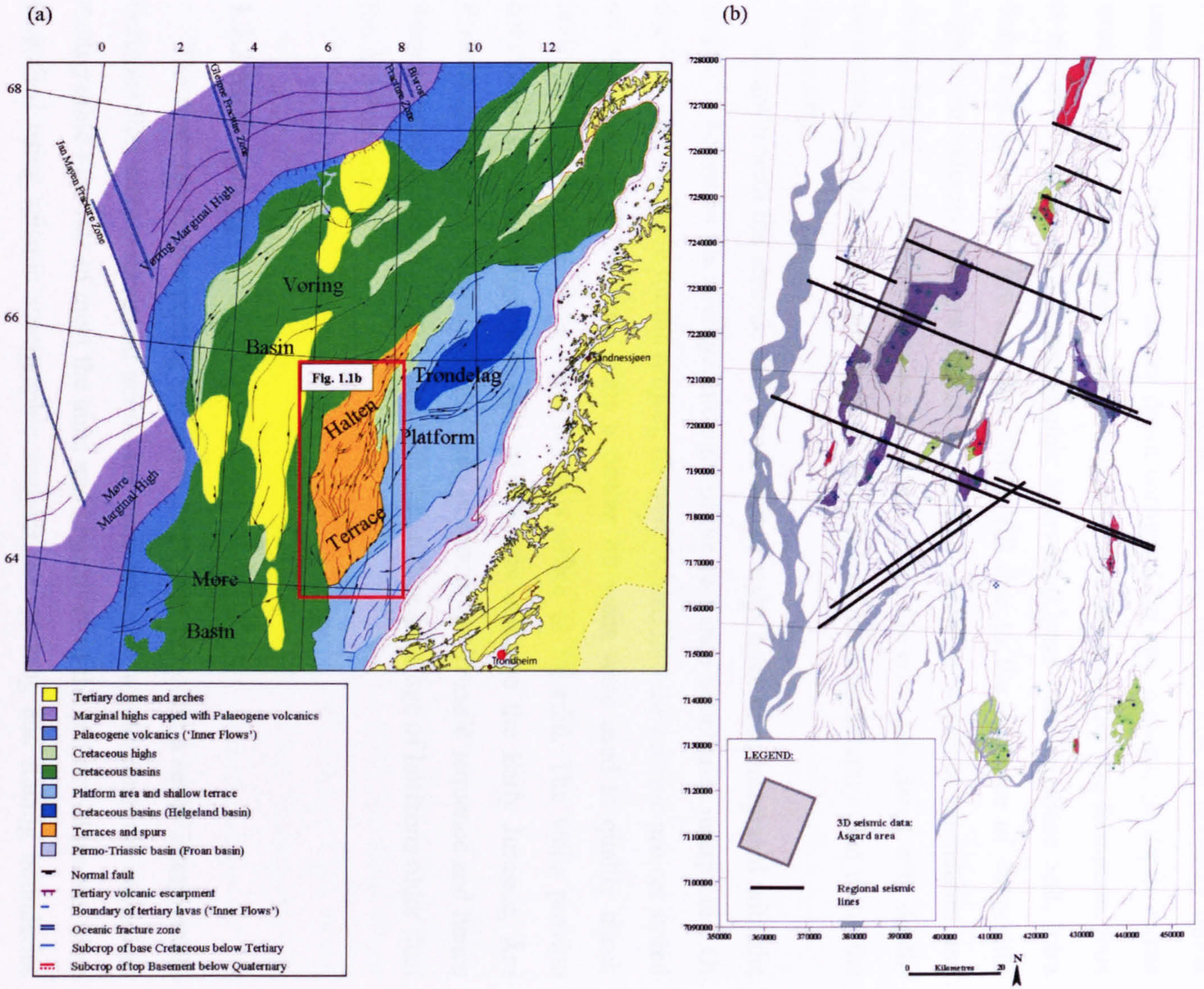

Figure 1.1: (a) Regional study area showing the location of the Halten Terrace with offshore platforms and terraces. (b) Fault polygon map for the Halten Terrace with the location of fields (purple = gas condensate, green = gas, red = oil). The Åsgard survey is shaded in the grey box and the location of regional lines highlighted.

The Åsgard dataset covers an area of approximately 20 x 30 km with a spacing of 12.5 m, on which horizons and faults were interpreted manually every 20 lines across the whole survey and every 10 lines around fault tips. Data quality is relatively consistent, with a resolution of c. 25 metres at the depth of top reservoir, and reaches a maximum two-way travel time of 6500 milliseconds (ms), with the exception of the survey edges where seismic diffraction interrupts the continuity of the data.

The seismic data have not been depth-converted and so the cross sections and isochron maps in this study are presented with the vertical axis in two-way travel time (TWTT). The data was not depth converted for two reasons; (i) depth versus time data from the available wells is only available down to Top Åre formation, thus is not available for earlier stratigraphic intervals (Upper Permian, Base Salt, Intra Salt, Top Salt, Intra Åre and Åre Coal), (ii) due to the presence of evaporites significant velocity changes across stratigraphic units or sequence boundaries and strong lateral velocity changes are expected. Thus, the error associated with depth-converting the data is potentially high, resulting in more uncertainty than using the data in time.

Coupled with the seismic data, a number of wells have been integrated with the project to constrain the stratigraphic ages of the sequence boundaries interpreted. Of the well data available for the project, 63 were loaded into the seismic project stored on workstations in Durham, while a further 80 wells were used to quality check horizon interpretations from StatoilHydro's office in Stjørdal. The wells provide constraints on the stratigraphic ages of horizons down to the Early Jurassic, Åre Formation. None of the wells in this area penetrate the Triassic sequence and hence there is more uncertainty associated with the stratigraphic age of horizons older than the Åre Formation.

1.2.2 Methodology

The first step in interpreting the seismic data was to define a set of interpretable horizons that were widespread across the area, and that would constrain sufficient stratigraphic intervals to meet the aims and objectives of the project. Horizons were identified using seismic stratigraphic analysis, i.e. picking and tracing boundaries between significant seismic sequences from the seismic datasets. The timing of seismic sequences was constrained using formation tops, biostratigraphic data and

internal reports (Brockbank & Hanssen, 2004), however due to confidentiality constraints, further details of biostratigraphic dating methods cannot be included as a part of this thesis. The available data was used to divide the sedimentary succession into eleven mega-sequences from the Permo-Triassic to Cretaceous to include pre-, syn- and post-tectonic sequences (see Chapter 2). Interpreted seismic reflection events are described by their formation name and the location of the seismic response within the formation, i.e. top, intra or base, for example, 'Top Ile' refers to a seismic reflection event at the top of the Ile formation.

1.2.2.1 Data Analysis

A fault/horizon model was constructed using a combination of Schlumberger's IESX™ and Badley's TrapTester™ software. By using Badley's TrapTester™ software, the hangingwall and footwall intersections for each horizon can be accurately modelled on the fault surface. The hangingwall and footwall cut-offs of a given stratigraphic horizon on a fault surface define a fault polygon (**Figure 1.2a**). Interpreted horizon and fault surfaces from the Åsgard survey area were exported from Schlumberger's seismic interpretation software package into Traptester™, where fault sticks were correlated to create fault surfaces. Fault polygons, generated on the fault surfaces, were quality checked for errors due to mis-picks in horizon data, or due to interactions with adjacent faults. Once modelled, the fault polygons were used to calculate fault displacement-length profiles (see 1.2.2.3).

The fault attributes calculated in Badley's Traptester™ software, were sampled within the software using a sampling grid of regularly spaced lines with a fixed azimuth that has been manually set by the interpreter (**Figure 1.2b**). Values of throw were measured in a plane perpendicular to the strike of the fault (**Figure 1.2c**), where throw is the vertical component of fault displacement (**Figure 1.2d**). Throughout this thesis the term displacement is used to refer to the vertical component of displacement, or throw. This method was used to export fault length and displacement data used in chapter 5. The data were exported in ascii file format and imported into Microsoft Excel for analysis. The result is a database of fault attributes that describes the amount of throw on each horizon at regularly spaced points along the length of each fault (**Figure 1.2b, c**).

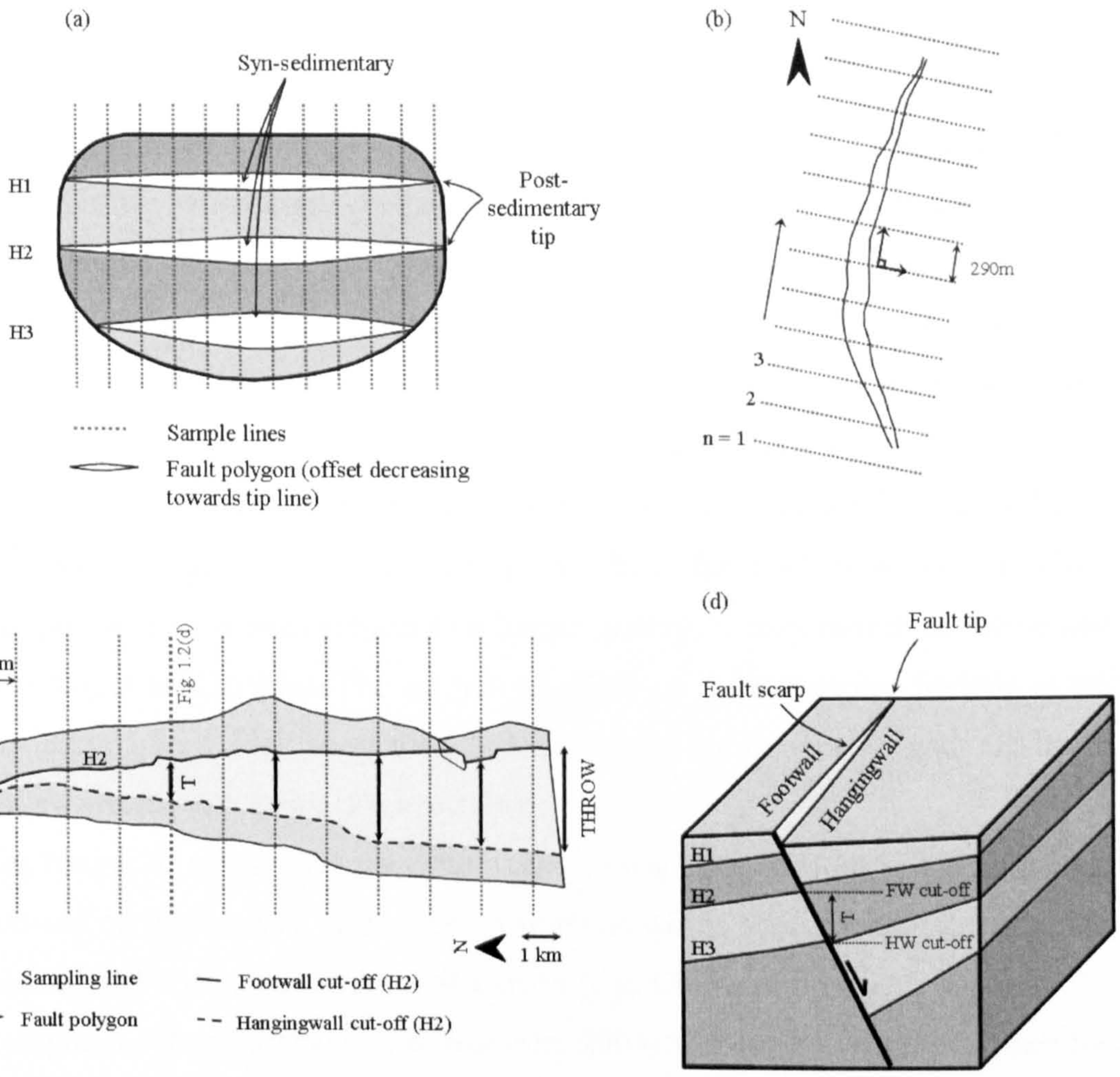

Figure 1.2: Constraining the timing of fault movement. (a) Strike-view of a fault plane with an orthogonal sample grid. The magnitude of offset on each horizon is sampled along each gridline. The fault centre shows a decreasing upwards offset indicating syn-sedimentary fault movement from horizon H3 onwards. The fault tip shows equal offset on all three horizons indicated that movement occurred after the deposition of H1. The fault tip is younger than the fault centre, the fault has grown laterally through time. (b) Map-view of a fault plane and sampling grid used in Badley's TrapTester software. The cut-off polygons for one horizon are shown for a single fault dipping towards ESE. A sampling grid with a spacing of 290 m was used at sampling intervals, n, for cut-off polygons on each horizon. (c) Strike-view of a fault plane with footwall and hangingwall cut-offs which constrain the fault polygon highlighted. Values of throw were measured at intervals along the fault plane as defined in (b). Note the location of (d) which shows the geometry of the fault in cross-section. (d) 3D sketch of a syn-sedimentary fault intersecting three horizons (H1, H2, H3). Upward decreasing offset on successive horizons indicates syn-sedimentary fault movement. Note syn-sedimentary packages are thicker in hangingwall relative to footwall.

1.2.2.2 Constraining the timing of fault movement

Syn-sedimentary normal faults are those that were active during the deposition of the sedimentary sequence. In contrast to the blind faults described by Barnett *et al.* (1987), syn-sedimentary faults always displace the Earth's surface (**Figure 1.2d**). The downthrown hangingwall creates a synclinal depression at the surface into which sediment can be deposited. The footwall is often uplifted, which, depending on the overall basin subsidence, the location of the fault within the basin and the eustatic sea level, may then be subject to erosion. The difference in elevation between the footwall and hangingwall controls the relative sediment thickness change across the fault and produces a thicker sedimentary sequence in the hangingwall (**Figure 1.2d**). Because the stratigraphy is being deposited whilst the fault is active, the older stratigraphy will have been subject to a longer history of fault movement compared to the younger stratigraphy. The amount of offset on a stratigraphic horizon is the accumulation of all fault movement subsequent to its deposition and results in increasing offsets with depth (**Figure 1.2a**).

The timing of syn-sedimentary fault activity has been constrained for modelled faults based on the analysis of thickness variations within stratigraphic intervals used to constrain the onset and duration of growth (e.g. Childs *et al.*, 1993, 1995, 2003). Biostratigraphic data (Brockbank & Hanssen, 2004) was used to accurately date the seismic stratigraphic boundaries interpreted, and thus to constrain the onset of growth associated with thickness changes across the faults.

In the present study, two types of syn-sedimentary faults are recognised: (i) emergent faults, which intersected the free surface at the time of activity; and (ii) blind-faults that were active at depth - typically beneath evaporite layers - leading to the development of fault propagation folds. The latter group of faults did not intersect the free surface at the time of folding. Active emergent faults were identified based on the recognition of reflector geometries that define distinct syn-rift wedges (Prosser, 1993). Rift-related sedimentary wedges commonly thin onto the crests of fault blocks, where truncation and onlap are observed. Reflectors diverge and thicken down dip from the footwall crest and towards the adjacent bounding fault (**Figure 1.3a**). Markedly different structural characteristics define blind faults where fault propagation folds are associated with the development of a buried fault tip (**Figure 1.3b**). Typically, they comprise upward-widening zones of distributed

deformation with anticlinal and synclinal bends that form above blind normal faults (Withjack & Callaway, 2000). Reflectors diverge into the hangingwall depocentre at a point offset into the hangingwall of the basement fault trace and onlap onto the limb of the anticline (Gawthorpe *et al*, 1997) (**Figure 1.3b**). Thus, the location of the hangingwall depocentre can be used to distinguish emergent faults from those with a buried tip. Isochron maps show changes in the vertical time difference between two horizons and are calculated by a simple subtraction of one horizon from the other. Isochron maps for successive intervals can therefore be used to investigate changes in the spatial distribution of stratal thickness – and therefore active faulting and associated folding - throughout rifting.

In order to make a valid analysis, it is important to be aware of the assumptions and measurement errors associated with the methods used. Interpretations of across-fault thickness variations can be applied only where sedimentation rates exceeded, or were comparable to fault displacement rates (e.g. Childs *et al.* 2003), a condition which is likely valid on the Halten Terrace. Well data from the survey area indicate that the depositional environment during the Early to Upper Jurassic rift phase was a shallow marine/tidal environment, where an adequate supply of siliclastic sediment is expected. Evidence to suggest relatively rapid fault displacement rates such as the formation of fault scarps, the underfilling of hangingwall basins and the erosion of uplifted footwalls is generally not observed in the area, with the exception of extensive erosion associated with the development of the base Cretaceous Unconformity (BCU) which is accounted for in the interpretation of thickness variations.

Additional evidence such as displacement contours (Childs et al., 2003), interactions between adjacent faults, e.g. cross cutting relationships and upward decreasing fault offsets (**Figure 1.2a**) have been used wherever possible to further constrain fault timing. Upward decreasing fault offsets were used to quality check the interpretation using the amount of offset on each horizon cut by a fault from the 3D fault model. This method was used to compare the amount of offset on one horizon with that on the horizon above at the same point along the fault strike. An increase in the amount of offset between a younger horizon and an older horizon is an indication that the fault was active during the time between the deposition of those two horizons **(Figure 1.2a)**.

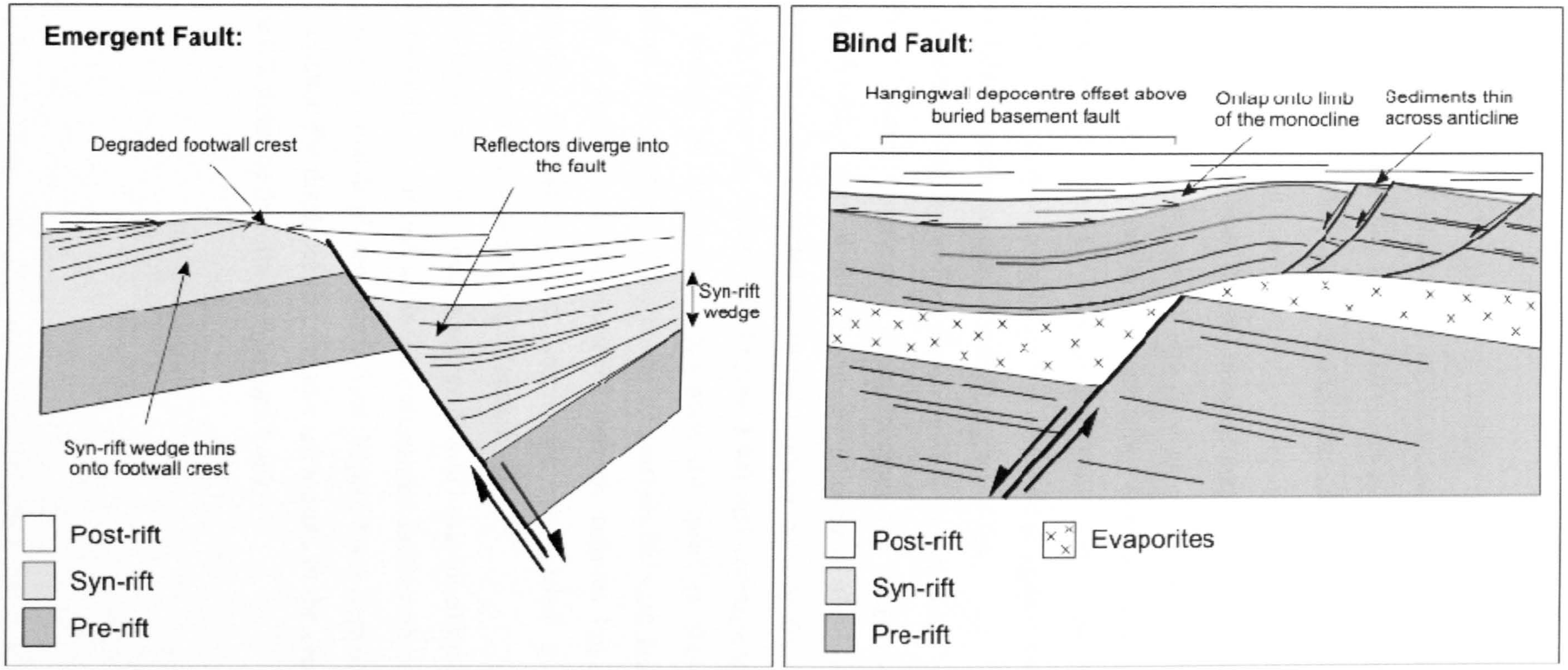

Figure 1.3: (a) The development of syn-rift wedges in the hangingwall of active emergent faults during syn-sedimentary faulting (b) Sedimentary growth patterns associated with the propagation of a buried fault tip.

1.2.2.3 Displacement-length analysis

Fault displacement-length (d-L) profiles were generated by systematically recording the vertical component of displacement (throw) in milliseconds (ms) (TWTT) at intervals of 290m along the length of the fault zone (**Figure 1.2b, c**). An interval spacing of 290m was selected to adequately sample the shortest faults in the survey, whilst ensuring that splays and overlap zones were sufficiently sampled. The seismic data have not been depth-converted therefore true displacements cannot be accurately measured because of uncertainties in measuring the dip of the fault; consequently throw, which is measured along vertical planes perpendicular to the fault, is used as a proxy for displacement. Throw data in ms TWTT was exported from TrapTester at each sampling point and plotted against sampling number, (n), **(Figure 1.2b)** to generate displacement-length profiles.

Displacement-length profiles were recorded for the Åre Coal horizon which is free from footwall erosion and hence footwall and hangingwall cut-offs can be determined with a good deal of accuracy. In contrast, the top of the Åre and Ile formations have been eroded along the footwall crest of the largest displacement faults (e.g. Trestakk, Smørbukk, **Figure 1.4a)** and consequently footwall cut-offs cannot always be determined accurately. d-L profiles show the displacement distribution along individual faults and interactions between faults, and can be used to assess if fault growth has occurred through segment linkage (see chapter 2). Additionally, displacement and length data were used to generate plots of displacement maxima against length (section 4.5.1.1).

In all the data analysis only faults with well constrained tip-lines i.e. where both tips of the fault are constrained in the dataset, and faults with one well-imaged fault tip and well defined displacement maxima **(Figure 1.4a)** were used. In the latter case it was assumed the displacement maxima are located in the centre of the fault, at a distance L/2 from the fault tip line **(Figure 1.4b)**.

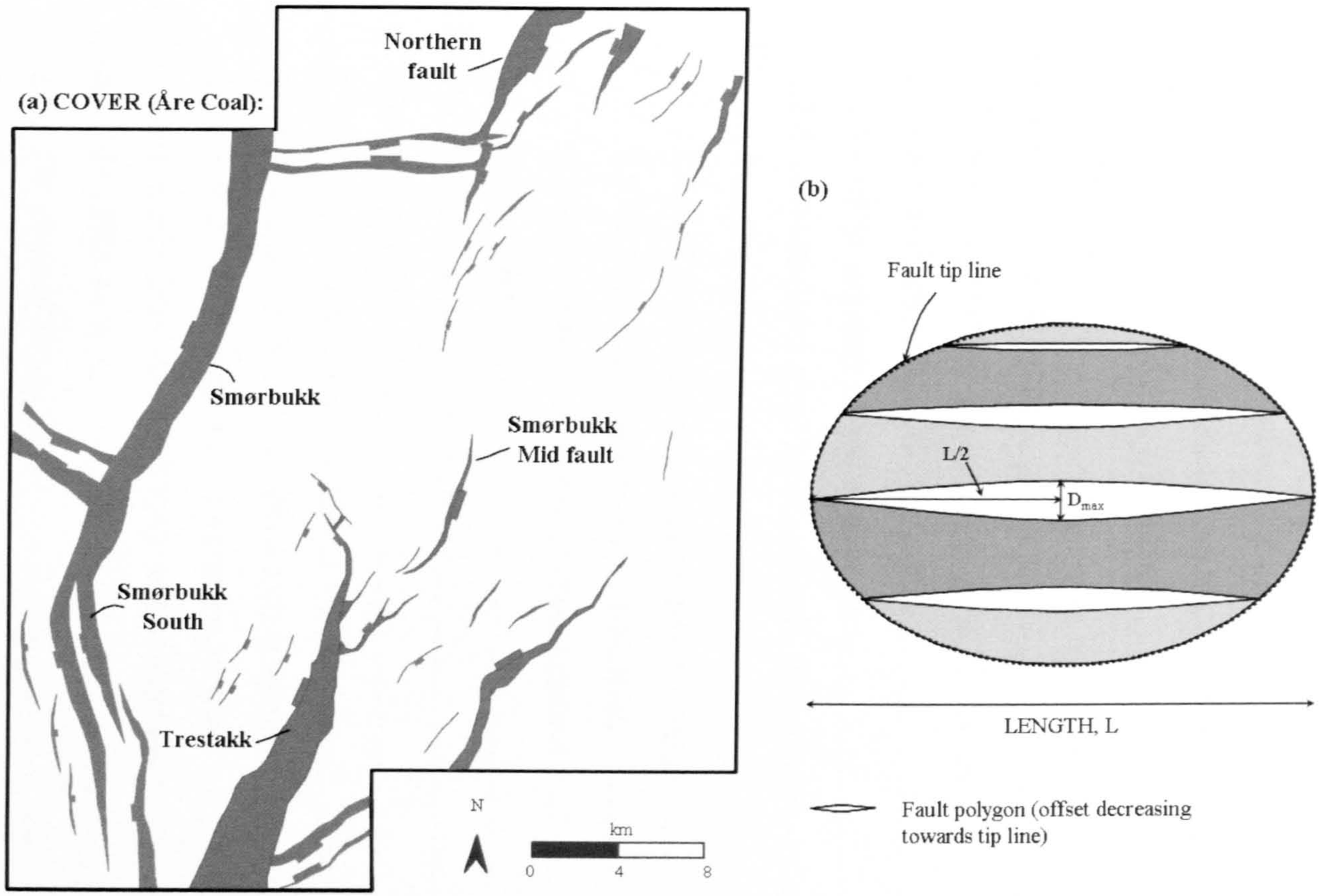

Figure 1.4: Sampling method used for D_{max}-length profiles. (a) Map of cover fault polygons used to generate displacement-length data. (b) Conceptual model of an ideal post-sedimentary blind fault (after Barnett *et al*, 1987). Strike view of the fault surface with throw decreasing towards the tip line. The length, L, of the fault and throw maxima, Dmax, are highlighted. For faults whose full length is not sampled by the survey area e.g. Trestakk fault, we assumed the displacement maxima is located in the centre of the fault, at a distance L/2 from the fault tip line.

CHAPTER 2

2: CONCEPTUAL MODELS OF FAULT GEOMETRY AND GROWTH

2.1 FAULTING

2.1.1 Post-sedimentary normal faults

The idealised geometry of an isolated post-sedimentary normal fault is described by Barnett *et al.* (1987) (**Figure 2.1**). The fault surface is elliptical, with an average aspect ratio of ~2:1 and a sub-horizontal major axis (Walsh and Watterson, 1989). The displacement decreases in all directions from a maximum at the fault centre to zero at the tip line loop, with displacement contours forming concentric ellipses (Barnett *et al.* 1987; **Figure 2.2c**). In 3-D the displacement also decreases away from the fault, normal to the fault surface to form an ellipsoidal tip surface that defines a volume of near-field strain (**Figure 2.1a**). The variation in strain across the fault surface must be accommodated by ductile strain (distortion, dilation) of the hangingwall and footwall rocks and results in reverse drag adjacent to the fault surface (Barnett *et al.* 1987; **Figure 2.1a**).

The displacement gradient - the rate of change in displacement across the fault surface in a particular direction - can be measured vertically or horizontally. In an ideal fault model, where the length of the horizontal axis is roughly twice that of the vertical axis, the horizontal displacement gradient should be roughly half that of the vertical displacement gradient (Walsh & Watterson, 1991). The gradient is influenced by the material properties of the rock volume, particularly the shear modulus, and the size (length) of the fault. The non-linear growth relationship predicted by analysing fault displacement-length populations (Eq. 2.1, see below) implies that larger faults should have higher displacement gradients compared with smaller faults. This contention is supported by values for throw gradients reported in Nicol *et al.* (1996), from faults measured on mining plans and seismic datasets. Coal-field faults, with widths of 0.2-2.6 km have gradients of 0.001 to 0.007 (horizontal) and 0.007 to 0.03 (vertical), whilst seismically imaged faults with widths of 1.3-9.7 km have gradients of 0.007-0.06 (horizontal) and 0.04-0.22 (vertical).

The ideal geometry described above is relevant only for isolated normal faults formed at depth. The majority of faults formed in regions of active rifting interact

with neighbouring faults or the Earth's surface, restricting the vertical or lateral growth of the fault. This results in reduced curvature of the tip line and displacement contours (Nicol *et al.*, 1996), locally increased displacement gradients (Walsh and Watterson, 1989) and changes to the fault surface aspect ratio.

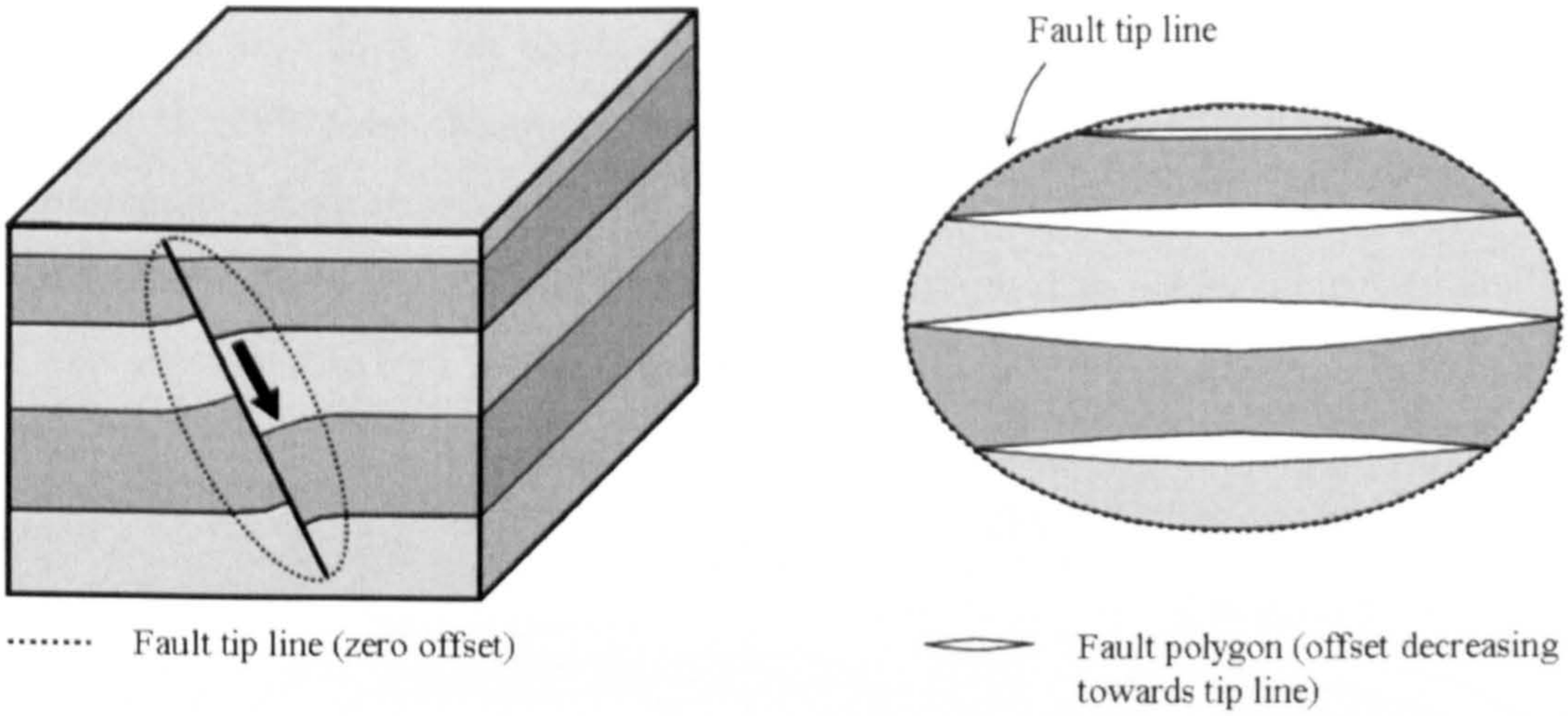

Figure 2.1: Conceptual model of an ideal post-sedimentary blind fault (after Barnett *et al*, 1987). a) Fault in cross section. Fault tips out below the earth surface. Offset decreases towards the tip line and note the reverse drag (footwall uplift; hangingwall rollover) in the wallrocks. b) Strike view of the fault surface. Fault polygons are in white. Offset decreases towards the tip line.

2.1.2 Syn-sedimentary normal faults

Syn-sedimentary normal faults or growth faults are those that were active during the deposition of the sedimentary sequence that they cut and offset (**Figure 2.2**). In contrast to the blind fault described above, syn-sedimentary faults always deform the Earth's surface. The downthrown hangingwall creates an asymmetric depression at the Earth's surface into which growth sediments can be deposited. The footwall is often uplifted and, depending on the overall basin subsidence, the location of the fault within the basin and the eustatic sea level, may be subject to erosion. Provided the sedimentation rate keeps pace with the fault displacement rate, the difference in elevation between the footwall and hangingwall controls the relative sediment thickness across the fault and produces a thicker sedimentary sequence in the hangingwall (**Figure 1.3a**).

Because the stratigraphic sequence is deposited during fault movement, an older stratigraphic sequence is generally subjected to a longer history of fault movement than the younger sequence and the amount of offset on a stratigraphic horizon is the accumulation of all fault movements subsequent to its deposition. This results in increasing offsets with depth, but is different to the variation in offset from a maximum at the fault centre to zero at the tip line as seen in the case of post-sedimentary faults (Barnett *et al.* 1997; **Figure 2.2c**). The displacement gradients on syn-sedimentary faults can be much larger than those of post-sedimentary faults. Nicol *et al.* (1997) report vertical displacement gradients of 0.16 to 1.5 for onshore and offshore syn-sedimentary faults of a range of sizes from 30m to 6km maximum displacement. They suggest that these values are larger than post-sedimentary faults of a comparable size by a factor of at least 2.

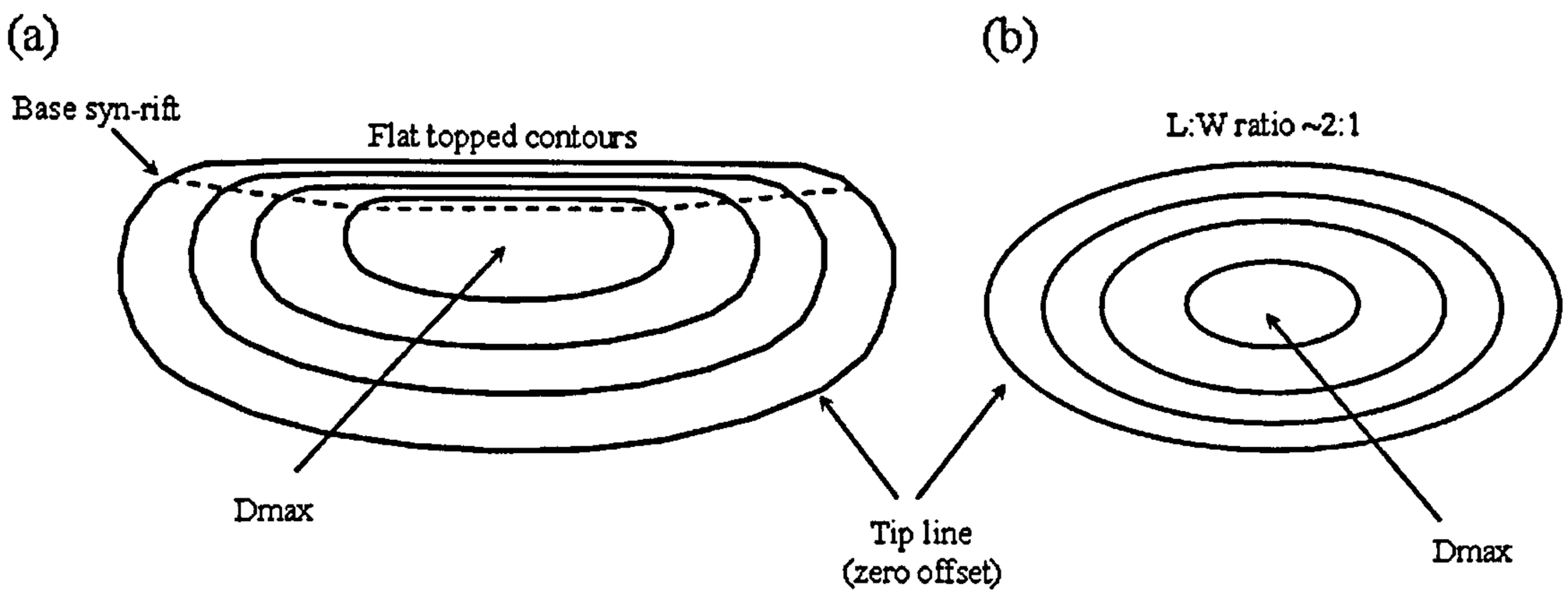

Figure 2.2: Model of syn-sedimentary faulting. a) Displacement contours for an ideal syn-sedimentary fault. Maximum displacement is in the fault centre (D_{max}). The contours are flat topped above the maximum displacement indicating syn-sedimentary fault movement. The dashed line marks the base of the syn-sedimentary part of the fault, recognised by the horizontal contours. Below this line the fault is post-sedimentary and the contours resemble those of a post-sedimentary fault. After Childs et al. (2003). b) Displacement contours for an ideal post-sedimentary blind fault. Contours are concentric ellipses and the fault has an ~2:1 length to width (L:W) ratio. After Barnett et al. (1987).

Interactions between neighbouring faults can cause the tips of syn-sedimentary faults to propagate, remain static or retreat through time. The shapes of the upper tip line and displacement contours on syn-sedimentary faults reflect the high vertical displacement gradients where the fault intersects the Earth's surface and are horizontal rather than curved (**Figure 2.2b, c**; Childs *et al.* 2003). In reality, many faults include a syn-sedimentary section and a post-sedimentary section in which the

fault geometry resembles that of a blind fault. The post-sedimentary section is that part of the fault that cuts the pre-faulting sequence, which was deposited prior to fault initiation. Such faults should show sub-horizontal, closely spaced displacement contours in the younger, syn-kinematic sequence and concentric displacement contours in the pre-faulting sequence (**Figure 2.2b**). Many seismic datasets do not extend to the base of the faults and so the lower, curved tip line and the lower concentric contours of the post-sedimentary section are often absent. In these cases, the pre-faulting sequence is identified by the curved, sub-vertical displacement contours that define the lateral component of fault growth. The point on the fault surface where there is a switch from sub-vertical contours to sub-horizontal contours marks the base of the syn-kinematic sequence (**Figure 2.2b**; Childs et al. 2003). A shift in the lateral position of this point reflects the lateral propagation of the fault tip during syn-sedimentary activity and can be used to identify fault growth or fault retreat.

2.1.3 Fault growth, linkage and fault population evolution

By plotting maximum displacement against width for a variety of faults, Watterson (1986) proposed a fault growth model:

$$D = W^2/P \qquad (2.1)$$

where D is maximum displacement within the fault plane, W is the maximum dimension of the fault surface normal to the slip direction (along-strike length for normal faults) and P is a variable relating to rock properties. The model shows a non-linear relationship, i.e. the displacement increases disproportionately more than the fault width (or length). Conventional models of fault growth based on mathematical analyses of dip-slip fault displacement-length populations suggest that faults grow by the simultaneous accumulation of both displacement and length (Walsh and Watterson, 1988). A more recent model proposed by Walsh *et al.* (2002), which was based upon an analysis of syn-sedimentary growth faults, suggests that the displacement to length ratio of faults progressively increases as they grow. In this model, fault growth is divided into two stages. During the first stage, the fault grows predominantly through the rapid (near-instantaneous on geological timescales) lateral

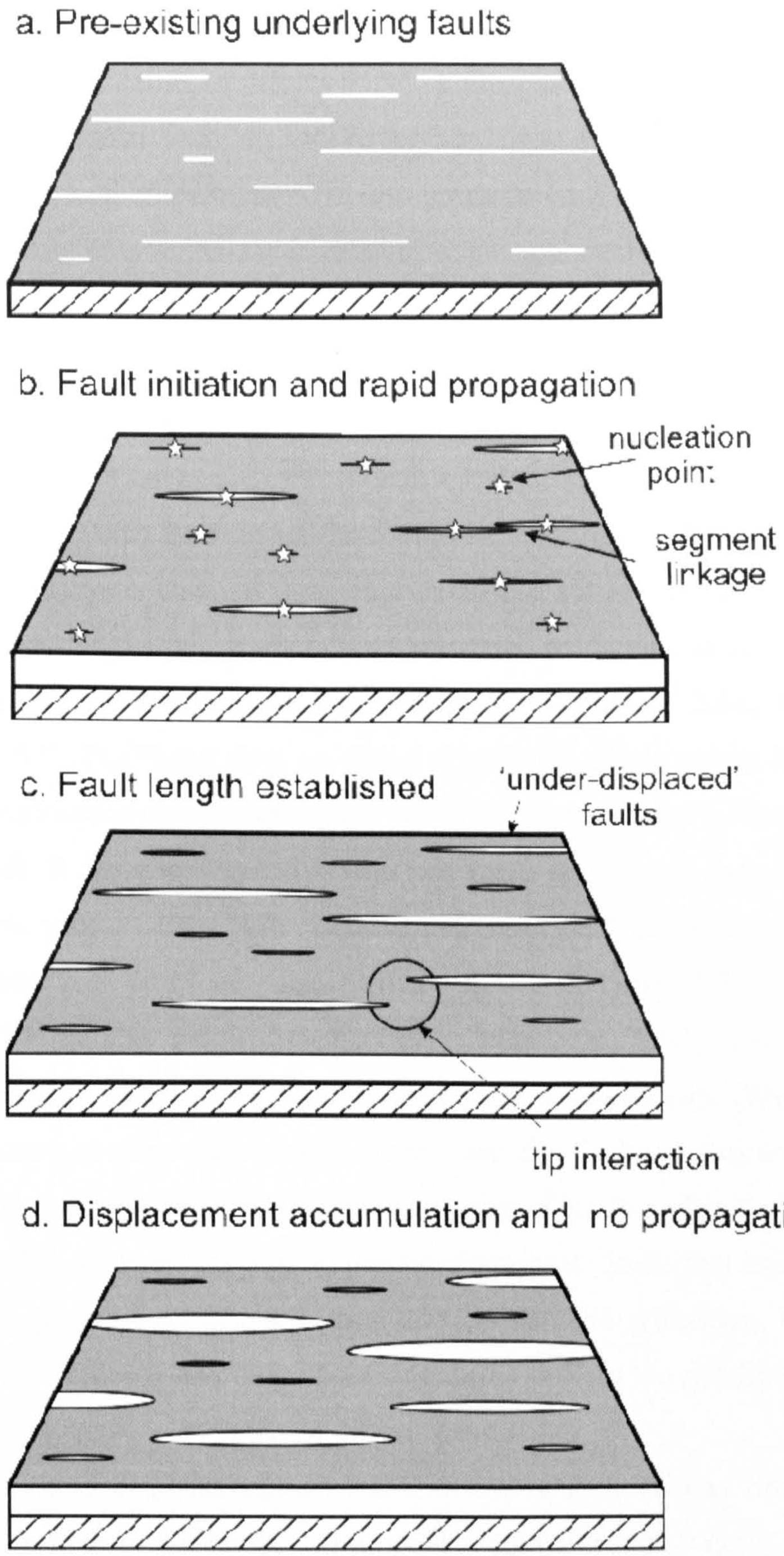

Figure 2.3: Schematic block diagram illustrating the alternative model of fault growth (redrawn from Walsh et al, 2002) using sequential fault maps from the base of a syn-faulting sequence (b–d). (a) The location of pre-existing faults beneath the faulted horizon. (b) Faulting initiates on the horizon above the pre-existing fault system with nucleation close to the centre of each fault. Fault lengths increase rapidly while displacements accrue relatively slowly. (c) Propagation ceases when the faults begin to interact, while displacement continues to accumulate at near constant rates. Fault lengths are inherited from a pre-existing fault system (a). (d) Fault lengths remain fixed while displacements accrue.

propagation of the fault tips until the length of the fault is established (**Figure 2.3b, c**). In the second stage, lateral growth is retarded and the fault continues to grow mainly by the accumulation of displacement (**Figure 2.3d**). This model is consistent with reactivated normal faults in the Timor Sea, in which the fault lengths in the cover sequence are inherited by rapid up-dip propagation from pre-existing basement structures (Walsh *et al.*, 2002). It may also be applicable to many other fault populations which are not necessarily reactivated (Childs *et al.*, 2003). The switch from lateral growth to displacement accumulation could occur because the lateral growth is impeded, as the faults in a population begin to interact at the fault tips (Walsh *et al.*, 2002; Nicol *et al.*, 1996; Walsh and Watterson, 1989).

As faults grow, they interact and link with neighbouring faults. Synthetic faults, which have the same polarity of dip, can overlap and act as a single coherent fault. The displacement on the two faults is accommodated by ductile strain in the form of a relay ramp, which develops in the overlap zone (**Figure 2.4a**; Peacock and Sanderson, 1991). The faults show an abrupt decrease in displacement and increased horizontal displacement gradients within the zone of overlap (Childs *et al.*, 1995; **Figure 2.5d-f**). If the displacement on the two faults is summed and contoured, the resultant displacement pattern will resemble that of an ideal isolated fault and should typically show very little net displacement deficit (**Figure 2.5e**; Peacock and Sanderson, 1991; Walsh and Watterson, 1991; Childs *et al.* 1995). The faults in this case are said to be "soft-linked", at least at the scale of observation (**Figure 2.4a**). It is often the case that some deficit will remain when the displacements are summed in this way. This could be due to a ductile component of strain within the relay zone – for example, due to shear strain accommodated on small faults that exist on a scale too small to be seen on seismic reflection data (Walsh and Watterson, 1991). Faults with aggregate displacements that show significant deficits do not form a coherent structure and may have been active at different times.

With increasing displacement on the faults, a relay ramp can breach (**Figure 2.4b**). Either or both of the faults will propagate across the relay ramp to physically link with the other. Alternatively, a new fault could initiate within the overlap zone and link with both faults (Peacock and Sanderson, 1991; Imber *et al.*, 2004). The faults are then said to be hard-linked. This process of growth by linkage results in an increasing amount of the strain being accommodated on fewer, larger faults as the system evolves (Meyer *et al.*, 2002; Walsh *et al.*, 2003).

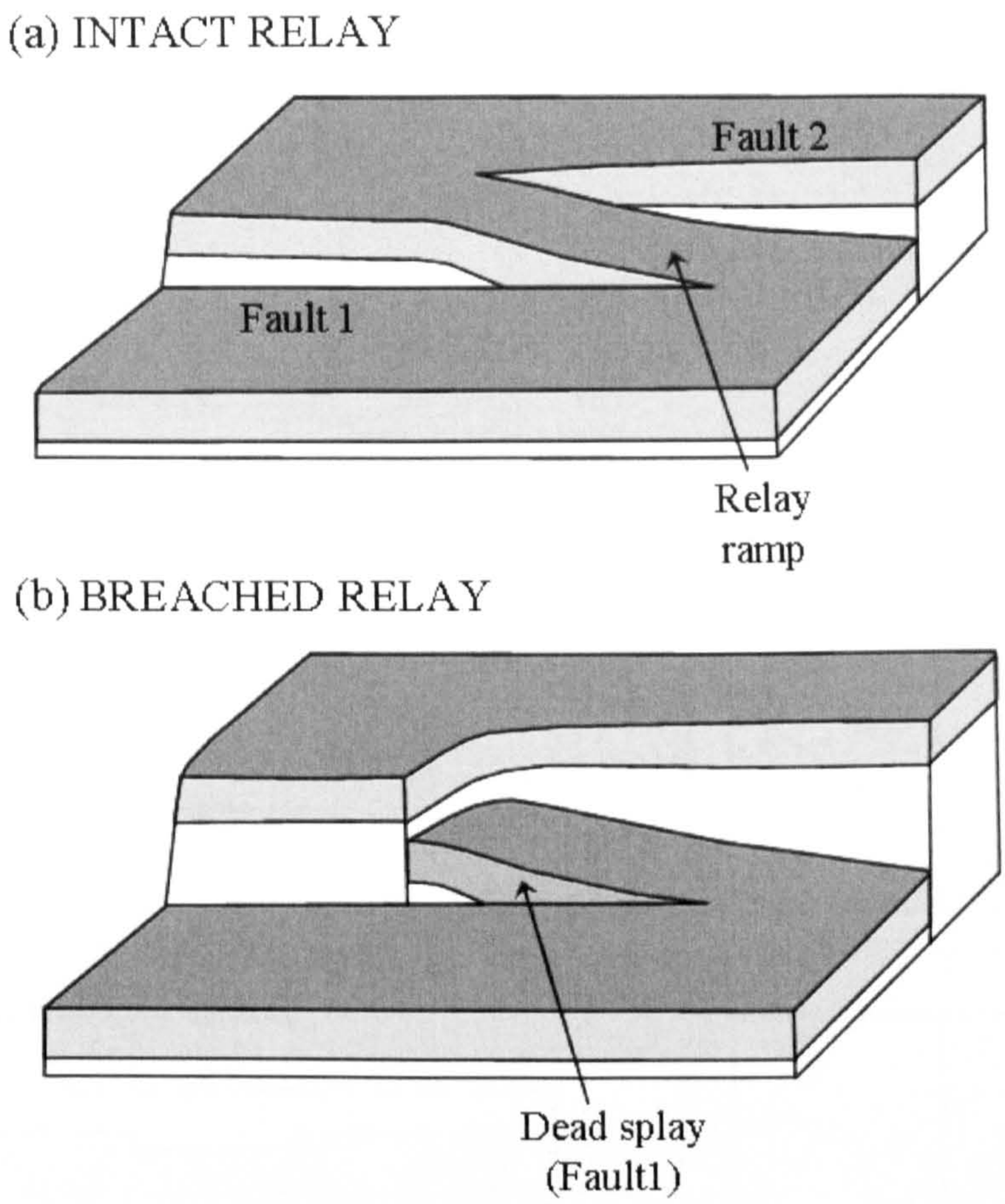

Figure 2.4: The geometry of relay ramps. a) 3D block diagram of an intact relay ramp. b) As displacement increases faults grow and the relay ramp is breached by one or both fault tips or by newly formed faults.

Existing models of fault growth describe the evolution of relay zones through one of two mechanisms (**Figure 2.5a-c**). The conventional and most cited model for relay formation describes the lateral propagation and coincidental overlap of initially kinematically isolated faults (Childs *et al*, 1995; Cartwright *et al*, 1996; **Figure 2.5b**). This model is based on an entirely 2D perspective of fault propagation, in which faults are assumed to propagate within the plane of inspection. An alternative model, based on a 3D perspective of fault growth, describes the bifurcation (or splaying) of an individual kinematically coherent array (Childs *et al*, 1995, 1996b; Huggins et al, 1995, **Figure 2.5c**). The model suggests that local retardation in the propagation of a tip-line due to material anisotropy will lead to out-of-plane propagation of the fault surface and to the generation of overlapping fault segments. At all stages, individual fault segments form a kinematically coherent fault array

even if they appear not to be physically linked (Walsh and Watterson, 1991; Nicol et al, 1996).

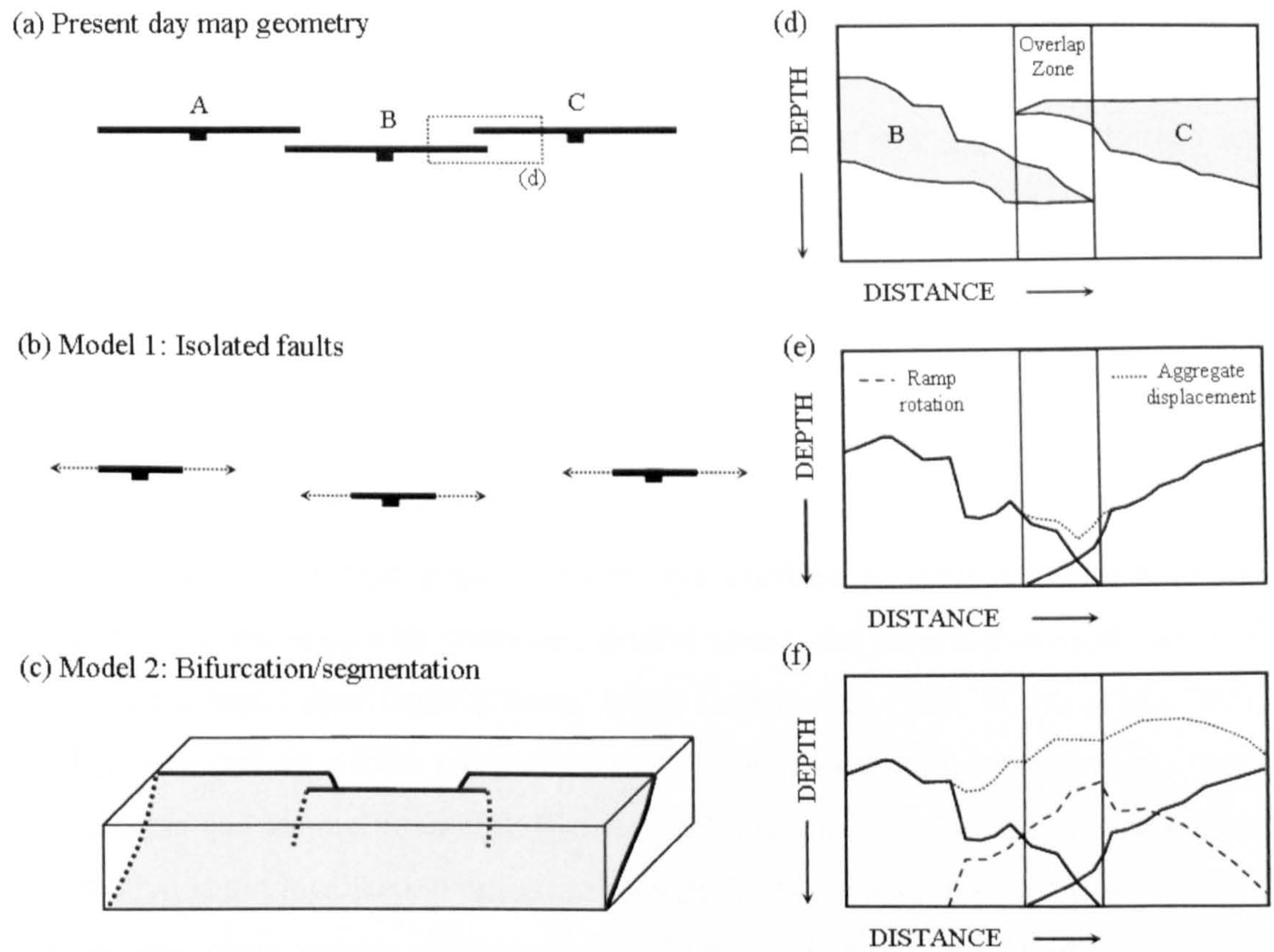

Figure 2.5: Existing models for the growth of faults and relay zones. (a) Present day fault geometry. (b) Conventional model for relay formation due to in plane propagation and coincidental overlap of originally kinematically isolated faults. (c) Alternative model of fault growth due to bifurcation of a kinematically coherent array of unconnected segments. (d) – (e) relationships between fault displacement and length for isolated and bifurcated faults (d and f redrawn from Walsh *et al*, 1996). (d) Horizon separation diagram for faults B and C. (e) Throw profiles for faults (solid lines) and aggregate throws (dotted lines) demonstrating the presence of a displacement minima in the overlap zone of B and C. Throw profile as expected for isolated faults such as Model 1. (f) Throw profiles (solid lines) and aggregate throws (dotted line) including the ramp rotation (dashed lines). The sum of fault throw plus ramp rotation produces a more regular profile than in (e) suggesting that faults are a kinematically coherent structure as in Model 2.

The relationship between fault displacement and length can be used to reconstruct the growth histories of faults and to differentiate between faults that formed due to the 'isolated' or 'bifurcated' models described above (**Figure 2.5e, f**). In the isolated model displacement-length measurements are used to locate the sites of fault linkage on previously isolated faults where the point of linkage is represented by a displacement minima (e.g. Peacock & Sanderson, 1991; Trudgill & Cartwright, 1994; Cartwright *et al*, 1995). Figure 2.5e shows that aggregate displacement

variations for overlapping isolated fault segments have distinct displacement minima centred upon the relay zone. Walsh *et al* (1996) presented a new interpretation of displacement-length analyses in which they suggested that ductile strains, such as sub-resolution faulting and plastic deformation processes, should be taken into account in the analysis of fault displacements. They demonstrated that bed rotation and minor faulting together largely compensate for the low aggregate throws on overlapping faults resulting in a more regular aggregate profile (**Figure 2.5f**). The displacement variations on faults can thus be used to distinguish between the two models of fault growth; isolated and bifurcated.

2.1.4 Models of strain localisation

The evolution of fault populations is characterised by early generation of the main fault pattern and, with continued displacement, the progressive localisation of strain onto a few, larger faults (Cowie, 1998; Gupta *et al*, 1998; Walsh *et al*, 2003). Analogue modelling studies (Ackermann et al, 2001; Mansfied & Cartwright, 2001) and numeric and geometric models (Cowie, 1998; Gupta et al, 1998) have shown that progressive strain localisation onto increasingly longer and simpler fault systems is a fundamental characteristic of the spatial and temporal evolution of fault systems. In Cowie's (1998) model, the spatial and temporal evolution of faults is explained using a stress feedback mechanism in which the seismic rupture of a fault perturbs the surrounding stress field, advancing the occurrence of future earthquakes on optimally oriented faults, while relaxing stress levels on others. In the model, a positive feedback is set up so some faults develop higher displacement rates and grow more rapidly whilst others experience reduced rates or become inactive. This mechanism drives rapid strain localisation and the formation of major through-going faults whilst faults that are optimally positioned in the overall fault population experience enhanced displacement rates.

Walsh *et al* (2003) results support earlier work on strain localisation. They used seismic sections from the Inner Moray Firth to demonstrate that a clear positive relationship exists between the longevity of fault growth and fault displacement. Given that larger faults are also longer in length, fault maps show that early phases of fault growth are characterised by many small faults, whereas later stages of rifting are dominated by larger faults.

2.1.5 Reactivation

Reactivation is defined as *"the accommodation of geologically separable displacement events on pre-existing structures"* (Holdsworth *et al.* 1997). The reactivation of pre-existing faults and fabrics in the continental crust is known to influence the locations and structural architectures of rift basins. Structures such as faults and shear zones are thought to be long-lived zones of weakness that can reactivate repeatedly and may do so in preference to the formation of new faults (Holdsworth *et al.* 1997). Geometric reactivation describes a situation in which a deformation inherits the location or geometry of a pre-existing structure, but with a different sense of movement. During kinematic reactivation the sense of displacement is similar between successive reactivation events (Holdsworth *et al.* 1997). Pre-existing fabrics can be discrete or pervasive (Morley, 1999). Discrete fabrics include faults, shear zones or major rheological or compositional boundaries. Pervasive fabrics are present throughout a large rock volume and induce a marked strength anisotropy. These include metamorphic fabrics such as cleavage, schistosity and gneissic foliation (Morley, 1999). Pervasive fabrics tend to influence the majority of the faults within a rift whereas discrete fabrics tend to influence more isolated structures to produce faults which may be atypical in terms of their location, geometry or orientation.

Fault orientations can directly reflect the orientation of the regional stress field, with localised re-orientation of structures due to the influence of pre-existing fabrics within the rift. Often, faults are either parallel to the basement fabric or perpendicular to the regional extension direction, or some combination of these two end-member types. Natural rifts commonly develop where there are a variety of pre-existing fabric orientations, locations and types, some of which may be exploited whilst others are ignored. It is often difficult to confidently identify reactivation, particularly in offshore settings where the basement or deep structure may be below the range of the seismic data, whilst the relatively poor resolution of the data prevents the use of traditional outcrop-scale identification criteria. Often geometric similarity – in which offshore structures have the same orientation as basement faults and shear zones exposed onshore – is relied upon to infer reactivation, but this is not always a reliable indicator (Holdsworth *et al.* 1997).

2.2 SALT TECTONICS

The deformation of buried salt accumulation is known to play a significant role in controlling the spatial and temporal distribution of sedimentary facies at the surface, and the generation, migration and entrapment of hydrocarbons. It is therefore vital to study the evolution of such systems in order to understand their impact on the development of salt-related hydrocarbon bearing provinces around the world.

Understanding of the geometry and evolution of salt bodies and associated strata has advanced in the last few decades with advances in seismic imaging, experimental and numerical modelling, and structural restoration techniques. The main interest in salt tectonics stems from the oil and gas industry because many of the world's largest hydrocarbon provinces lie in salt basins (e.g. Atlantic margins of Brazil and West Africa, the Gulf of Mexico and the Middle East; **Figure 2.6**). The presence of salt in a basin can create structural traps, influence reservoir distribution and act as a seal to fluid migration, as well as effectively conducting heat to elevate the thermal maturation of nearby source rocks, therefore affecting almost every aspect of the hydrocarbon system. Salt also produces some of the most complex and fascinating deformational features on the Earth's surface, e.g. La Popa Basin, onshore NE Mexico (**Figure 2.6**), attracting the attention of structural geologists, stratigraphers and petroleum geologists alike.

The mechanics of salt flow, the process of diapir growth and the interaction of these processes with regional deformation produce a variety of salt structures (**Figure 2.7**). It is the unique deformation style in salt basins which make salt tectonics an important component in the analysis of sedimentary basins (Hudec & Jackson, 2007).

2.2.1 What is salt?

In the context of this work, and in line with most salt tectonics literature, the term 'salt' refers to all salt bodies composed primarily of halite (NaCl) that may also include varying, but subordinate amounts of other evaporites, such as anhydrites, gypsum and potassium and magnesium salts, and non-evaporite rocks (Warren, 1999).

Evaporites are precipitated from saturated surface or near-surface brines during intervals driven by solar evaporation. Typically they are deposited in restricted basins, where the outflow of water by evaporation exceeds inflow (Warren, 1999).

Salt basins occur primarily in rift basins and along passive margins, as well as in their deformed counterparts such as the Alpine/Himalayan system. The history of rift basin formation is often conducive to evaporite deposition. As a result of high heat flow and regional uplift during extension of the continental crust, graben are commonly initially filled with non-marine clastics. Subsidence during post-rift thermal and loading-related subsidence leads to marine incursion. It is during the transition from non-marine to marine environments that evaporites are formed, if the climatic conditions are appropriate (Rowan, 2006). Typically, this is followed by continued subsidence leading to true marine conditions and the cessation of evaporite deposition.

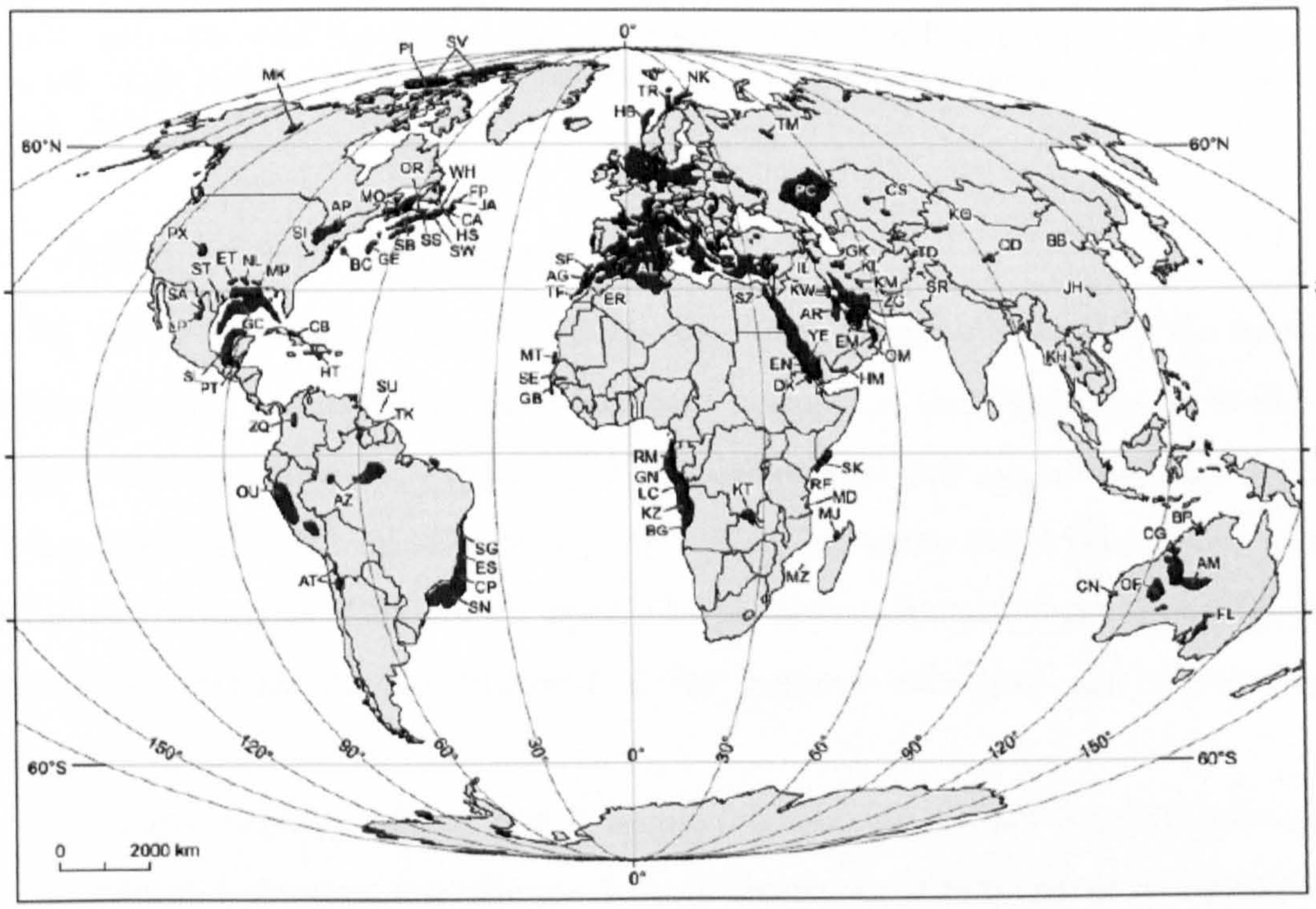

Figure 2.6: The global distribution of basins containing salt structures (black areas). Basins containing undeformed salt are omitted. Note, HB = Haltenbanken, offshore mid-Norway, GC = Gulf of Mexico, CP = Campos, LC = Lower Congo and LP = La Popa (from Hudec & Jackson, 2007).

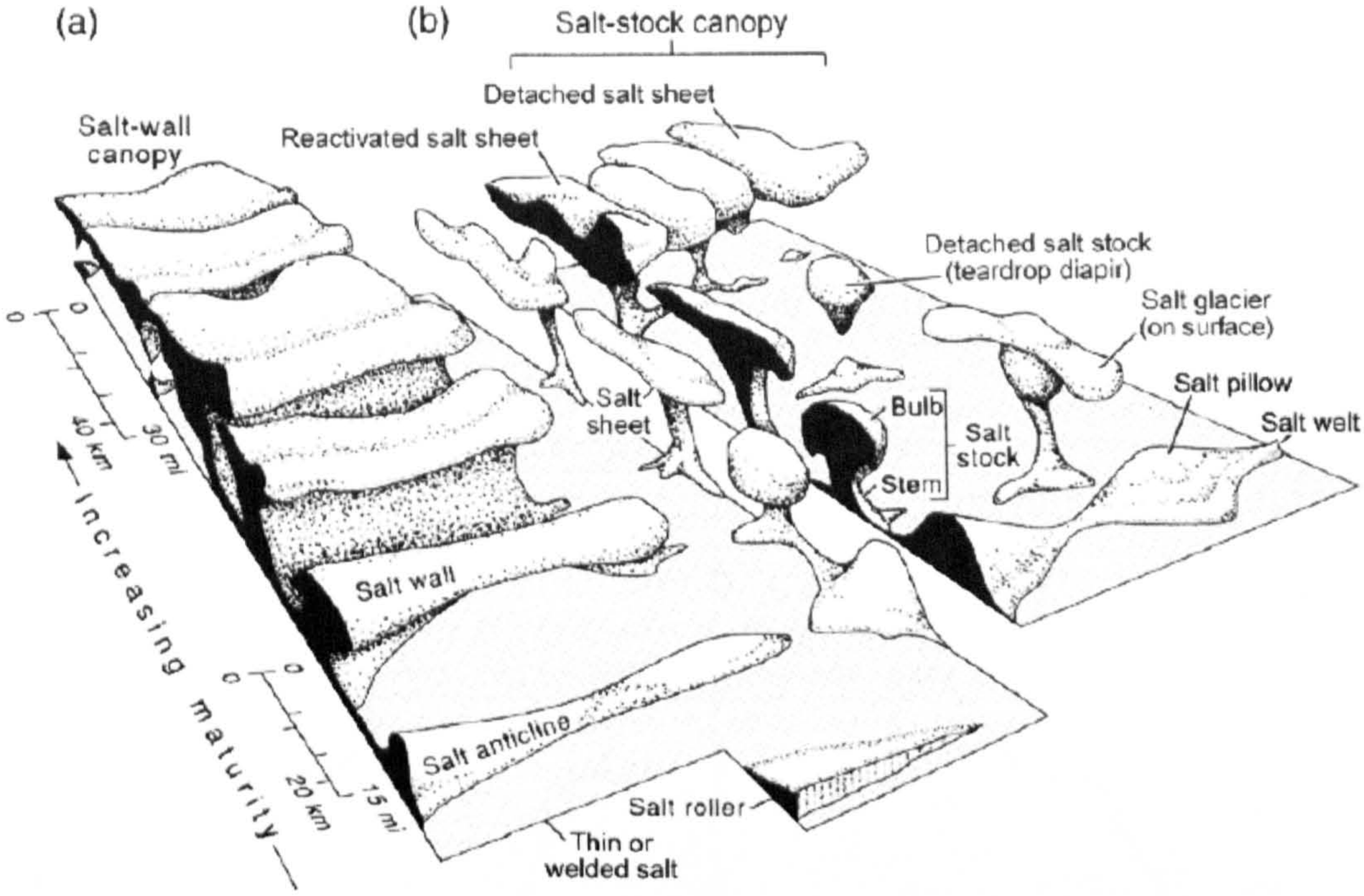

Figure 2.7: Block diagram showing the schematic shapes of salt structures. Structural maturity increases with increasing size and coalescence of salt structures. (a) Elongate structures rising from line sources, (b) structures rising from point sources. From Hudec & Jackson, 2007

2.2.2 Mechanics of salt deformation

The ability of a salt horizon to creep and form diapirs depends on the creep mobility which is controlled by the evaporate composition (with mobility increasing in sequence from anhydrite, gypsum, halite, to potassium and magnesium salts) and the percentage of mechanically competent materials within the interval. Salt has mechanical properties different to most clastic and carbonate rocks resulting in profound differences in deformational styles between salt- and non-salt-bearing basins.

The unique rheology of salt, which is much weaker than other lithologies under both tension and compression (**Figure 2.8**), is one factor which makes it inherently unstable under a wide variety of conditions. Under high strain rates, salt fractures like most other rocks and yet under most geological conditions a majority of evaporites deform viscoelastically (Weijermars *et al*, 1993). The relatively high relaxation rates of evaporites mean that the elastic component of geological deformation can be ignored and the strain treated as purely viscous (Hudec *et al*, 2007). As a result evaporites typically are able flow exhibiting negligible yield

strengths in the sub-surface and surface and consequently salt bodies are much weaker (**Figure 2.9**) and therefore more easily deformed than other rocks. At the surface, flow rates up to 15 metres per year have been recorded in exposed diapirs in Iran (Talbot & Aftabi, 2004).

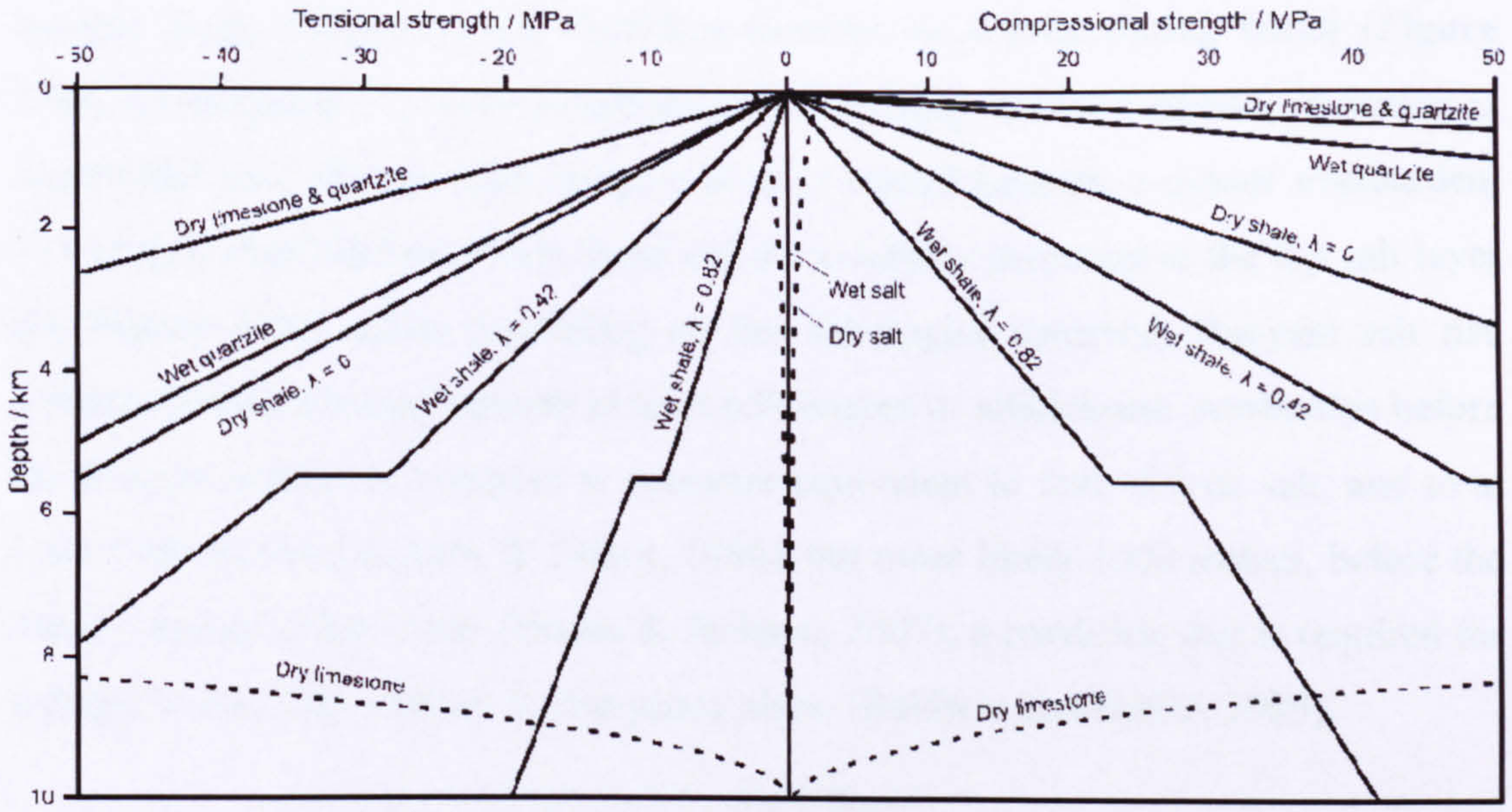

Figure 2.8: Comparison of creep and frictional strengths of various rock types in both tension and compression (Redrawn from Jackson & Vendeville, 1994). Note that wet salt effectively falls on the axis of zero strength.

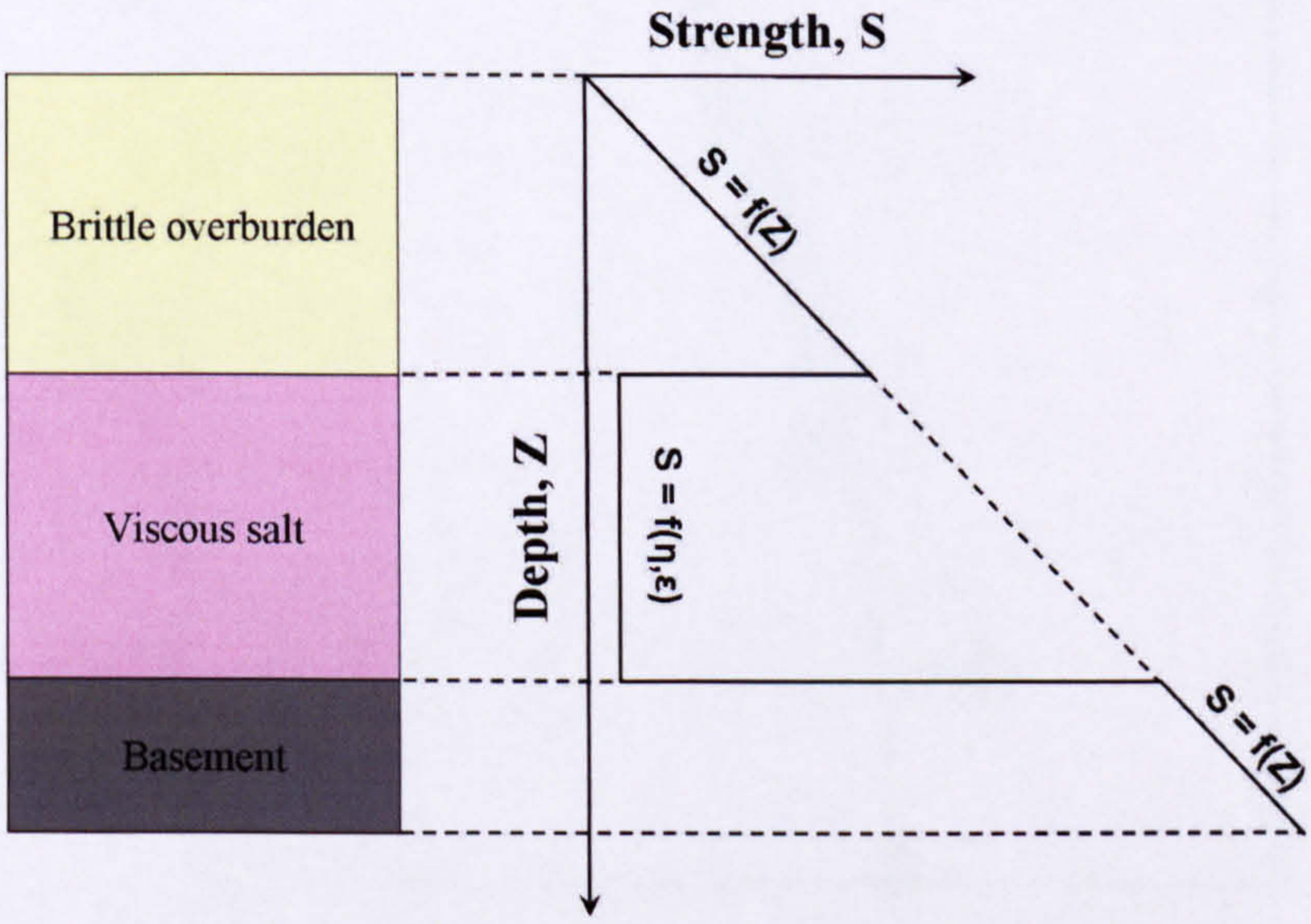

Figure 2.9: Simple 3-layer model of the crust with a weak, constant-strength salt layer between two brittle layers whose strength increases with depth. The strength of the salt layer is independent of depth, but is instead dependent on, ε = Strain rate and η = viscosity (redrawn from Vendeville and Jackson, 1993).

A second important aspect of salt is that its density is effectively invariant with depth, i.e. it shows no affect of compaction with increasing depth of burial. In fact the density typically decreases slightly due to the effect of rising temperature (**Figure 2.10**). Slightly impure rock salt (ρ = 2200kg/m^3) is less dense than most carbonates and moderately to fully compacted siliciclastic rocks (Warren, 1999), both of which become more compacted and therefore increase in density during burial (**Figure 2.10**). Consequently in most salt-bearing sedimentary basins a density inversion is established and salt becomes buoyant as it is buried beneath a denser overburden. The critical depth below which there will be a density inversion at the top salt layer (D, **Figure 2.10**) varies depending on the lithologies involved. Buoyant salt rise typically requires burial beneath at least 650 metres of siliciclastic overburden before the deepest sediments compact to densities equivalent to that of rock salt, and to at least 1000 metres (Jackson & Talbot, 1986), but more likely 1600 metres, before the density exceeds that of salt (Hudec & Jackson, 2007), a condition that is required for a diapir to reach the surface by buoyancy alone (Baldwin and Butler, 1985).

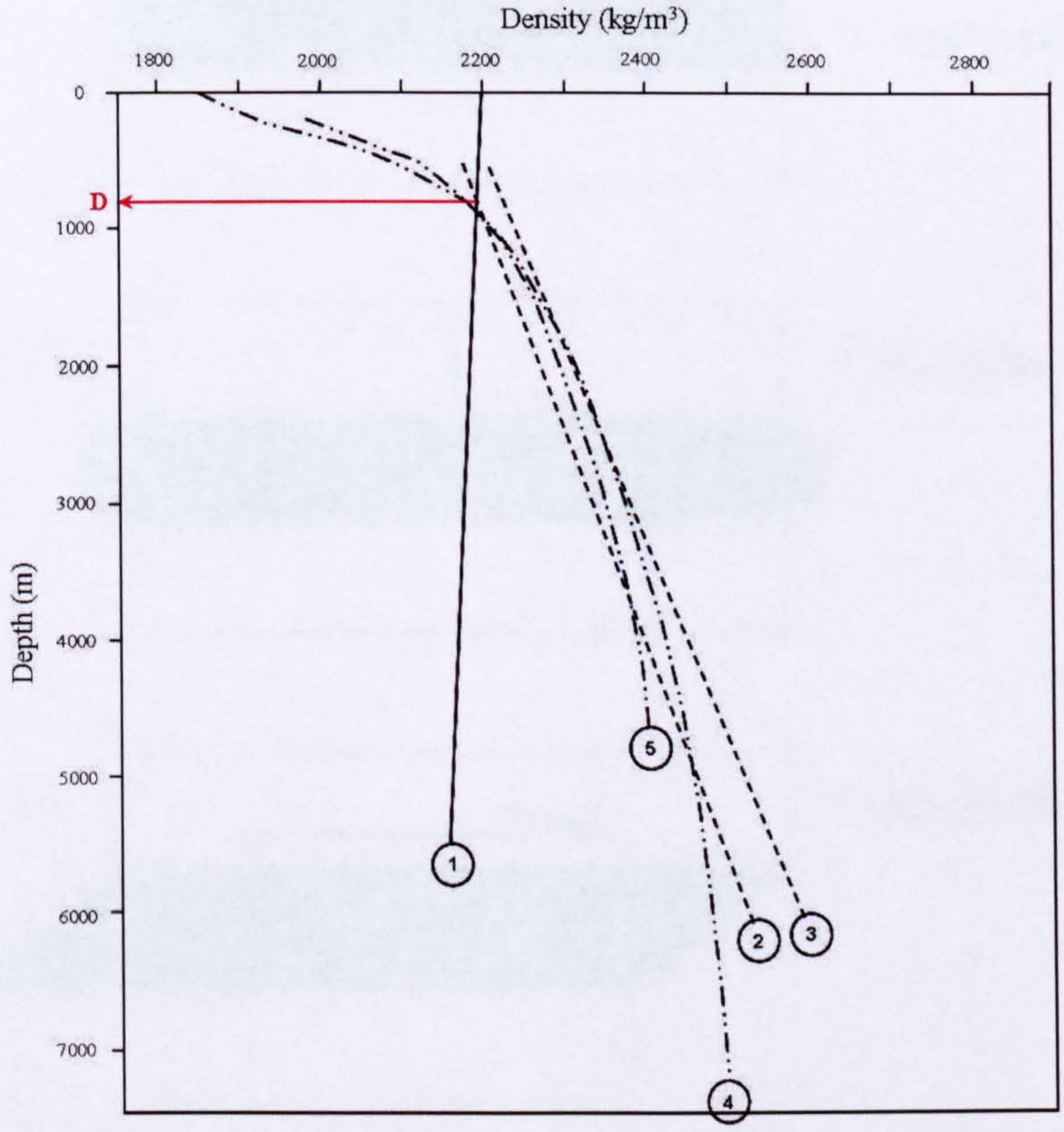

Figure 2.10: Density vs. Depth curves for various lithologies (1 = salt, 2 = dry sand, 3 = wet sand, 4 = wet shale, 5 = dry shale). The density of salt remains approximately constant with depth, whereas sand and shale increase in density during burial so that buried salt is less dense than its overburden at a critical point (D), (Modified from Jackson and Vendeville, 1986).

Salt which exists at any depth below the critical loading thickness (i.e. >650 m) is gravitationally unstable and is liable to lose potential energy by overturning (Hudec & Jackson, 2007). Once the system is destabilised, salt flows by a combination of Poiseuille flow due to overburden loading (**Figure 2.11b**) and Couette flow due to overburden translation (**Figure 2.11c**). Importantly, the presence of a weak, viscous salt layer between brittle overburden and basement (**Figure 2.9**), can act as an excellent detachment surface onto which faults cutting the overburden sole out, decoupling strain between basement and cover during periods of tectonism further enabling salt to flow in response to loading or unloading. It is the unique mechanical properties of salt that make salt-related basins unstable and therefore much more likely to deform when compared to basins that form in the absence of salt.

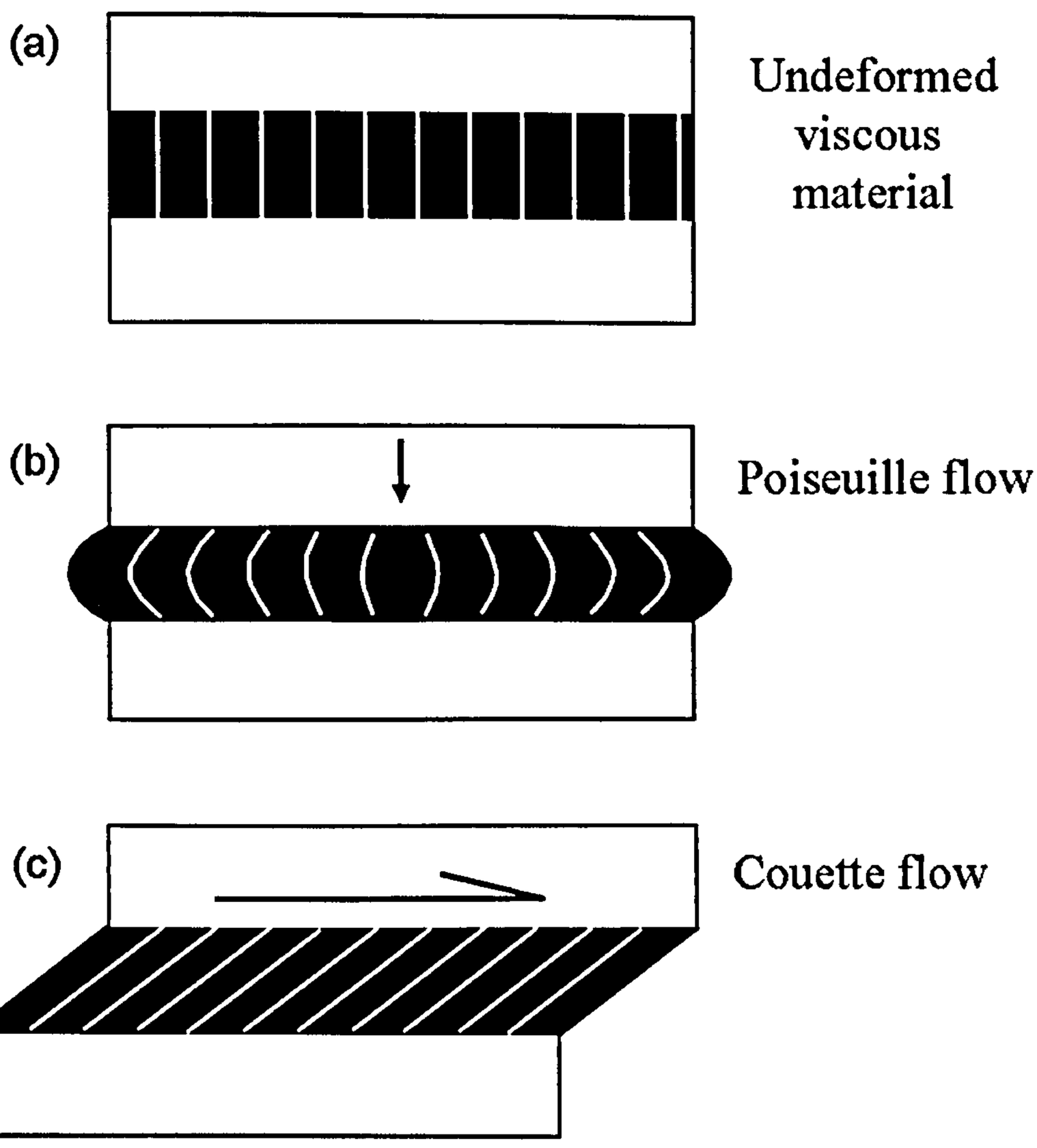

Figure 2.11: Types of viscous flow of an undeformed viscous material (a): (b) Poiseuille flow in which overburden pressure drives lateral flow in an unconfined layer. Velocities are slower at the boundaries because of viscous drag; and (c) Viscous material is sheared due to lateral translation of the overburden during Couette flow (redrawn from Rowan, 2006)

2.2.3 A brief history of salt tectonics

Salt tectonics refers to the study of deformation involving the flow of salt which may involve regional extension and shortening or purely gravity-driven deformation and differential loading in the absence of tectonic forces. A vast quantity of literature on salt tectonics exists, dating as far back as the 1850's, so that a review of all these contributions is beyond the scope of the present work. This review concentrates on those papers that present major conceptual breakthroughs.

Understanding of salt tectonics has changed dramatically over the last 150 years, initiated by the search for a general hypothesis for salt diapirism following the first recorded discovery of a salt dome in the literature (Ville, 1856). Nettleton (1934) investigated vthe fluid mechanics of salt domes by assuming that salt and its overburden could be represented by two viscous fluids of negligible strength (oil and syrup). He demonstrated that gravity alone could generate diapirs and a surrounding peripheral sink from an undeformed source layer. Nettleton's basic assumption that the mechanical properties of salt and sediment alone could control diapirism prevailed for the next 55 years and his modelling approach was widely applied (e.g. Ramberg, 1967, 1981). These models predict that once initiated, diapirs rise continuously until the salt source is exhausted, which does not account for the recognition that many diapirs have, in reality, developed episodically during short pulses separated by long periods of quiescence (Jackson & Vendeville, 1994).

Attempts to model salt deformation changed in the 1980's when the overburden was modelled as a strong, brittle material, more in line with its recognised mechanical behaviour. The modelling approach of using dry sand over a viscous fluid (Vendeville *et al*, 1987; Vendeville & Cobbold, 1988) focussed on extension above a salt substratum and produced far more realistic salt structures than previously accomplished (Jackson, 1995). As a result, the importance of roof strength as a control on diapir growth was recognised. Hence, the position and shape of viscous salt bodies was seen to depend also on the brittle, mechanically competent deformed overburden.

The most significant breakthrough in the advent of these models was the recognition that stresses generated by differential loading were the dominant forces driving salt flow, resulting in a range of structural styles. Furthermore, upwelling salt structures were shown to be the response of salt flow to extension, rather than the

cause of extension above them (Cobbold, 1988). These results fundamentally changed understanding of salt deformation, demonstrating salt's passive role in reacting to, rather than being the cause of deformation in basins (Vendeville and Jackson, 1992a & b).

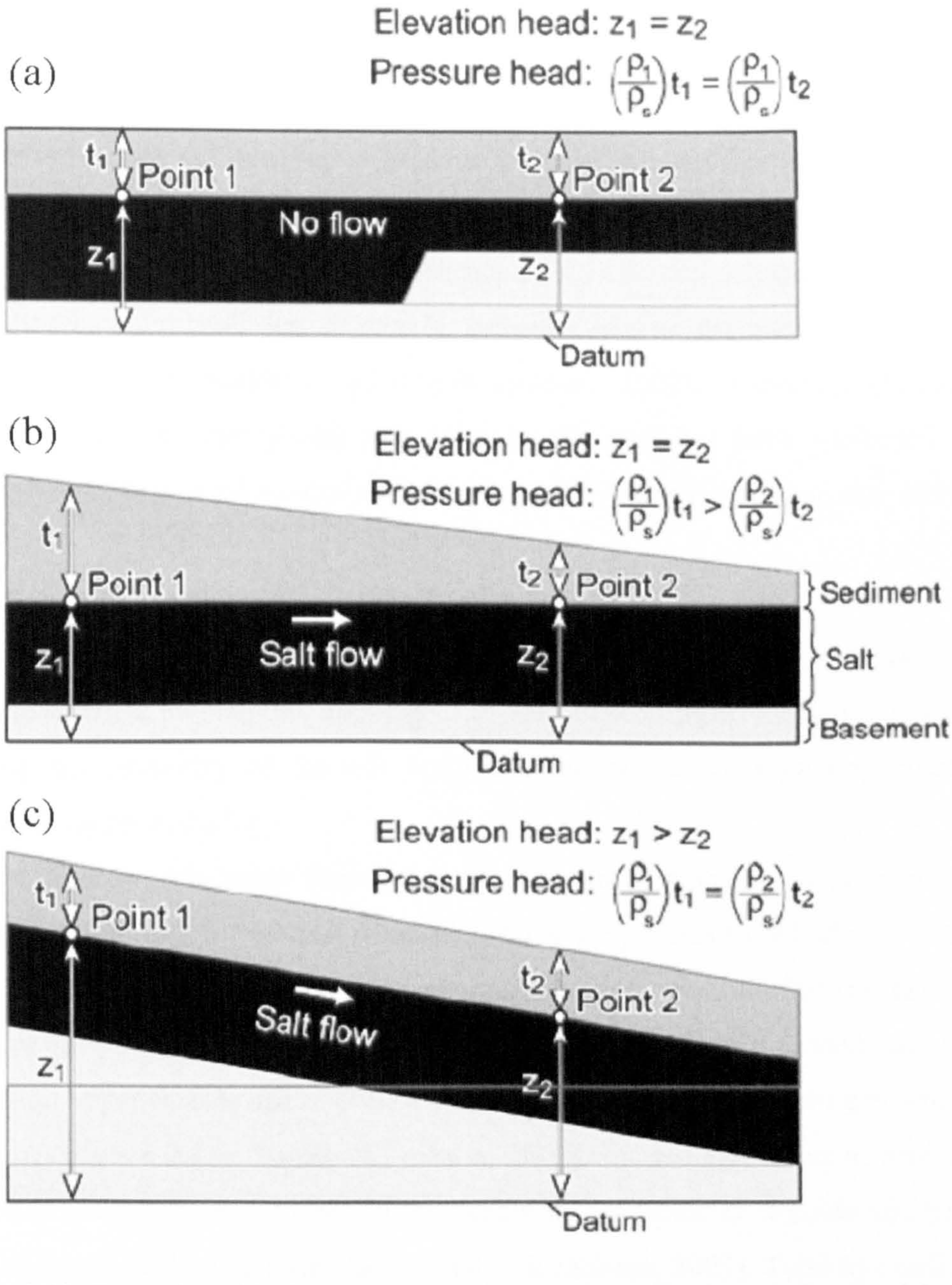

Figure 2.12: Examples of hydraulic-head gradient analysis in salt tectonics (modified from Hudec & Jackson, 2007). (a) A uniform overburden thickness above a flat lying salt layer produces no hydraulic head gradient, even though the salt thickness varies, thus salt remains at rest. (b) A laterally varying overburden thickness above a tabular salt layer produces a pressure gradient from point 1 to point 2 but no elevation head gradient. Salt will flow from left to right along the pressure gradient. (c) A uniform overburden thickness above an inclined, tabular salt layer produces an elevation head gradient from Point 1 to Point 2 but no pressure head gradient. Salt will flow from left to right down the elevation head gradient.

2.2.4 Salt mobility and fault growth: Why does salt start to move?

A number of mechanisms that account for the structural evolution of salt basins have been described in the literature including: erosional unloading; sedimentary differential loading; gravity-gliding and spreading; sub-salt deformation and thin-skinned extension; and tectonic shortening (Jackson & Vendeville, 1994). The majority of papers agree that differential loading is the dominant driving force for salt flow (Jackson & Vendeville, 1994; Jackson, 1995; Hudec & Jackson, 2007). If driving forces are sufficient to overcome the two principal resistant forces which oppose the flow of salt - strength of the overburden and boundary friction within the salt layer - then salt will flow. In the absence of such forces, salt can remain static in the subsurface for millions of year's subject only to groundwater dissolution, diagenesis and metamorphism (Hudec & Jackson, 2007). Bouyancy, although an important factor in maintaining salt rise after the roof has been weakened, is no longer thought to control the initiation of diapirism (Vendeville & Jackson, 1992a).

2.2.4.1 Driving force - differential loading

Salt flow is typically thought to be driven by two forces: gravitational loading and displacement loading, the importance of each depending on the depth of burial of the salt, the geometry of the salt body and the geological boundary conditions (Hudec & Jackson, 2007).

The flow of salt away from areas of high gravitational load is termed 'salt withdrawal', or 'salt expulsion' which describes the process by which salt is forced from its source layer into a diapir. It is common to describe fluid flow in response to pressure gradients. This concept is incorrect, since uniformly loaded salt with a horizontal upper surface does not flow even though a vertical pressure gradient exists within it (**Figure 2.12c**; Hudec & Jackson, 2007). Instead salt flows in response to hydraulic head-gradients, a concept applicable to salt tectonics because salt behaves as a fluid over geological time scales (Hudec & Jackson, 2007). Total hydraulic head is a function of two components: elevation head - the elevation of a particle of fluid above an arbitrary horizontal datum, and pressure head - the height of a fluid column that could be supported by the pressure exerted by the overlying rock (**Figure 2.12**). Head-gradients can be used to more accurately predict salt flow in response to gravitational loading.

Displacement loading refers to the forced displacement of one boundary of a rock body relative to the other (Suppe, 1985). In salt tectonics, this type of loading occurs when the flanks of a salt body move towards or away from one another during extension or shortening (**Figure 2.13**), a process common in basins with pre-existing salt structures (Hudec & Jackson, 2007). Displacement loading causes salt movement in response to extension or contraction of the salt walls.

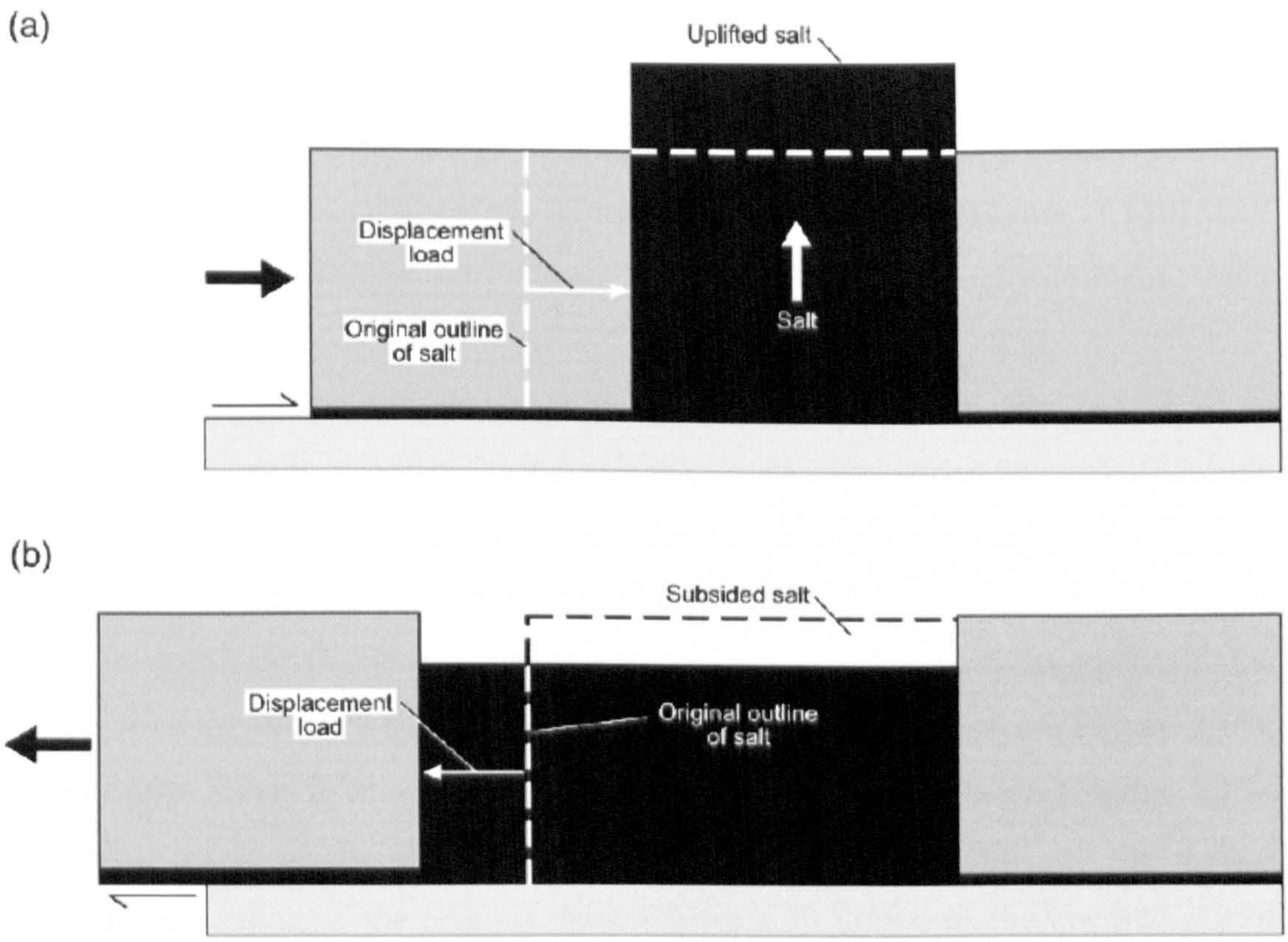

Figure 2.13: The effects of displacement loading on pre-existing salt structures. (a) Salt is horizontally loaded during shortening, by inward movement of one or both walls. The horizontal displacement load overcomes the vertical gravitational load forcing the salt to rise. In a natural example the top of the salt structure would flow out over the sediment surface rather than form a vertical column. (b) During extension, the salt is unloaded horizontally by outward movement of one or both walls. The vertical gravitational load then exceeds the horizontal displacement load so the salt subsides.

2.2.4.2 Tectonic differential loading

Until the 1990's the role of thin-skinned extension in initiating and promoting the diapiric rise of salt was generally ignored, with graben structures associated with diapirs typically being attributed to intrusion, withdrawal or dissolution of salt

diapirs. This view was only questioned when the first computerised structural restorations from the Gulf of Mexico were published (Worrall & Snelson, 1989).

Physical modelling by Vendeville & Jackson (1992a) demonstrated that diapirs in many of the world's salt provinces were initially triggered by regional extension regardless of the thickness, lithology and density of the overburden. By locally thinning and weakening the suprasalt overburden, extensional faulting allowed pressurised salt to pierce the overburden and to subsequently rise by downbuilding (Peripheral sink, I: **Figure 2.14a)** until depletion of the salt source was complete. This phase is termed 'reactive diapirism' because diapir rise stops whenever regional extension ceases; thus the salt is reacting to and is controlled by extension. Fault patterns above reactive diapirs are approximately symmetric **(Figure 2.14b)**. Salt rollers are less symmetric salt pillows associated with a single dominant fault **(Figure 2.14c)**.

Regional extension can also eventually slow the rise of diapirs and, in some cases, causes them to subside. During extension, salt walls widen between diverging blocks of overburden placing increasing demand on salt supply. As the source layer thins due to extension, the supply rate diminishes and may eventually cause the diapir to withdraw (Vendeville & Jackson, 1992b). Sedimentary deposits fill the space above the diapir's subsiding flanks or above its sagging crest **(Figure 2.15)**. Diapir crests invert from a topographic bulge to a subsiding graben **(Figure 2.15)**. Adjoining horns of the diapir project into each bounding fault of the graben recording the extent of the original crest. Figure 2.20 illustrates the rise and fall of diapirs during sedimentation.

Tectonic differential loading by extension initiates diapirism more effectively than sedimentary differential loading, providing the only mechanism for salt to pierce thick or thin overburdens of initially uniform thickness. Jackson & Vendeville (1994) surveyed 18 of the world's salt basins recording a close and consistent temporal link between onset of diapirism and regional extension, with diapirism initiating soon after salt deposition, or significantly delayed until the basin extended.

Most diapir provinces around the world initiated during thick- or thin-skinned extensional tectonics (Jackson & Vendeville, 1994), suggesting that regional extension is the trigger for salt diapirism. Many faults adjoin the crests and/or flanks of diapirs, reflecting their early extensional histories **(Figure 2.13a, b)**.

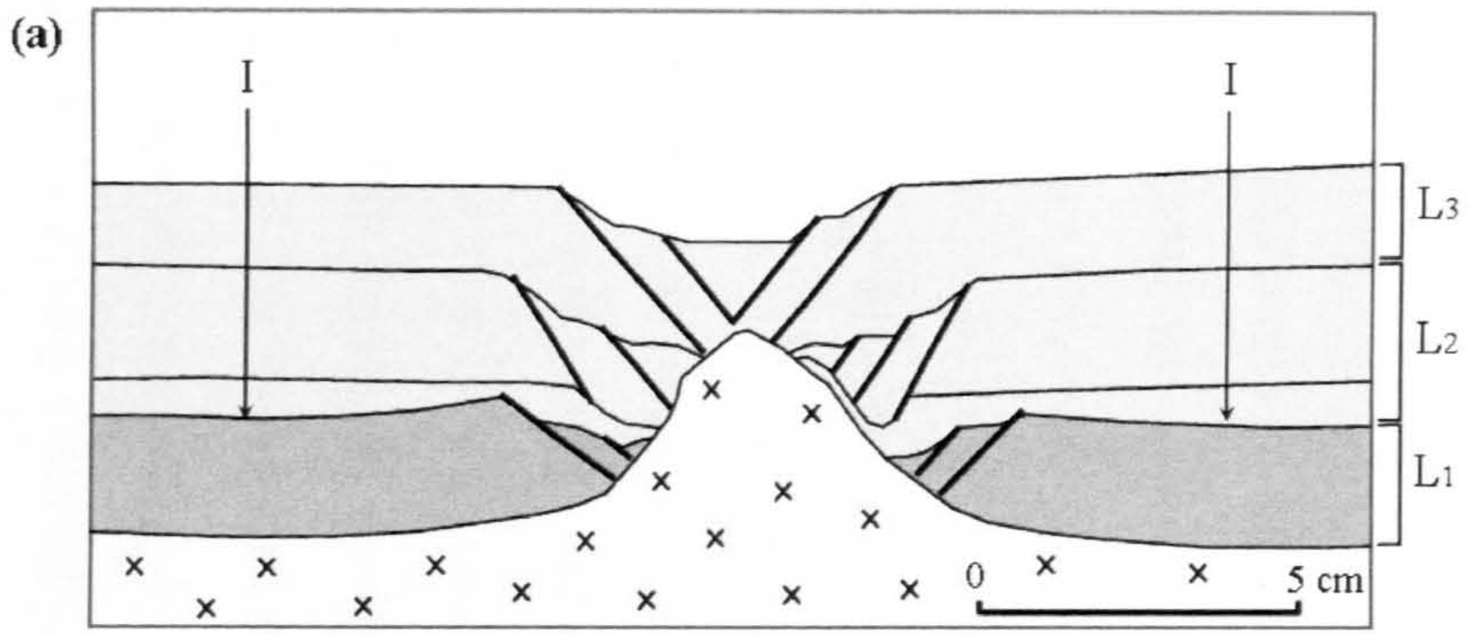

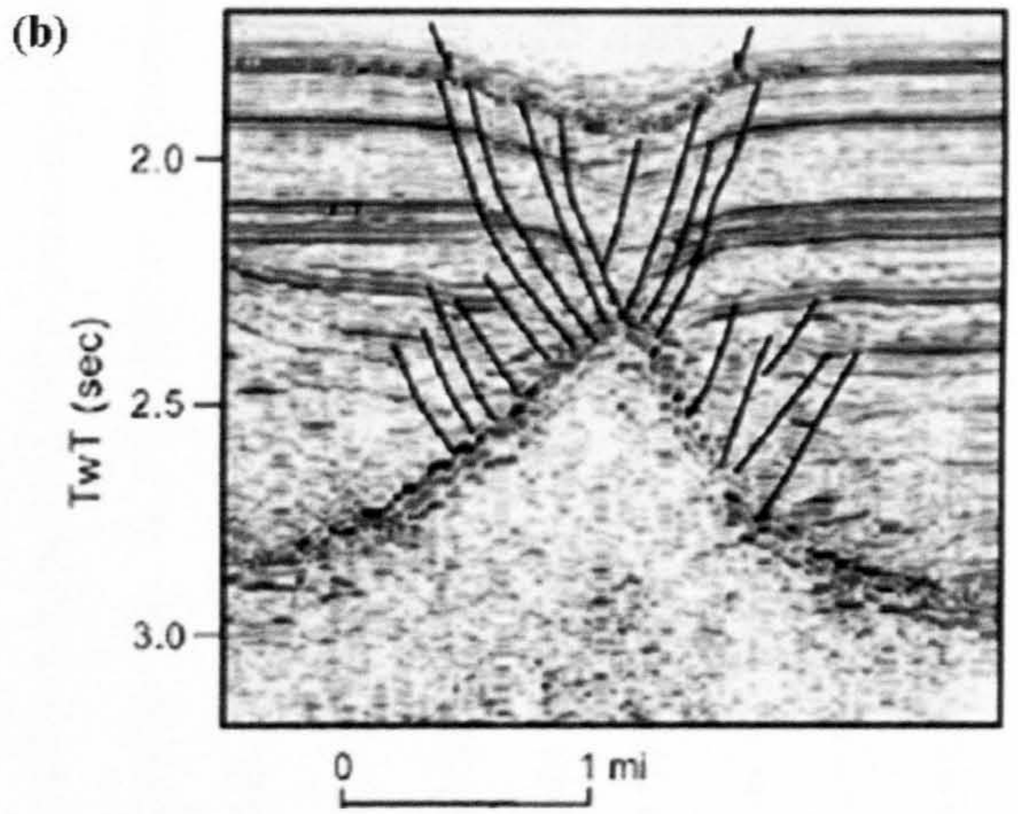

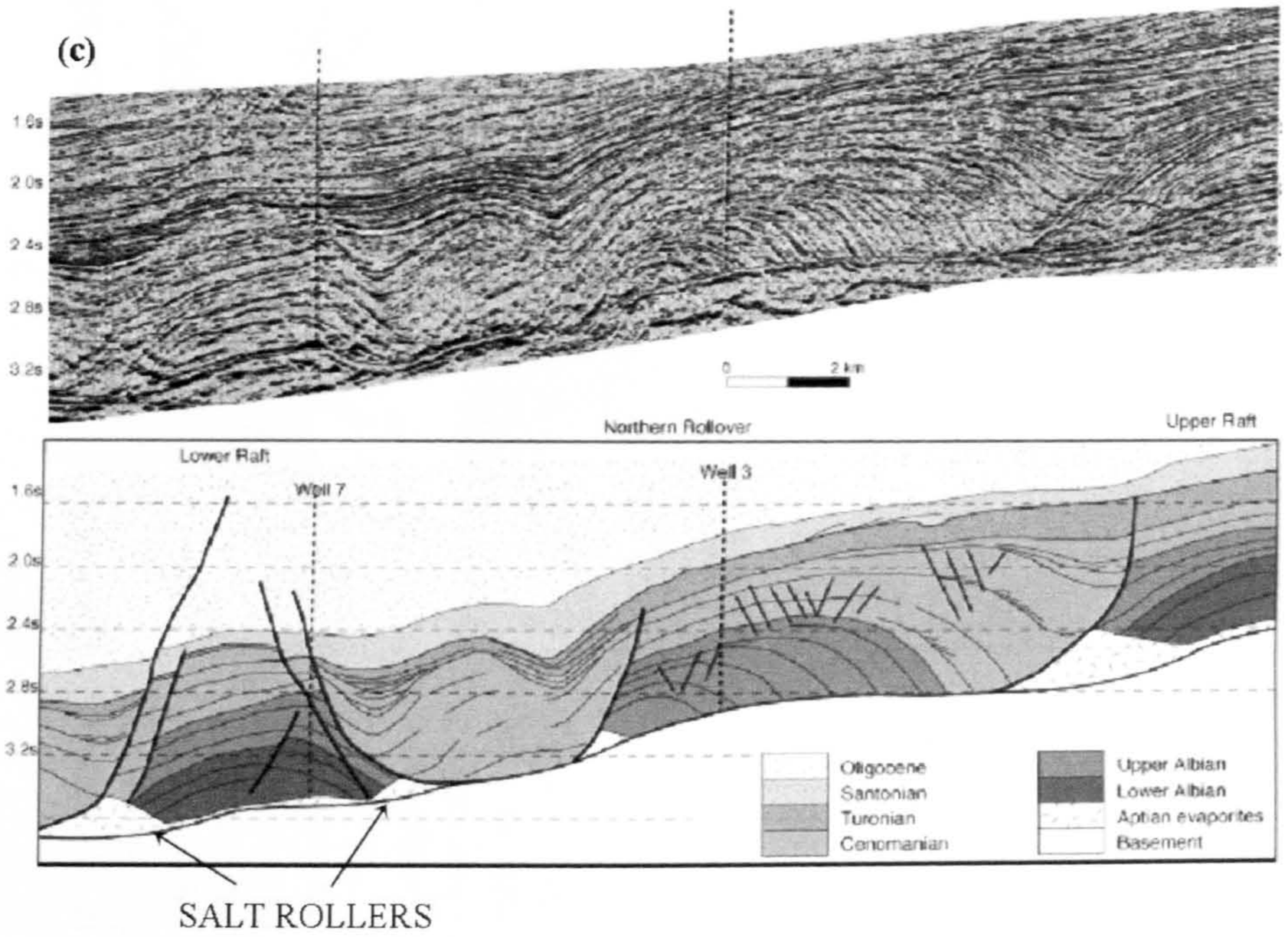

Figure 2.14: (a) Cross section in an experimental model illustrating the formation of a reactive diapir and primary peripheral sink in response to graben faulting. The overburden comprises one prekinematic layer (L1) and two synkinematic layers (L2 and L3), each made of several stratified sub-layers. The lowermost layer was flexed upwards as the shoulders of the graben and underlying reactive diaper rose. I indicates the location of the primary peripheral sink indicated by thinning of the basal layer toward the diapir (Redrawn from Vendeville, 2002). (b) Example of a reactive diapir in the Gulf of Mexico (from Hudec and Jackson, 2007). (c) Cross-section from the West African margin illustrating the geometry of salt rollers (from Rouby et al, 2002)

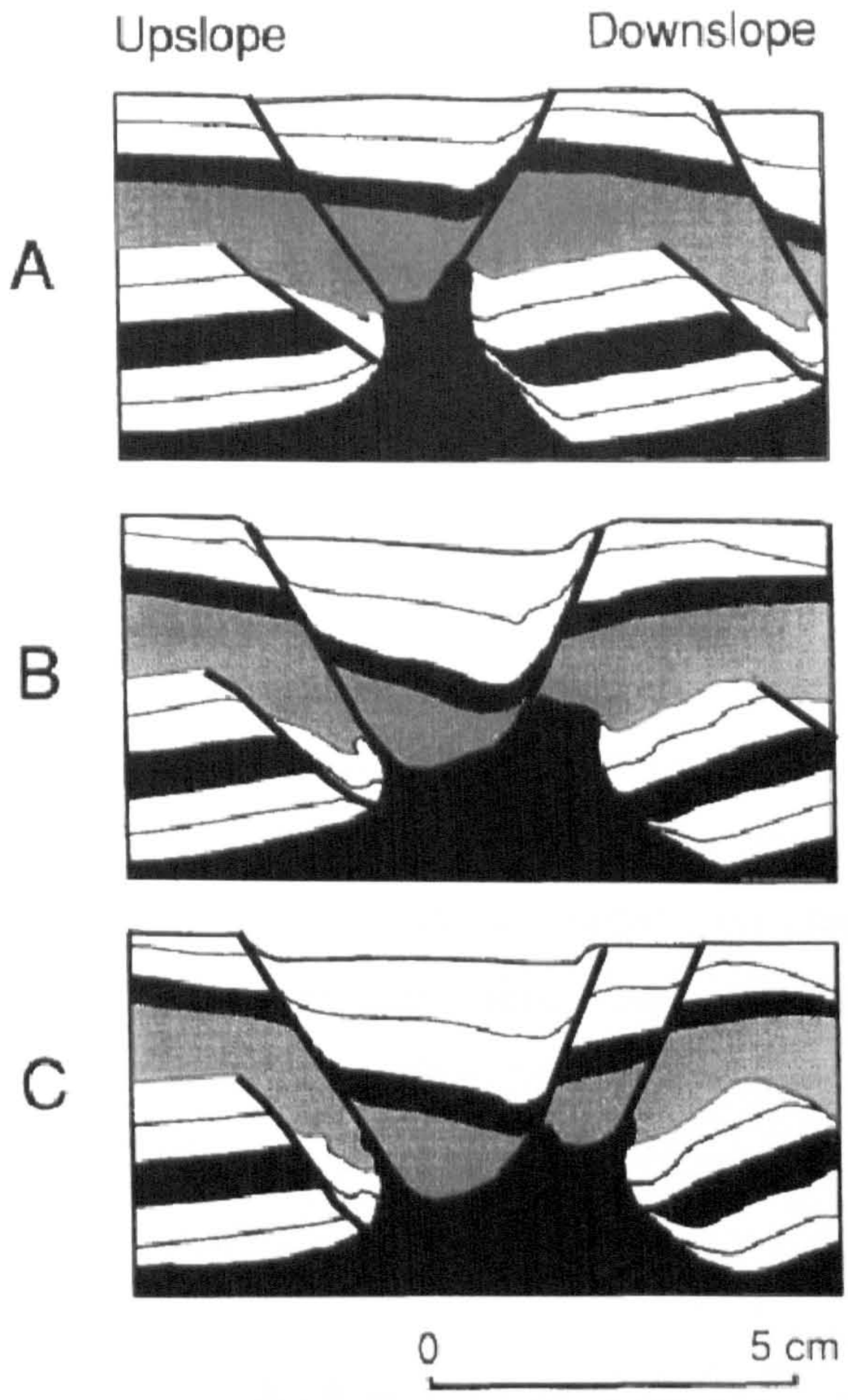

Figure 2.15: Vertical sections through an experimental model showing progressive fall of a diapir. Diapir subsidence increases with increasing extension. The diapir becomes wider and lower, the overlying graben deepens and the slip of the crestal faults increases. The overlying growth graben subsides into and indents the widening diapir (Modified from Vendeville et al, 1992b).

2.2.4.3 Sedimentary differential loading

Sedimentary differential loading is widely believed to initiate salt flow if the sediments are continually funnelled into the same depocentre (Jackson & Talbot, 1986; Jackson & Vendeville, 1994). Salt can be efficiently displaced beneath a depocentre of extra thick or dense sediments, causing it to well up adjacent to the depocentre. It is even possible for thin, partly compacted sediments which are less dense than salt to apply a differential load if their thickness varies laterally, i.e. delta lobes of restricted areal extent, or gravity driven-turbidity currents funnelled between structural barriers (Jackson & Vendeville, 1994). An established depocentre, which efficiently displaces salt from beneath it, will continually create space for further sediment deposition and associated compaction in the depocentre as long as salt displacement and sediment supply are ongoing to continually reinforce diapiric rise.

Sedimentary differential loading is one mechanism that can trigger lateral salt flow as the overburden flexes under vertical load, forming a pillow. It is however more difficult to trigger diapiric piercement because the strength of the overburden is

far greater than the pressure differences exerted by sedimentary differential loading (Jackson *et al*, 1994). However, if a diapir completely pierces its overburden and is exposed at the sediment surface, passive diapirism or downbuilding can maintain diapir growth (**Figure 2.16**). In passive diapirism, the diapir rises continually with respect to surrounding strata and remains exposed as sediments accumulate around it. The salt may rise through thousands of meters of overburden without ever having to forcibly break through overlying sediments. The relative rates of diapir rise and sediment aggradation then control the shape of the diapir (Jackson & Vendeville, 1994).

Sedimentary differential loading alone does not account for many of the salt structures observed around the world. Jackson & Vendeville (1994) addressed the issue of why some thick salt deposits become destabilised and rise as salt structures, whereas others remain stable. They concluded that extension is the most common initiator of salt upwelling. Many salt basins may not have undergone salt tectonism due to limited differential loading of salt, or absence of regional tectonism (Hudec & Jackson, 2007).

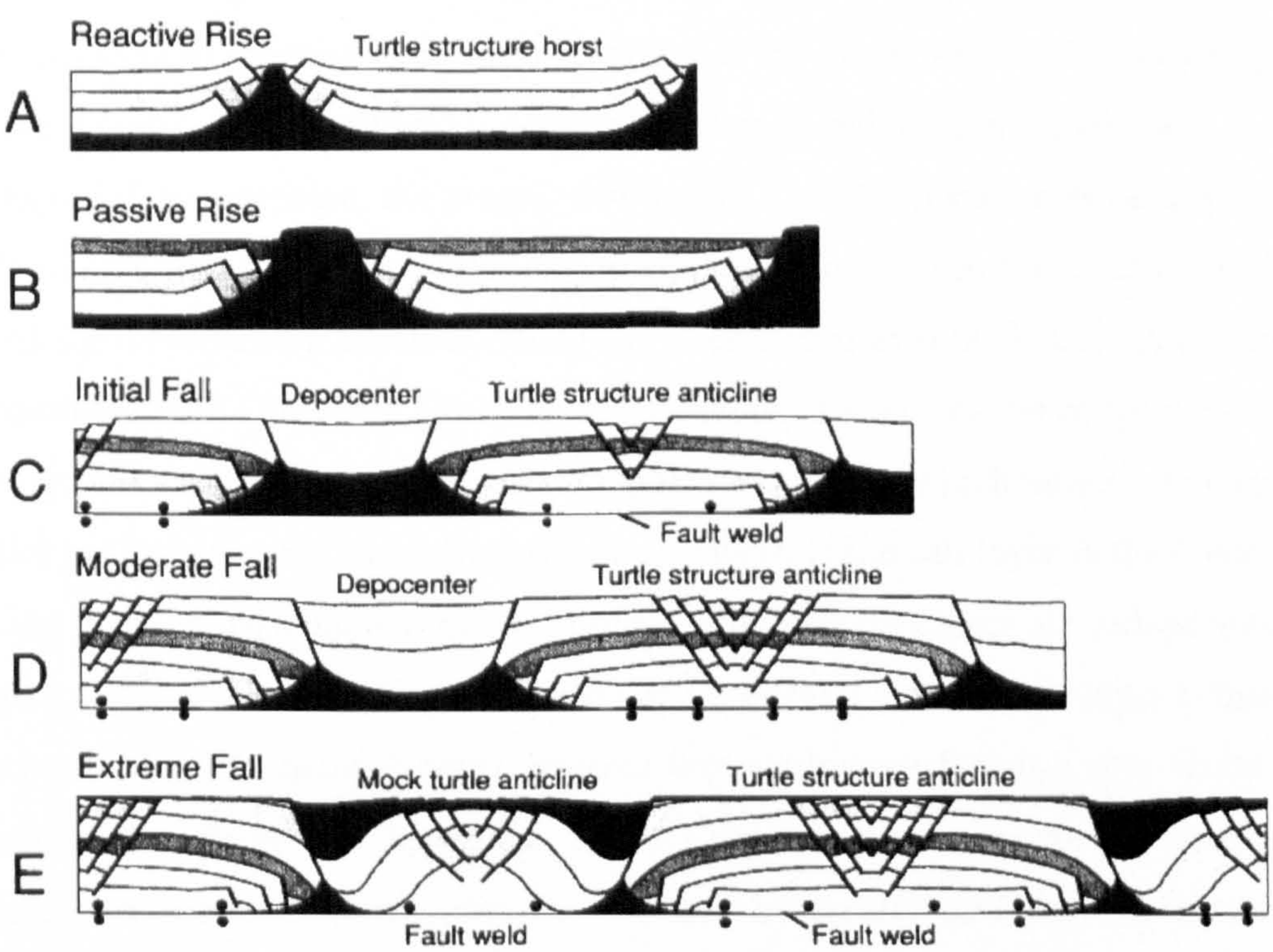

Figure 2.16: Schematic rise and fall of diapirs during sedimentation. Three types of extensional turtle structure successively form: turtle structure horst, turtle anticlines and mock turtle anticlines (from Vendeville *et al*, 1992b).

2.2.5 Role of basement

Thick-skinned extension stretches both the basement and cover. Normal offsets affecting the sub-salt basement have long been thought to initiate diapirs thus influencing their location and shape (Koyi *et al* 1993, Stewart *et al*, 1997). Modeling indicates that the affect of basement faulting can only propagate upward through the salt into the overburden (i.e. hard-link) due to either: (i) lateral salt flow; (ii) very rapid regional extension; or (iii) a very thin salt layer (Vendeville *et al*, 1992a). Hudec & Jackson (2007) argue that the shape of the base of the salt layer is not important for producing hydraulic head gradient and is thus not important for initiating salt flow, although it may influence the geometry of flow once it begins. However, modeling results and observations from seismic data (Withjack *et al*, 1989, 1990; Withjack & Callaway, 2000) suggest that sub-salt faulting that influences the geometry of the cover basin infill may be sufficient to cause passive salt flow.

Basement faults that slip at moderate rates or salt that is moderately thin cause the cover over the downthrown blocks to sag, forming a monocline above the basement fault (**Figure 2.17b**). Local stretching of the upper monoclinal hinge is exaggerated by regional extension to form a graben above the upthrown basement block, adjacent to the basement fault. Thinning of the overburden in this way triggers reactive diapiric piercement into the faulted graben (Vendeville *et al*, 1992a).

During slow extension, the presence of a thick (> 500 m) salt layer decouples the brittle overburden from the faulted basement. Salt flows from the upthrown block toward the downthrown block allowing the overburden to subside uniformly across the basement fault (**Figure 2.17b**). Regional extension stretches the cover with faults forming sub-parallel to the direction of regional extension, which may or may not be parallel to the basement faults (Jackson *et al*, 1994). If the salt layer is thick enough, then the location, spacing and throw of the overburden structures are independent of all but the larger basement faults (Jackson *et al*, 1994). Once the salt layer is thinned sufficiently, the basement footwall indents the overburden forming new faults and folds directly above the basement fault. Conversely, if the space created by downthrown basement blocks can be balanced by locally thickened synkinematic sediments situated above the draped overburden, rather than being filled by salt, the loading of sediments can reverse salt flow. In this case, salt is forced from above the downthrown block and above the upthrown block (Vendeville *et al*, 1992a).

It is important to point out that diapirism can occur without basement faulting under a mechanism that allows only the overburden to extend, e.g. gravity-sliding (**Figure 2.17**), although it is often the dip on the underlying basement surface that enables gravity-sliding to initiate (Vendeville, 1987; Gaullier *et al*, 1993; Mauduit *et al*, 1997). A sedimentary sequence with a basal layer of salt can glide under the effect of its own weight down a slope of less than 1° (Vendeville, 1987; Mauduit et al, 1997). Gravitational sliding induces thin-skinned extensional tectonics above a salt décollement and is characterised by normal growth faults, many examples of which have been imaged in seismic data from the Atlantic margins of Africa (Duval et al, 1992; Rouby et al, 2002) and Brazil (Cobbold & Szatmari, 1991; Demercian et al, 1993; Rouby et al, 1993). Knowledge of the process of gravity-induced faulting has been greatly improved by experimental models (Vendeville et al, 1987; Vendeville & Jackson, 1992a, b; Gaullier et al, 1993) which suggest that the geometry and dynamics of gravity-induced faults are controlled by the slope orientation, with listric growth faults and associated salt structures generally oriented perpendicular to the slope line (Gaullier *et al*, 1993). The slope line, which is the primary control on gravity-driven deformation, is controlled by the spatial and temporal variation in throw and linkage within basement fault systems (Stewart *et al*, 1997). The basement surface becomes sufficiently tilted to initiate cover sliding as basement faults increase in displacement.

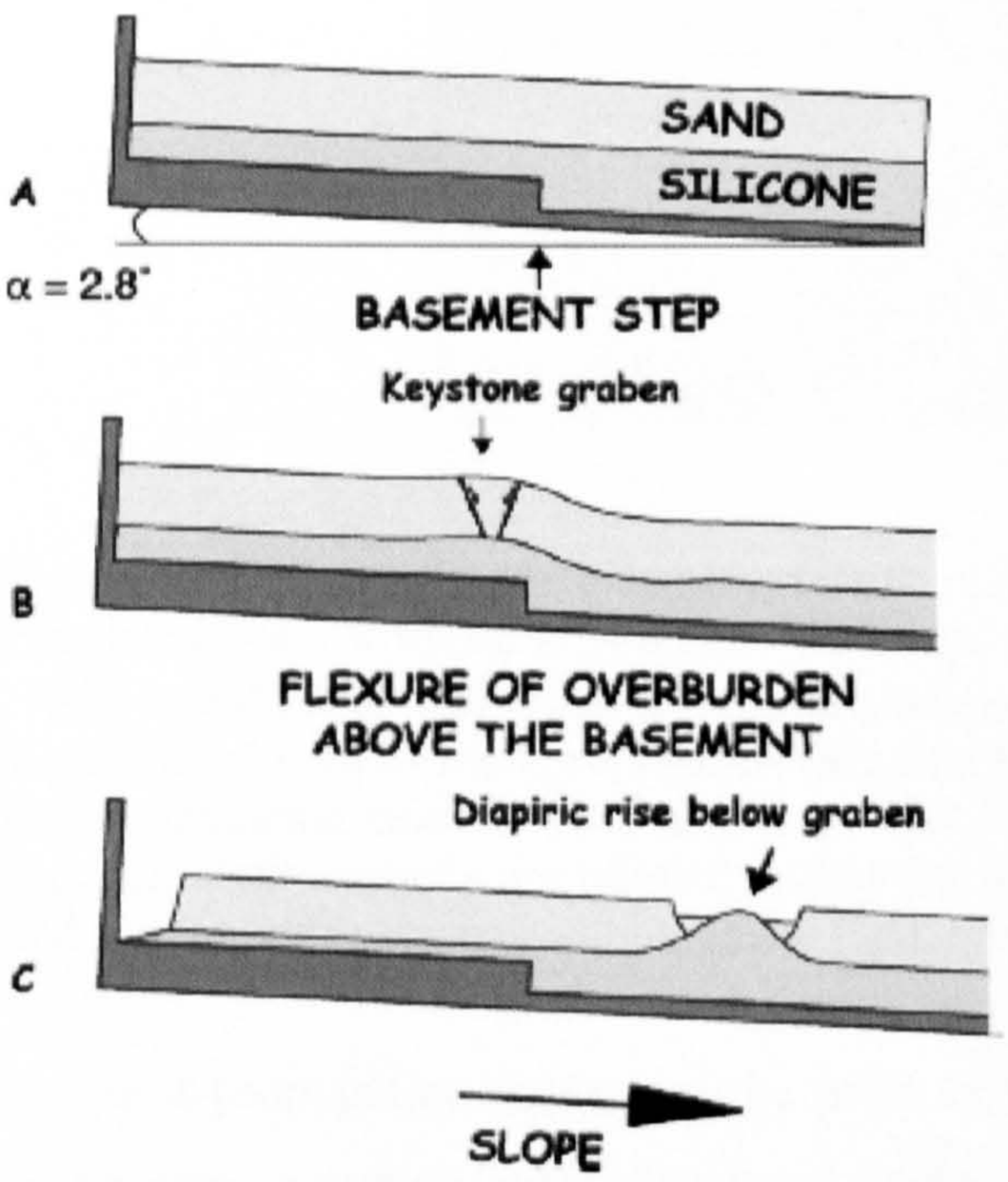

Figure 2.17: Schematic cartoon showing the deformation pattern of the viscous décollement and brittle overburden during gliding above a basement step (from Gaullier *et al*, 1993). The viscous source layer flows during gliding causing the overburden located above the step to flex, partly mimicking the topography of the underlying basement. A graben bounded by two normal faults formed in the upper hinge of the flexure trending parallel to the basement step. A ridge of salt rose reactively below the graben eventually piercing the graben floor diapirically.

2.3 FAULT-PROPAGATION FOLDING

2.3.1 Theory

Many types of folds and flexures are present in extensional tectonic settings, the majority of which are associated with the growth of normal fault systems (Schlische, 1995). Fault-propagation folds are typically produced by deformation of material beyond the tip-line of lengthening faults (White & Crider, 2006) (**Figure 2.18**) and are therefore quite distinct from folds and other compressional features formed during later basin inversion events. Inversion structures are formed by a different mechanism to extensional folds and thus the process of inversion will not be discussed again in this thesis.

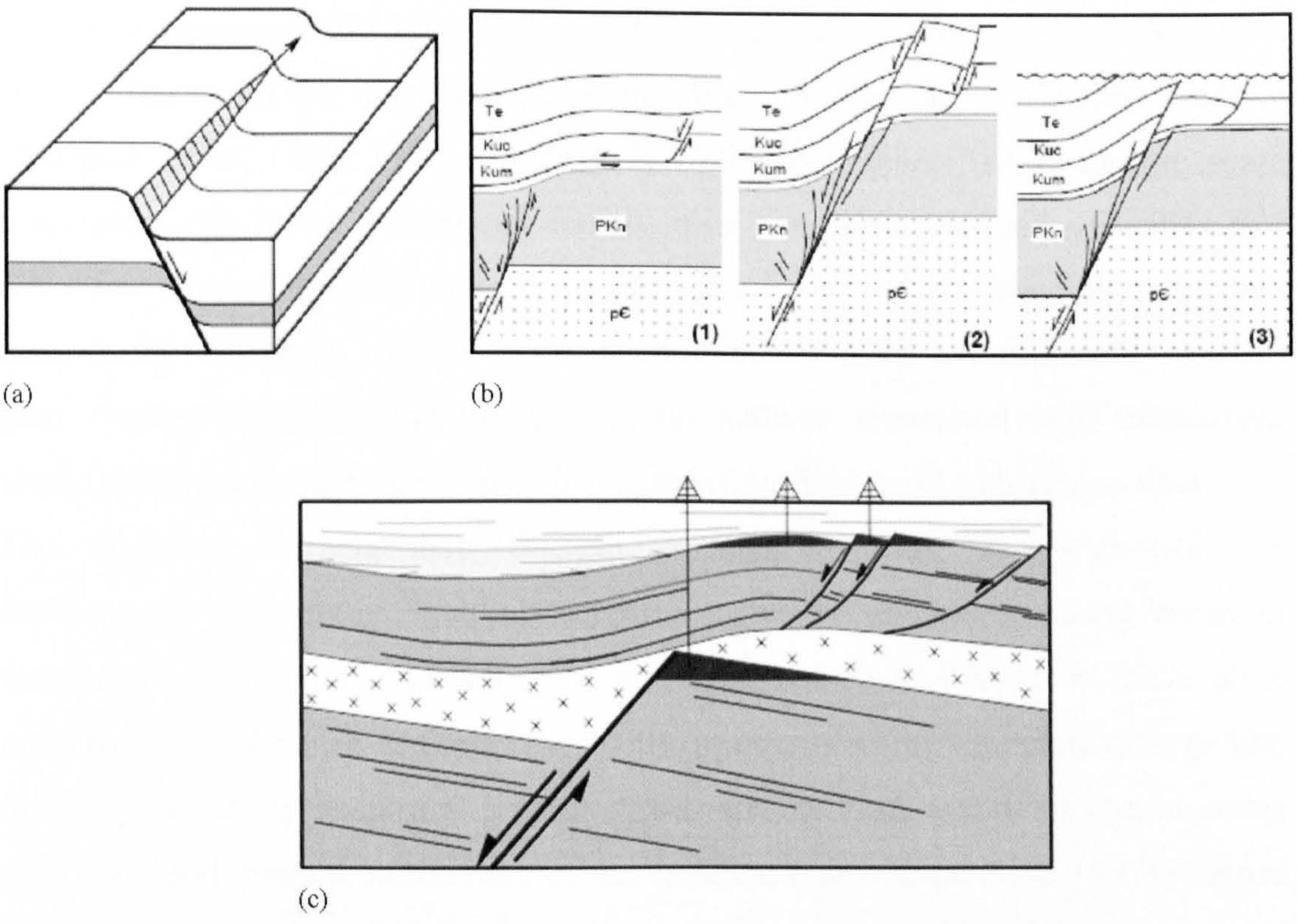

(a) (b)

(c)

Figure 2.18: Examples of extensional fault-propagation folds. (a) Fault-propagation fold associated with warping beyond the fault tip-line (Modified from Walsh & Watterson, 1987); and (b) Idealised cross-sections illustrating the evolution of folds in the Gulf of Suez as a result of vertical fault propagation (Modified from Withjack et al, 1990). (c) Sketch of a fault-propagation fold above a master normal fault. Crossed area represents an evaporitic package. Hydrocarbons are trapped within the secondary supra-salt structures produced by folding and within the sub-salt basement block (redrawn from Withjack & Callaway, 2000).

Fault-propagation folds may be produced ahead of both laterally and vertically propagating normal faults. However, field observations from the Modoc Plateau,

north eastern California suggests that fault-propagation folds are the result of faults with a dominant component of vertical propagation (White & Crider, 2006). In other words, most fault-propagation folds are rooted at depth in faults that are partially or completely blind. As the fault accumulates displacement, it propagates laterally and vertically through the overlying fold, forcing growth of a monocline (**Figure 2.18b**). Both lateral and vertical folds can change the local topography around near-surface faults, which in turn produces important controls on the pattern of erosion and deposition of sediments (Gawthorpe *et al*, 1997).

It is also apparent that in many cases, the presence of subsurface evaporites facilitates the development of extensional forced folds by partially decoupling the shallower, folded strata from the deeper faulted strata in the basement (Withjack *et al*, 1989). Examples include flexures within the Suez rift (Brown, 1980; Gawthorpe *et al*, 1997, **Figure 2.19a**), the Modoc Plateau, northeast California (White & Crider, 2006, **Figure 2.19b**) and throughout the Haltenbanken area, offshore Norway (Withjack *et al*, 1989, 1990; Withjack & Callaway, 2000). The evaporitic strata associated with many extensional forced folds have densities and velocities that differ from the surrounding strata, distorting seismic images and thus making seismic interpretation difficult. In such cases, experimental models are commonly used to gain a better understanding of deformation patterns associated with extensional forced folding, providing guidelines for interpreting field, well and seismic data.

The structural characteristics of fault propagation folds associated with the development of a buried fault tip comprise typically upward widening zones of distributed deformation with anticlinal and synclinal bends that form above blind normal faults (Withjack & Callaway, 2000). In cross-section, reflectors diverge into the hangingwall depocentre at a point offset into the hangingwall of the basement fault trace and onlap onto the limb of the anticline (Gawthorpe *et al*, 1997) (**Figure 2.18c**). The location of the hangingwall depocentre can be used to distinguish blind faults associated with the development of an extensional fold from those faults that were emergent at the surface.

Extensional forced folds are important hydrocarbon traps, most commonly with hydrocarbons trapped within shallow, secondary structures associated with the hangingwall basin. Hydrocarbons can also be trapped within the underlying fault blocks (**Figure 2.18c**), but precisely locating these structures, which lie beneath an evaporitic layer, can be difficult.

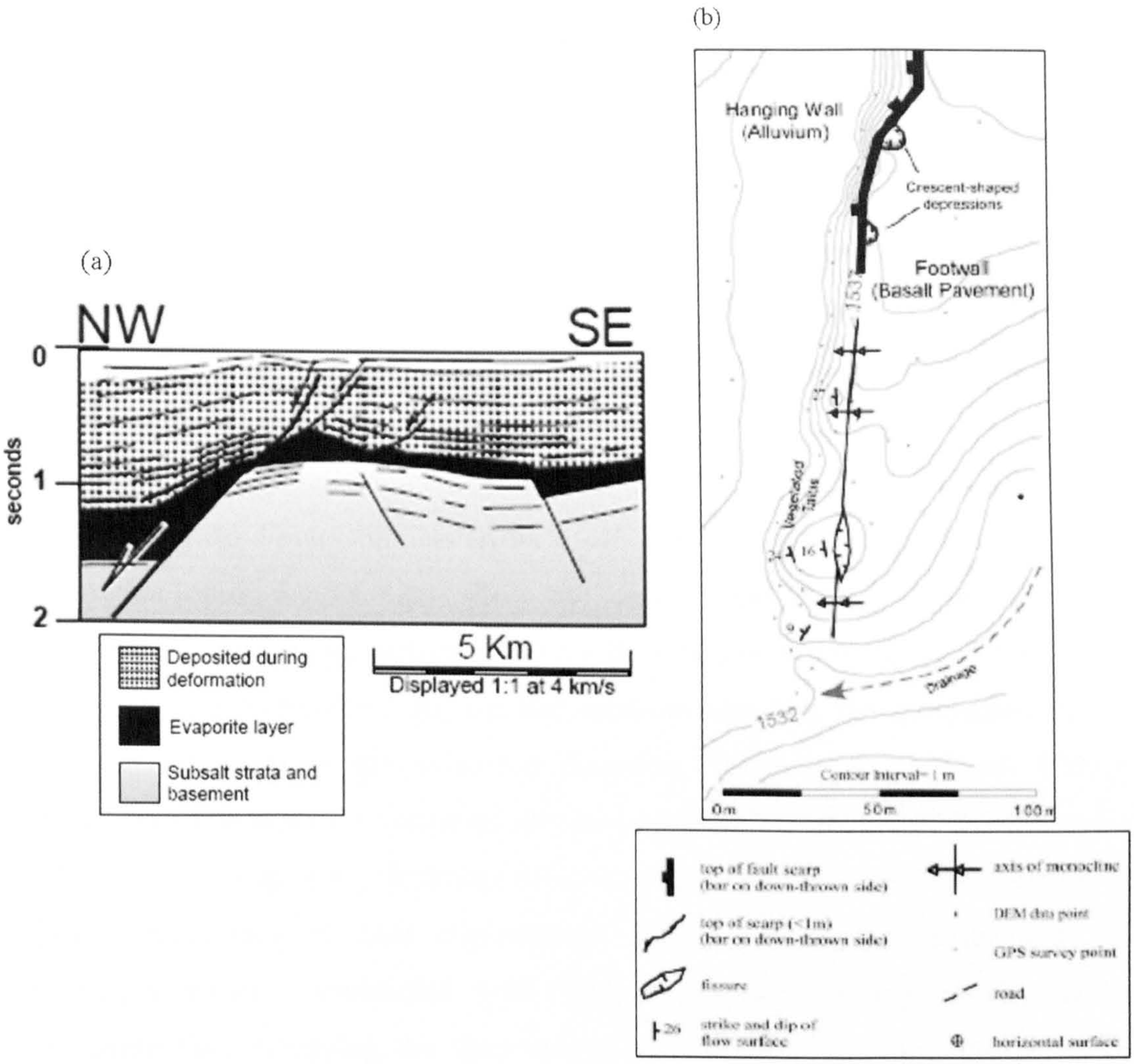

Figure 2.19: Examples of fault-propagation folds from seismic and field data. (a) Line-drawing of a seismic section from the Suez rift (from Patton *et al*, 1994), (b) Detailed topographic and structural map of the Porcupine Valley Fault scarp, Modoc Plateau, North East California (From White & Crider, 2006). Well-developed monoclines are mapped ahead of the emergent fault tip.

2.3.2 Analogue and experimental modelling

Experimental models can be used to aid the interpretation of structures in areas of structural complexity, uncertainty or poor data quality. Models are designed to simulate real geological conditions over much shorter time-scales and under conditions that are scaled to best represent material properties, stress regimes and boundary conditions.

Scaled experimental models have been used to define the geometry of fault-propagation folds and the controls on deformation patterns in brittle-ductile systems. Single-layer models composed of either clay or sand (Vendeville, 1987; Withjack *et al*, 1990), two-layer sand/putty models (Vendeville, 1987) and discrete-element

models (Finch *et al*, 2004) have all demonstrated that the dip of the master normal fault influences the deformation patterns associated with forced folding. Moderately-dipping master faults typically produce wide folds and gentle limb dips, whereas steeply-dipping master faults produce narrow folds with steep dipping limbs (Withjack *et al*, 1990). Thus as basement fault dip decreases, the width of the monocline at the surface increases (Finch *et al*, 2004). In both cases, secondary (cover) faults are upward-steepening normal faults. The propagation and linkage of secondary faults into through-going normal faults generally terminates the development of extensional forced folds (Withjack *et al*, 1990, **Figure 2.18b**).

Multilayer, sand/putty models (Koyi *et al*, 1993; Vendeville & Jackson, 1995) suggest that other factors also affect the deformation patterns associated with extensional forced folding, including: (i) the thickness of the viscous layer (Stewart *et al*, 1997) and overburden; (ii) the deformation rate; (iii) the orientation of the master fault relative to the extension direction. Withjack & Callaway (2000) supplemented this work by systematically investigating the impact of five variables (thickness of viscous layer, thickness of cover sequence, strength/ductility of cover sequence, magnitude of fault displacement and rate of fault displacement) on deformation patterns associated with fault-propagation folding. Their results demonstrate that increasing the thickness of the viscous layer and the cohesive strength and ductility of the overburden enhances decoupling between the basement and cover deformation (**Figure 2.20a, c**). By contrast, increasing the viscosity of the viscous layer, the thickness of the overburden, and the magnitude and rate of displacement on the master normal fault reduces the decoupling between basement and cover, leading to a more coupled, hard-linked system (**Figure 2.20b, d, e**). Crucially, results show that in the absence of a viscous layer, most of the deformation in the cover sequence occurs directly above the master normal fault (**Figure 2.20a**). With a viscous layer, deformation in the cover sequence is more widely distributed meaning that in general, the presence of evaporites will favour the development of fault-propagation folds.

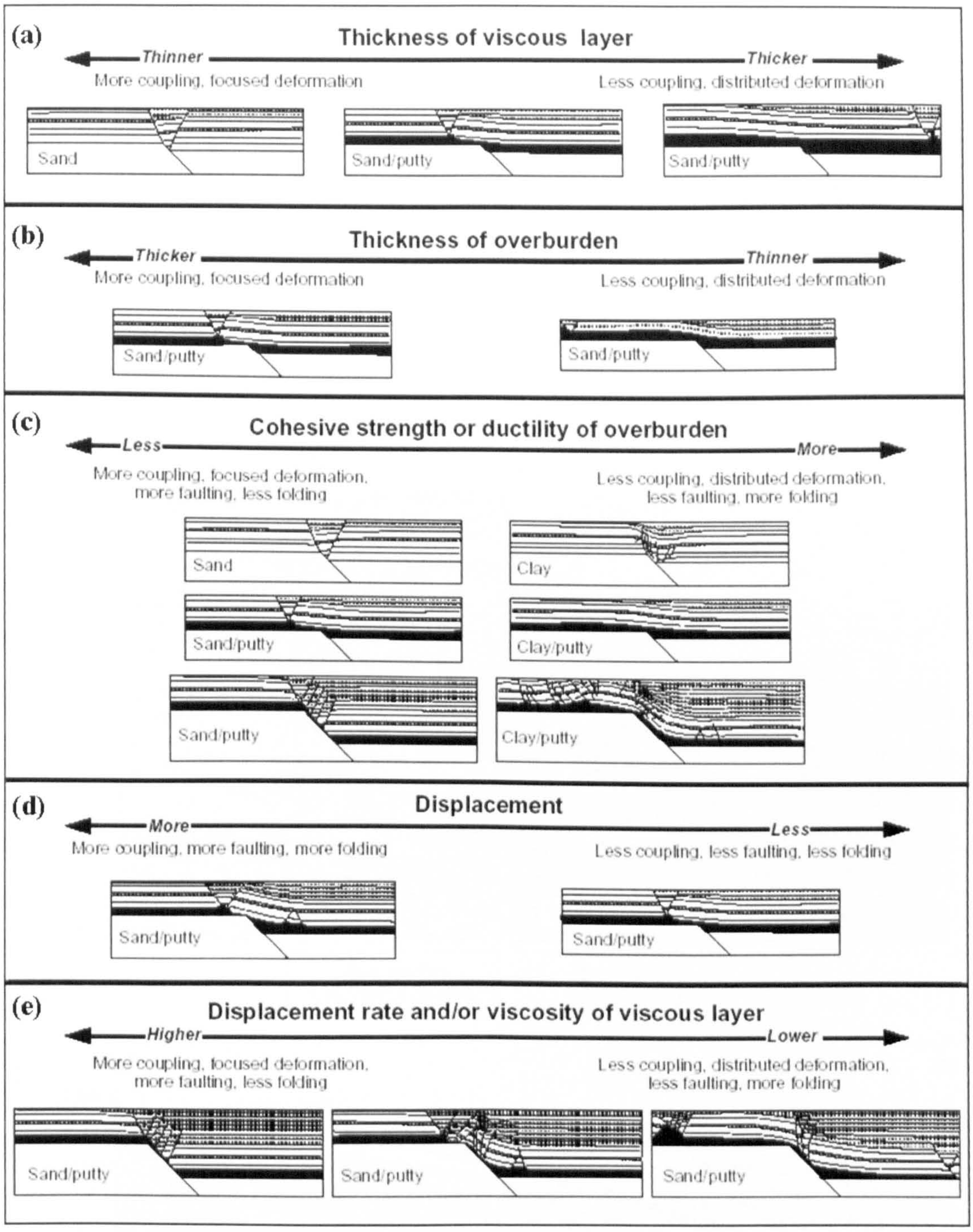

Figure 2.20: Results of experimental models summarising factors that control deformation patterns in the cover sequence above an active basement normal fault (from Withjack & Callaway, 2000).

2.3.3 Examples: Surface outcrop & sub-surface seismic

The results of the experimental models described above predict deformation patterns that closely resemble those observed in seismic and field data from the Gulf of Suez and offshore Norway (**Figure 2.21**).

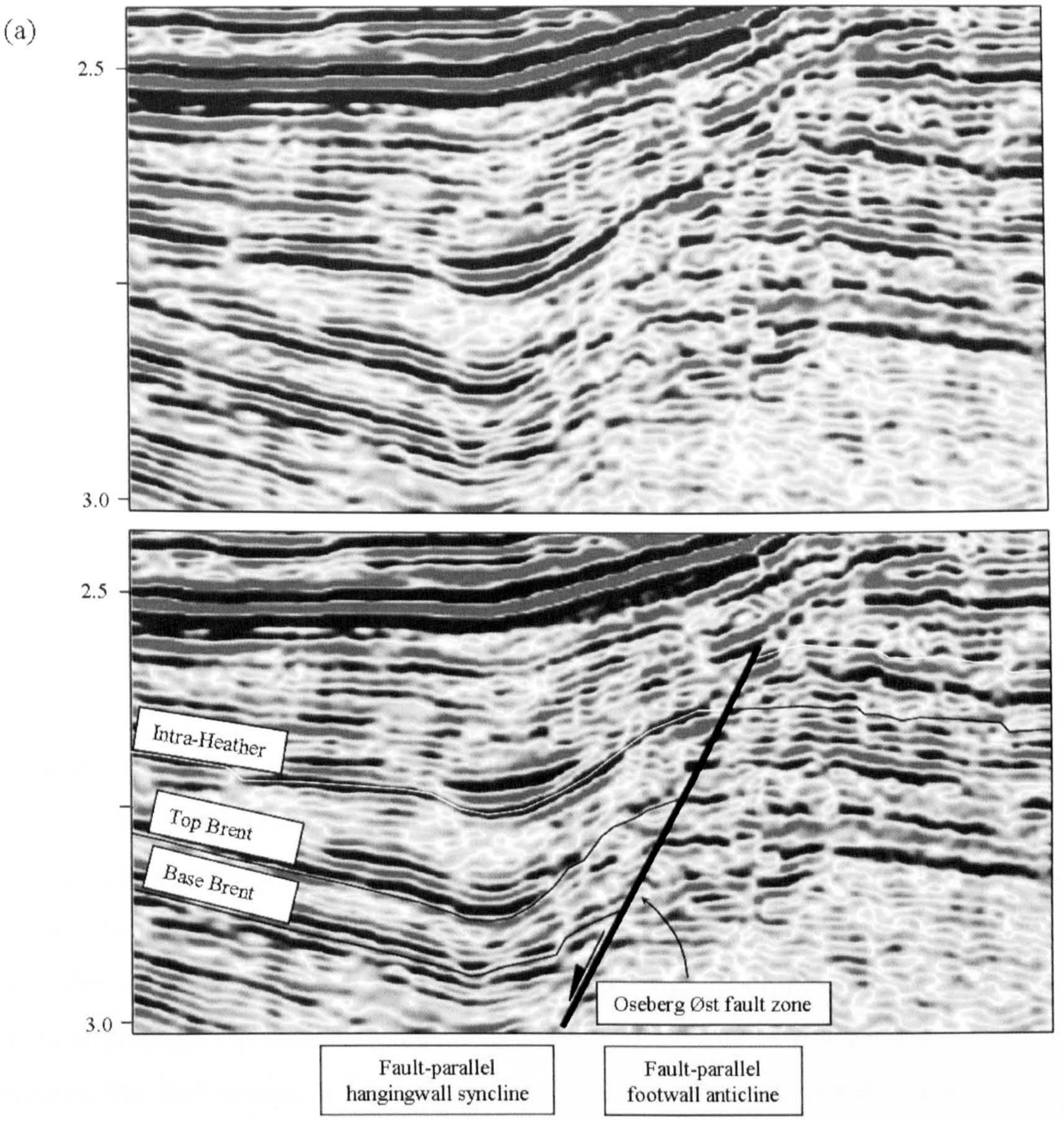

Figure 2.21: Examples of fault-propagation folds from field and seismic data. (a) Seismic expression of an extensional fault-propagation fold from the Oseberg East field, Norway (modified from Finch *et al*, 2004). (b) A breached fault-propagation fold, the Nakheil fault, Gulf of Suez (from Finch *et al*, 2004).

Breached folds are commonly recognised in natural examples of fault-propagation folds, in which localisation on a single fault produces hangingwall synclines and footwall anticlines as a result of breaching through the earlier monocline; they do not represent the effects of 'drag' against the fault (Finch *et al*, 2004). A seismic example from the Oseberg East field is shown in Figure 2.21a and a comparative field example from Wadi El Nakheil in the Gulf of Suez is shown in Figure 2.21b. Both cases show similar geometries to the modelling results (**Figure 2.20c, d**) in which the axis of the footwall syncline lies to one side of the fault, adjacent to which the bed dips are steep and in some cases sub-parallel to the fault.

Field observations of fault-propagation folds have come mainly from deformed pre- and syn-extensional strata associated with large normal fault systems in extended regions. Kilometre-scale fault-propagation folds have been recognised in the Gulf of California (Willsey *et al*, 2002), the Suez rift (Jackson *et al*, 2006), the Red Sea (Khalil & McClay, 2002) and northeast California (White & Crider, 2006; **Figure 2.19**). White and Crider (2006) use detailed mapping of surface deformation near the tips of small surface-breaking normal faults to present a detailed description of the geometry of fault-propagation folds. They describe the overall shape of the deformation in the near-tip regions as *'a monocline or highly asymmetric anticline with decreasing amplitude beyond the tip'*. Other structures that occur in conjunction to fault-propagation folds include fissures along the crests of folds whose long axes parallel the fault traces. It was suggested that these structures are the expression of small amounts of extension at the surface in response to folding. Outcrop-scale observations such as these are an invaluable addition to seismic data and analogue modelling results, providing an insight into features that perhaps cannot be resolved from seismic data but provide a crucial insight into the structural evolution of extensional fault-propagation folds.

2.3.4 Non-salt related fault-propagation folds

Examples of fault-propagation folds that form in the absence of evaporites have also been cited in the literature (Maerten *et al*, 2002; Finch *et al*, 2004; Smart *et al*, 2007). Smart *et al* (2007) describe the geometry of the Big Brushy Canyon monocline in the Sierra Del Carmen of west Texas. This fault-tip monocline developed in Cretaceous limestone and shale above a steep-dipping (80°) normal

fault with up to 30 m displacement. The master basement fault offsets thick limestones which are overlain by a monocline which developed in weak clay-rich shale and a limestone unit with interbedded argillaceous limestone. Brittle deformation of the interbedded argillaceous limestone units is concentrated in the monocline limb. Finite element modelling using mechanical stratigraphy, fault architecture, and boundary conditions simulating the Brushy Canyon monocline confirm the correlation of increased layer extension and up-dip bedding plane slip with increasing limb dip (Smart et al, 2007).

Localisation on a single master fault which form in the absence of salt similarly produces hangingwall synclines and footwall anticlines which are recognised in natural examples e.g. from the Oseberg East field in Norway (Finch et al, 2004).

2.4 REGIONAL GEOLOGICAL SETTING: MID-NORWAY

The Halten Terrace and neighbouring structural elements form part of a passive continental margin stretching from the North Sea to the Barents Sea. The opening of the North east Atlantic Ocean at the Paleocene-Eocene transition (c.55Ma) marked the culmination of a c.340Ma history of extensional deformation and sedimentary basin formation since the end of the Caledonian Orogeny (ended late Silurian – early Devonian). Following extensional collapse of the Caledonian Orogeny in the Devonian, several well-documented rift events affected the present North east Atlantic margin. Five main rift episodes are identified; Early – Middle Devonian, Carboniferous, Late Permian – Early Triassic, late Middle Jurassic to Early Cretaceous and Late Cretaceous to Early Eocene (Bukovics *et al*, 1984; Blystad *et al*, 1995; Doré *et al*, 1999; Brekke, 2000 & Skogseid, 2000).

It is well documented that Mesozoic rifting in Mid-Norway is characterised by repeated reactivation of pre-existing basement structures inherited from the Caledonian Orogeny.

The continental margin offshore Norway between 62° and 69°N consists of a central area of deep NE-SW trending Cretaceous basins, the Vøring and Møre Basins, flanked by shallower platforms to the east and west. The platforms to the west, termed the Vøring and Møre Marginal Highs, are characterised by thick, Early Eocene basalt flows overlying an unknown substrate (Brekke, 2000), whereas the

eastern side is dominated by the Late Jurassic – Early Cretaceous Trøndelag platform (**Figure 1.1a**).

The Vøring Basin is bound to the north by the NW-SE trending Bivrost Fracture Zone, which separates the deep Vøring Basin to the south, from the narrow, tectonically uplifted continental margin around the Lofoten Ridge (**Figure 1.1a**), and is defined by an apparent dextral shift in NE-SW trending structures. Further south, the Vøring and Møre Basins are separated by the Jan Mayen Lineament (**Figure 1.1a**), which is defined by a distinct c.250km scale sinistral shift of NE-SW trending basins. Brekke (2000) suggests these two fracture zones reflect an old structural grain in the crystalline basement which exerted major control on the post-Caledonian structural development of the region, such as the position and formation of the Trøndelag platform.

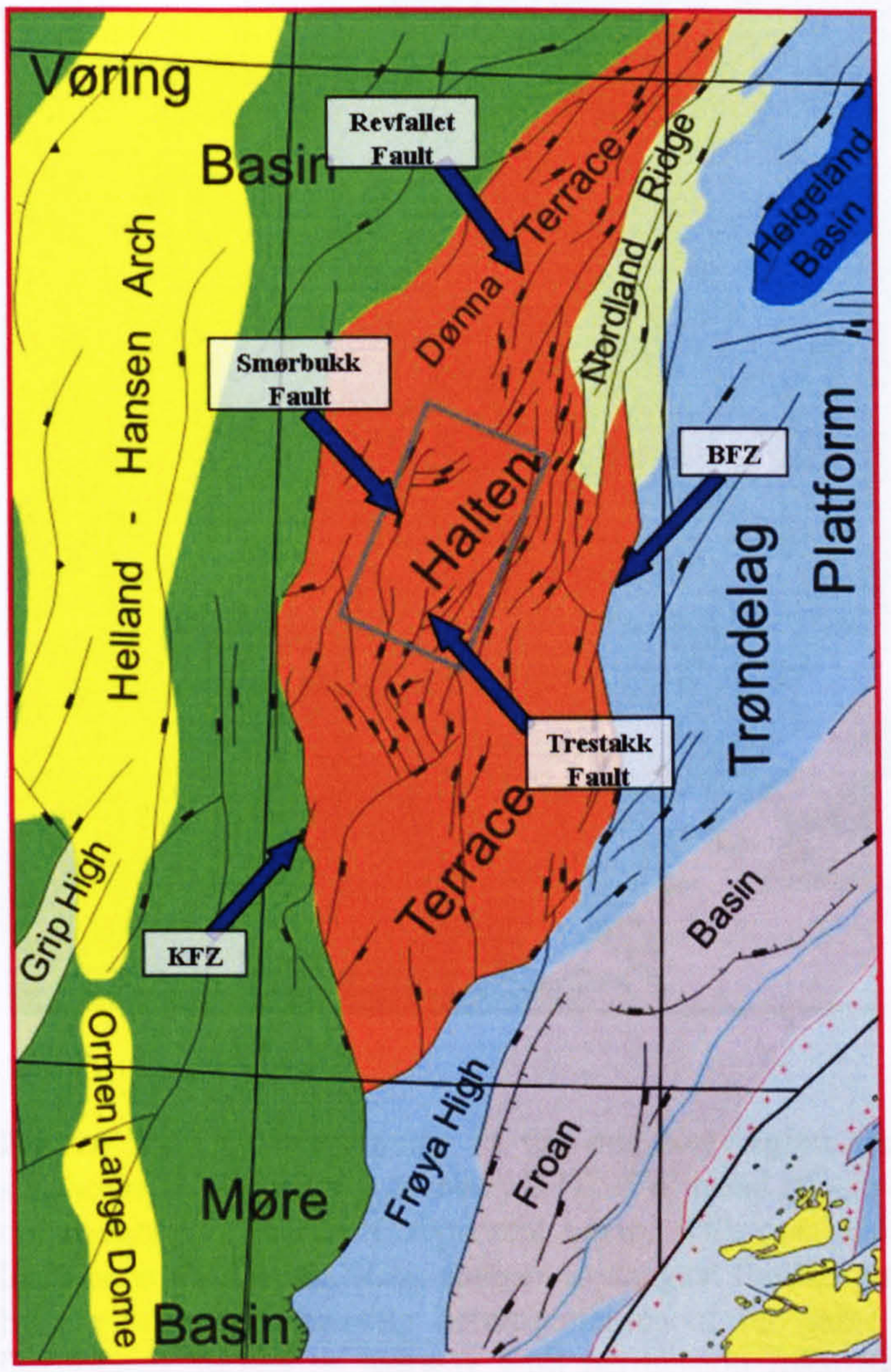

Figure 2.22: Structural map of the Halten Terrace highlighting key structural features (KFZ = Klakk Fault Zone, BFZ = Bremstein Fault Zone). The grey box outlines the study area covered by the seismic survey in Figure 3b.

These NW-SE trending lineaments thus coincide with and define the northern and southern boundaries of the rhomb-shaped Trøndelag platform (**Figure 1.1a**), subdividing the continental margin into three structural provinces; (i) a northern province, (ii) a middle province and (iii) a southern province (Brekke, 2000). The Halten Terrace lies within the middle province (**Figure 2.22b**), which is the main focus of this study.

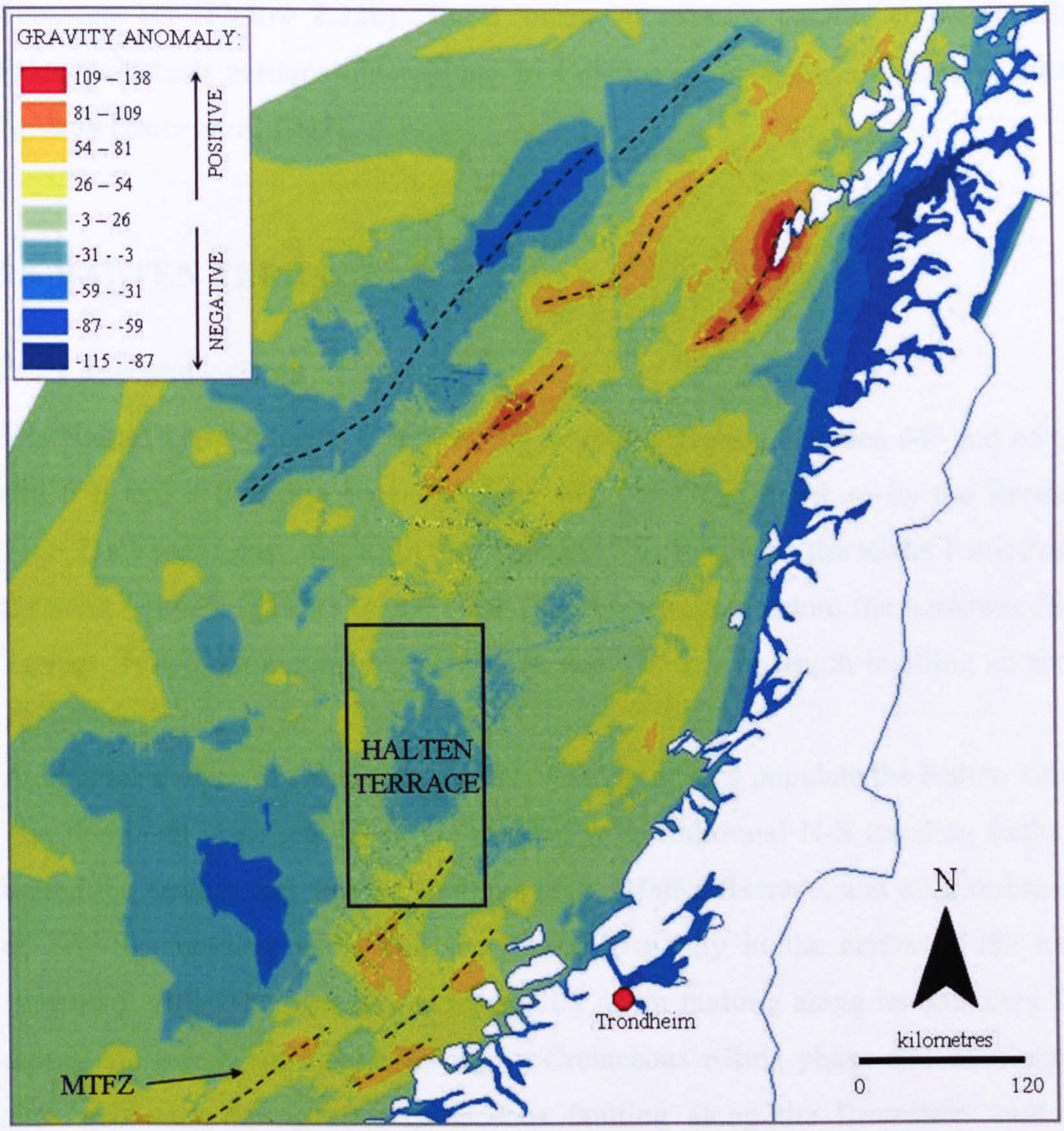

Figure 2.23: Gravity image of the mid-Norwegian shelf based on regional coverage of shipborne data showing an overall NE-SW trend of gravity anomalies. Such anomalies are commonly interpreted to represent basins with contrasting densities. Similar gravity maps have been used by existing authors to suggest the Norwegian continental margin developed by exploiting pre-existing heterogeneities of the same trend. Raw data provided by the Geological Survey of Norway with permission from Statoil. Abbreviations: MTFZ, Møre Trøndelag Fault Zone.

The structural configuration of the continental margin, offshore Norway is highlighted on gravity and aeromagnetic maps across the area, (e.g. **Figure 2.23**) which show contrasts in basement relief. The gravity image shows a series of elongate highs and lows which represent the contrast in density between basement rocks and sediments, i.e. the edges of depocentres or intra-basinal highs. The area is characterised by three major fault trends: (i) a dominant NE-SW structural grain; (ii) a less common, but distinct N-S grain and (iii) a more diffuse cross-cutting NW-SE lineament set (**Figure 2.22b**). These lineament patterns parallel similar trends in Palaeozoic fault patterns outcropping in Caledonian crystalline basement, onshore Norway (Doré *et al*, 1997).

2.5 HALTEN TERRACE

2.5.1 Tectonic setting

The Halten Terrace forms a rhomboidal structural feature between 64° and 65°30'N and 6°E and 8°E and is separated from the Trøndelag Platform by the Bremstein Fault Zone to the east, and from the Møre and Rås Basins by the Klakk Fault Zone to the west (**Figure 2.22b**). To the north, the terrace merges into the narrower Dønna Terrace. It is approximately 80 km wide and 130 km in length totalling an area of 10,400km^2.

A complex pattern of extensional faults of different ages populate the Halten Terrace. The dominant structural trend is NE-SW, with additional N-S trending faults that bound the eastern and western margins of the Halten Terrace, and a subordinate set of NW-SE trending faults that are localised mainly in the centre of the terrace (**Figure 2.22b**). The terrace was formed by down-faulting along its boundary faults during the late Middle Jurassic– Early Cretaceous rifting phase and developed its final geometry during Late Cretaceous faulting along the Bremstein fault zone (Blystad *et al*, 1995).

2.5.2 Åsgard area

The area consists of a series of dominantly NE-SW trending faults (**Figure 2.24b**) with steep westerly dips and apparently listric geometries. Two faults, the

Smørbukk and Trestakk faults, dominate the area which is strongly influenced by interactions with salt at depth during extension. The Smørbukk field lies in the crest of a Jurassic fault block that is bound to the west by the Smørbukk fault and to the north by an east-west trending graben that transects the crest of the fault block (**Figure 2.24b**). Most fields on the Halten Terrace reside in the footwall crests of tilted fault blocks similar to the structural setting of the Smørbukk field, e.g. Trestakk and Midgard fields. These major fault blocks are dissected by smaller faults causing variable degrees of internal fault block deformation, ranging from relatively low in Smørbukk to high in Trestakk and Midgard.

One exception is the Smørbukk Sør field which is located on the crest of a complexly faulted domal structure to the south-east of Smørbukk. It is reported to have developed from a combination of lateral salt movement and the doming of block-faulted stratigraphy during the Late Jurassic (Jackson & Hastings, 1986; Martinius *et al*, 2005).

2.5.3 Significance as a petroleum producing province

The Norwegian authorities acquired the first seismic data for exploration purposes in 1969, followed soon after by the Ekofisk discovery which initiated over a decade of increased seismic, gravity and magnetic data acquisition. The first licences on the Norwegian continental shelf were allocated on the Halten Terrace in 1980, closely followed by the discovery of Midgard and Tyrihans in 1981 and 1983, respectively, and a peak in drilling activity in 1985, by which time all the major fields had been found (Koch *et al*, 1995). A significant number of hydrocarbon fields have been discovered on the Halten Terrace making it the most prolific hydrocarbon province offshore mid-Norway (Koch *et al*, 1995) (**Figure 2.24a**).

Today there are 50 fields in production on the Norwegian continental shelf, ranking Norway as the world's third largest oil and gas exporter in the world (NPD, 2006). Historically production on the Norwegian continental shelf has been dominated by a few large fields, e.g. Åsgard. With production from a number of these fields now in decline, several new smaller fields have been developed, e.g. Kristin, Tyrihans, (**Figure 2.24a**) resulting in distributed production over a larger number of small fields (NPD, 2006).

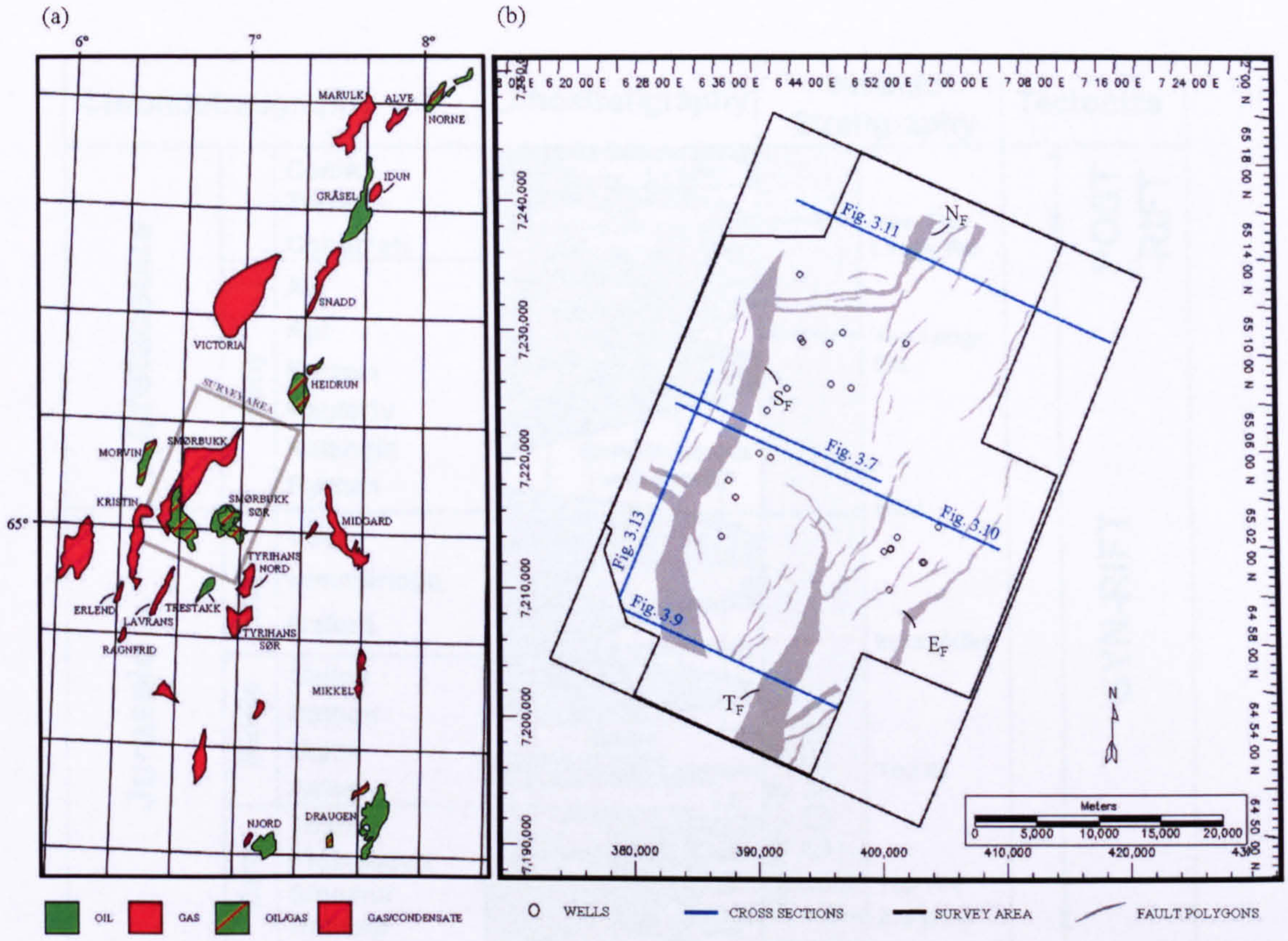

Figure 2.24: (a) Location of hydrocarbon fields with respect to survey area. The survey straddles two major fields, the Smørbukk and Smørbukk Sør fields. (b) Outline of survey area (irregular black box), available well data (circles) and cross sections (blue lines) referred to in the chapter 3.

To date only approximately 30 percent of expected total resources on the Norwegian continental shelf have been produced (NPD, 2006) leaving plenty of opportunity for further growth and development. With forecasts predicting that activity in the Norwegian petroleum industry will remain high over the long term, it is therefore important to invest time in understanding of fault systems and their impact on the petroleum system to maximise recovery from both old and new developments.

2.6 TECTONOSTRATIGRAPHIC EVOLUTION

Based on existing well data, it is assumed that the platforms and terraces offshore Mid-Norway comprise sedimentary rocks of Carboniferous to Permian in age on top of crystalline basement, similar to those found onshore East Greenland (Surlyk, 1990). The tectonostratigrahic evolution of the Halten Terrace from the Permian to Early Cretaceous is summarised below (**Figure 2.25**).

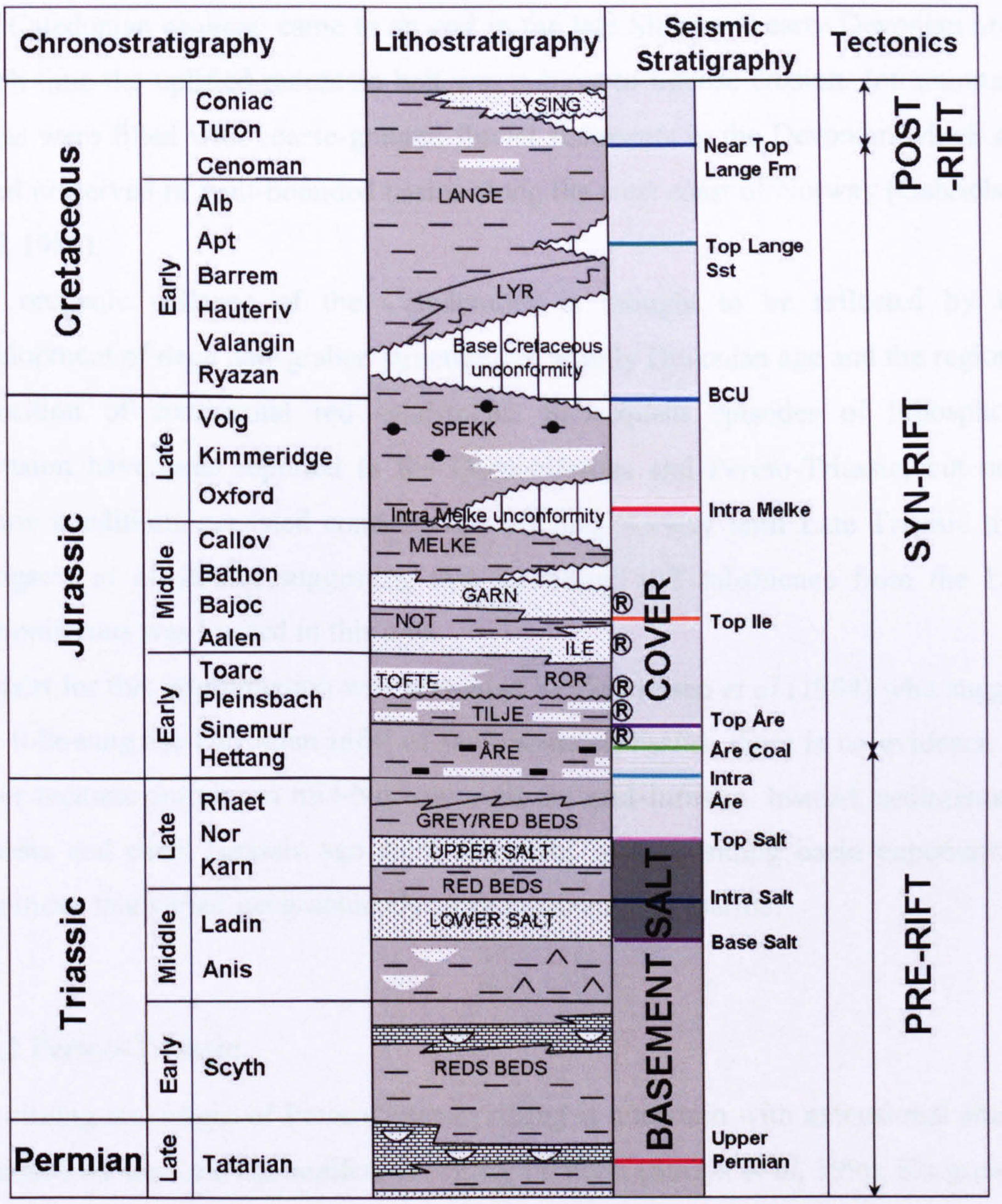

Figure 2.25: Stratigraphic framework, showing the ages and representative lithologies of the formations present in the Halten Terrace (redrawn from Hermanrud et al, 1998a and Müller et al, 2005), and our interpretation of the main tectonic events in the area. Colour codes and names used for seismic marker horizons interpreted as part of the study and their relative position with respect to reservoir formations are highlighted, see text for detail.

2.6.1 Pre-Permian

The Caledonian orogeny came to an end in the late Silurian – early Devonian after which time the uplifted mountain belt was subject to intense erosion. Intramontane basins were filled with coarse-grained fluvial sediments in the Devonian which are found preserved in fault-bounded basins along the west coast of Norway (Gabrielsen *et al*, 1984).

The orogenic collapse of the Caledonides is thought to be reflected by the development of deep half-graben structures of mainly Devonian age and the regional deposition of continental red sandstones. Subsequent episodes of lithospheric extension have been reported in the Carboniferous and Permo-Triassic, but non-marine conditions persisted continuously off mid-Norway until Late Triassic time (Skogseid *et al*, 2000), suggesting that stretching and subsidence from the Late Carboniferous was limited in this area.

Support for this interpretation was presented by Gabrielsen *et al* (1984) who suggest that following the Devonian infill of fault-bounded basins, there is no evidence for major tectonic activity in mid-Norway until the mid-Jurassic. Instead, sediments of Triassic and early Jurassic age were deposited in a subsiding basin experiencing conditions that varied geographically from continental to marine.

2.6.2 Permo-Triassic

The timing and origin of Permo-Triassic rifting is uncertain with extensional phases proposed for the Late Carboniferous – early Permian (Surlyk *et al*, 1990; Skogseid *et al*, 2000)), earliest Permian (Brekke and Riis, 1987; Ehrenberg *et al*, 1992; Blystad, 1995), late Permian (Schmidt, 1992), early Triassic (Dam *et al*, 2002) and early to late Triassic (Pascoe *et al*, 1999).

Existing work describes the introduction of post-rift evaporites on the Halten Terrace in the late Middle Triassic due to a tectonically-induced transgressive event following Late Permian – Early Triassic rifting of the northern North Atlantic **(Figure 2.26a)** (Ziegler, 1986; Blystad *et al*, 1995; Doré *et al*, 1999; Müller *et al*, 2005). However quantification of the degree of Permo-Triassic stretching is difficult given the lack of detailed stratigraphic information and knowledge about the post-Caledonian crustal and lithospheric structure (Skogseid *et al*, 2000).

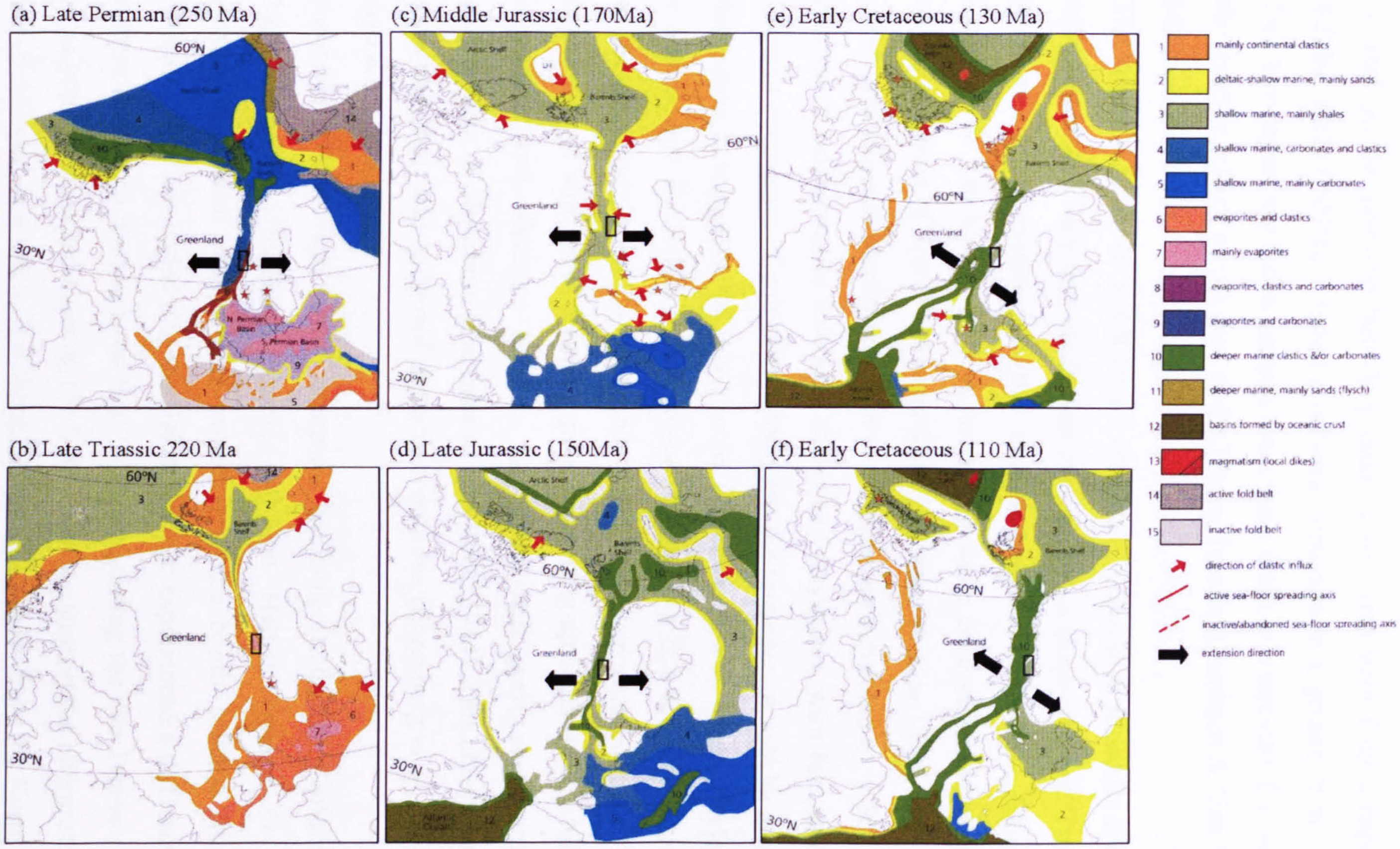

Figure 2.26: North Atlantic paleogeography from the Late Permian to Early Cretaceous (modified from Torsvik *et al*, 2002). The location of the Halten Terrace is indicated by the black box and black arrows highlight the direction of extension for each interval.

Although rarely a primary prospect, the Triassic was penetrated in a number of wells during the allocation of licenses and drilling of deep wells in the 1980's (Jacobsen & Van Veen, 1984). On the Halten Terrace two wells penetrate thick Late and possibly Middle Triassic deposits (**Figure 2.26b**). 6507/12-2, the deepest well, is situated on the platform boundary fault of the Bremstein fault complex (**Figure 2.22b**), while 6507/12-1 tested a roll-over structure in a graben west of this fault. Two key papers use facies analysis from these wells as a template for reconstructing the tectonic history of the area in the Permo-Triassic (Jacobsen & Van Veen, 1984; Müller *et al*, 2005).

The lowermost interval in 6507/12-2 consists of calcareous siltstones and claystones intercalated with very fine sandstones overlain by an evaporitic unit. Two 400 metre thick halites are recorded in this unit, interbedded with thin, dolomitic shales (Jacobsen & Van Veen, 1984). A restricted marine environment is suggested based on the presence of scarce microplankton (Jacobsen & Van Veen, 1984), deposited under arid climatic conditions. The two halites are separated by a 500 metre thick interval of calcareous to dolomitic shales and claystones, with few sandstones, and frequent occurrence of anhydrite throughout the sequence. A sabkha environment of deposition is suggested for this interval (Jacobsen & Van Veen, 1984). The upper evaporitic unit is overlain by calcareous claystones with a few limestones, probably of lacustrine origin, with a noticeable absence of evaporitic intervals. The gradual appearance of sandstones defines a gross coarsening upwards trend, whilst dominant claystones and siltstones become red, green and grey, suggesting a fluvial environment of deposition (Jacobsen & Van Veen, 1984). This change represents the transition from arid to humid climatic conditions (Ehrenberg *et al*, 1992) during a period of sea-level fall.

Jacobsen & Van Veen (1984) compared available stratigraphic information from East Greenland, Svalbard, Troms and the Halten Terrace to model the palaeogeographical and tectonic evolution of the North Atlantic rift during the Triassic. They concluded that the Halten Terrace experienced a different subsidence pattern relative to Svalbard and East Greenland during the late Triassic. Differences in palynological assemblages on the Halten Terrace support the interpretation that the area developed as a small, fault-bounded basin, separate from the North Atlantic rift basin, with a restricted connection to the open-sea (Jacobsen & Van Veen, 1984). High evaporation rates led to the deposition of evaporites (**Figure 2.26b**), with

hypersaline brines and pure halites deposited in the basin centre, and interbedded anhydrites and dolomites on the margins. During the middle Late Triassic (end Norian), a decrease in subsidence and a change in climate to more humid conditions led to the termination of evaporite deposition on the Halten Terrace (Jacobsen & Van Veen, 1984).

Based on detailed facies analysis of available core and well data from across mid-Norway, Müller *et al*, (2005) present a detailed study of the Permo-Triassic tectonic and sedimentological development. Their work describes a late Permian initial rift phase, an early Triassic syn-rift phase and middle to late Triassic post-rift phase with minor faulting (**Figure 2.27)**. In their model, Ladinian to Carnian evaporites are post-rift sediments infilling isolated half-grabens of late Permian – early Triassic age which produced lateral variations in the depositional thickness of evaporites. Müller *et al*'s (2005) structural model is based on the present-day thickness of evaporites on the Halten Terrace which is problematic given their nature as weak, ductile strata that deform under successive deformation or loading events.

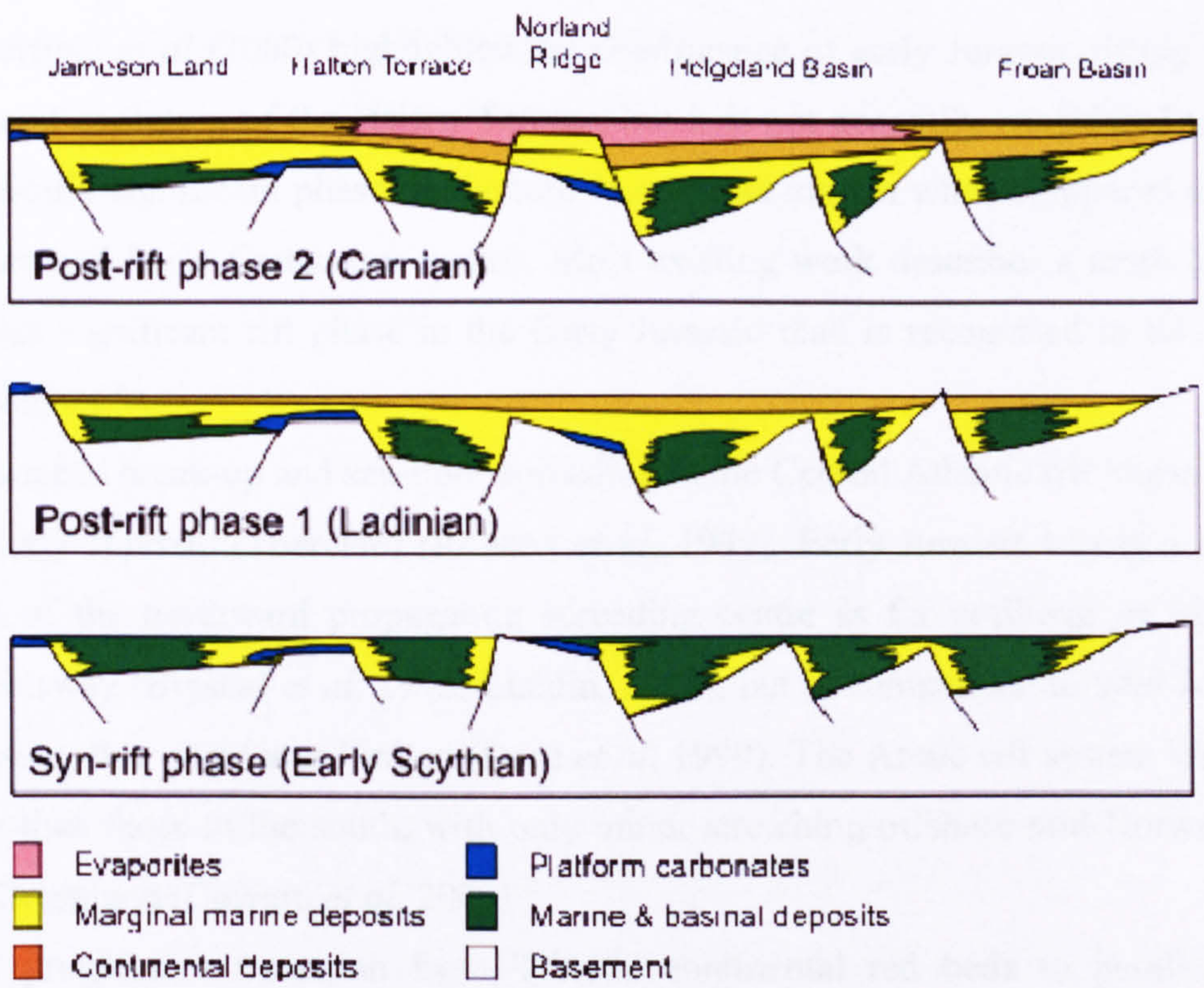

Figure 2.27: Permo-Triassic basin infill history of the northeastern part of the Proto-Atlantic region (Modified from Müller et al, 2005). Evaporites were deposited in structurally isolated basins formed during post-rift subsidence which control the present-day thickness distribution of evaporites.

2.6.3 Jurassic

The Jurassic interval has been the focus of intensive research for a number of years given its importance as the main hydrocarbon-bearing interval on the mid-Norwegian margin. Hydrocarbons are contained within five Early to Middle Jurassic sandstone formations (Åre, Tilje, Ile, Tofte and Garn) deposited in tidally influenced nearshore and braided delta front environments (Ehrenberg *et al*, 1992).

Existing work recognises the importance of Late Jurassic to Early Cretaceous rifting in the structural development of the Norwegian margin (Bukovics *et al*, 1984; Blystad *et al*, 1995; Doré *et al*, 1999; Brekke, 2000 & Skogseid, 2000). However there is considerable variation in dating the onset of earlier rift events ranging from limited Early Jurassic rifting (Blystad *et al*, 1995), significant Early Jurassic rifting (Corfield *et al*, 2000), and rift initiation in the Middle Jurassic (Gabrielsen *et al*, 1984). As a consequence of such variation in timing, further work is required to constrain the extent and duration of Early to Middle Jurassic rift events.

2.6.3.1 Early Jurassic

Corfield *et al* (2000) highlighted the significance of early Jurassic rifting in the structural evolution of the Halten Terrace, but it is not generally considered to be a tectonically significant phase on the mid-Norwegian margin when compared to Late Jurassic and Early Cretaceous events. Most existing work describes a more limited and less significant rift phase in the Early Jurassic than is recognised in this work (see chapter 3).

Pangean break-up and sea-floor spreading in the Central Atlantic rift began in the late Early Jurassic (Toarcian) (Roberts *et al*, 1999). Early Jurassic rifting occurred ahead of the northward propagating spreading centre as far northeast as offshore mid-Norway (Blystad *et al*, 1995; Lundin, 2002), but in comparison to later Jurassic extension, this event was limited (Doré *et al*, 1999). The Arctic rift system was less active than those in the south, with only minor stretching offshore mid-Norway and East Greenland (Coward *et al*, 2003)

A progressive transition from Triassic continental red beds to paralic coal-bearing sediments and coastal facies is compatible with a model of minor rifting during this interval. Müller *et al* (2005) describe the cessation of intra-basinal tectonic activity during the latest Triassic (Rhaetian) and associated with this, limited

thickness variation of sediments deposited during the subsequent tectonically quiet period, i.e. during the Early Jurassic.

A new interpretation of Early Jurassic fault activity was presented by Corfield *et al* (2000) who used isochron maps to highlight significant fault-related thickness variations across the Smørbukk and Trestakk faults, which they interpreted to have had surface breaks in their active, southern segments during the end Sinemurian to end Aalenian (Top Åre - Top Ile). Prior to this study, no major fault activity had been postulated for the Early Jurassic succession.

2.6.3.2 Middle Jurassic

By the Middle Jurassic, Pangea continued its stepwise break-up with the opening of the Central Atlantic and sea-floor spreading in the Gulf of Mexico. More locally, rifting in the North Sea was synchronous with the deposition of major reservoir units in the area (**Figure 2.26c**). Sea-level fall during the Bajocian caused rapid progradation of deltaic sediments along the Norwegian-Greenland rift and Barents Sea (Torsvik *et al*, 2002).

There is considerable uncertainty surrounding the importance of a Middle Jurassic rift event in the region. Blystad *et al* (1995) describe the Middle Jurassic, Aalenian to late Bathonian interval as a period of relatively little fault activity during a tectonically quiet episode. Gabrielsen *et al* (1984) suggest that extensional tectonics was initiated in the Mid-Jurassic, which combined with Cretaceous differential subsidence, created most of the structures described in the area, i.e. N-S, NE-SW and ENE-WSW trending normal faults. This is supported by Corfield *et al* (2000, 2001), who describe clear tectonic controls on Ile, Garn and Melke depositional patterns across Smørbukk and Smørbukk Sør, suggesting Middle Jurassic rifting intiated in the earliest Jurassic Aalenian period.

2.6.3.3 Late Jurassic

The most intense phase of rifting occurred during the Late Jurassic interval, although the precise timing of the onset of this event varies between authors as mentioned above (Badley *et al*, 1988; Blystad *et al*, 1995; Corfield *et al*, 2000; Gabrielsen *et al*, 1984; Rattey & Hayward, 1993).

By the Late Jurassic a continuous rift had evolved from the Barents Sea to the Southern North Sea. Plate motions indicate that the main rift direction was E – W

favouring the brittle reactivation of pre-existing N – S structures observed in onshore western Norway (Torsvik *et al*, 2002). Sea-level rise that commenced in the late Bathonian continued to the early Kimmeridgian, was synchronous with the deposition of organic-rich open-marine claystones (**Figure 2.26d**) and most likely marks the initiation of the latest Middle to Late Jurassic rift phase (Doré *et al*, 1999).

2.6.4 Cretaceous

Several phases of tectonic activity have been described for the Cretaceous evolution of the Norwegian Sea (Blystad *et al*, 1995; Brekke, 2000; Doré *et al*, 1999; Gabrielsen *et al*, 1999). Early Cretaceous fault patterns strongly influence the present-day structural topography of the Halten Terrace, and have led to the complete erosion of the pre-existing Jurassic stratigraphy in some parts of the region, e.g. the Nordland Ridge. Late Jurassic and Early Cretaceous events are often referred in the literature as a single event due to persistent activity on some Late Jurassic faults continuing into the Early Cretaceous on the Halten Terrace (Blystad *et al*, 1995).

Tectonics on the future Atlantic margin switched from a system dominated by N-S rift propagation to one dominated by NE-SW rifting (Mosar *et al*, 2002) (**Figure 2.26e, f**), and a rift system was established from the Rockall Trough to the Barents Sea. The Late Jurassic and Early Cretaceous rift events may have been continuous in time, but they were spatially separate events with different trends (Doré *et al*, 1999). This change in fault trend records the rotation of the regional direction of tectonic extension from E-W to NW-SE in the Early Cretaceous (Doré *et al*, 1999).

The majority of existing work attributes Cretaceous structures to periods of deep-seated crustal stretching and associated normal faulting (Blystad *et al*, 1995; Brekke & Riis, 1987; Bukovics *et al*, 1984; Doré *et al*, 1999; Gabrielsen *et al*, 1999). Active faults in the Early Cretaceous have been described in and around the Halten Terrace, e.g. the Klakk fault system generated significant footwall erosion which separated the Møre and Vøring basins from the Halten Terrace during this interval. However, Færseth *et al* (2002) demonstrate that some features said to be indicative of Cretaceous faulting can be explained without invoking tectonism, based on evidence from the northern North Sea where similar geometries and depositional profiles are included in the post-rift development of the basin.

2.7 STRUCTURAL EVOLUTION OF THE HALTEN TERRACE: EXISTING MODELS

The Mesozoic structural evolution and the mechanisms behind the development of the Halten Terrace have been widely debated in the literature. Published models which discuss the Permo-Triassic to Cretaceous structural evolution of the margin can be grouped into three end-member categories: (i) Extension and basement fault reactivation; (ii) Salt tectonics and fault-propagation folding and; (iii) Dextral and/or sinistral strike-slip movements.

Such distinctly different models for the timing and nature of deformation on the Halten Terrace exist, despite using similar datasets, due to uncertainties associated with seismic interpretation, particularly in areas of poor quality or limited data coverage, e.g. poor imaging of basement reflectors. Such ambiguity is inherent when interpreting seismic data which, in the absence of piercing points, fails to provide reliable constraints on the kinematics of the fault system, e.g. slip vectors and sense of offset. Furthermore, seismic cross sections of limited lateral extent which may omit some of the deformation on faults that lie outside the realms of the seismic survey can be interpreted in a number of ways which, in the absence of regional seismic lines, can lead to a variety of structural models for one area. The use of data from a range of scales (well data, 3D seismic, 2D regional lines and plate reconstructions) reduces such uncertainty, enabling us to build a more consistent structural models for the evolution of the area.

2.7.1 Extensional normal faulting and basement fault reactivation

Perhaps the most well documented model for the structural evolution of offshore mid-Norway describes the presence and probable reactivation of Palaeozoic detachments (Osmundsen, 2002; Brekke, 2000; Doré *et al*, 1997; Ziegler, 1975, 1986) during Mesozoic extension and normal faulting. It has been suggested that the NE-SW, N-S and NW-SE fault trends that dominate the continental margin offshore mid-Norway resemble the orientation of Palaeozoic fault patterns observed onshore to the east and that these trends were reactivated during later rift phases (Bukovics *et al*, 1984; Doré *et al*, 1997).

Doré *et al* (1997) & Skilbrei *et al* (2005) correlate NE-SW and NW-SE trending lineaments on gravity and aeromagnetic data with fault patterns mapped on seismic profiles to infer the reactivation of Proterozoic and Caledonian basement faults such as the Møre-Trøndelag Fault Zone, during Mesozoic to Cenozoic extension (**Figure 2.23**). In so doing, they concluded that the Norwegian continental margin developed by exploiting pre-existing heterogeneities associated with the structure of the Caledonian collision zone.

It is common practice to use similarities in geophysical signatures of basement rocks underlying the shelf and those exposed on land to extend basement units into offshore areas such as Mid-Norway (Skilbrei *et al*, 1995; Olesen, 1997a; Osmundsen *et al*, 2002). Butler *et al* (1997) & Holdsworth *et al* (1997) stressed the need for caution when correlating the map-trends of faults in offshore basins with structures exposed in adjacent onshore basement outcrops. Basement structures beneath offshore sedimentary basins are rarely imaged on commercial shallow seismic reflection profiles, meaning that underlying structural control is often inferred solely on the basis of trend ('geometric similarity'; Butler *et al*, 1997; Holdsworth *et al*, 1997). However, the correspondence between onshore and offshore trends does not necessarily require a basement control on Mesozoic basin development, offshore mid-Norway (Gabrielsen *et al*, 1995), although there is increasing evidence at least some Mesozoic reactivation of major onshore faults such as the More-Trondelag Fault Complex (e.g. Watts, 2002; Sherlock *et al*, 2004) and the Dalsfjord Fault (Torsvik *et al*, 1992).

Laboratory experiments on two-layer brittle-ductile models suggest that similarities between basement and cover fault patterns decoupled by a salt layer can be explained by gravity gliding over a passive residual topography inherited from the rifting stage, rather than by reactivating basement faults (Gaullier *et al*, 1993). Such models are supported by observations from the Campos Basin (Guardado *et al*, 1990) and the Gulf of Lion (Gaullier *et al*, 1993) and often overlooked in models invoking basement fault reactivation offshore mid-Norway.

2.7.2 Salt tectonics and fault-propagation folding

Elsewhere in the literature, it is generally recognised that the presence of Triassic evaporites has significantly influenced the structural development of the Halten

Terrace by mechanically decoupling Triassic and younger strata from older basement stratigraphy (Withjack *et al*, 1989; Pascoe *et al*, 1999; Withjack & Callaway, 2000; Corfield *et al*, 2000; Richardson *et al*, 2005), resulting in the development of both low-angle detachment faults and generally steeper-dipping through-going structures that cut the entire salt sequence (Jackson & Talbot, 1986; Withjack *et al*, 1989, 1990; Pascoe *et al*, 1999). Nevertheless, some workers persist in regarding the role of salt tectonics on the mid-Norwegian shelf as being less significant than in other areas, such as northwest Europe, the southern North Sea, the central North Sea and the Barents Sea, where halokinesis greatly influenced structural evolution (Gabrielsen *et al*, 1995). Comparatively, present-day diapirism is less common on the mid-Norwegian shelf where salt appears to play a more passive role as a detachment layer. As a result, the role of salt tectonics in the structural evolution of the Halten Terrace is often understated (Brekke, 2000; Bukovics *et al*, 1983; Doré *et al*, 1997, 1999).

The first work recognising the potential of salt tectonics in structuring fields and prospects on the Halten Terrace was published in the 1980's (Jackson and Hastings, 1986; Withjack *et al*, 1989). Jackson and Hastings (1986) observed a number of broad domes in the cover sequence of the Halten Terrace, e.g. the Smørbukk Sør and Njord fields, which they describe as salt-cored folds caused by the swelling of evaporites beneath the cover stratigraphy (**Figure 2.28a**). Withjack *et al* (1989) proposed an alternative interpretation in which folds or broad monoclines were described as extensional forced folds that form above normal faults (**Figure 2.28b**). Forced folds observed in field and seismic data commonly develop above steeply dipping normal faults, and in the presence of ductile units which decouple the folded strata from underlying faulted strata and basement. The formation and importance of fault-propagation folds on the Halten Terrace was highlighted by Withjack *et al* (1989, 1990 and 2000) and Corfield *et al*, 2000. Pascoe *et al* (1999) extended this model to the north where they observed similar fault-related folds at the southern termination of the Nordland Ridge. Despite this, many recent papers describe the presence of a 'salt dome' beneath the Jurassic cover of the Smørbukk Sør field, but do not discuss fault propagation folding as a mechanism for their formation (Caselli, 1987; Martinius *et al*, 2005).

The impact of Triassic evaporites on the timing of active faulting within the cover sequence is also debated, particularly during the Cretaceous. Most workers

attribute Cretaceous structures, the majority of which are mapped on the platforms and terraces in the east, to periods of deep-seated crustal stretching and associated normal faulting during the Early Cretaceous (give example references). Færseth *et al* (2002) propose an alternative model whereby the majority of these faults are related to the mobility of Triassic evaporites rather than Cretaceous extension.

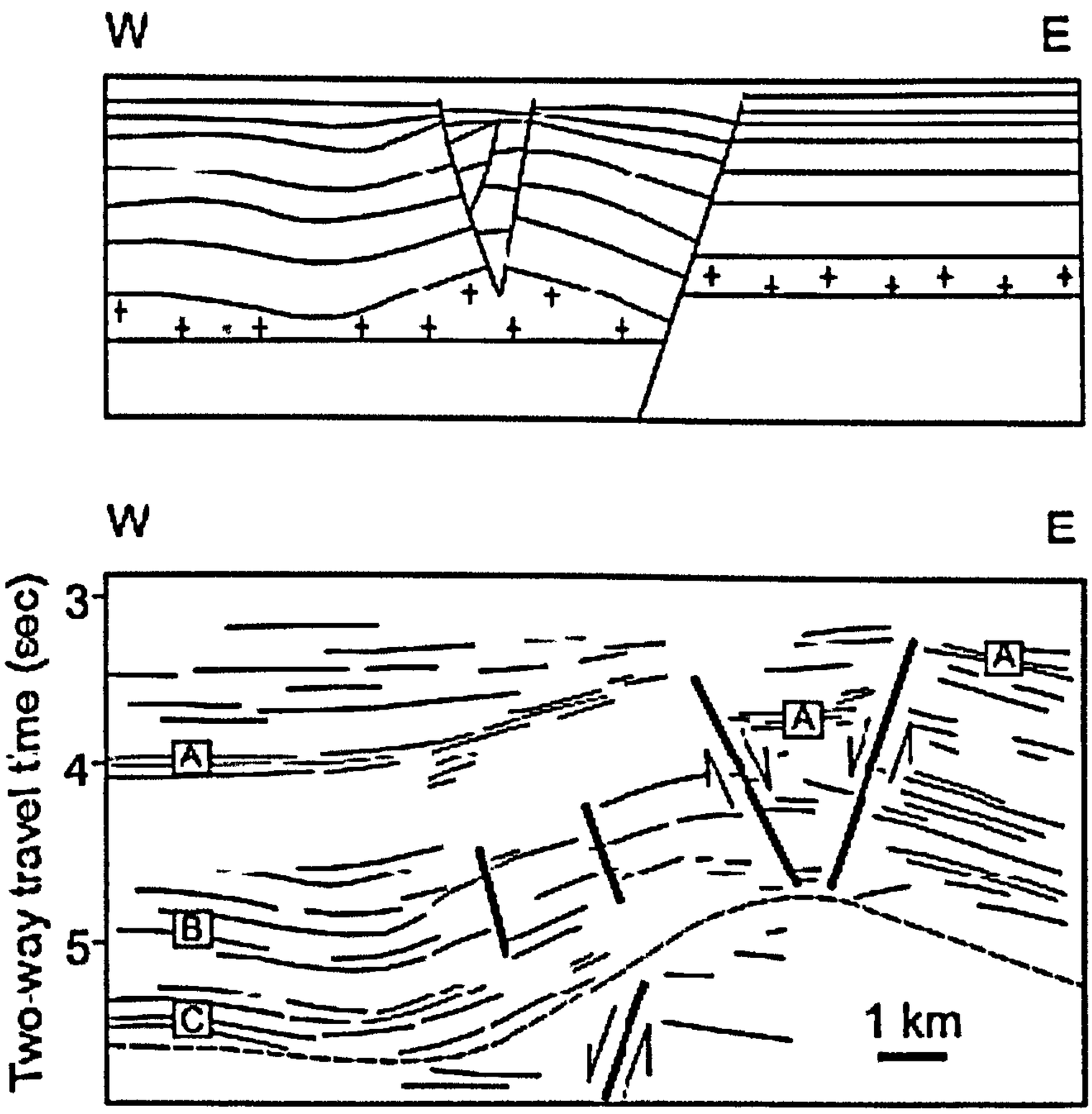

Figure 2.28: Contrasting interpretations of salt-related deformation on the Halten Terrace (a) Salt pillow development as proposed by Jackson & Hastings (1986). Redrawn from Jackson and Hastings, 1986) (b) Extensional fault-propagation fold developed above a blind basement fault in the presence of a ductile layer (Withjack et al, 1989) where A = Base Cretaceous, B = Top Salt and C = Base Salt reflectors

2.7.3 Strike-slip tectonics

A number of papers in the 1980's sought to explain some of the observed structures offshore mid-Norway in terms of strike-slip tectonics along NE-SW pre-existing basement grains.

Gowers and Lunde (1984) describe wrench-related structures in the Trænabanken area of Oligocene age, which they conclude were a result of spreading

reorganisations in the Atlantic, an idea supported by Brekke and Riis (1987) based on their interpretation of mid-Cenozoic inversion structures in the Vøring Basin. Gabrielsen and Robinson (1984) added that wrench-movements could have started as early as the late Mesozoic.

Perhaps the most extreme view was taken by Caselli (1987) who describes large-scale, deep-seated dextral strike-slip movement as the dominant structural style along specific lineaments during the Late Jurassic to Cretaceous structural evolution offshore Mid-Norway. Within this setting, the rhomb-shaped Halten Terrace was interpreted as a pull-apart basin associated with a releasing bend (**Figure 2.29**) on which Caselli (1987) describes negative flower structures. These same structures had previously been interpreted as salt-related features by Jackson and Hastings (1984) **(Figure 2.28a)**.

Caselli (1987) presented evidence in support of dextral strike-slip tectonics including faults characterised by horizontal displacements, complex sinuous fault zones made up of branching and anastomosing faults and the development of folds implying both compressional and extensional strains characteristic of strike-slip tectonics (**Figure 2.29**). Færseth *et al* (2002) disagree with Caselli's (1987) interpretation given that subsequent work has shown that faults showing evidence of wrenching are rare. In particular, the absence of piercing points to support the interpretation of large-scale horizontal displacements and the absence of restraining/releasing bends along faults at high angle to the suggested strike-slip movements suggests that such models are unlikely to be correct.

Interestingly, Caselli's (1987) work also suggests that salt flow due to mobilisation of Triassic evaporites during the Late Jurassic and throughout the Cretaceous was a feature of the Halten Terrace, lending support to Færseth *et al*'s (2002) later models of salt-related faulting.

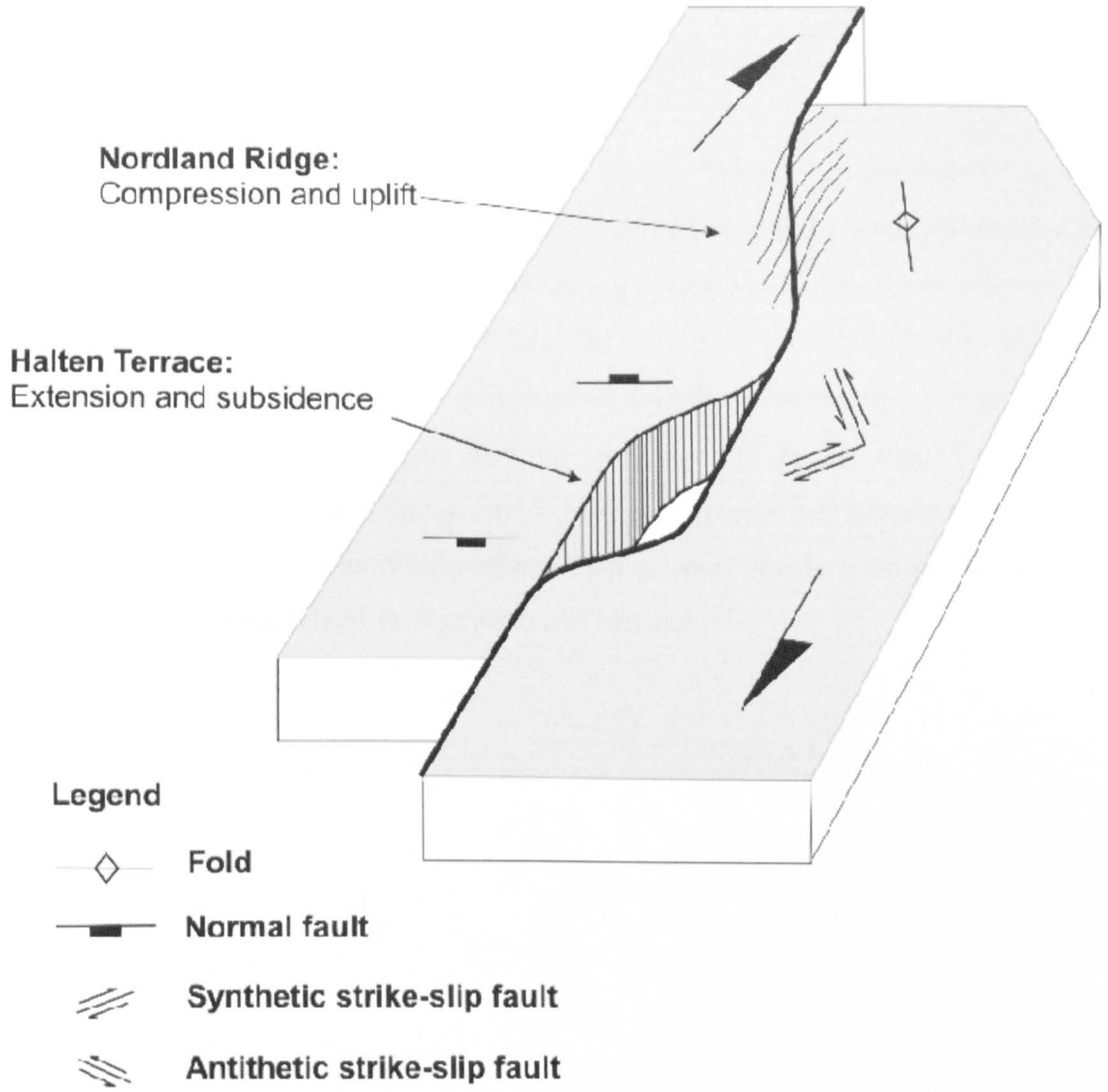

Figure 2.29: Dextral strike-slip movement on a sinuous fault producing a pull-apart basin (Halten Terrace) close to compressional uplift (Nordland Ridge). (Modified from Caselli, 1987).

The following chapters of the thesis use the existing research described as background information to support new results and hypotheses, which are presented in three chapters as follows;

- A new, regionally consistent structural framework for the Halten Terrace is established from the Permo-Triassic to the Early Cretaceous, and a new model for the structural evolution of the area is proposed. The results presented are based on thickness variations within these intervals that are used to constrain the onset and duration of growth across syn-sedimentary faults and fault-propagation

folds. Existing structural models for the evolution of the Halten Terrace are challenged and a new interpretation of the rift history prior to well-documented Jurassic events is presented

- Observations of structural styles on the Halten Terrace are presented and the dominant mechanisms controlling the degree of coupling between basement and cover faults is discussed. The results are supported by existing knowledge of the unique mechanical properties of salt, the results of analogue models and the interaction between thick- and thin-skinned extensional tectonics.
- Finally, a conceptual model for the evolution of faults which undergo a component of thick- and thin-skinned tectonics is presented. Results are based on the 3-D geometry of the fault surface, displacement-length profiles and existing knowledge of models of fault growth and linkage.

CHAPTER 3

3: Structural evolution of the Halten Terrace, offshore Mid-Norway: new insights into fault growth in a brittle-ductile system and implications for hydrocarbon prospectivity

3.1 INTRODUCTION

There are currently 52 fields in production on the Norwegian continental shelf, ranking Norway as the fifth largest oil and third largest gas exporter in the world. To date, approximately 35 percent of the predicted total hydrocarbon resources on the Norwegian continental shelf have been produced (NPD, 2007), leaving much scope for further field development. However, many parts of the Halten Terrace (**Figure 1.1**), which has been the most prolific hydrocarbon province in offshore mid-Norway (Koch & Heum, 1995), are now considered mature (NPD, 2007).

Historically, production on the Halten Terrace has been dominated by a few large fields (e.g. Smørbukk and Heidrun) but, with production now in decline, several other fields are presently in early development and appraisal (e.g. Morvin, Tyrihans, Lavrans), resulting in distributed production over a larger number of often deep, challenging or marginal fields. A more distributed production profile, with ventures into less familiar areas increases the uncertainties associated with drilling and calculating recoverable reserves from new fields. Current forecasts therefore predict a gradual decline in production from the Norwegian continental shelf over the next decade (NPD, 2007). The aim of this study is to develop a regional structural and stratigraphic framework for the Halten Terrace, which may help to optimise recovery and increase the lifespan of production from existing fields whilst potentially opening up new developments.

Despite its status as an important hydrocarbon province, there are substantial differences in the published structural models for the Mesozoic development of the Halten Terrace, with disagreements on the kinematics, timing and causes of deformation. Three end-member models for the Permo-Triassic to Early Cretaceous evolution of the area have been proposed: (1) extension and basement fault reactivation (e.g. Ziegler, 1975, 1986; Bukovics *et al*, 1984; Doré *et al*, 1997; Brekke, 2000; Osmundsen, 2002; Skilbrei *et al*., 2005); (2) salt tectonics and fault propagation folding (Withjack *et al*, 1989; Pascoe *et al*, 1999; Withjack & Callaway,

2000; Corfield *et al*, 2000; Richardson *et al*, 2005); and (3) strike-slip tectonics (e.g. Caselli, 1987). The precise timing of deformation is also contentious. Several authors regard the principal extensional event as being Late Jurassic to Early Cretaceous in age (e.g. Bukovics *et al*, 1984; Brekke & Riis, 1987), but interpretations of the onset of Jurassic fault activity also include limited Early Jurassic rifting (Blystad *et al*, 1995), major Early Jurassic rifting (Corfield *et al*, 2000) and rift initiation in the Middle Jurassic (Gabrielsen *et al*, 1984). Each model has significantly different implications for the timing and distribution of active faults, and thus depocentre development and hydrocarbon potential in the area.

This ambiguity in the timing and kinematic significance of deformation on the Halten Terrace has arisen from the tendency of some previous workers to focus on the Jurassic reservoir interval at the expense of the pre- and post-Jurassic strata. In this paper, it is shown that a more holistic approach is essential as the presence of evaporites can facilitate gravity-driven deformation and/or decouple tectonic faults in the pre-evaporite "basement" from those in the post-evaporite cover. Both these effects can give rise to complex and apparently unrelated deformation patterns within basement and cover strata. A specific objective of this study is, therefore, to constrain the spatial and temporal evolution of faulting within the entire Permo-Triassic to Cretaceous interval on the Halten Terrace, with a particular focus on deformation within the lesser known Permo-Triassic to Middle Jurassic sequence.

Well data is integrated with structural and stratigraphic interpretations of a high-quality 3D seismic dataset from the Åsgard area (see below) and regional knowledge derived from interpretations of 2D seismic lines. Crucially, these seismic datasets image faults and horizons within the sub-evaporite basement. These interpretations have allowed us to develop a new structural model which considers the relative contributions and impacts of basement faulting, gravity sliding and salt tectonics on the development of the Halten Terrace. Additionally, the model provides new constraints on fault activity during the deposition of Early and Middle Jurassic (Åre, Tilje, Tofte, Ile and Garn Formations) and earliest Cretaceous (Lange and Lysing formations) reservoir sands. Identifying faults that were active during reservoir deposition provides a much-improved method of predicting and interpreting reservoir distribution and quality.

3.2 TECTONIC SETTING & STUDY AREA

No record of the pre-Jurassic rift events can be seen on seismic data from the Halten Terrace. Here, the seismic data show that the Permo-Triassic basement rocks are overlain by a thick sequence of Triassic evaporites, which separate the basement from Jurassic-Cretaceous cover. As a result of multiple rift episodes and salt-related deformation, the Halten Terrace is characterised by a complex fault pattern. The dominant structural trend is NE-SW. N-S trending faults bound the eastern and western margins of the Halten Terrace, whilst a subordinate set of NW-SE and E-W trending faults is local to the centre of the terrace (**Figure 2.22**).

The results presented here are based on the interpretation of data from the Åsgard area, a region of approximately 1400 km^2 covering the Smørbukk and Smørbukk Sør hydrocarbon fields (**Figure 2.22 & 2.24**) in the north-western part of the Halten Terrace. The area is strongly influenced by salt-related extension and is characterised by dominantly NE-SW trending normal faults that display westerly dips and both planar and listric geometries (**Figure 2.24a**). Two structures, the Smørbukk and Trestakk faults, and a major NE-SW trending fold dominate the region.

The Smørbukk field lies in the crest of a Jurassic fault block that is bound to the west by the Smørbukk fault and to the north by an east-west trending graben that transects the crest of the fault block (**Figure 2.24**). Most fields on the Halten Terrace reside in the footwall crests of tilted fault blocks similar to the structural setting of the Smørbukk field (e.g. Trestakk and Midgard fields). One exception is the Smørbukk Sør field which is located on the crest of a complexly faulted domal structure to the south-east of the Smørbukk field, reported to have developed from a combination of lateral salt movement and the doming of block-faulted stratigraphy during the Late Jurassic (Jackson & Hastings, 1986; Martinius *et al*, 2005).

3.3 DATA AND METHODOLOGY

The 3D seismic data set used in this study was selected based on its high-quality and optimal orientation with respect to the main fault trends. The survey covers an area of 1400 km^2 and has a line spacing of 12.5m. Horizons and faults were interpreted manually every 20 lines across the entire survey and every 10 lines around fault tips. The seismic data, which has its vertical axis in two-way travel time (TWTT), has not

been depth-converted and so the cross sections and isochron maps in this study are presented with the vertical axis in time.

63 wells (Appendix 5 & 6) have been integrated with the seismic data to constrain the stratigraphic ages of the horizons down to the Early Jurassic Åre Formation (**Figure 2.25**). Where possible, seismic horizons were defined at trace positions (peak, trough, zero-crossing) that tied most closely with formation tops from well data (Appendix 5 & 6). None of the wells within the Åsgard area penetrate below the Åre Formation, so there is increased uncertainty associated with the stratigraphic age of older horizon interpretations. Two wells approximately 50km northwest and west of the Åsgard area penetrated two intervals of Triassic evaporites (Jacobsen & Van Veen, 1984) providing constraints on the nature of seismic reflections from the top salt interval (Appendix 7.3). Reflectors were traced along 2D regional seismic lines to aid interpretations in the Åsgard area. The Smørbukk fault is the only fault with well constraint in both the footwall and hangingwall. The well picks show a marked thickening of the Early Jurassic (Åre Formation) to Base Cretaceous Unconformity (BCU) interval across this fault from footwall to hangingwall (Appendix 7.1 & 7.2).

To constrain the timing of movements on individual faults, the Permo-Triassic to Early Cretaceous interval was divided into twelve regionally mappable seismic stratigraphic marker horizons which bound eleven stratigraphic intervals (**Figure 2.25**). Thickness variations within these intervals constrain the onset and duration of growth (e.g. Childs *et al.*, 1993, 1995, 2003) across two types of syn-sedimentary faults that cut basement (pre-Jurassic) strata: (i) emergent faults, which intersected the free surface at the time of activity; and (ii) blind-faults that were active beneath the evaporite layer leading to the development of fault propagation folds. The latter group of faults did not intersect the free surface at the time of folding. Active emergent faults were identified based on the recognition of reflector geometries that define distinct syn-rift wedges (Prosser, 1993). Rift-related sedimentary wedges commonly thin onto the crests of fault blocks, where truncation and onlap are observed. Reflectors diverge and thicken down dip from the footwall crest and towards the adjacent bounding fault (**Figure 1.3a**).

Markedly different structural characteristics define blind faults where fault propagation folds associated with the development of a buried fault tip (**Figure 1.3b**). They comprise typically upward widening zones of distributed deformation

with anticlinal and synclinal bends that form above blind normal faults (Withjack & Callaway, 2000). Reflectors diverge into the hangingwall depocentre at a point offset into the hangingwall of the basement fault trace and onlap onto the limb of the anticline (Gawthorpe *et al*, 1997) (**Figure 1.3b**). Thus, the location of the hangingwall depocentre can be used to distinguish emergent faults from those with a buried tip.

Isochron maps show changes in the vertical time difference between two horizons and are calculated by a simple subtraction of one horizon from the other. Isochron maps for successive intervals can therefore be used to investigate changes in the spatial distribution of stratal thickness – and therefore active faulting - throughout rifting. However, in order to make a valid analysis, it is important to be aware of the assumptions and measurement errors associated with this method. Interpretations of across-fault thickness variations can be applied only where sedimentation rates exceeded, or were comparable to fault displacement rates (e.g. Childs *et al*. 2003), a condition which is likely valid on the Halten Terrace. Evidence to suggest relatively rapid fault displacement rates such as the formation of fault scarps, the underfilling of hangingwall basins and the erosion of uplifted footwalls is generally not observed in the area, with the exception of extensive erosion associated with the development of the BCU which is accounted for when interpreting thickness variations.

The process of calculating time-thickness maps can also lead to misinformation about thickness changes for a given interval. Isochron maps measure vertical time thickness (T_{vert}, in seconds) between two surfaces regardless of their dip. Thicknesses can be overestimated where beds are strongly tilted, i.e. in the footwall and hangingwall of faults, relative to areas of gentle dip, i.e. $T_{vert} > T_{true}$ (**Figure 3.1a**). As a result, steeper dipping beds will have overestimated thicknesses relative to those with gentler dips. Hence time thickness deviations across a fault trace may not be indicative of growth, but reflect instead changes in the relative vertical thickness of an interval due to variations in stratal dip. The same problem applies when measuring thickness changes across folds where beds steepen from the fold hinge zone into the limbs resulting in apparent thickness changes across an interval of constant thickness (**Figure 3.1b**). Inaccuracies in the analysis have been minimised by using cross-sections and displacement profiles to visually verify whether changes

in vertical thickness reflect true variations in stratigraphic thickness rather than being due to changes in dip.

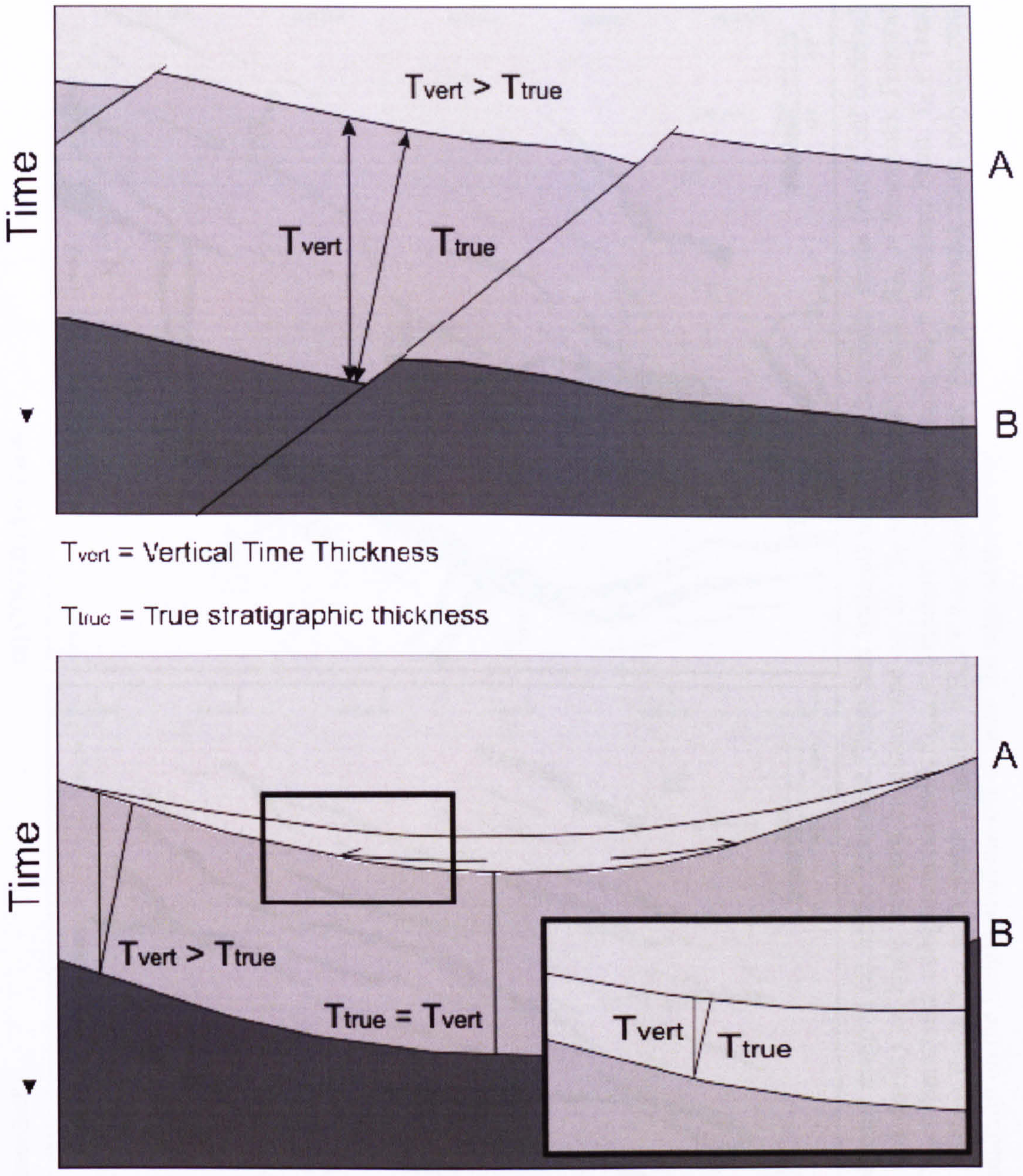

Figure 3.1: (a) Sampling the vertical time thickness of an interval leads to an overestimation of the 'true' thickness of beds in the hangingwall of a tilted fault block, the same occurs in the footwall. Across fault measurement errors occur if the footwall and hangingwall beds dip at different angles; (b) An overestimation of 'true' thickness also occurs in synclines where beds dip at a higher angle towards the limbs of the syncline than near the axis where $T_{vert} = T_{true.}$ An interval of equal thickness will show apparent growth towards the limbs of the syncline (A to B). Similarly, an underestimation of the change in thickness across a syn-folding interval will occur due to an overestimation of thickness on its limbs (inset).

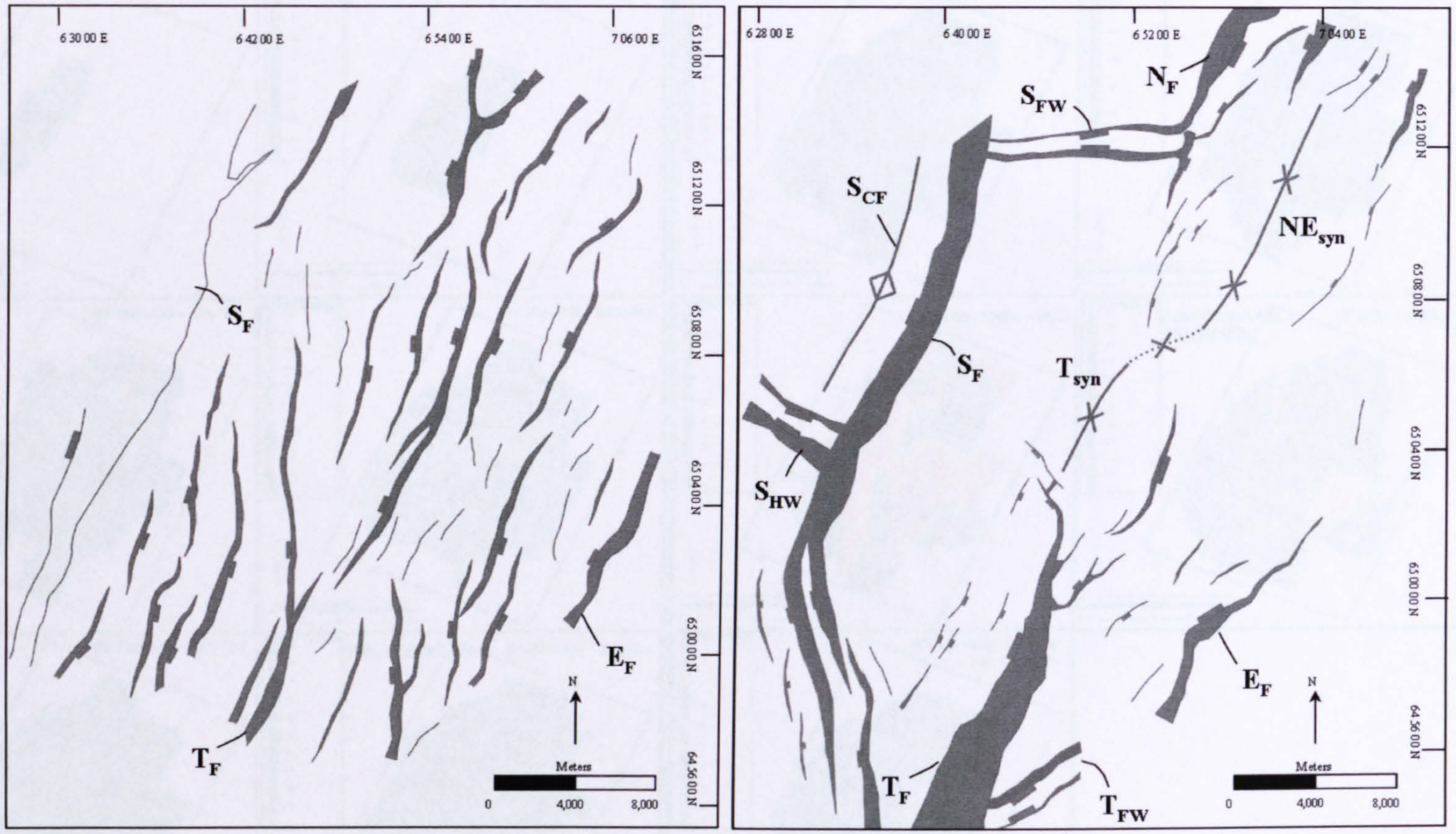

Figure 3.2: Present-day fault polygons mapped (a) in the basement (Base Salt horizon) and (b) in the cover strata (Åre Coal horizon) showing a clear upward decrease in the number and density of faults between basement and cover. S_F = Smørbukk Fault, S_{FW} = Smørbukk Footwall Graben, S_{HW} = Smørbukk Hangingwall Graben, S_{CF} = Smorbukk compressional fold, S_{South} = Smorbukk southerly trace, N_F = Northern Fault, T_F = Trestakk Fault, T_{FW} = Trestakk Footwall Graben, E_F = Eastern Fault, T_{syn} = Trestakk syncline, NE_{syn} = Northeast syncline. The Smørbukk fault polygon remains unshaded at basement level due to a lack of constraint on the hangingwall cut-off close to the edge of the survey.

Missing pages are unavailable

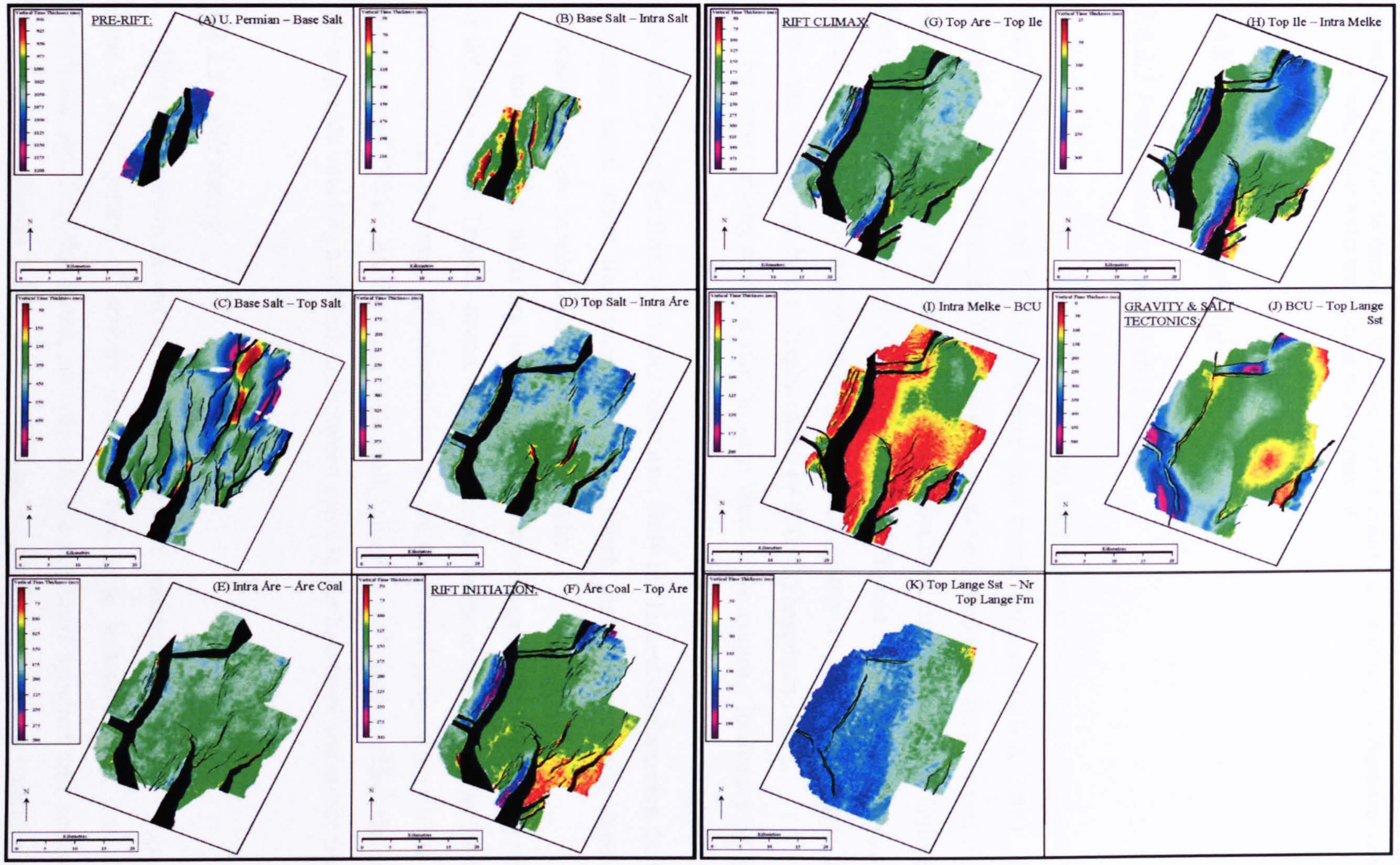

Figure 3.5: Figure caption on following page.

Figure 3.5: Time-thickness maps for eleven stratigraphic intervals used to constrain the timing of fault and fold growth from the Upper Permian to Early Cretaceous (see Figure 2 for seismic stratigraphic intervals). Thickness changes across A, D & E are due to measurement errors associated with calculating the vertical thickness of intervals. B & C represent thickness changes within the salt layer which we suggest records the passive flow of evaporites in response to Jurassic rifting. F records the onset of fault growth during rift initiation. Faults remained active during the remaining intervals (G – K). Note, colour scales are different for each interval.

3.4.2 Rift Initiation: Early Jurassic

3.4.2.1 Fault geometry and distribution

In map view a clear NE - SW fault trend dominates in the cover sequences, with local ENE - WSW and N - S subsidiary fault trends (**Figure 3.2b & 3.8F**). Fault orientation plots indicate a 10° rotation of mean fault strike towards the east (029°), and a larger spread in the mean orientation of faults relative to basement faults (53°, **Figure 3.3b**). The dominant NE - SW trend is followed by a few, large, regularly spaced faults, with an average spacing of approximately 11 km. These major faults follow the trend of the largest displacement (> 400 ms) basement faults.

The most striking characteristic in map view is the contrast in density of faults above and below the salt, with far fewer faults in the Jurassic cover sequence than faults offsetting the Permo-Triassic basement. Only the largest displacement faults at basement level offset the entire salt layer, which therefore generally decouples extension between basement and cover stratigraphy.

In cross section, faults are both planar and listric in geometry terminating within or detaching upon Triassic evaporites and in many cases extending above the Base Cretaceous Unconformity. Displacements at Åre Coal level range from 40 ms to a maximum of 700 ms on the Smørbukk fault, which is sufficient to offset the entire salt sequence enabling hard-linkage between some larger basement and cover faults.

3.4.2.2 Fault timing

Thickness variations within the Early Jurassic interval (Åre Coal – Top Åre) show a clear pattern of activity across a few large structures, e.g. across the Smørbukk and Trestakk faults, growth into the northeast syncline and across the Northern fault (**Figure 3.5F**). Cross sections through these structures typically show

divergent reflectors, wedge-shaped packages (**Figure 3.6**) and thicker intervals in the hangingwalls of active faults relative to the footwall (**Figure 3.7, 3.11**). Activity migrated to the north on the Trestakk fault and southwards on the Smørbukk fault until the faults overlapped by 2 - 3 kilometres in map view (**Figure 3.5F**).

Divergence of reflectors into the syncline in the northeast (**Figure 3.8**) reflects subsidence in response to movement on underlying basement faults. Further to the

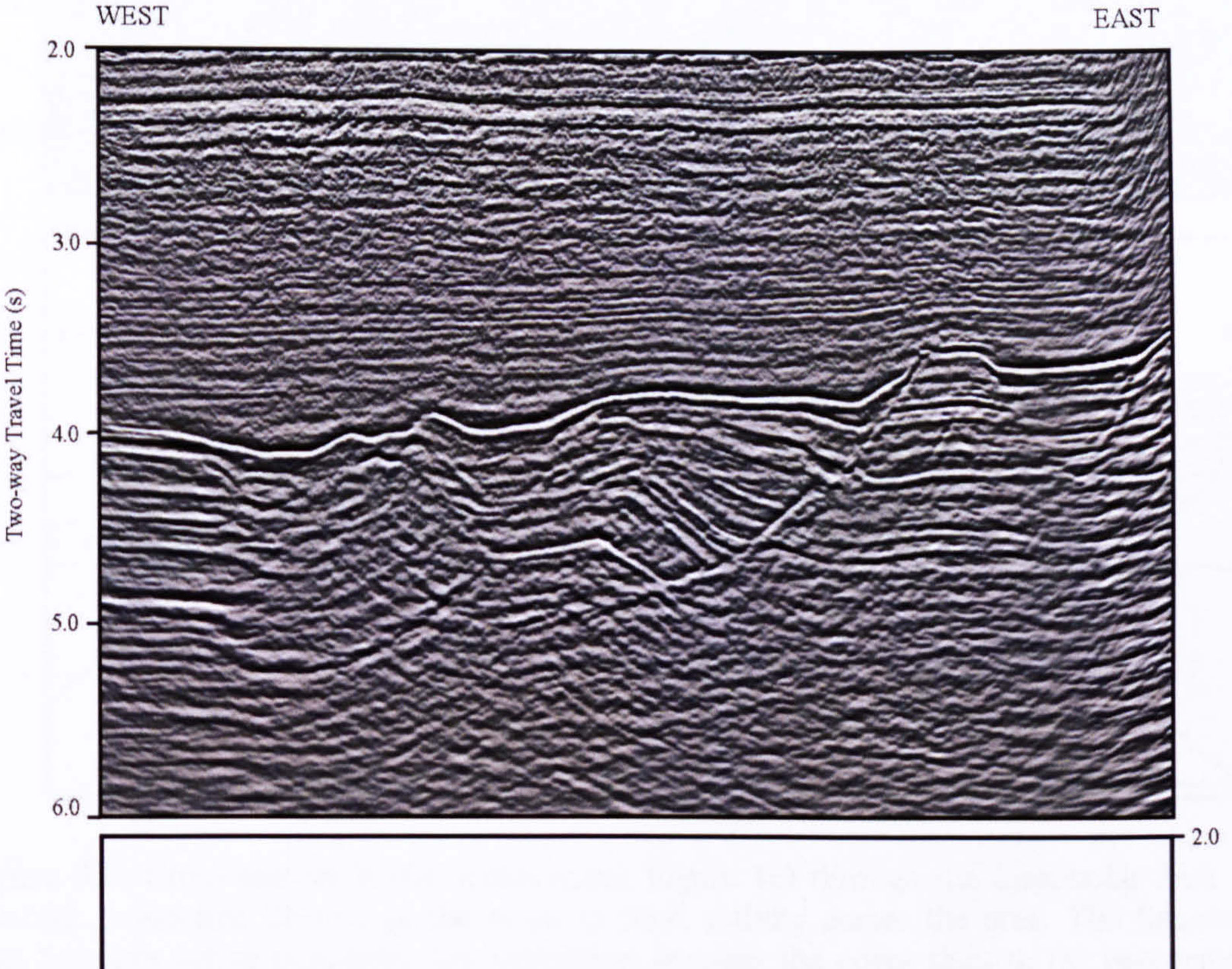

Figure 3.6: Cross section D (see Figure 1c for location) across the south of the Trestakk fault, an area of complex interaction between basement-cover faulting, gravity sliding and salt diapirism. Pink shaded area highlights the period of salt withdrawal indicated by thickening above the footwall of S_{south}. See Figure 5 for fault annotations. Key to seismic marker horizons and intervals are shown in Figure 2.

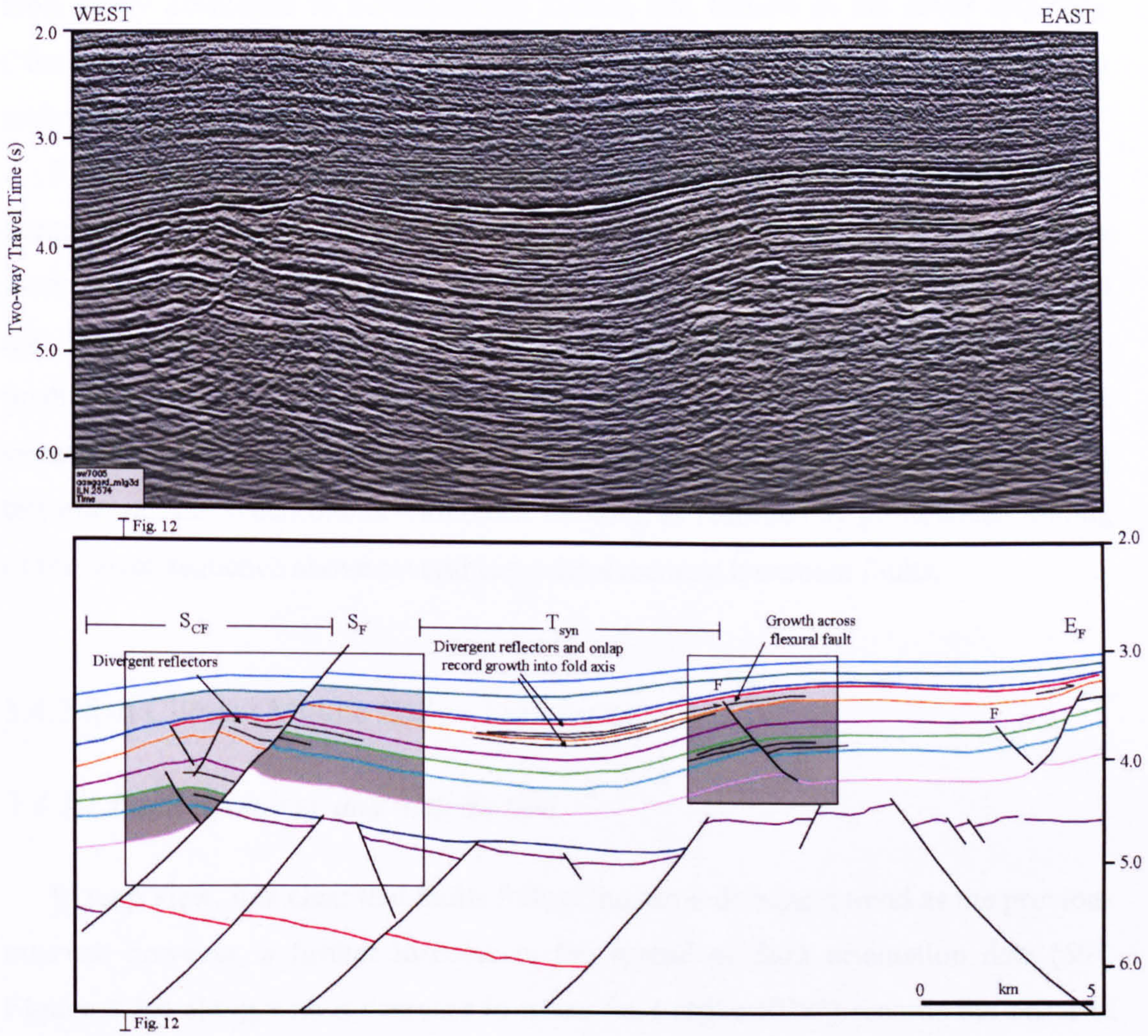

Figure 3.7: Cross section B (for location see Figure 1c) through the Smørbukk fault and Trestakk monocline illustrating the onset of fault activity across the area. The Smørbukk fault becomes active post-Intra Are deposition whereas the cover fault to the east remains inactive until post-Top Ile deposition, synchronous with the development of the cover monocline above a basement horst. See Figure 5 for fault and fold annotations, F = flexural fault. Key to seismic marker horizons and intervals are shown in Figure 2.

east, thinning across the footwall of the Trestakk fault and over Smørbukk Sør records uplift above an active basement horst block.

A number of small displacement en echelon faults which offset this interval have their displacement maxima within the Early Jurassic Åre Coal horizon and are restricted to Early Jurassic stratigraphy, dying out up sequence. In plan view, the faults are distributed around the margins of the present-day north east syncline, in the hangingwall of the Smørbukk and Trestakk faults and across Smørbukk Sør (**Figure 3.5f)**. A large number of small faults may reflect the initial stages in the evolution of a fault population, prior to strain localisation onto a few, large faults. However, the restricted distribution of these faults in areas of subsidence and flexure suggests they

most likely developed to accommodate folding and flexure in the cover sequence ('flexural faults', F, **Figure 3.7, 3.11**) in response to localisation of displacement on underlying basement faults.

Fault activity during the Earliest Jurassic (Åre coal – Top Åre) is well defined, constraining the onset of fault activity to be earlier than suggested by previous workers (Corfield *et al*, 2000). Activity was localised on a few, large structures and not distributed over a large number of small displacement faults contrary to the predictions made by some models of fault growth and strain localisation in brittle systems (e.g. Cowie and Scholz, 1992a,b). Basement fault activity initiated during this interval, i.e. synchronous with cover faulting, as recorded by pronounced folding of the cover sequence above several large displacement basement faults.

3.4.3 Rift Climax: Middle Early - Late Jurassic

3.4.3.1 Fault geometry and distribution

In map view, it is clear that faults follow the same dominant trend as the previous interval; however, a further increase in the spread of fault orientation data (59°, **Figure 3.3c**) along with a decrease in mean fault strike (028°) records the onset of growth across new structures oblique to the dominant basement fault trend.

3.4.3.2 Fault timing

The Middle Early to Late Jurassic interval is sub-divided into three seismic stratigraphic units that best define the onset and duration of rift climax in the area. Formation tops from well data have been used to constrain the interpretations during this interval.

Activity becomes focussed on a few structures during rift climax, with growth into the hangingwalls and pronounced thinning of sediments across the footwalls of the Smørbukk and Trestakk faults (**Figure 3.5G, H, I**). Activity migrates northwards with time across the Trestakk fault, which curves towards the Smørbukk fault, and southwards across the Smørbukk fault resulting in the widening of depocentres in their hangingwalls and the development of a more pronounced south-westerly

dipping ramp between the increasingly overlapping fault traces (by up to 10km) **(Figure 3.5G)**.

In cross-section, distinct wedge-shaped packages of divergent reflectors are developed in the hangingwalls of major active faults from the Top Åre to BCU intervals **(Figures 3.9 & 3.10)**. During the same period, the northeast syncline remains an area of active subsidence, with the growth and divergence of sediments into the axis of the syncline, and growth continued across the Northern fault **(Figure 3.8)**. The initiation of growth across the Trestakk syncline is recorded by thickness changes into the axis of the syncline during Top Åre to Top Ile deposition **(Figure 3.5G, 3.10)**.

The Trestakk fault continues to propagate north during the Top Ile to Intra Melke interval extending across the northern branch of its splaying tip **(Figure 3.5H)**. Synchronous with this, ongoing lateral migration on the Smørbukk fault results in the maximum overlap of the faults (up to 15 km) without breaching the overlap zone, which remains intact to the present day. Well-developed growth along the axis of a pronounced NE-SW trending syncline ahead of the propagating buried tip of the Trestakk fault is recorded by onlap and growth into the hinge zone of the underlying fold **(Figure 3.7)**, and activity initiates across cover faults which develop on the limbs of the fold, due to flexure of strata during folding **(Figure 3.7)**. The uplifted area to the east of the Trestakk fault is the crest of an anticline which sits above an area of uplifted basement faults **(Figure 3.7)**.

The initiation of growth across the Smorbukk hangingwall graben, which formed oblique to the main fault trend, leads to an increase in the spread of fault orientations during this interval **(Figure 3.3c)**. Vertical displacement profiles suggest that both graben-bounding faults initiated post-Ile formation deposition **(Figure 3.9)**. Furthermore, it is worth noting the development of a compressional fold which initiated in the hangingwall of the Smørbukk fault synchronous with growth across the hangingwall graben. The interval thins across, and onlaps onto the crest of the fold **(Figure 3.7)**, which runs parallel to the trace of the Smørbukk fault **(Figure 3.2)**, whilst thickening occurs over the fold limbs and into the immediate hangingwall of the fault, which remains active during this interval. It is suggested that the fold is a gravity-driven compressional feature that formed above an inclined salt surface **(Figure 3.7)**, with up-dip gravitational slumps on its western flank. Evaporites flow

into space created in the hangingwall of the fault which initiates down-slope gravitational collapse of the overlying cover sequence.

The Upper Jurassic (Intra Melke to BCU interval) is bound on its upper surface by an extensively mappable erosional surface (the BCU). Footwall uplift and erosion during this interval must be taken into account when interpreting relative thickness changes across faults. Erosion and thinning of strata in the footwall of the Smørbukk fault is particularly prominent, migrating north across the present-day Smørbukk footwall graben (**Figure 3.5I**), which remains inactive during this interval. Survey-wide fault activity remains the same with the addition of growth across the Eastern fault (**Figure 3.5I**). However, erosion of the Upper Jurassic sequence in the footwall of the fault makes interpretations of thickness changes across faults during this interval impossible. The most striking development is the erosion and thinning of sediments in the footwall of the Smørbukk, Trestakk and Eastern faults and across Smørbukk Sør and the compressional fold in the hangingwall of the Smørbukk fault (**Figure 3.5I**), which has implications for the removal of important reservoir sands.

Regionally during rift climax, extensional tectonics remains localised on the same few structures whilst more pronounced growth into subsiding fault propagation folds and the progressive development of more widespread depocentres in the cover records ongoing, and more localised growth across faults in the sub-salt basement. The basement surface at depth becomes progressively tilted during ongoing sub-salt extension, resulting in salt movement and the onset of gravity sliding in the hangingwall of the Smørbukk fault, recorded by the growth of structures oblique to the maximum extension direction. Extensive erosion, which removes Middle and Upper Jurassic stratigraphy across large parts of the area, marks the culmination of rift climax in the area.

3.4.4 End of rifting, gravity-sliding & salt withdrawal: Early Cretaceous

Over the past decade, Cretaceous sediments have become increasingly important in the exploration for hydrocarbons in the Norwegian Sea (NPD, 2007), with more companies turning their attention to post-rift plays. Cretaceous sands are generally thin and isolated and thus difficult to locate. For this reason a detailed understanding of the interplay between tectonics and sedimentation during the Cretaceous is required to constrain the distribution of sands across the area.

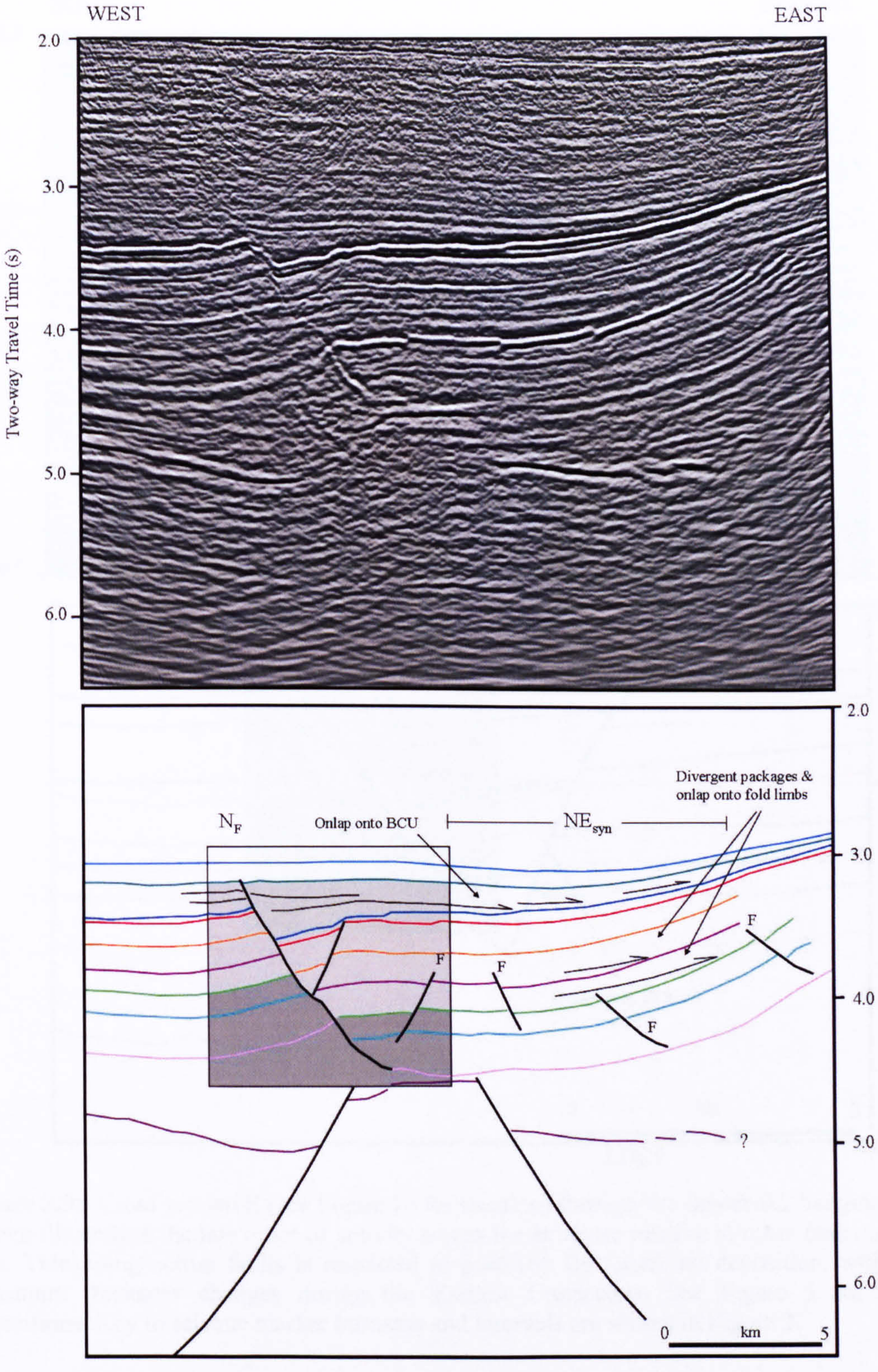

Figure 3.8: Cross section C (for location see Figure 1c) through the Northern fault and adjacent northeast syncline. Growth across the northern fault initiates post-Åre Coal deposition continuing until Top Lange Sandstone deposition in the Early Cretaceous. Onlap and thinning onto the Base Cretaceous Unconformity in the east supports our interpretation of ongoing tectonic activity until at least Early Cretaceous Top Lange Sandstone deposition, with thinning of the subsequent succession suggesting activity continued synchronous with Near Top Lange Formation deposition. See Figure 5 for fault and fold annotations. Key to seismic marker horizons and intervals are shown in Figure 2.

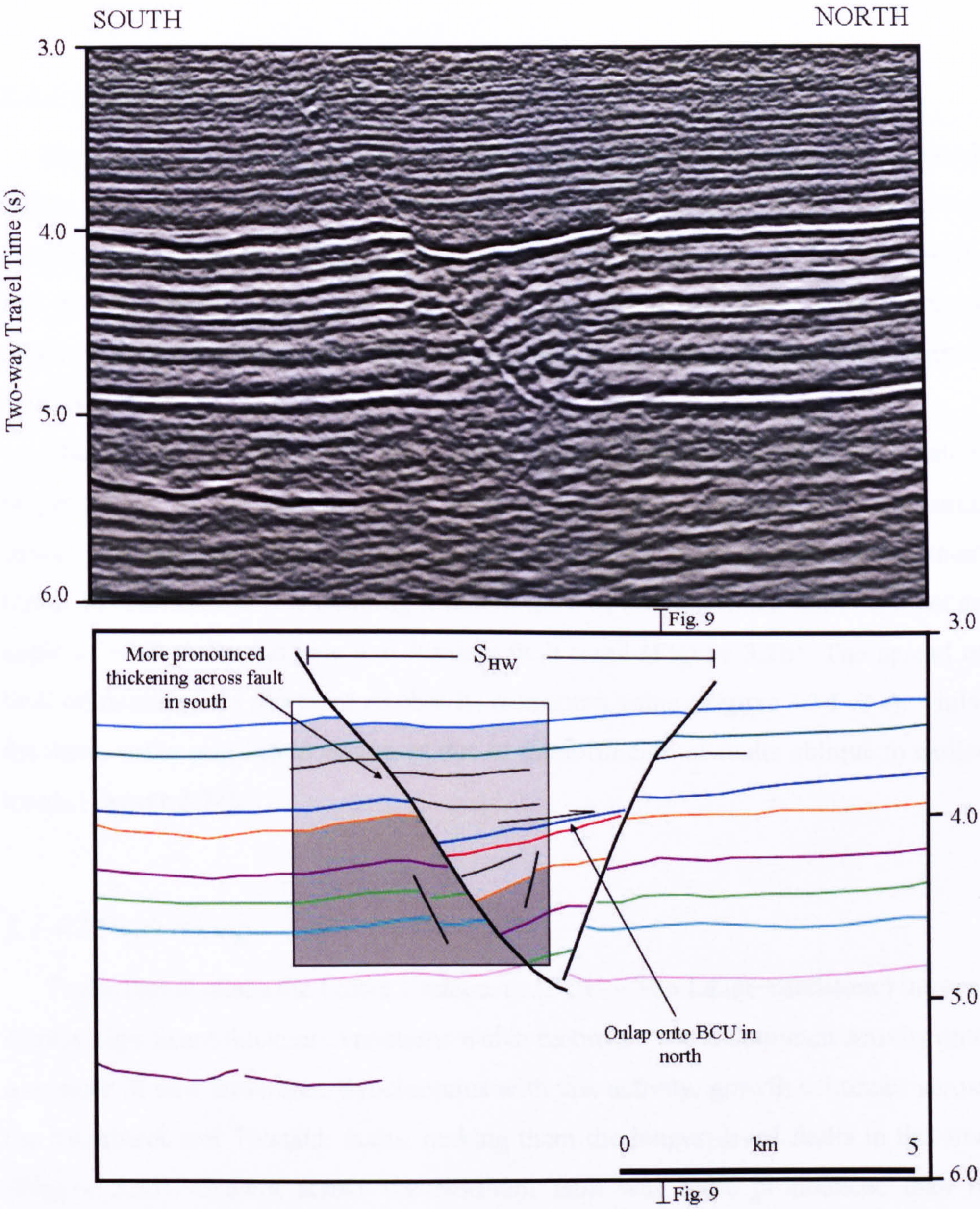

Figure 3.9: Cross section E (see Figure 1c for location) through the Smørbukk hangingwall graben illustrating the late onset of activity across the structure relative to other faults in the area. Thickening across faults is restricted to post-Top Ile formation deposition, with the maximum thickness changes during the Earliest Cretaceous. See Figure 5 for fault annotations. Key to seismic marker horizons and intervals are shown in Figure 2.

Two Cretaceous successions (BCU-Top Lange and Top Lange-Near Top Lange Sandstone) have been mapped during the period following Late Jurassic rifting. The precise age of the Top Lange Sandstone is unknown, however along with the Near Top Lange Formation (between Cenomanian to Coniacian age from well data), these horizons provide some broad constraint on deposition within the Early Cretaceous.

3.4.4.1 Fault geometry and distribution

The geometry and distribution of faults that intersect the Cretaceous interval differs from the dominantly NE – SW and N – S pattern observed in the Triassic and Jurassic. Instead faults are observed at a variety of orientations, E-W, WNW-ESE and NW-SE and NE-SW, and with less predictable distributions, with spacings ranging from a maximum of 12km to a minimum of approximately 2km (**Figure 3.2b, S_{FW}, S_{HW}, E_F, T_{FW}, S_{South}**).

The Smørbukk footwall and hangingwall grabens trend approximately perpendicular to the orientation of Jurassic and Triassic structures, terminating downwards into the Triassic evaporites without linking to the underlying basement faults. In contrast, the N-S trending southern trace of the Smørbukk fault trends at an angle of ~20° to the Triassic and Jurassic fault trend (**Figure 3.2b**). The spread of fault orientation data therefore reaches its maximum value (**Figure 3.3d & e**), whilst the mean strike orientation decreases due to the formation of faults oblique to earlier trends (**Figure 3.3e**).

3.4.4.2 Fault timing

Faults that displace the Lower Cretaceous (BCU – Top Lange Sandstone) interval display significant thickness variations which record a shift in dominant activity onto a number of new structures. Synchronous with this activity, growth continues across the Smørbukk and Trestakk faults, making them the longest-lived faults in the area (**Figure 3.5J**). Growth across the Northern fault was more pronounced than in previous intervals and more localised to the very north of the study area, perhaps suggesting a shift of activity towards the more northerly Revfallet fault. The presence of thicker Lower Cretaceous deposits is noted over the axis of the present-day Trestakk syncline which continued to subside synchronous with thinning across the anticlinal crest of the monocline (**Figure 3.5J**), suggesting that activity across basement faults below the salt continued during this interval.

The initiation of activity on a number of new structures is the most striking difference from earlier intervals. Growth continued and became more pronounced into the Smørbukk hangingwall graben (**Figure 3.9**) and activity initiated across the

Smørbukk footwall graben, the Trestakk footwall graben and across the N-S trending southerly trace of the Smørbukk fault (**Figure 3.5J**). Clear cross cutting relationships are observed between graben that form in the Cretaceous and earlier Jurassic faults (**Figure 3.6**), a relationship that is also noted from 2D seismic lines through the Tyrihans field to the south east of the study area. Furthermore, growth of the compressional fold (S_{CF}) continued post-BCU deposition when thinning and onlap over the crest of the fold, and thickening west of the fold crest is observed (**Figure 3.5J**).

The youngest mapped interval (Top Lange Sandstone – Near Top Lange Formation) thickens from the northeast to the west and southwest (**Figure 3.5K and 3.11**), with a noticeable thickening across a NE-SW trending boundary parallel to the trace of the buried Trestakk fault (**Figure 3.6**). Fewer faults cut the interval, namely the Smørbukk fault which becomes segmented into a central and southerly trace, the Smørbukk footwall graben and the Eastern fault, highlighting that faults are dying out up-sequence. Thickness variations across these faults most likely represent fault activity in a low strain-rate localised rift environment, with the most thickening across the longest-lived structures. Activity across the southern segment of the Smørbukk fault and the Smørbukk footwall graben may reflect a continuation of gravity-sliding and salt-withdrawal from the previous interval.

A new interpretation of Early Cretaceous thickness variations is presented in which a number of new faults initiated whilst activity continued on a few long-lived faults. The orientation of new faults within this interval cannot be accounted for by the simple rotation of the maximum horizontal extension direction to NW-SE, as suggested in previous work (Mosar *et al*, 2002). Fault activity maps (**Figure 3.11E**) illustrate the varied orientation of Cretaceous faults with respect to the NW-SE stretching event. Significantly, grabens are instead oriented approximately perpendicular to the maximum dip on underlying basement faults which at a critical point could enable gravity sliding of the cover above evaporites. Furthermore, thickening of Cretaceous intervals is observed over the footwall and hangingwall of the southerly trace of the Smørbukk fault, which is suggested here to be due to salt-withdrawal above a falling reactive diapir. A detailed discussion of salt diapirism is beyond the scope of the present paper.

The youngest interpreted interval (Top Lange Sandstone – Near Top Lange Formation) records the gradual cessation of fault activity across the area, with fault

displacements decreasing up-dip and tipping out during or immediately following Post Lange deposition. Layer-parallel reflector packages and a lack of faults characterising younger stratigraphy support the interpretation suggesting the onset of relative tectonic quiescence.

3.5 DISCUSSION

3.5.1 Conceptual model

Fault-related thickness variations have been used to reconstruct the history of active faults from the Permo-Triassic to Early Cretaceous, and to propose a new structural model for the evolution of the Åsgard area of the Halten Terrace. This can be divided into four key stages; (i) pre-rift, (ii) rift initiation, (iii) rift climax and (iv) end of rifting, gravity sliding and salt withdrawal **(Figure 3.10A-D)**.

Mapping intervals within the Permian and Triassic presents an important, new interpretation of the rift history prior to well-documented Jurassic events. The results challenge existing models for the structural evolution of the Halten Terrace by demonstrating that faults were not active in the interval prior to evaporite deposition **(Figure 3.10A)**. Instead activity within these intervals initiates synchronous with the onset of cover faulting as recorded by growth into synclines during the Early Jurassic **(Figure 3.10B)**. Thickness variations have been used in the pre-salt basement and internal geometries within the evaporitic interval, along with knowledge of the unique mechanical properties of salt which accommodates strain by internal salt flow, to propose a new structural model for the Permo-Triassic. It has been shown that fault geometries observed in the basement and cover stratigraphy can be accounted for without the need for basement fault reactivation. The results also highlight the importance of salt in decoupling fault activity between the basement and cover strata, which is the main control over the structural evolution of the area.

The Jurassic evolution of the Åsgard region is intimately related to strain localisation on faults in the basement and the propagation of a few, large faults and the development of folds and associated smaller faults in the cover. Basement and cover fault activity initiated during the Early Jurassic interval (Åre Coal to Top Åre) **(Figure 3.10B)**, earlier than previously recognised. Strain within the basement was initially distributed across a large number of small faults, which progressively

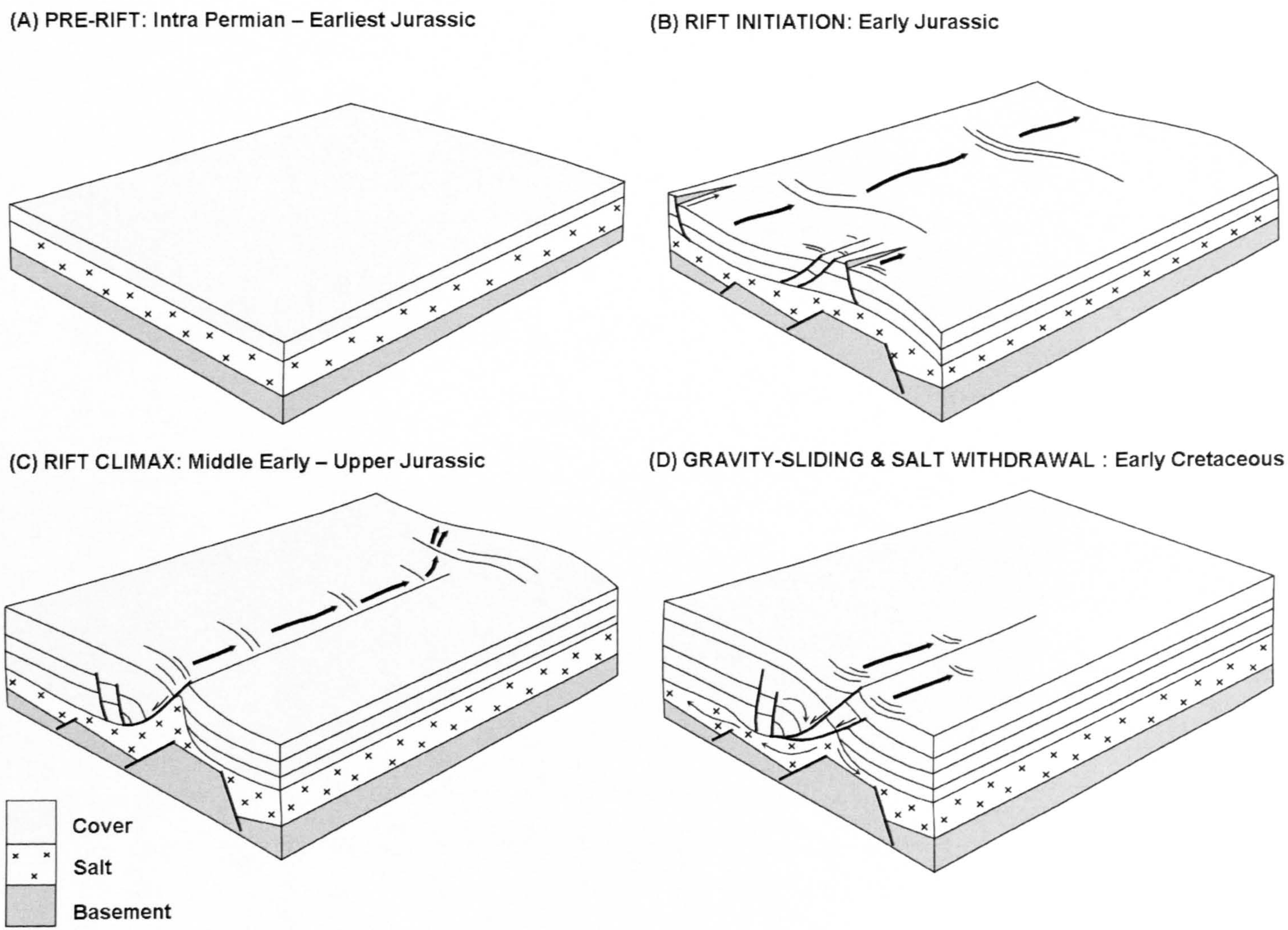

Figure 3.10: Figure caption on following page

Figure 3.10 (previous page): (A) Layer parallel strata in a pre-rift setting, including the deposition of Triassic evaporites (highlighted with crosses). (B) The onset of faulting in the basement causes folding and flexure of cover strata where faults form and depocentres develop above basement lows. (C) The localisation of strain onto a few faults in the basement causes increased folding, flexure and faulting in the cover. Strain in the cover localises onto a few major faults and around areas of flexure e.g. hangingwall rollovers, synclines and anticlines. The most significant depocentres follow the axis of major faults and folds. (D) Fault growth in a low-strain rate syn-rift environment leads to salt withdrawal as sedimentation rate out paces salt supply rate. Sufficient dip on the underlying basement surface initiated gravity-driven deformation. The thickening of Early Cretaceous sediments in the footwall and hangingwall of faults records the onset of salt withdrawal. Salt evacuates up or down dip of the fault causing the collapse and rotation of overlying faults synchronous with withdrawal.

localised displacements onto a few, large structures as predicted by models of strain localisation in brittle systems (Cowie and Scholz, 1992a,b) (Basement, **Figure 3.10A-D**) and recognised across the Heidrun Field on the Halten Terrace (Richardson *et al*, 2005). As strain localised in the sub-salt stratigraphy, basement faults gained sufficient displacement to deform the cover by distributing strain across broad, monoclinal flexures **(Figure 3.10B)** and through the formation of a few, large faults which localised above the largest displacement basement faults **(Figure 3.10C)**. Reactive diapirs formed in response to ongoing extension as faults in the cover continued to grow. Displacement localised on basement faults synchronous with the development of progressively larger faults and broad monoclinal flexures in the cover, demonstrating that the magnitude and distribution of faults and folds in the cover is controlled by the synchronous growth and linkage in the underlying basement fault system. Activity remained focussed on these faults until the onset of gravity-driven deformation initiated in Middle Jurassic. The interpretation therefore supports existing publications that recognise the role of salt tectonics and fault-propagation folding in the structural evolution of the Halten Terrace (Corfield *et al*, 2000; Færseth *et al*, 2002; Pascoe *et al*, 1999; Withjack *et al*, 1989, 1990, Withjack & Callaway, 2000).

The gradual decline of extension in the Early Cretaceous is marked by the fall of diapirs and the initiation of growth across new faults trending at high-angles to Triassic and Jurassic fault trends. This interval marks a change in the dominant mechanism for fault growth from extensional tectonics to gravity-sliding and salt withdrawal **(Figure 3.10D)**. Gravity sliding initiated as the basement surface tilted sufficiently for down-dip translation of the overlying cover. There is no evidence for Early Cretaceous strike-slip activity in the area (Caselli, 1987), but instead it is here

suggested that gravity-sliding and salt tectonics account for structural characteristics that seem to differ from those expected in a purely brittle extensional regime (e.g. extensional and compressional folds, 'inversion and flower structures' (Caselli, 1987)).

The model presented here illustrates the complexities of fault system evolution in basins where active extensional faulting is decoupled by the presence of a regionally extensive ductile salt layer. The interactions between salt movement, faulting in the basement and folding and faulting in the cover fundamentally controls the surface morphology. This in turn has a direct impact on the development of accommodation space and on sediment pathways across the area.

3.5.2 Implications for Hydrocarbon Prospectivity

3.5.2.1 Rift initiation

The development of accommodation space with the onset of rifting in the Early Jurassic has implications for the distribution of Jurassic reservoirs whose structurally controlled depocentres first evolved during this interval. Deposition of Åre formation sands from the West – the only reservoir deposited synchronous with rift initiation – was widespread, crossing the main faults in the region (e.g. Smørbukk and Trestakk) suggesting that sedimentation rates at least kept pace with fault displacement rates **(Figure 3.11A)**.

The development of local, isolated depocentres in the hangingwalls of the Smørbukk and Trestakk faults, along with the onset of subsidence into the northeast syncline suggests that the thickest syn-rift sediments are most likely to be confined to depocentres in central and north-eastern areas **(Figure 3.11A)**, which is where the best quality reservoir sands (i.e. sands undergoing optimal production) are recorded from well data – an observation which suggests a tectonic control over the distribution of the best quality sands in the Early Jurassic. There is potential for the reworking and redeposition of sands from the uplifted area in the east, into depocentres to the west (e.g. Smørbukk, Trestakk and northeast syncline) **(Figure 3.11A)**.

Åre formation sandstones have previously been described as a 'pre-rift play' (Koch & Heum, 1995), but the observations suggest that a structural control over

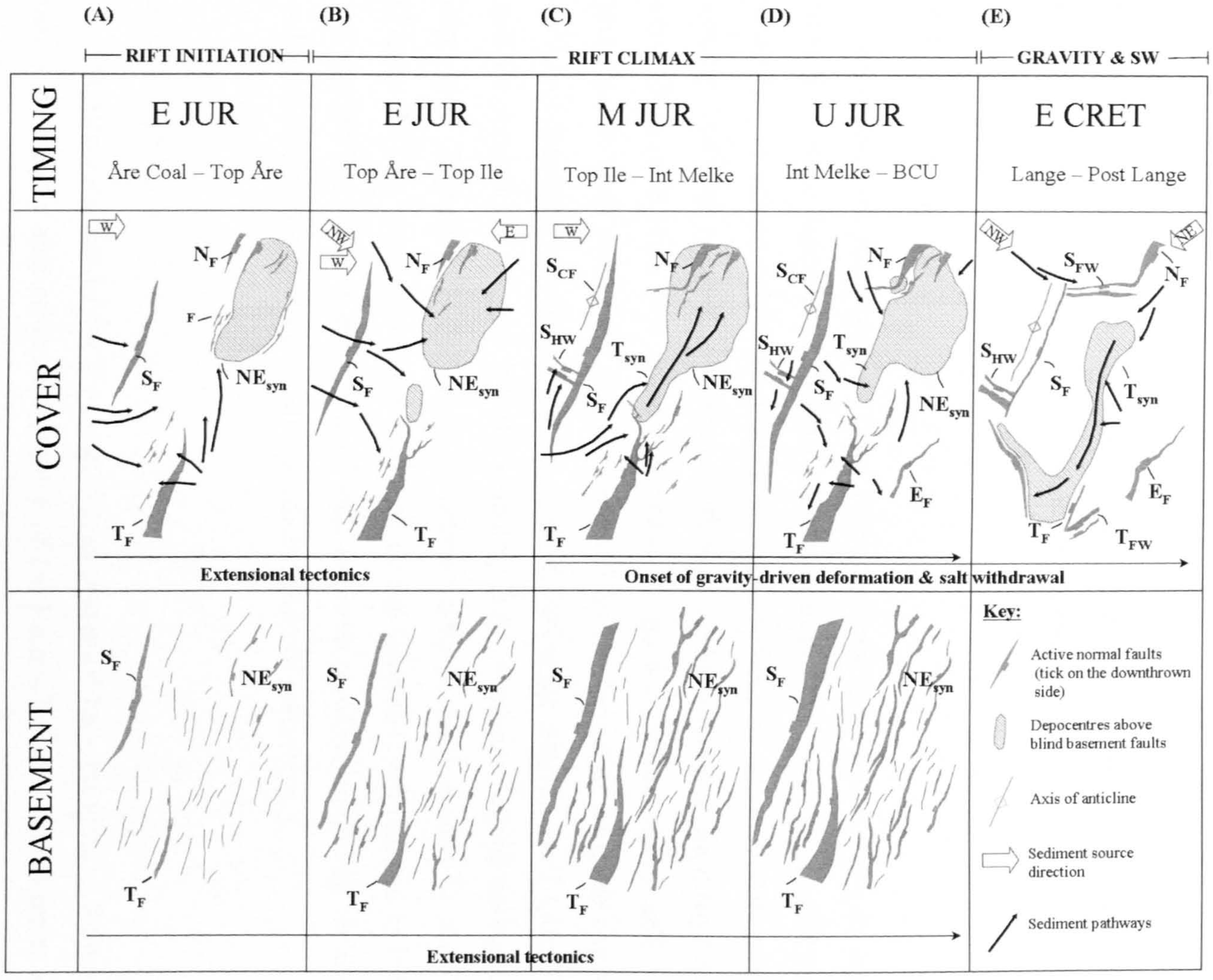

Figure 3.11: Figure caption on following page

Figure 3.11 (previous page): Fault activity maps tracking the evolution of faults in the basement and cover sequence from the Early Jurassic to Early Cretaceous. The basement behaves as a pure brittle system in which strain becomes progressively localised through time, whereas in the cover sequence more faults develop as the basin evolves with the onset of gravity sliding and salt withdrawal in the Middle Jurassic. Depocentres that form above deforming basement blocks become more widespread as basement faults gain sufficient displacement to fold the cover.

reservoir deposition existed much earlier in the Jurassic than previously recognised, thus reclassifying Åre formation sandstones as a syn-rift play.

3.5.2.2 Rift Climax

Four reservoir formations – Tilje, Tofte, Ile and Garn sands (early to middle Jurassic) – were deposited during rift climax. Fault growth remained focused on the same few structures which controlled the development of accommodation space synchronous with reservoir deposition, although source directions are interpreted to vary (**Figure 3.11B**). An overall increase in growth across faults and fault-propagation folds during rift climax is marked by the formation of more extensive sediment depocentres, which remained isolated during the deposition of Tilje, Tofte and Ile formations (**Figure 3.11B**), reaching their maximum extent during Garn deposition (**Figure 3.11C**); these were subsequently partially eroded by the BCU (**Figure 3.11D**). Constraining the evolution of depocentres (from isolated to linked) and identifying areas of erosion is of vital importance when producing models of sediment dispersal patterns to predict the distribution of reservoirs.

3.5.2.3 Summary

The structural model for the Åsgard area presented here provides a framework that is potentially applicable across much of the Halten Terrace. Whilst many areas will have more or less complex fault and fold patterns, the regional presence of a ductile salt layer means that the driving mechanisms for deformation will likely be similar. Constraining the timing and distribution of active faults and the development of accommodation space throughout the Jurassic and Early Cretaceous provides a much-improved method of predicting reservoir distribution. The results highlight the impact of tectonic activity on sediment pathways, local sediment sources and the

development of depocentres for sediment ponding. The complexity of the system should be emphasised, particularly in relating reservoir quality to the distribution of depocentres and depth of burial.

The impact of basement faulting on the spatial distribution and size of faults and folds in the cover has been demonstrated, which has implications for well planning and reservoir development around the Smørbukk and Smørbukk Sør fields. The results highlight the importance of mapping faults and stratigraphic marker horizons that formed at all stages of rifting. Furthermore, it has been demonstrated that basement faults do not necessarily form during an earlier rift event than faults in the cover, as is commonly assume, highlighting the danger of inferring basement fault reactivation based purely on geometric similarity, e.g. fault trend.

3.6 CONCLUSIONS

- The development of fault-propagation folds records the onset of sub-salt basement fault activity during the Early Jurassic, subsequent to the deposition of Middle to Late Triassic evaporites, which were deposited during a period of relative tectonic quiescence in an un-faulted basin.
- Jurassic fault activity initiated earlier than previously recognised during the Early Jurassic (Hettangian - Pliensbachian) interval, synchronous with Åre Coal to Top Åre deposition.
- A new interpretation of Cretaceous fault activity highlights the initiation of new fault growth in the earliest Cretaceous due to gravity sliding and salt-withdrawal over a tilted basement surface.
- Extensional basins that form in the presence of a ductile layer undergo an alternative process of strain localisation than proposed for purely brittle basins. Sub-salt basement faults behave as in a purely brittle system, whereas post-salt cover faults undergo rapid strain localisation followed by the development of new faults oblique to main trends due to gravity sliding and salt withdrawal.
- Constraining the timing and distribution of active faults and the development of accommodation space throughout the Jurassic and Early Cretaceous provides a much-improved method of predicting reservoir distribution and for identifying areas for more detailed interpretation. The results highlight that the interaction between salt movement and faulting in the basement and cover fundamentally

controls the surface morphology which in turn has a direct impact on the development of accommodation space and on sediment pathways across the area.

CHAPTER 4

4: The evolution of structural styles in a brittle-ductile system: examples from the Halten Terrace, offshore mid-Norway

4.1 INTRODUCTION

The unique fluid rheology and incompressibility of salt - which is much weaker than other lithologies under both tension and compression - together with its buoyancy make it inherently unstable under a range of geological conditions, resulting in often complex structural geometries. Compared to most other rock types, evaporites are able to deform with relative ease in a viscous manner and can therefore readily accommodate strain by ductile deformation. Thus, the presence of evaporites may detach deformation in the pre-evaporite "basement" from that in the post-evaporite "cover" and give rise to varying degrees of linkage ("coupling") between basement and cover faults, ranging from coupled, to partially coupled and decoupled (Stewart *et al*, 1997). Here, the term 'coupling' is used to describe the degree of linkage between basement and cover faults, where coupled faults offset the entire salt layer, kinematically linking basement and cover strata **(Figure 4.1a)**; partially coupled faults are kinematically linked via detachments in the salt layer **(Figure 4.1b)**; and decoupled cover faults are independent of basement structure **(Figure 4.1c)**. In this paper, both thick-skinned extensional systems are considered, which includes coupled and partially coupled faults, and thin-skinned, decoupled faults.

Extension of the basement beneath a regionally extensive detachment, such as a salt layer, can give rise to two kinematically distinct types of structure in the post-salt cover. Thick-skinned cover structures, i.e. those that are coupled or partially coupled to the basement structures, evolve during crustal extension to balance basement stretching (Rowan, 1993; Stewart *et al*, 1997). 'Thin-skinned' refers here to decoupled faults that detach on or within mechanically weak evaporites and are not kinematically related to basement extension. The thin-skinned structures described here are most likely to have developed due to gravity-driven deformation, which arose due to translation of material either down the *regional* dip or in response to *local* tilting of the detachment surface. In particular, basement extension can result in the rotation of major basement fault blocks either through isostatic footwall uplift

(e.g. Contreras *et al.* 1997), reverse drag **(Figure 4.2a)** (e.g. Barnett *et al.* 1987) and/or by rotation of strata in relay zones between overlapping fault segments **(Figure 4.2b)** (e.g. Peacock & Sanderson, 1991). These rotational strains tilt the detachment layer and may give rise to the development of gravity-driven, thin-skinned faults and folds (Duval *et al*, 1992; Vendeville & Jackson, 1992a; Jackson *et al*, 1994a, b). Three factors are used to identify gravity-driven faults: (i) their orientation perpendicular to the local or regional dip direction; (ii) the absence of basement faults with a similar trend; and (iii) the onset of fault activity, which initiate post-Middle Jurassic, subsequent to activity on thick-skinned faults.

In the absence of a free-surface at the toe of a gravity slide, up-dip gravity-driven extension may terminate down-dip in detachment folds and/or reverse faults (Hesthammer & Fossen, 1999). The crucial point is that crustal extension is required to initiate the formation of both thick- *and* thin-skinned structural styles. As a result, (normal and reverse) thin-skinned faults will interact with those cover structures that directly balance basement extension (Stewart *et al*, 1997), giving rise to complex structural architectures and the potential to develop a wide range of hydrocarbon trap geometries.

Analogue models, supported by examples from seismic data and field outcrops, suggest that a number of factors control the degree of coupling between basement and cover fault systems. These are: the dip of the basement faults (Vendeville, 1987; Withjack *et al*, 1990; Finch *et al*, 2004); the magnitude of basement fault displacement (Stewart *et al*, 1997; Withjack & Callaway, 2000); the thickness and viscosity of the viscous (salt) layer (Stewart *et al*, 1997; Koyi *et al*, 1993; Vendeville & Jackson, 1995; Withjack & Callaway, 2000); and the thickness and strength of the overburden and the rate of fault displacement (Koyi *et al*, 1993; Vendeville & Jackson, 1995; Withjack & Callaway, 2000). These results demonstrate that increasing the thickness of the viscous layer and the cohesive strength and ductility of the overburden enhances decoupling between the basement and cover deformation. In contrast, increasing the viscosity of the viscous layer, the thickness of the overburden, and the magnitude and rate of displacement on the master normal fault enhances the degree of coupling between basement and cover structures. Seismic examples from the Oseberg East field (Finch *et al*, 2004) and comparative outcrop examples from Wadi El Nakheil in the Gulf of Suez (Khalil & McClay, 2002) show similar geometries to, and thus support the results of the analogue

experiments. These models, which are designed to simulate real geological conditions over much shorter time-scales and under conditions that are scaled to best represent the material properties, stress regimes and boundary conditions, have therefore been used to aid interpretation of salt-related deformation in areas of structural complexity, uncertainty and poor data quality.

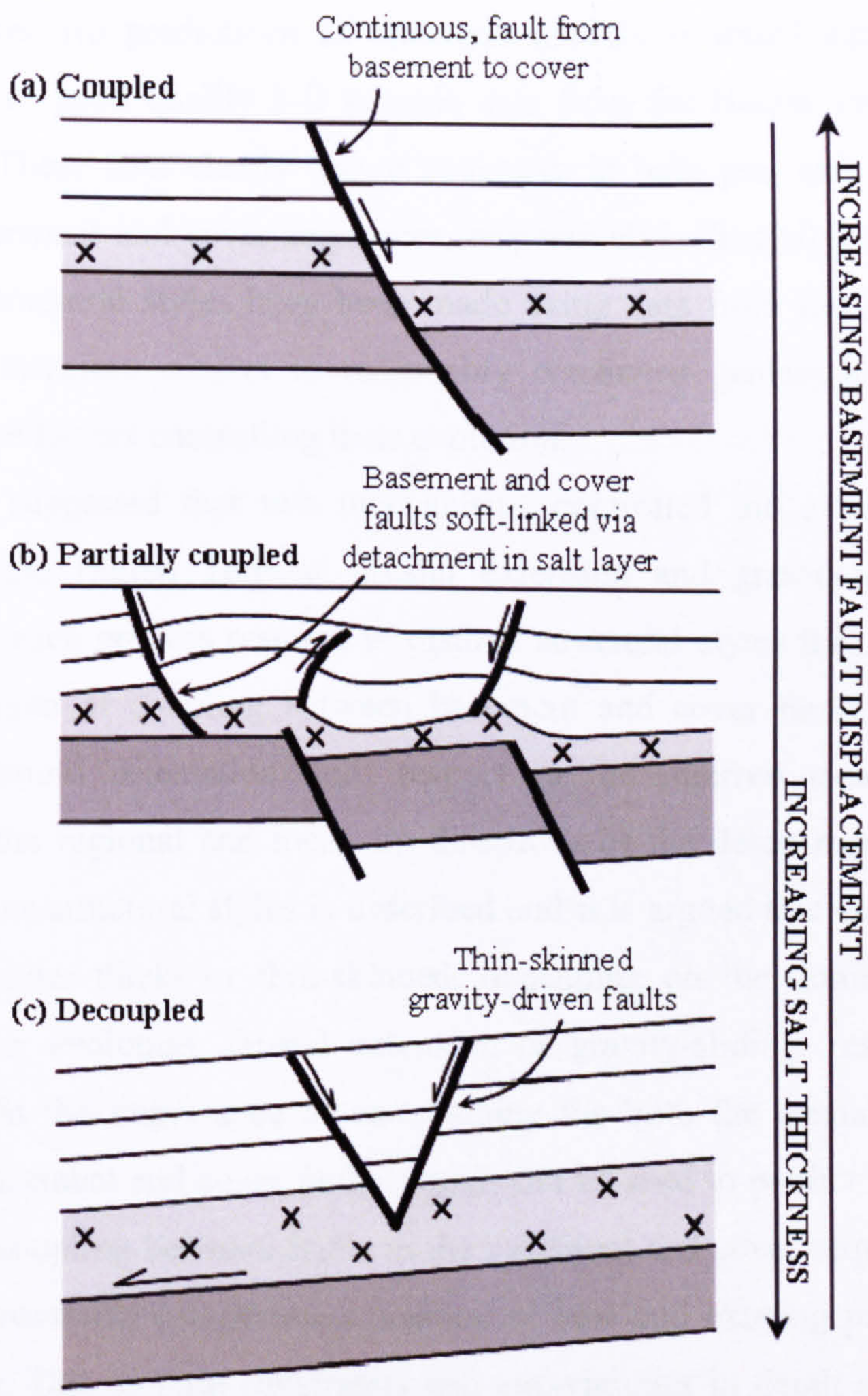

Figure 4.1: Basement-cover fault linkage scenarios in a system influenced by ductile evaporites, based on observations made in the Channel Basin by Stewart et al, 1997. Experimental models and observations from seismic data suggest the nature of linkage evolves as basement fault displacement relative to detachment layer thickness increases through time: (a) A coupled system in which a continuous fault links basement and cover strata by offsetting the entire evaporite sequence; (b) Partial coupling of the basement and cover via a detachment in the salt layer and (c) A decoupled system in which cover extension initiates due to gravity-sliding above an inclined basement surface. Large displacement basement faults and a thin salt layer favour coupled basement-cover fault growth whereas thick salt and low displacement basement faults favour decoupled faults.

Despite the good correlation that exists between the modelled geometries and structures observed in salt basins worldwide, it is difficult to use these general observations to test the influence of specific factors (e.g. overburden thickness) on fault kinematics and the degree of coupling. This problem arises because each basin has experienced a unique combination of stretching rates, subsidence rates and sedimentation rates that, in many cases, can be only partially constrained. In this study, the geometric predictions of analogue models is tested against structural interpretations of good quality 3-D seismic data from the Halten Terrace, offshore Mid-Norway. These data clearly image structures in both pre- and post-salt strata (i.e. within basement and cover sequences, respectively). Crucially, observations of the different structural styles have been made using data from the *same* structural province and therefore subject to reasonably consistent geological conditions in which to test the factors controlling their evolution.

Here it is suggested that two mechanisms controlled the evolution of cover structures on the Halten Terrace: crustal extension and gravity-sliding, and in particular, that each process resulted in distinct structural styles that can be defined by: (i) the degree of coupling between basement and cover faults; and (ii) their dominant structural orientation with respect to the inferred tectonic extension direction and the regional and local dip directions of the detachment surface. The geometry of nine structural styles is described and it is argued that each style can be classified as either thick- or thin-skinned, depending on the dominant processes controlling their evolution: crustal extension or gravity-sliding, respectively. The results highlight the importance of constraining the both the spatial and temporal evolution of basement and cover faults, which can be used to predict the distribution and degree of coupling between faults in the basement and cover sequence, and thus the degree of reservoir compartmentalisation in new and existing prospects on the Halten Terrace. Due to time constraints and uncertainties in depth converting fault and horizon interpretations, section balancing was not carried out to test whether *specific* structures developed in response to tectonic- or gravity-driven extension. Nevertheless, the factors that control the evolution of each structural *style* can be discussed based on existing knowledge of the regional structure and stratigraphy, and supported by work from analogue models. Thus, this study provides a new working hypothesis for the structural evolution of the Halten Terrace.

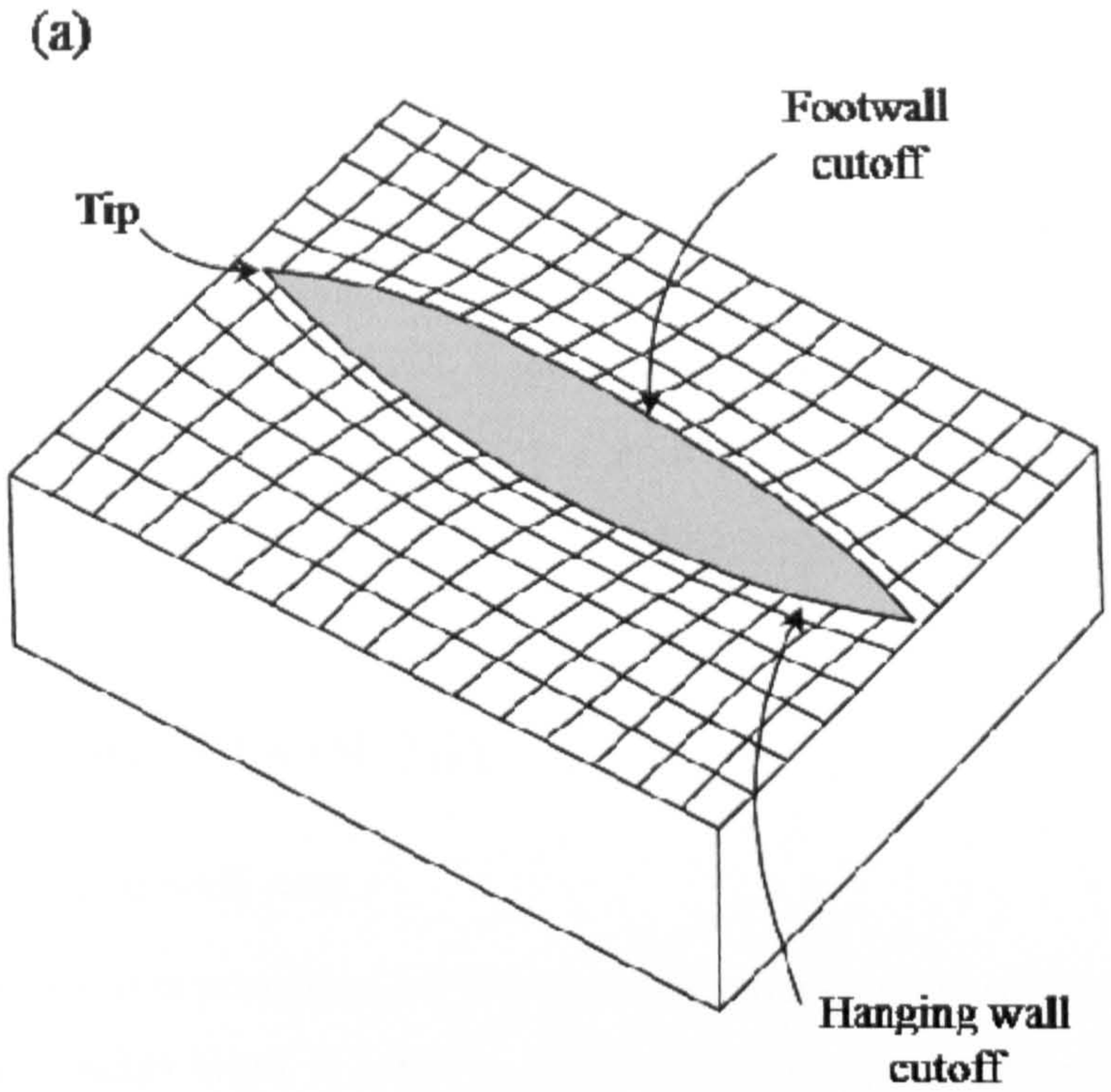

Figure 4.2: 3D block diagrams showing the development of a dipping surface during normal faulting. (a) The displacement along the strike of an isolated normal fault (redrawn from Freeman *et al*, 1990). Note the variation in dip around the fault due to footwall uplift and hangingwall rollover. (b) During the evolution of a relay ramp between overlapping fault segments bedding is reoriented to accommodate displacement transfer between fault segments resulting in a dipping surface in the relay zone (redrawn from Peacock, 2003). Note, the evolution of dip on a basement surface which is separated from the cover by an intervening detachment layer, will initiate gravity-sliding when the surface gains sufficient dip.

4.2 REGIONAL SETTING

Permo-Triassic basement rocks on the Halten Terrace are overlain by a thick sequence of Triassic evaporites, separating basement and cover stratigraphy. Fault activity within Permo-Triassic basement and Jurassic cover stratigraphy initiated synchronously in the Early Jurassic and was ongoing until the Early Cretaceous in the Åsgard area (see chapter 3) and the mid-Cretaceous further north across the Heidrun field (Pascoe *et al*, 1999).

4.3 DATA & METHODOLOGY

4.3.1 Seismic and well data

The observations presented are based on the interpretation of 14 regional seismic lines (**Figure 4.3a**) from a large merged 3D seismic dataset across the Halten Terrace, along with a more detailed interpretation of a 3D seismic dataset from the Åsgard area of the Halten Terrace (**Figure 4.3a**). In the context of this work, 'Åsgard' refers to an area covering the Smørbukk and Smørbukk Sør hydrocarbon fields (**Figure 4.3a**) in the north-western part of the Halten Terrace, approximately 230km north-west of Trondheim in water depths of 250 – 300 m. The Åsgard survey covers an area of 1400 km^2 and has a line spacing of 12.5 m. Horizons and faults in the Åsgard area were interpreted manually every 20 lines across the entire survey and every 10 lines around fault tips.

Stratigraphic control was provided by a total of 63 wells in the Åsgard area, along with an extensive database of well data from across the Halten Terrace. On the regional seismic lines, four prominent reflectors have been mapped to define the basement and cover fault geometries: Base Salt; Top Salt; Åre Coal (interpreted as onset of rifting, see chapter 3); and Base Cretaceous (**Figure 2.25**). More stratigraphic intervals are constrained on seismic lines local to individual fields and prospects where well picks were used to constrain the interpretation of nine regionally mappable seismic stratigraphic marker horizons that bound eight stratigraphic intervals (**Figure 2.25**). Where possible, additional seismic reflectors have been interpreted to constrain intervals significant to a given area. The seismic data has not been depth-converted and so the cross sections in this study are presented with the vertical axis in two-way travel time (TWTT).

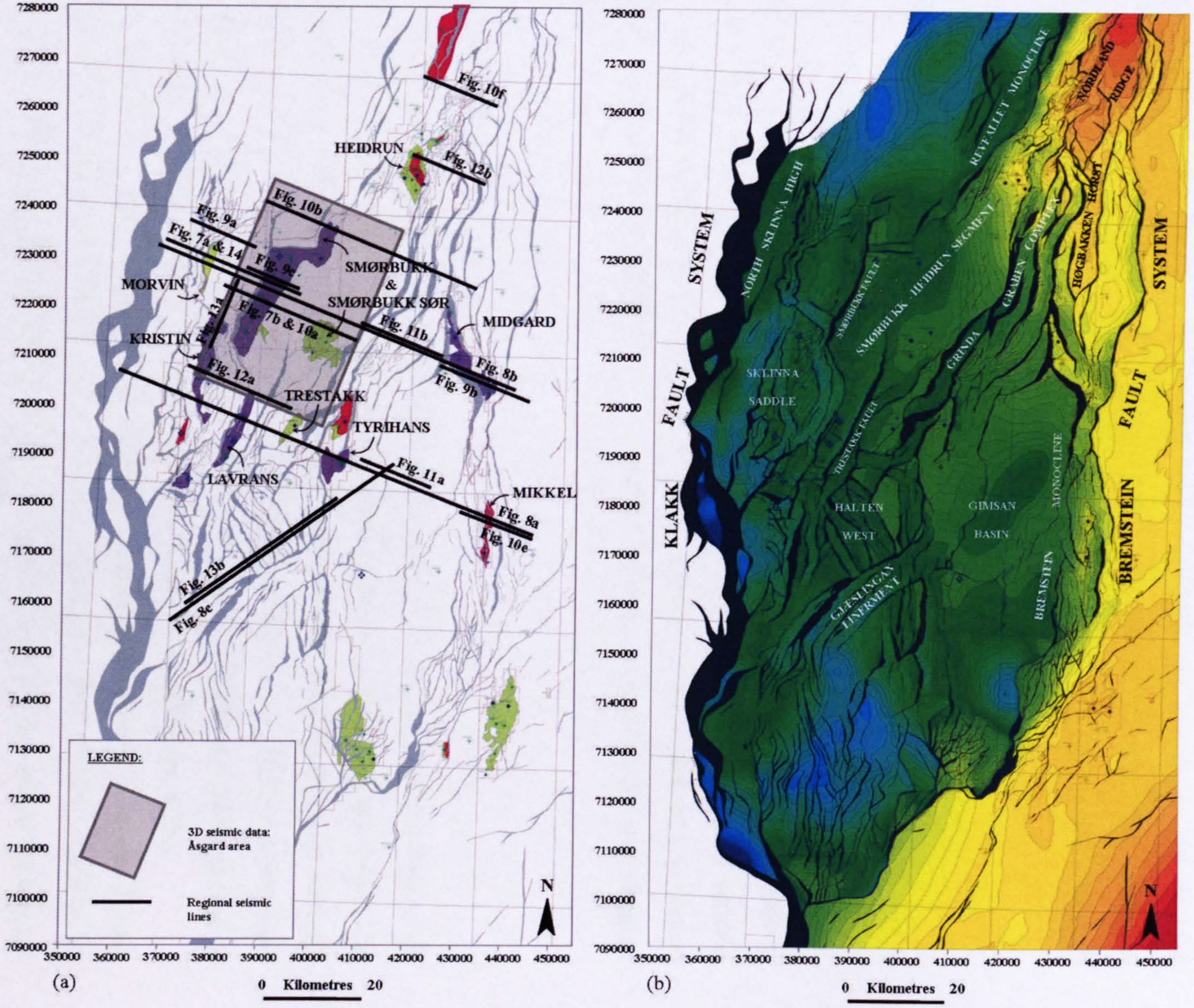

Figure 4.3 (a) Fault polygon map from the Halten Terrace with the location of hydrocarbon fields (purple = gas/condensate, green = oil/gas and red = gas) the Åsgard area (grey box) and regional seismic lines referred to in the text. (b) Time structure map from Middle Jurassic Top Garn interval (see Figure 4.4) across the Halten Terrace highlighting the distribution and nomenclature of structures across the region. Co-ordinates are for UTM zone 32N. Figures modified from Brockbank & Hanssen, 2004.

To investigate the relationship between fault displacement and the degree of coupling, plots of maximum throw (as a proxy for maximum displacement, D_{max}) against fault length (L) were generated, measured at Åre Coal level using the detailed horizon and fault model for the Åsgard area (section 4.5.1.1). These plots only include data from faults where both lateral tips occur within the 3-D seismic dataset, and from faults with one well-imaged fault tip. In the latter case, it was assumed the maximum *observed* throw is located in the centre of the fault, i.e. at a distance L/2 from the observed lateral tip. Thus, D_{max} is likely to be greater than or equal to the maximum observed throw, whilst the actual fault length may be more or less than the calculated value for faults that extend beyond the limits of the 3-D survey area. The assumptions were quality checked for regional consistency using the fault polygon maps generated for the Halten Terrace **(Figure 4.3)**.

4.4 REGIONAL STRUCTURAL ANALYSIS

4.4.1 Map view: Fault populations and domains

Fault populations and domains are described qualitatively based on observations of map-view fault patterns. A simple analysis of fault trends, using regional seismic lines and local fault polygon maps was used to sub-divide the region into structural domains or 'systems' highlighting the variation in fault strike across the area **(Figure 4.4)**.

4.4.1.1 Halten Terrace

Regional 3-D seismic data were used to define a set of fault polygons in the post-salt cover sequence at Top Garn level throughout the Halten Terrace **(Figure 4.4a)**. The distribution and density of faults varies across the area, ranging from an average spacing of c. 4 km in the northeast (Grinda Graben, Høgbakken Horst and Nordland Ridge) to c. 3 km in the centre of the terrace (Halten West) and c. 20km spacing in the Åsgard area (Smørbukk - Heidrun and the Gimsan Basin) **(Figure 4.3b)**.

The Halten Terrace has three fault trends, dominated by N-NNE (system 1) and NNE-NE (system 2) trending structures, with subsidiary NE-E, N-NW and NW-W trends (system 3) **(Figure 4.4a)**. The major bounding fault on the east of the terrace follows a dominant N-NNE (system 1) structural trend in the north and centre of the

terrace, changing to NE-SW (system 2) along its southerly trace. A more complex trend defines the western boundary fault, which changes from NW-trending (system 3) in the south to N-NE trending (systems 1 & 2) further north.

In the north-eastern part of the terrace, to the north and immediately east of the Åsgard area, the dominant fault trend is that of system 2, i.e. NNE-NE (**Figure 4.4a**). There are no system 3 faults in this area. Within the Åsgard area the trend is dominated by system 2 and system 3 faults (section 4.4.1.2). However, the majority of more complex, obliquely oriented fault sets of system 3 are found within the centre and towards the west of the terrace (**Figure 4.4a**). Fewer examples of system 3 faults can be found on the south-east of the terrace where the density of faults decreases and changes to dominantly NNE-NE and N-NE trending.

4.4.1.2 Åsgard area

A more detailed analysis of fault orientations in the basement (**Figure 4.4b**) and cover (**Figure 4.4c**) has been used to compare fault trends above and below the salt horizon within the Åsgard area. The orientation of faults in the basement follows a more systematic pattern than those in the cover, with more regularly spaced faults (average spacing of c. 3km) all following N-NNE (system 1) and NNE-NE (system 2) trends. There are no basement faults of system 3 that form oblique to these trends.

In the cover (Åre Coal level) faults have a larger average spacing (c. 10km) and the dominant trend is that of system 2 faults (NNE-NE). N-NNE trending faults of system 1 are the least dominant trend present only along strike of the largest displacement Smørbukk and Trestakk faults (**Figure 4.4c**) as displacement decreases and the basement and cover progressively decouple to the north (see Chapter 5). The most striking difference between basement and cover is the presence in the latter of system 3 fault trends in the footwall and hangingwall of the Smørbukk fault (S_{FW} & S_{HW}, Figure 4.4c) and at the tip of the Trestakk fault. These faults have variable distributions, orientations and spacings in both the Åsgard area and elsewhere on the Halten Terrace (**Figure 4.4**).

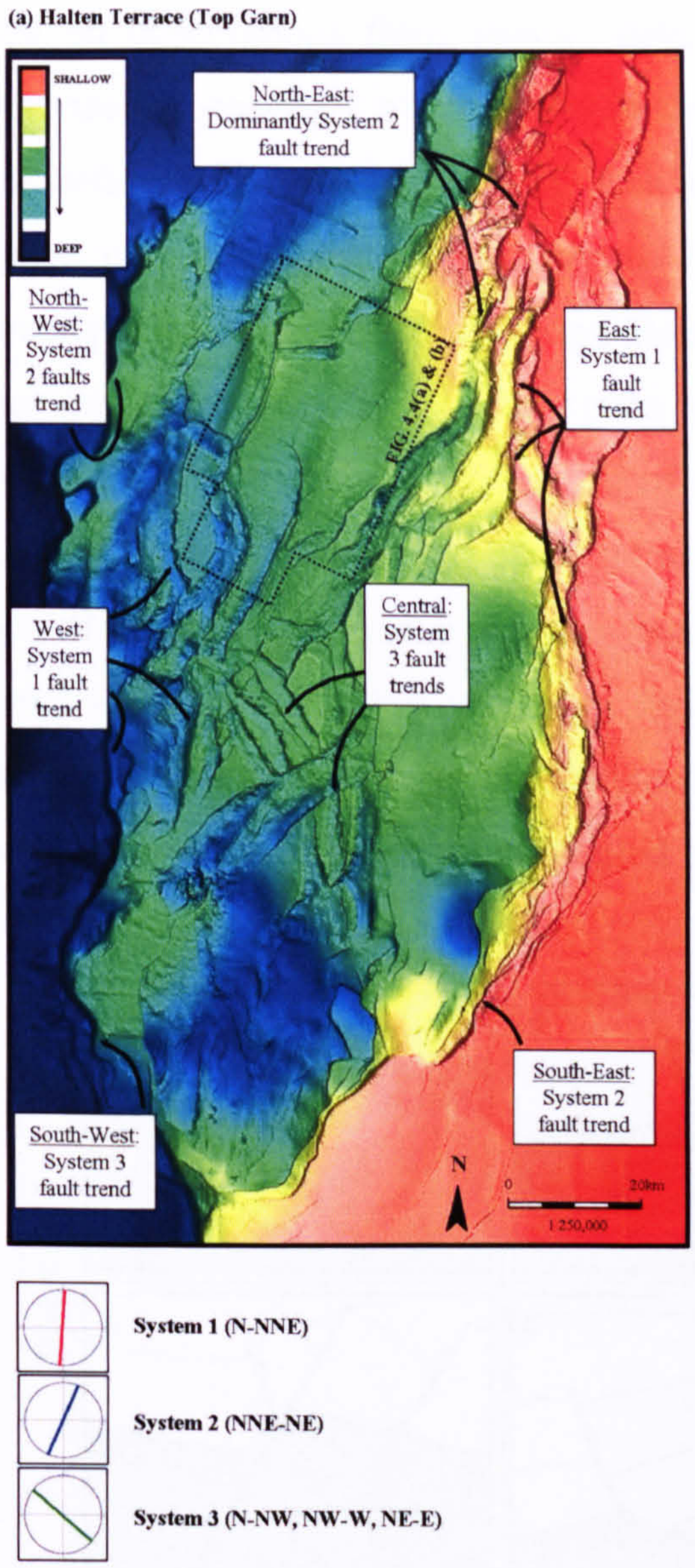

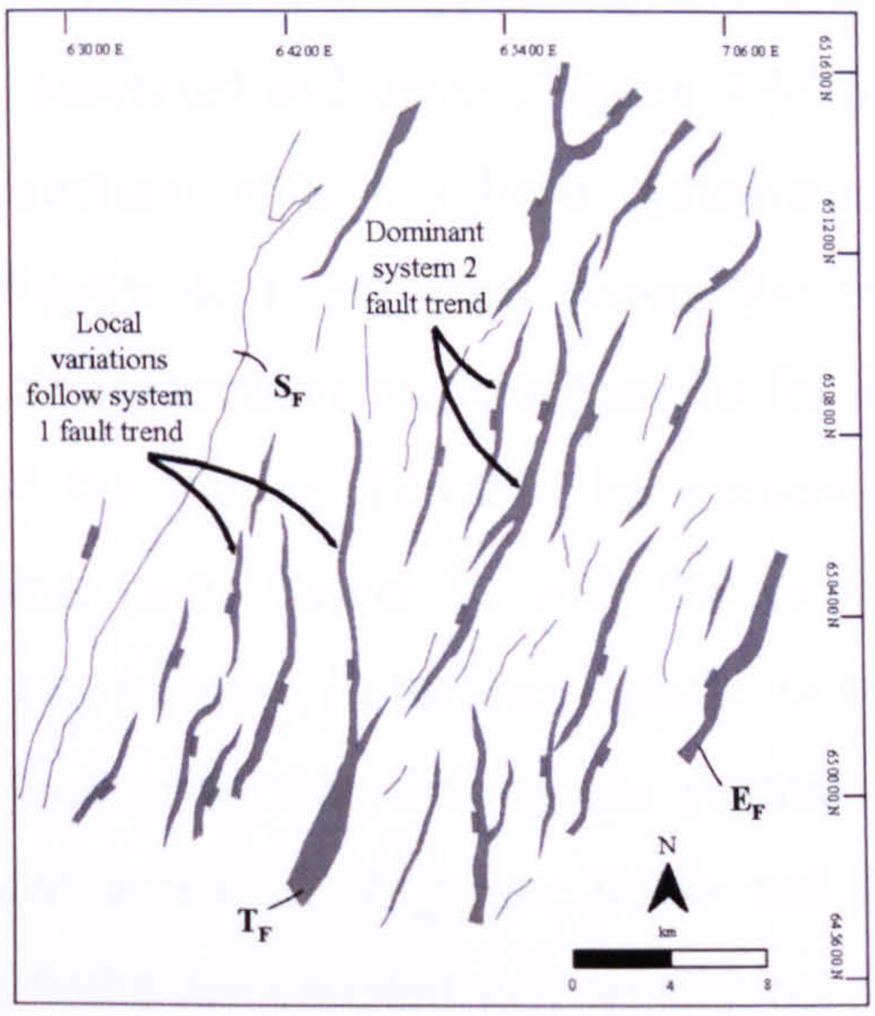

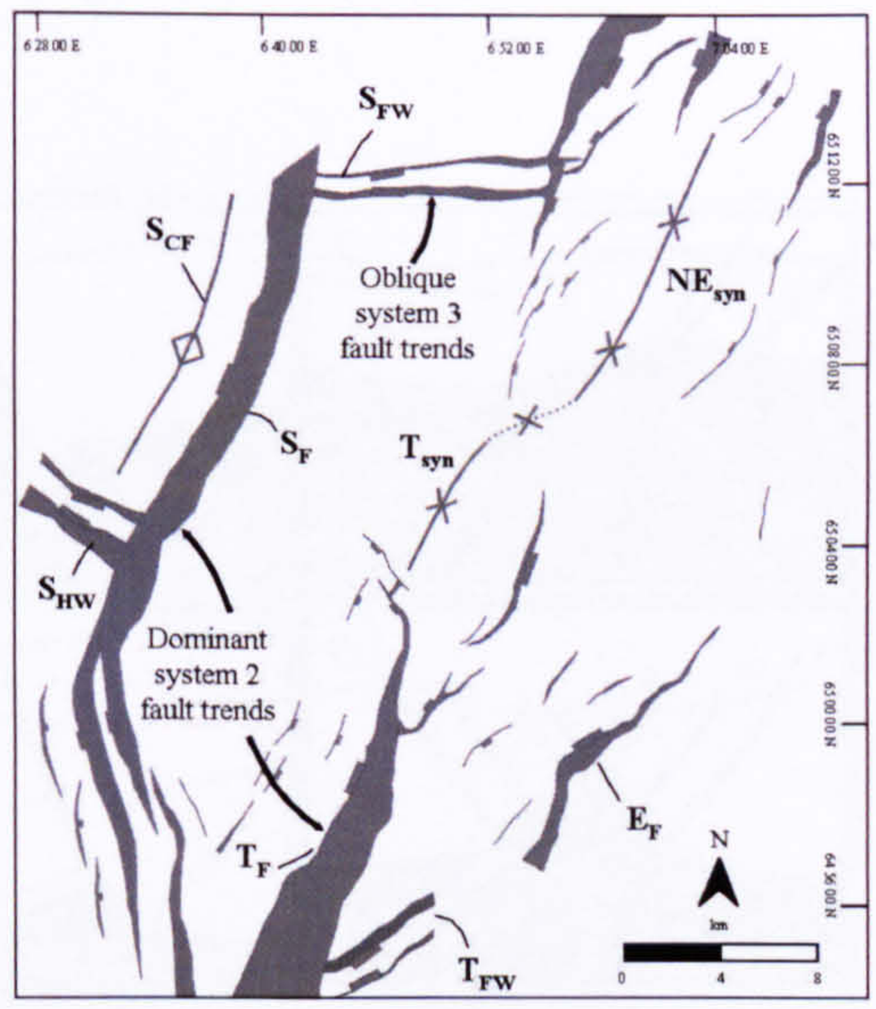

Figure 4.4: Fault population orientation data sub-divided into three systems: System 1 includes faults striking between N-S and NE-SW, System 2 includes those striking between NE-SW and E-W and System 3 is all other orientations. (a) Time structure map (Top Garn) illustrating fault orientation data across the Halten Terrace where the dashed box outlines the Åsgard area (modified from Brockbank & Hanssen, 2004). Fault orientation data for the Åsgard area is divided into (b) basement faults and (c) cover faults. S_F = Smørbukk Fault, S_{FW} = Smørbukk Footwall Graben, S_{HW} = Smørbukk Hangingwall Graben, S_{CF} = Smorbukk compressional fold, T_F = Trestakk Fault, T_{FW} = Trestakk Footwall Graben, E_F = Eastern Fault, T_{syn} = Trestakk syncline, NE_{syn} = Northeast syncline. The Smørbukk fault polygon remains unshaded at basement level due to a lack of constraint on the hangingwall cut-off close to the edge of the survey.

4.4.2 Cross-sections: Geometry of Structural Styles on the Halten Terrace

From observations in map-view, there is a significant variation in the spacing and orientation of faults across the Halten Terrace. In order to understand the mechanisms controlling the distribution and evolution of faults in this area, and

based on observations from seismic data, nine structural styles, that are used to categorise the geometry of structures in the basement and cover (**Figure 4.5**), have been defined. The distribution of each structural style has been systematically mapped over the entire Halten Terrace (**Figure 4.6**). For each group, the main characteristics are described with example seismic sections and mechanisms for their development suggested. In many parts of the Halten Terrace, the present-day geometries evolved over long periods of time (see Chapter 3), with two or more structural styles evolving, and overprinting one another, in the same place. In these cases, the area is defined using the structural style that defines the present day geometry. Structural styles have been divided into two categories; thick- and thin-skinned (**Figure 4.5**), where thick-skinned faults are coupled or partially coupled, whereas thin-skinned faults are decoupled.

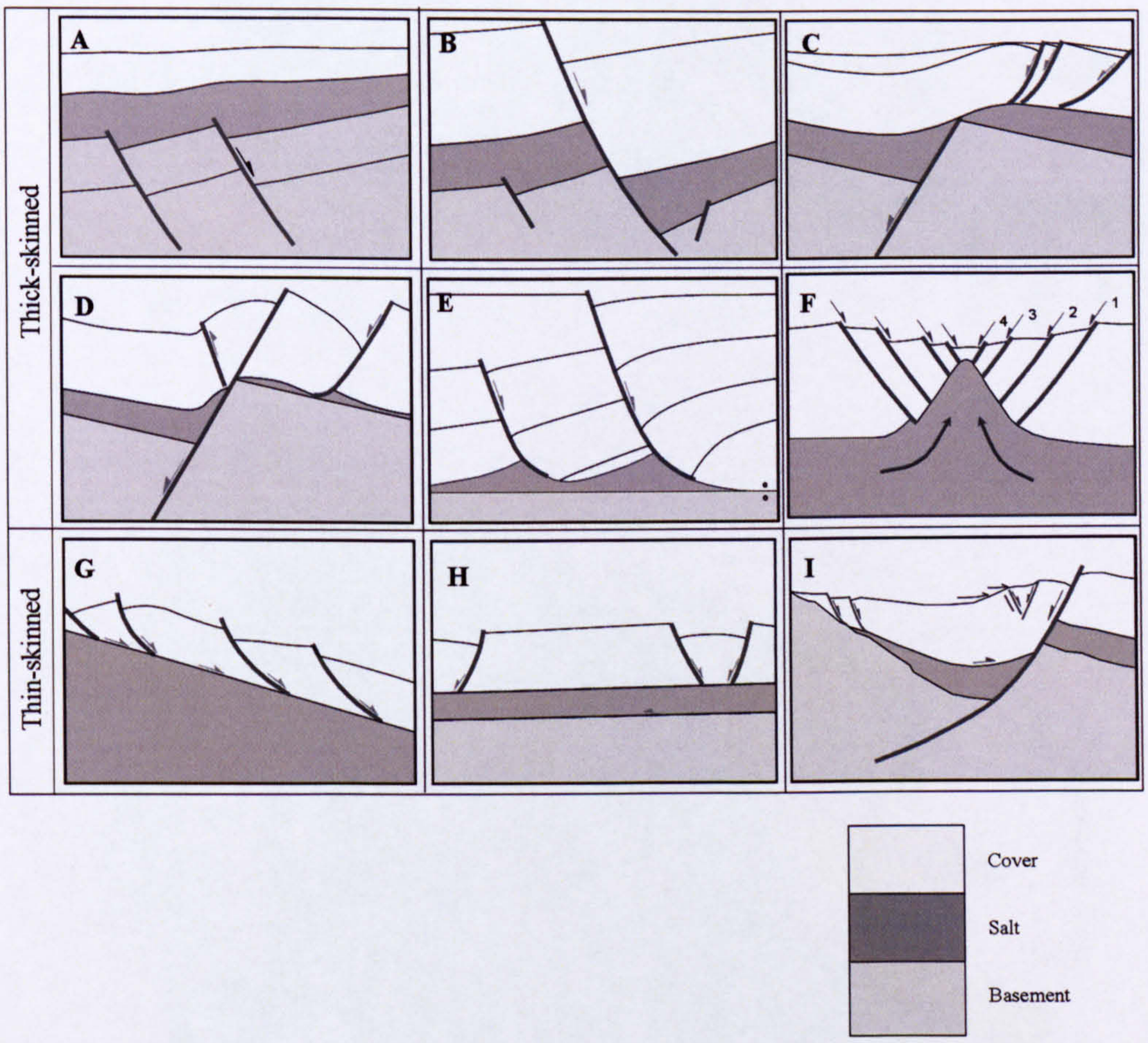

Figure 4.5: Common structural styles identified in the Åsgard area and regionally across the Halten Terrace. Structural styles are divided into two categories thick- and thin-skinned (see text for detail). A = Low-relief basement rift blocks, B = Coupled faults, C = Fault propagation folds, D = Breached folds, E = Simple rollers and grabens (dots represent salt weld), F = Reactive diapirism, G = Gravity-sliding, H = Raft tectonics, I = Compressional fold.

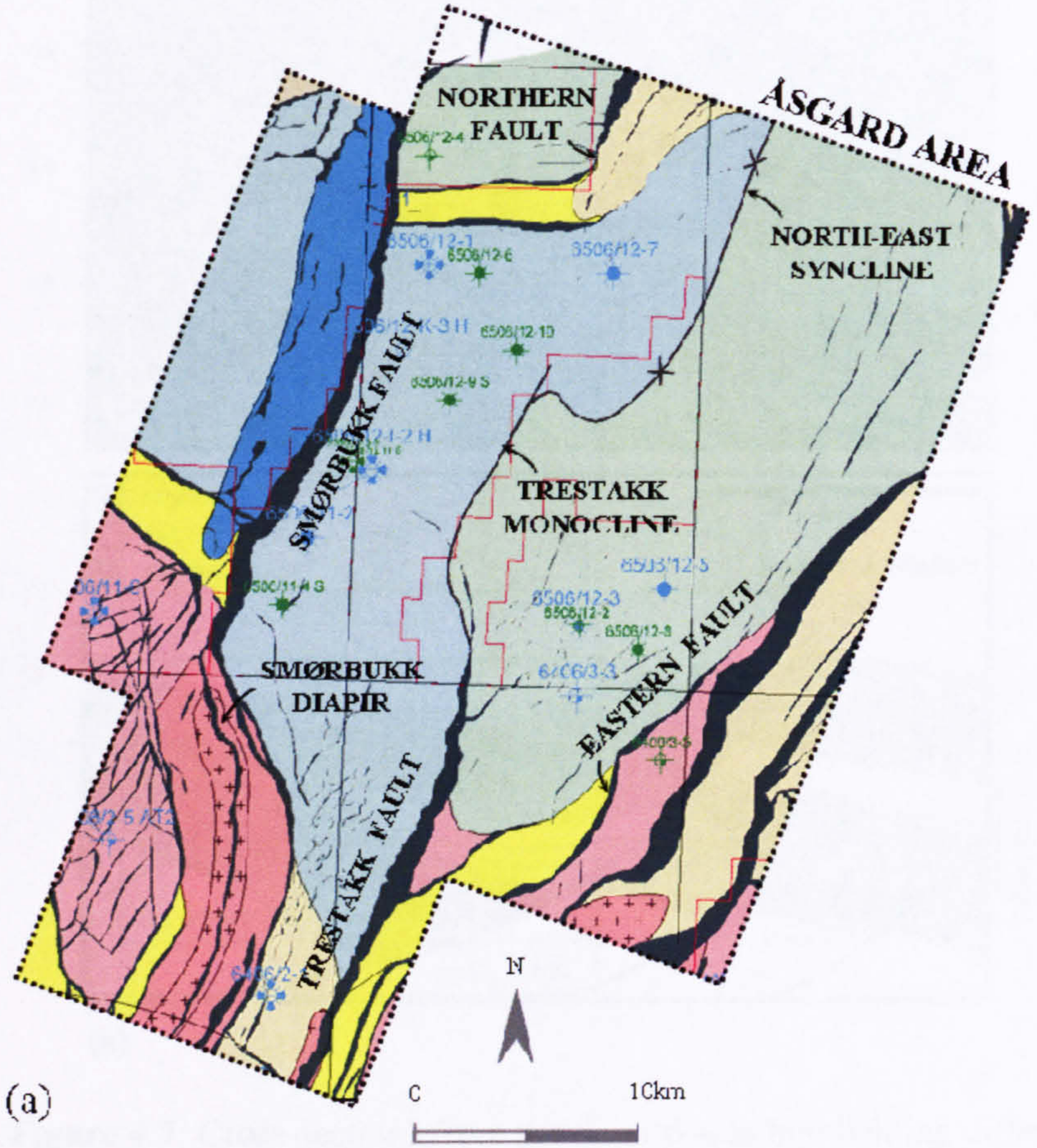

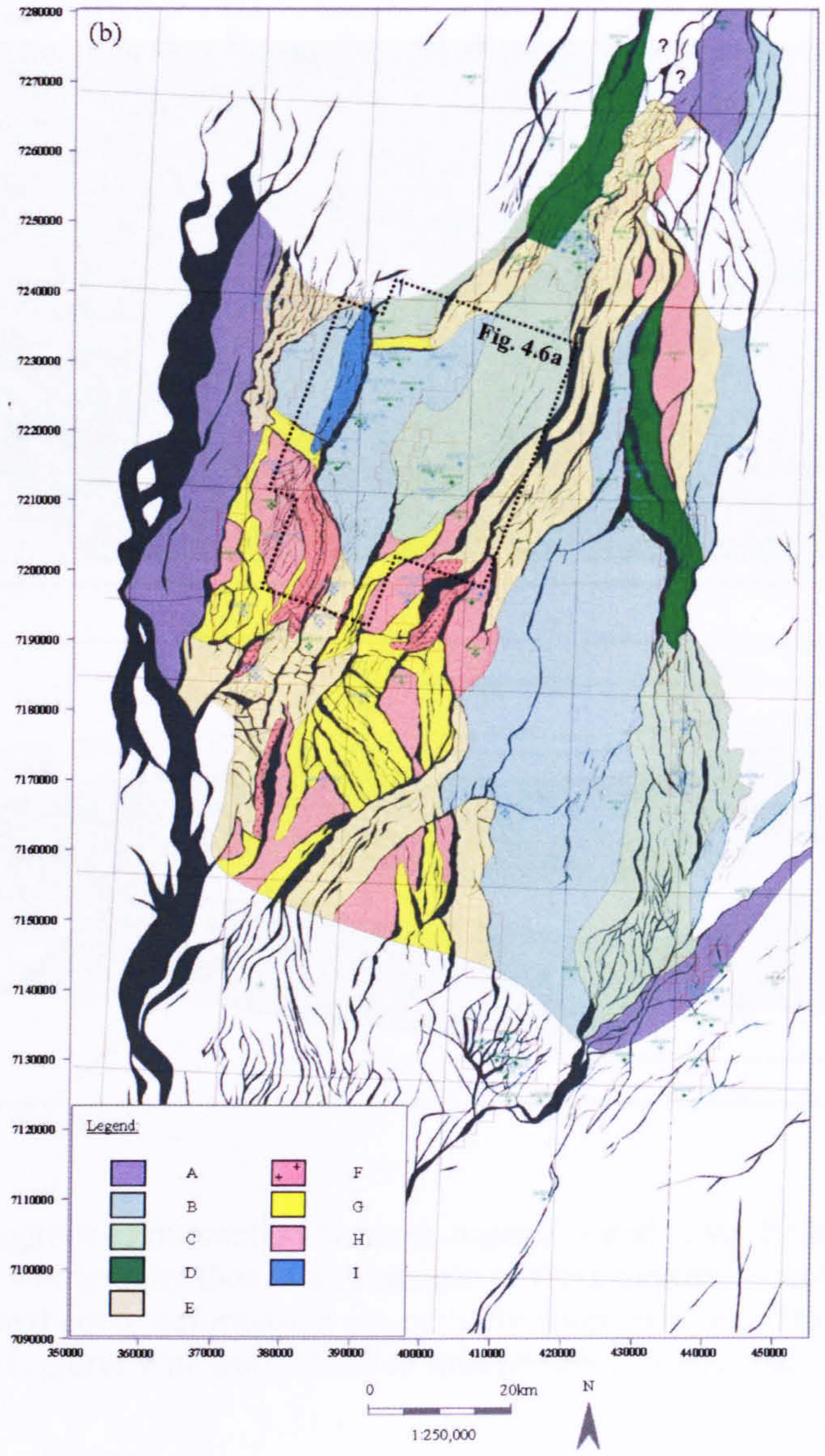

Figure 4.6: Figure caption on following page.

Missing pages are unavailable

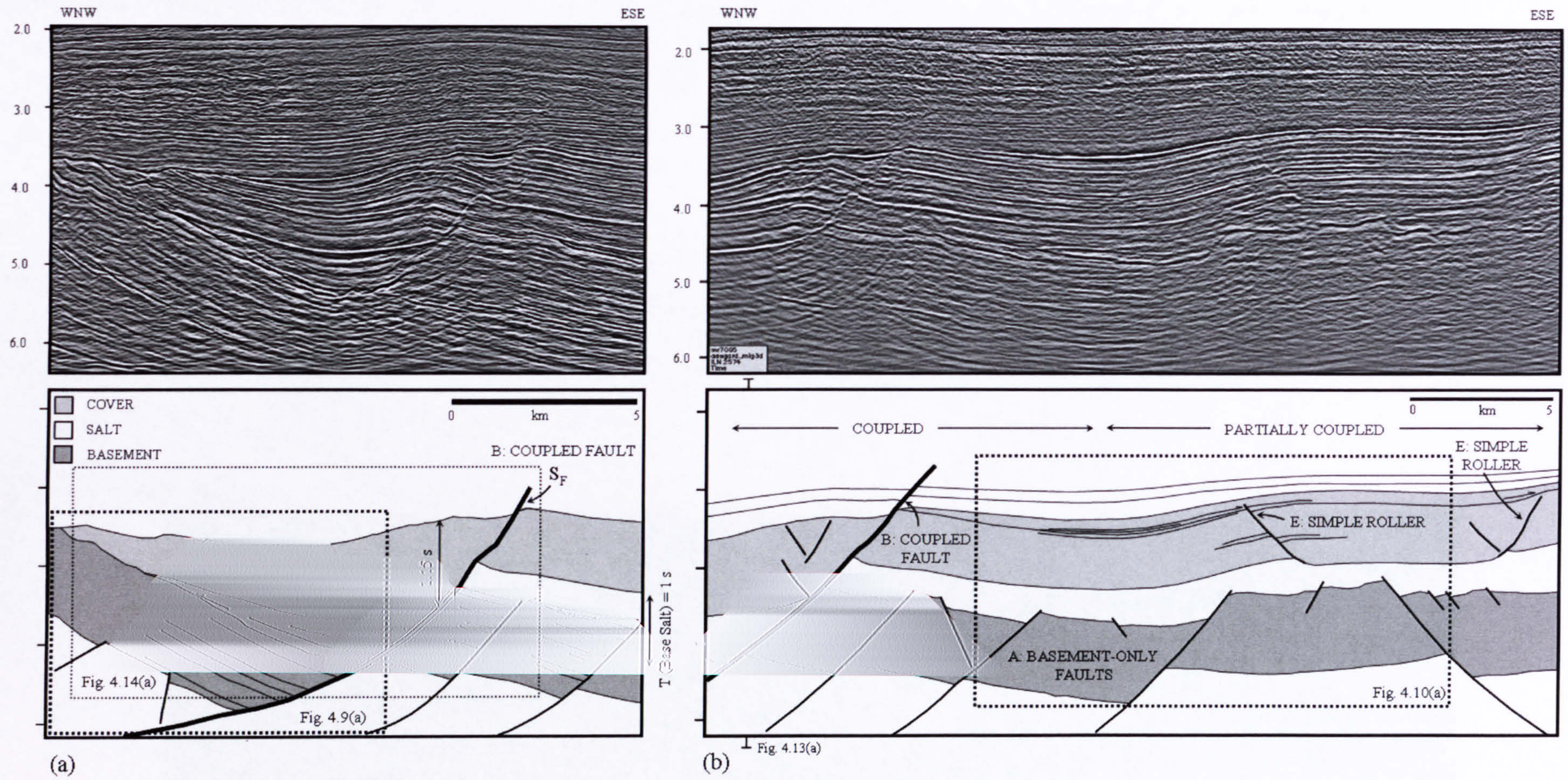

Figure 4.7: Cross-sections from the Åsgard area highlighting different degrees of interaction between basement and cover faults formed due to thick-skinned deformation; (a) The Smørbukk fault (S_F) is rooted in sub-salt basement stratigraphy thus is an example of thick-skinned coupled deformation. T (Base Salt) is the throw at base salt level. (b) East of the Smørbukk fault, basement and cover deformation are partially coupled. Cover faults detach on the mechanically weak evaporites, e.g. simple rollers (E) in the cover only. The locations of figures with more detailed interpretation are outlined by dashed boxes.

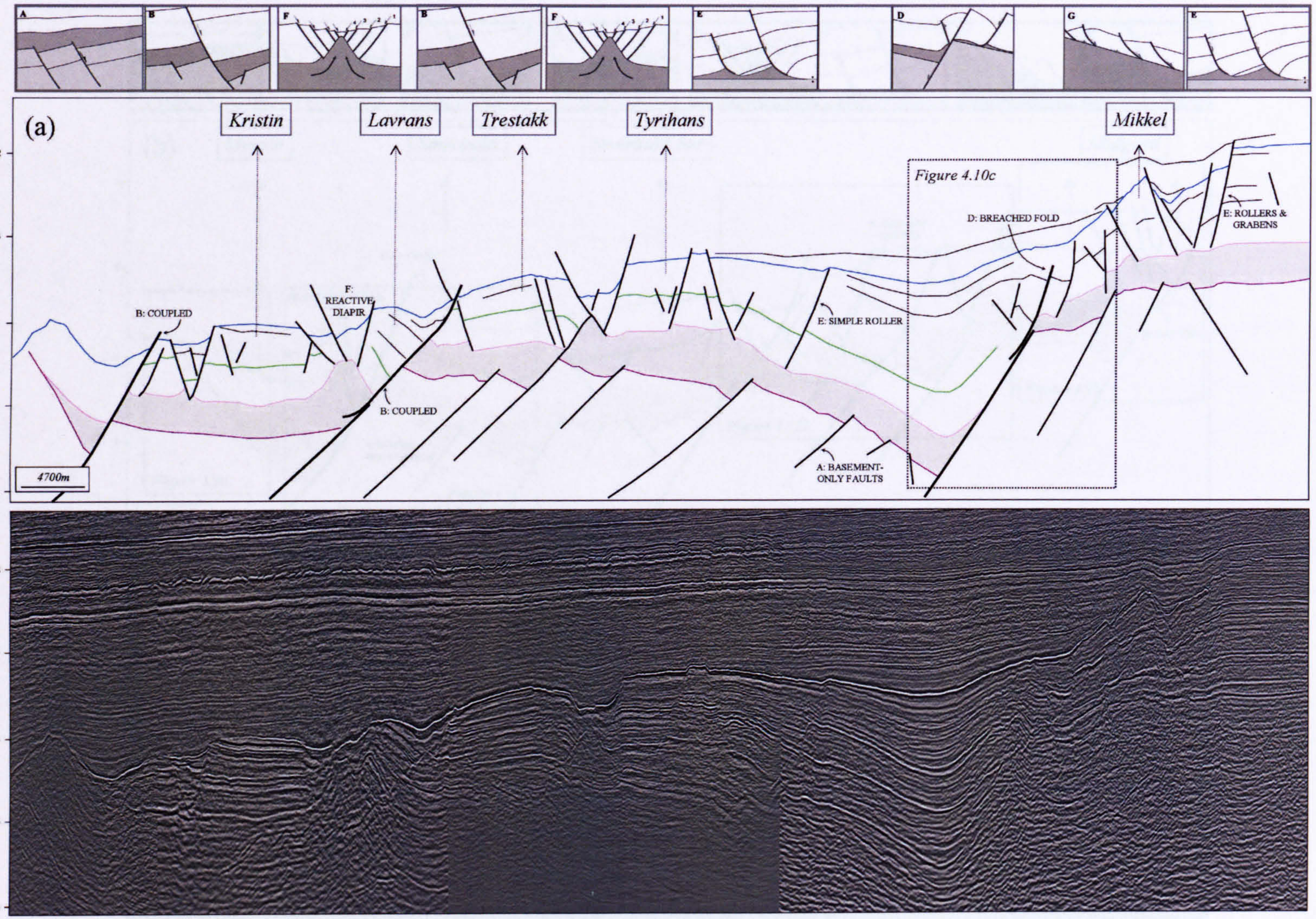
A
B
F
B
F
E
D
G
E
(a)
Kristin
Lavrans
Trestakk
Tyrihans
Mikkel
Figure 4.10c
D: BREACHED FOLD
E: ROLLERS & GRABENS
B: COUPLED
F: REACTIVE DIAPIR
E: SIMPLE ROLLER
B: COUPLED
A: BASEMENT-ONLY FAULTS
4700m
2
3
4
5
6
2
3
4
5
6

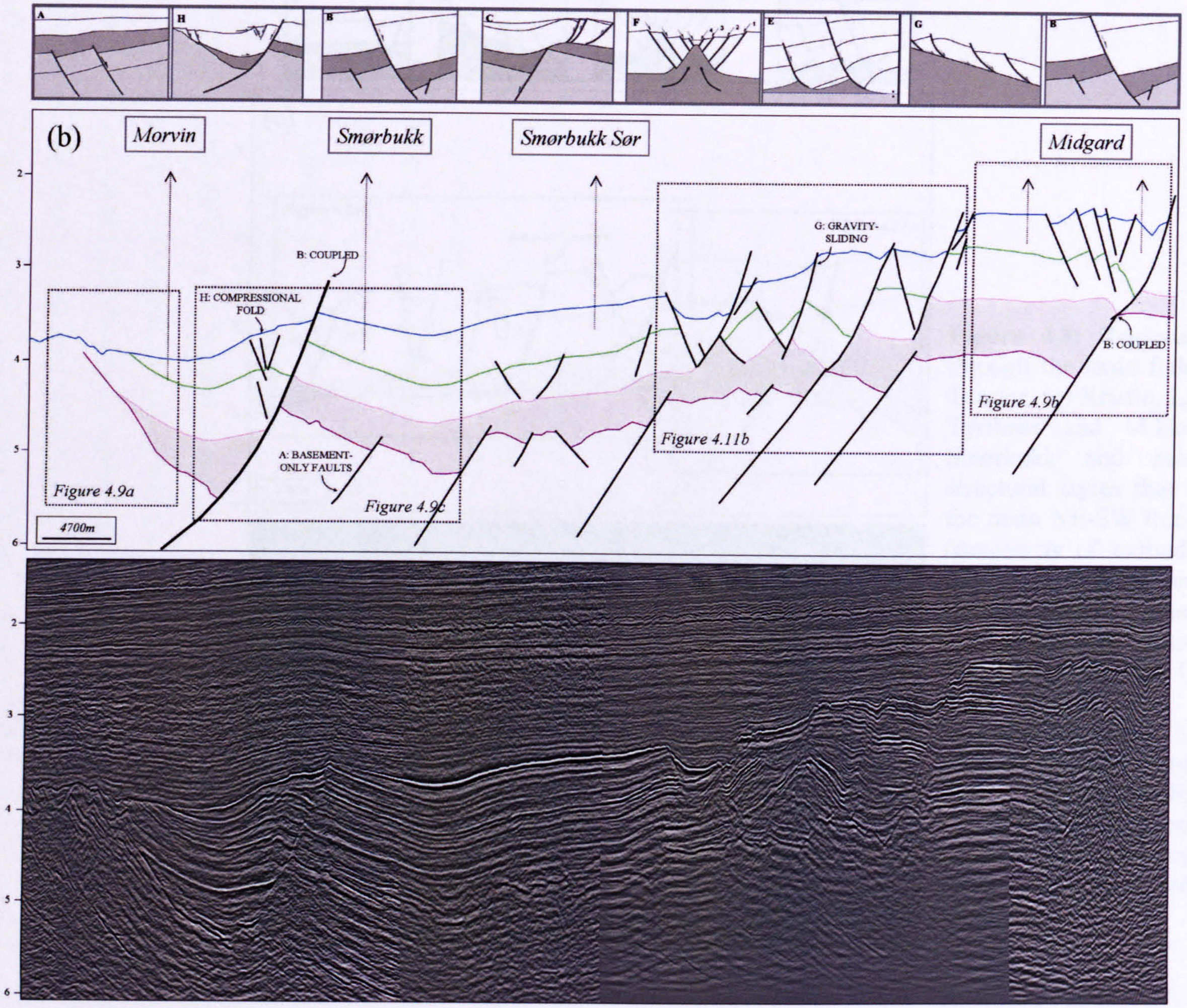
A
H
B
C
F
E
G
B
(b)
Morvin
Smørbukk
Smørbukk Sør
Midgard
B: COUPLED
H: COMPRESSIONAL FOLD
G: GRAVITY-SLIDING
A: BASEMENT-ONLY FAULTS
B: COUPLED
Figure 4.9a
Figure 4.9c
Figure 4.11b
Figure 4.9b
4700m
2
3
4
5
6
2
3
4
5
6

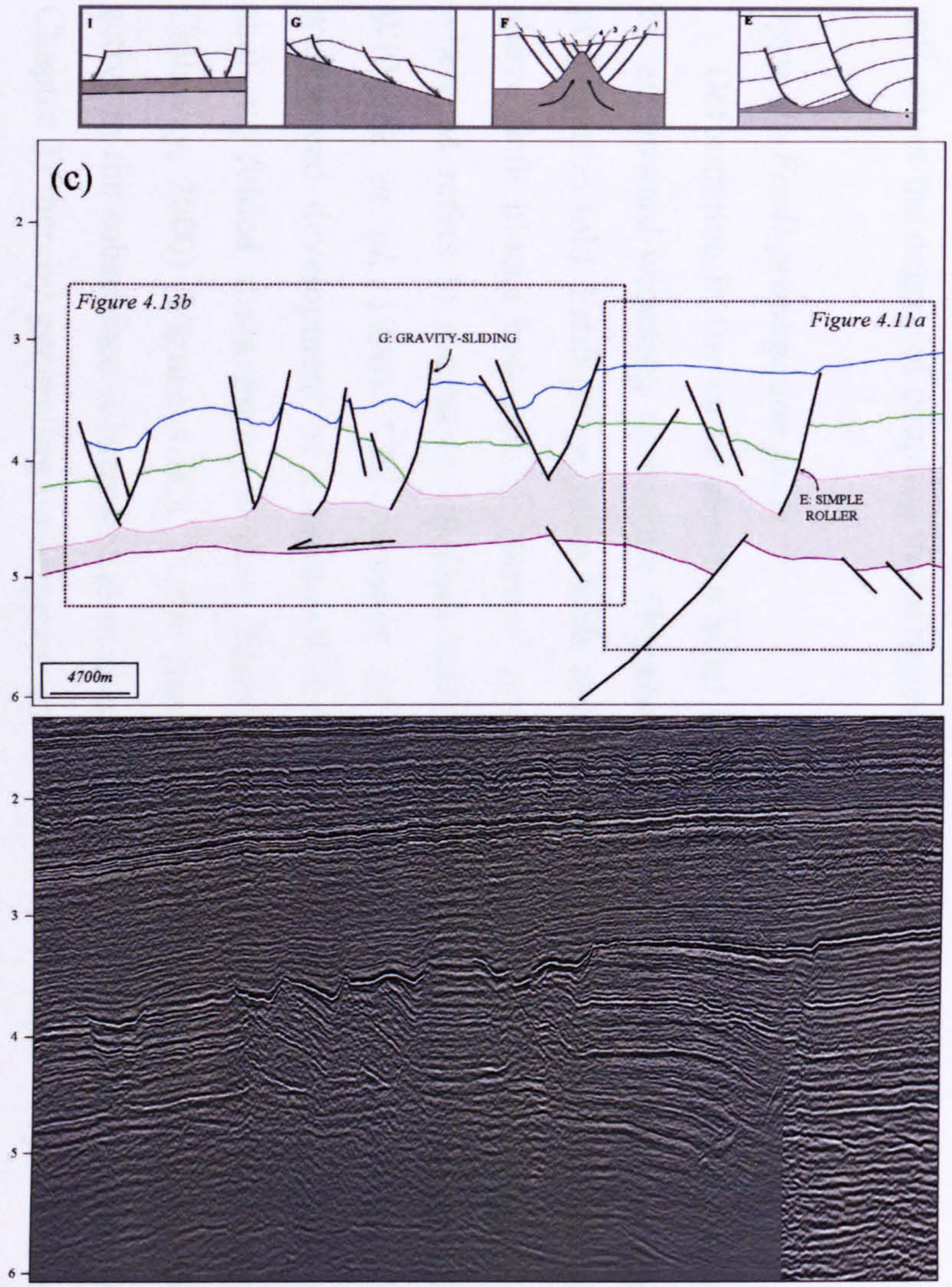

Figure 4.8: Regional cross sections through the main fields on the Halten Terrace. (a) Kristin, Lavrans, Trestakk, Tyrihans and Mikkel. (b) Morvin, Smørbukk and Midgard and (c) structural styles that form oblique to the main NE-SW trend. The structural complexity of individual fields varies greatly across the area. Each figure shows blank seismic data and interpreted lines (Base Salt (purple), Top salt (pink), Åre Coal (green) and BCU (blue)). The distribution of structural styles is highlighted in a series of sketches along the top of each figure, whilst hard-linked faults are also highlighted in bold on the cross sections. The locations of figures with more detailed interpretation are highlighted.

Examples of coupled faults include the Smørbukk and Trestakk faults from the Åsgard area. The Smørbukk fault is a thick-skinned listric fault with throws of up to 1 second TWTT (**Figure 4.7a**). Other examples include the coupled fault east of the Midgard field (**Figure 4.9b**) and the Smørbukk fault (**Figure 4.9c**).

Coupled faults, which initiated with the onset of extension in the Early Jurassic (see Chapter 3) remained active throughout rifting as strain became progressively localised onto a few, large displacement faults. The observations presented, supported by knowledge of the orientation and timing of activity on these faults, demonstrate that the longest-lived and largest displacement faults are the most coupled, which again suggests that the magnitude and duration of extension influences the degree of coupling in the region.

Type C - Fault-propagation folds

Deformation in the cover above a blind basement fault is initially characterised by an upward-widening monocline (**Figure 4.10a**) (Finch *et al*, 2004), or fault-propagation fold. Fault-propagation folds are defined here as 'forced folds that form above fault blocks bounded by 'master' normal faults at depth, (M in Fig. 4.11), where M refers to the basement fault controlling deformation in the cover (after Withjack *et al*, 1990). The presence of subsurface evaporites facilitates the widespread development of extensional forced folds by partially decoupling the shallow, folded strata from the deep faulted strata in the basement (Withjack & Callaway, 2000) (**Figure 4.5C**). In the Åsgard area, master basement faults were active in the subsurface subsequent to evaporite deposition in the Early Jurassic (see Chapter 3) thereby generating deformation in the cover in the form of synclines and anticlines synchronous with Jurassic extension.

There are two examples of preserved fault-propagation folds on the Halten Terrace, in the Smørbukk-Heidrun segment and the Gimsan Basin (**Figure 4.3b**). In both cases, fold axes are oriented NNE to NE, with hinge lines up to 25 – 30km long with fold azimuths that vary in map-view (**Figure 4.6a, b**). This structural style is associated with regions where there is the lowest density of larger cover faults on the terrace (c. 20 km spacing).

The geometry of folds in the area varies with the magnitude of displacement on the master basement fault. The Trestakk Monocline (**Figures 4.7a, 4.11a**) is a wide fold (after Twiss, 1988) with an amplitude (A, from Top Salt to BCU) of 1.3 seconds

or 1.6 km (assuming an average seismic velocity for sedimentary rocks of 2500m/s) and a wavelength ($\lambda/2$, distance between the crest & trough of the fold) of 7.3 km. Thus, the fold has an aspect ratio, which is define here as $A/(\lambda/2)$, where A is measured in depth, of 0.22. Further north, the north-east syncline (**Figure 4.10b**) is also a wide fold with an aspect ratio of 0.2. Here the amplitude of the fold is 2 seconds, or 2.5 km (applying the same assumptions as above), whilst the wavelength is 13km. In the former case, the throw on the master basement fault is 0.3 seconds whilst in the later case the throw is over three times larger at 0.93 seconds. Although the aspect ratios of both folds are similar, the larger displacement basement fault generates a higher amplitude, wider fold - an observation that supports the results of experimental models which suggest that the magnitude of displacement on the basement faults controls the geometry of the fold in the cover (Withjack *et al*, 1990; Koyi *et al*, 1993; Vendeville *et al*, 1995; Stewart, 1997).

Based on the interpretation of faults in the Åsgard area, master basement faults that trend parallel or sub-parallel to fold hinge lines (NNE-NE) are observed. Faults are west-dipping, planar surfaces with average along strike lengths of 10 km and displacements ranging from 500 to 1000 ms, although it is suggested that displacements of >300 ms may be sufficient to initiate deformation in the cover (see Chapter 5). Synthetic or antithetic faults form to accommodate flexure in the cover stratigraphy above the footwall of the master basement fault, sometimes displaced several kilometres up-dip from the fold hinge (e.g. Grinda Graben, **Figure 4.10b**). Individual faults vary in geometry from planar up-dip to listric down-dip where they detach on the salt (**Figure 4.10c**). Displacements range from 100 – 300 ms, increasing with displacement on the underlying basement fault. With increasing basement displacement, the amplitude of the monocline increases and more complex fault geometries initiate closer to the fold hinge (**Figure 4.10b**) which it is suggested form to accommodate basement extension. In addition, as the amplitude of the monocline increases, the down-dip translation of footwall cover blocks over the fold hinge often opens up large graben in up-dip locations, which are likely influenced by gravity-sliding above an inclined detachment surface. This process controls internal faulting within fields such as Smørbukk Sør and Mikkel (**Figure 4.10e**).

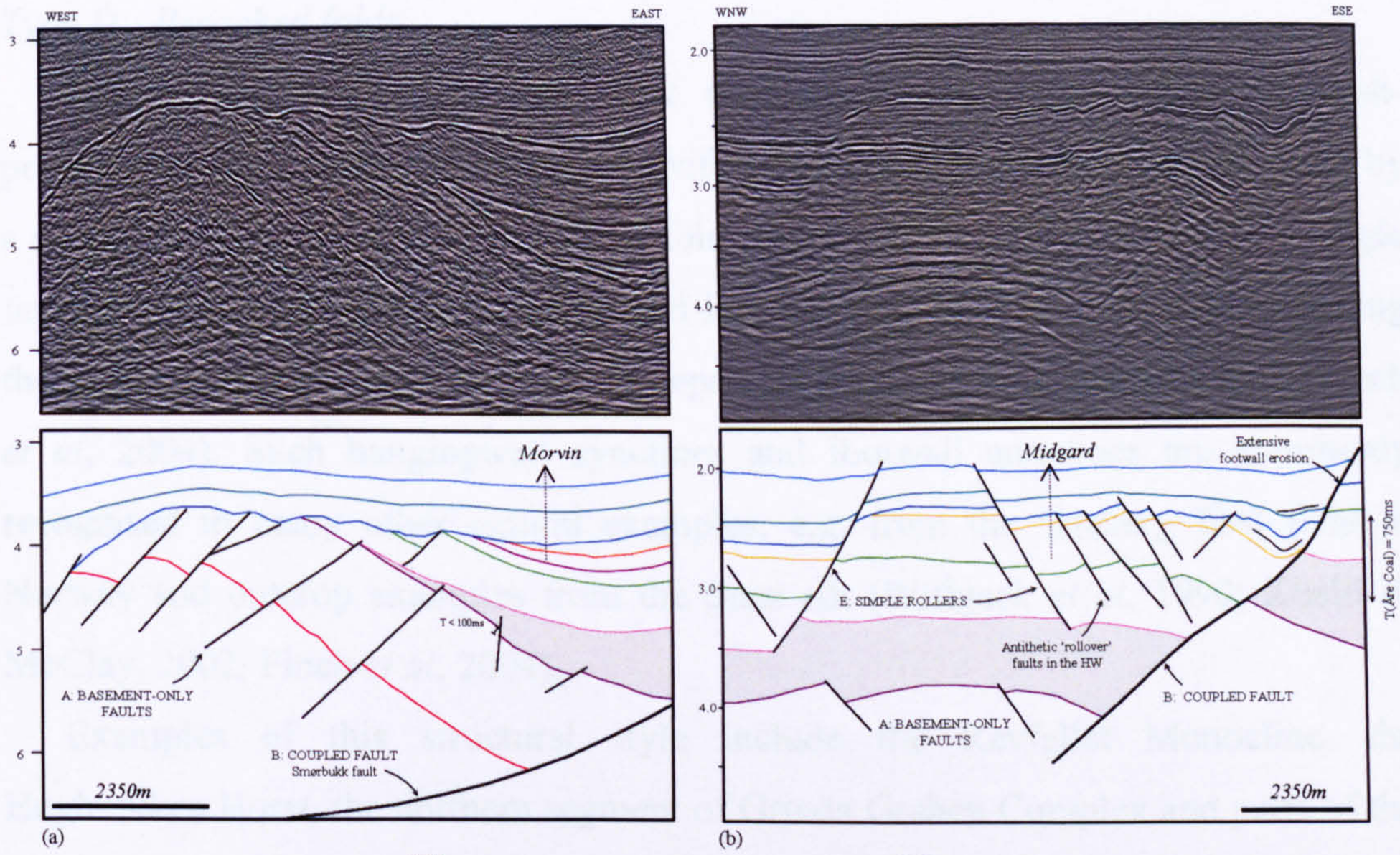

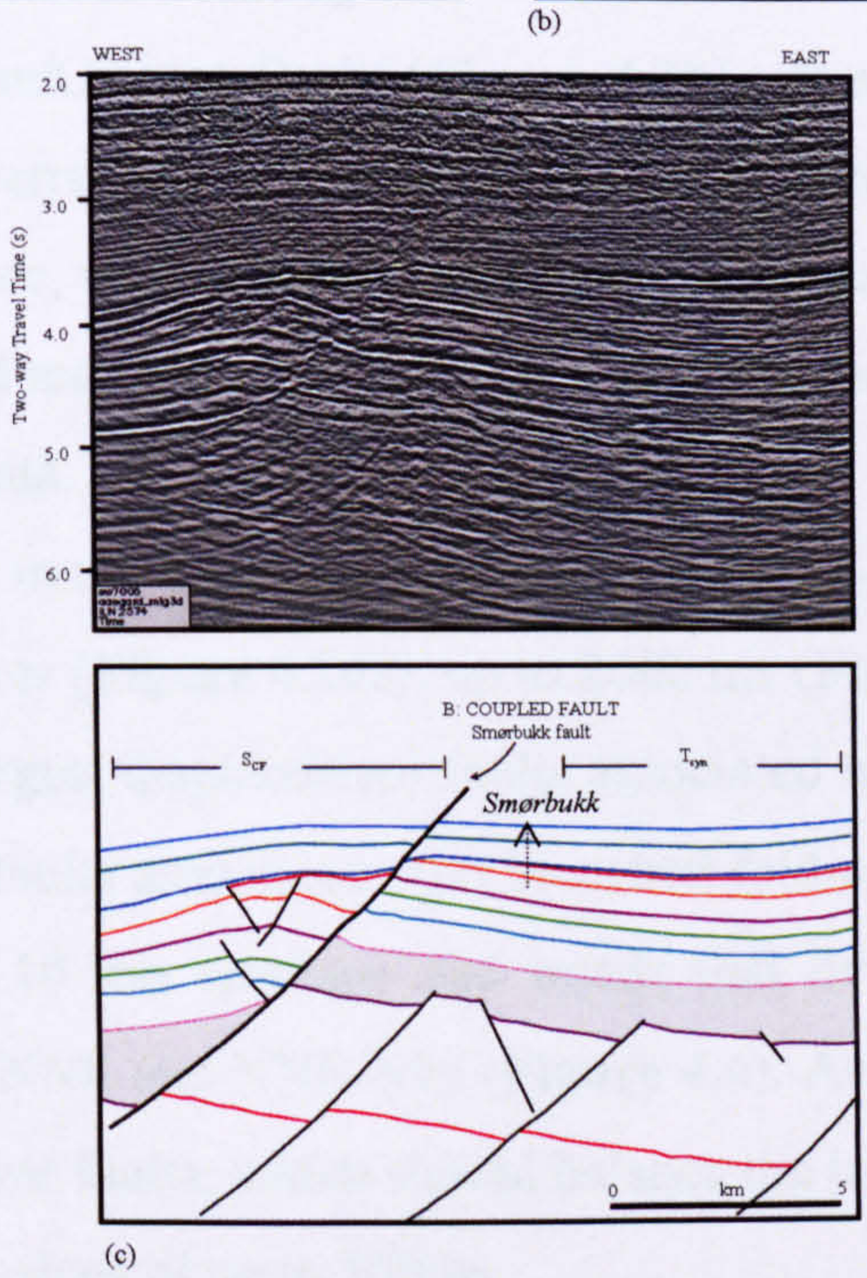

Figure 4.9: (a) Low-relief, basement blocks (structural style A) west of the Morvin field. Permo-Triassic basement faults decoupled from the cover are draped by the BCU due to extensive erosion in the west. (b) Coupled fault (bold) west of the Midgard field (see Figure 4.8b for location) offsets the entire salt sequence, linking basement and cover strata. (c) The Smørbukk fault which offsets the entire salt layer, coupling basement and cover faults. See Figure 2.25 for colour codes used for seismic marker horizons.

Type D - Breached folds

Upward widening monoclines that characterise the initial stages of fault-propagation folding are often replaced, with continued slip on the basement fault, by a single, through-going fault (breached fold, **Figure 4.10d**). Localisation on a single fault produces hangingwall synclines and footwall anticlines as a result of breaching the earlier monocline and which do not represent frictional drag against a fault (Finch *et al*, 2004). Such hangingwall synclines and footwall anticlines are commonly recognised in many other natural examples, e.g. from the Oseberg East field in Norway and outcrop examples from the Suez rift (Withjack *et al*, 1990; Khalil & McClay, 2002, Finch *et al*, 2004).

Examples of this structural style include the Revfallet Monocline, the Høgbrakken Horst, the northern segment of Grinda Graben Complex and parts of the Bremstein Monocline/Gimsan Basin (**Figure 4.3b**), all of which are located on the east of the Halten Terrace. It is possible that similar breached folding took place on the west of the terrace, where shallow detached geometries equivalent to those in the footwall of breached monoclines are observed, but basement faults are too deep to be imaged in seismic data.

Faults that form in the basement are planar and west-dipping with displacements that vary from 750 ms (**Figure 4.10e**), up to 2000 ms (**Figure 4.10f**), up to twice the magnitude of the largest displacement faults associated with fault-propagation folds. In the cover strata, faults associated with breached folding can have lengths up to 40 km, approximately 10 km spacings and trends that lie sub-parallel to underlying basement faults (N-NNE and NNE-NE) (**Figure 4.6**). As expected, the magnitude of displacement on cover faults, which should balance the larger displacement basement faults, increases to values of up to 500ms.

The footwalls containing detached faults associated with earlier fault-propagation folding are uplifted and eroded (**Figure 4.10e, f**). In the hangingwall, rotation and steepening of bedding and faults generates extreme dips which are difficult to image seismically (**Figure 4.10f**). Analogue models predict that normal faults will be rotated into reverse faults during fold breaching (Withjack & Callaway, 2000), an observation that supports the interpretation of reverse faults on the Heidrun field (**Figure 4.10f**). Thus, the geometries associated with breached folding could, without existing knowledge of the regional structural system, be incorrectly interpreted as compressional features (**Figure 4.5D**).

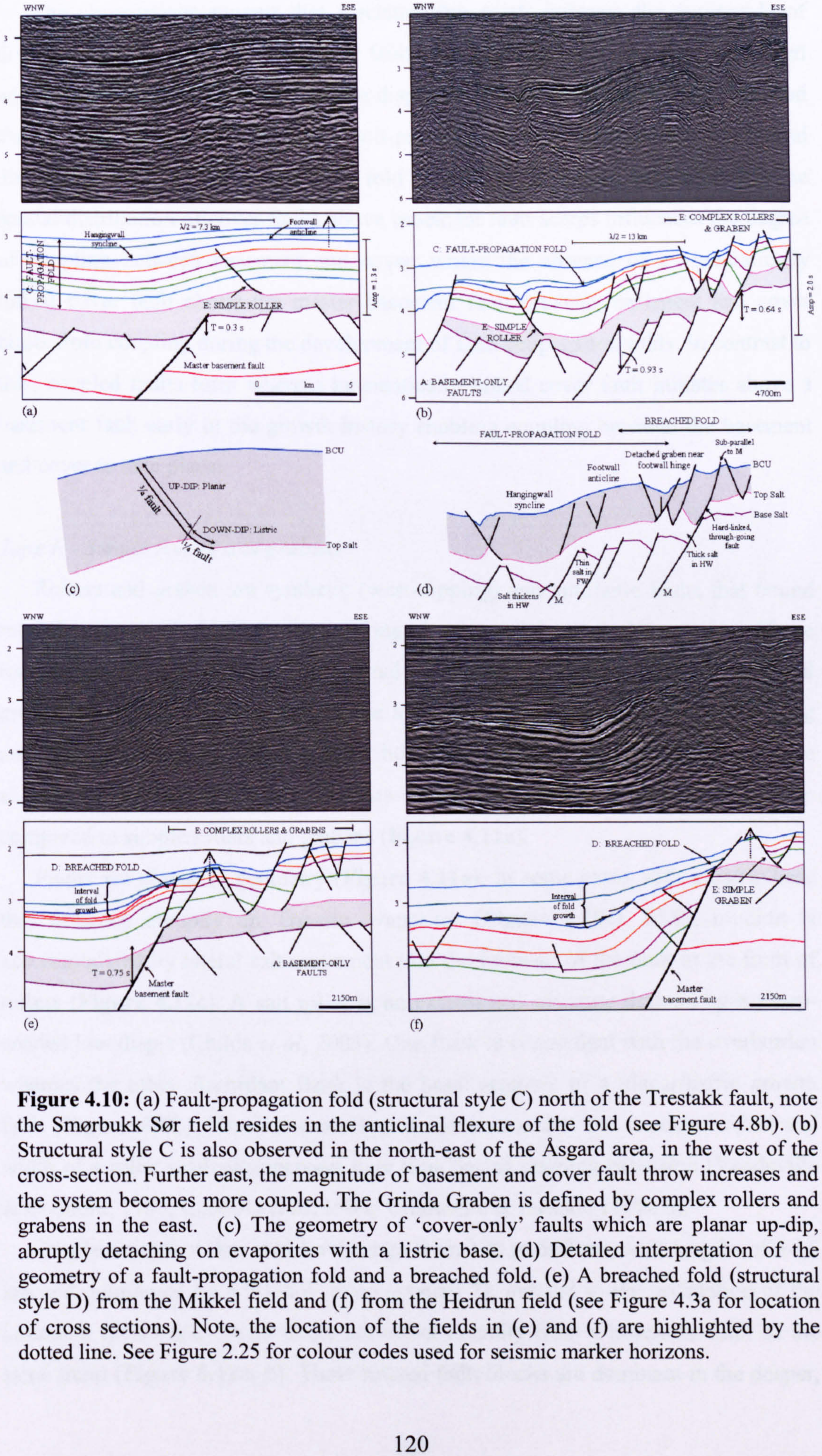

Figure 4.10: (a) Fault-propagation fold (structural style C) north of the Trestakk fault, note the Smørbukk Sør field resides in the anticlinal flexure of the fold (see Figure 4.8b). (b) Structural style C is also observed in the north-east of the Åsgard area, in the west of the cross-section. Further east, the magnitude of basement and cover fault throw increases and the system becomes more coupled. The Grinda Graben is defined by complex rollers and grabens in the east. (c) The geometry of 'cover-only' faults which are planar up-dip, abruptly detaching on evaporites with a listric base. (d) Detailed interpretation of the geometry of a fault-propagation fold and a breached fold. (e) A breached fold (structural style D) from the Mikkel field and (f) from the Heidrun field (see Figure 4.3a for location of cross sections). Note, the location of the fields in (e) and (f) are highlighted by the dotted line. See Figure 2.25 for colour codes used for seismic marker horizons.

The observations suggest that a relationship exists between the magnitude of displacement on basement and cover faults and the degree of coupling associated with extensional folding, where smaller displacement basement faults (<1000ms) and shorter fold axes associated with fault-propagation folds increase in length and displacement (up to 2000ms) during fold breaching. It is also suggested that the spatial distribution of cover faults above basement fault scarps influences the degree of coupling between basement and cover, where the absence of a kinematically linked cover fault above the master basement fault prevents basement and cover faults from coupling during the development of fault-propagation folds. In contrast to this, coupled faults form where a kinematically linked cover fault initiates above a basement fault early in the growth history enabling coupling between the basement and cover to take place.

Type E - Simple rollers and grabens

Rollers and graben are synthetic (west-dipping) and antithetic faults that bound rotated cover fault blocks with varying degrees of internal deformation. These include simple rollers with little internal deformation (**Figure 4.11a**) to horst and graben complexes that have undergone a larger degree of intra-fault block folding and faulting (**Figure 4.11b**). Complex horsts and grabens (**Figure 4.11b**) are more closely spaced with often complex cross-cutting relationships in cross-section when compared to simple rollers and grabens (**Figure 4.11a**).

Faults are planar in geometry (**Figure 4.11a**), in some cases with a listric base that detaches abruptly on Triassic evaporites (**Figure 4.10c**). Block rotation is accommodated by lateral salt movement into the footwall of the fault in the form of rollers (**Figure 4.11c**). A salt roller is an extensional structure defined by a sharp-crested low diapir (Childs *et al*, 2003). One flank is concordant with the overburden whereas the other discordant flank is the basal segment of a planar/listric growth fault (**Figure 4.5E**). Physical modelling demonstrates that the structural relief and width of a roller gradually increase over time during ongoing extension (Vendeville & Cobbold, 1987; Cobbold *et al*, 1989; Vendeville & Jackson 1992a,b).

Displacements at Åre coal level range from 100 to 500 ms, with lengths of 5-15 km and dominated by a NE-SW trend (system 2), parallel to the orientation of the basement fault trend. Many faults are offset laterally from a basement fault of the same trend (**Figure 4.11a, b**). These rotated fault blocks are dominant in the deeper,

western parts of the Halten Terrace, e.g. Gjæslingan lineament, Halten West Segment, Morvin Segment and further east throughout the Grinda Graben Complex **(Figure 4.3b, 4.7b)**.

Rollers and grabens of varying degrees of complexity form due to thick-skinned extension and are partially coupled to basement faults via detachment layers in the salt sequence. Displacements on cover faults increase with the displacement on nearby partially coupled basement faults and thus an increase in the degree of coupling is observed as the magnitude of displacement on basement *and* cover faults increases (**Figure 4.8a, b**). More complex rollers and grabens likely form where salt expulsion forms reactive diapirs (see section 4.4.1.6), which initiate during regional extension. This results in the development of new depocentres and thus the initiation of renewed fault growth.

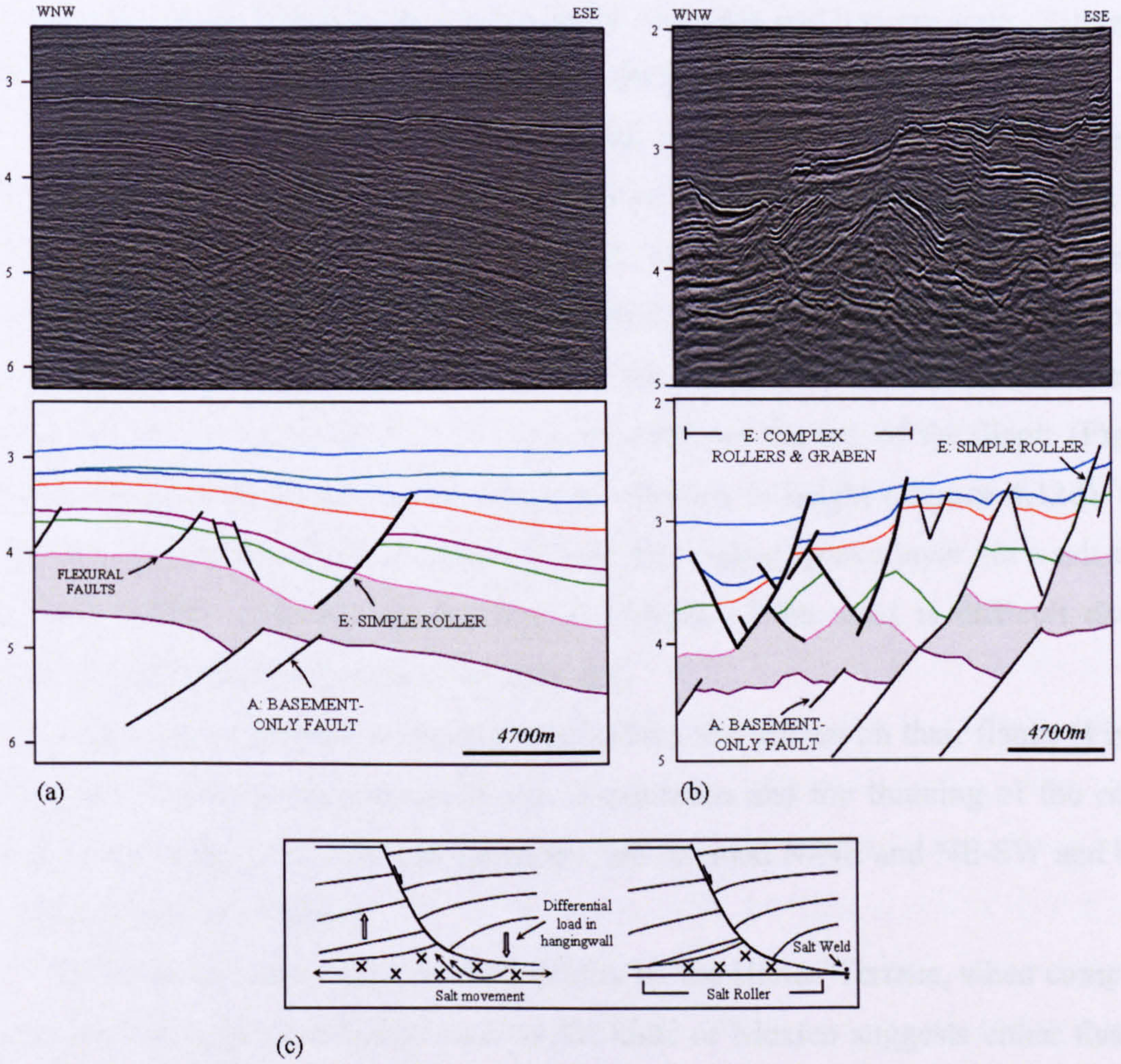

Figure 4.11: Examples of structural style E (a) A simple roller from the Gimsan Basin and (b) a series of complex rollers and graben through the Grinda Graben (see Figure 4.3a for the location of cross-sections. (c) Schematic diagram to illustrate the formation of a 'roller' due to differential loading in the hangingwall of a cover fault above mobile evaporites. See Figure 2.25 for colour codes used for seismic marker horizons.

Type F - Reactive diapirism

Faulting in the cover sequence, due to rifting or gravity-spreading, thins the brittle overburden initiating the rise of diapiric walls, or reactive diapirs, below the thinned floors of grabens (**Figure 4.5F**) (Vendeville & Jackson, 1992a). Reactive diapirism is controlled by the rate of extension and the volume of the salt source (Vendeville & Jackson, 1992a). The diapir will stop growing when extension ceases and/or when the source layer is depleted.

Reactive diapirs preserved at the present-day on the Halten Terrace are limited to the Sklinna Saddle (**Figure 4.12a**), Halten West and the Grinda Graben Complex (**Figure 4.3b**). In addition, a detached salt stock, or teardrop diapir (Jackson & Talbot, 1991), e.g. a diapir that is detached from the salt source via a salt weld, is preserved above a basement half-graben on the Nordland Ridge (**Figure 4.12b-d**). In general, the reactive diapirs are located in the footwalls and hangingwalls of coupled faults such as the Smørbukk and Trestakk faults (**Figure 4.12a, 6b**).

The most continuous diapirs, which reach a maximum of ~15-20 km in length (**Figure 4.6b**), lie beneath the graben east of the Kristin field and between the Trestakk and Tyrihans fields (**Figure 4.8a**). In cross-section, diapirs have an average width of 2-5 km and a maximum height of 500 ms. The salt spine preserved on the Nordland Ridge is geometrically unsual for the region. In map view, a pronounced elliptical feature, approximately 0.5 km wide defines the top of the diapir (**Figure 4.12c**) whilst in cross-section the diapir is ~850 ms in height (**Figure 4.12d**). One hypothesis is the salt stock is detached from the original source layer via a salt weld (**Figure 4.12d**), although constraining the height of the weld is difficult due to problems inherent in seismically imaging salt.

Diapirs are commonly associated with rollers and graben on their flanks (**Figure 4.8a**) which form during the initiation of extension and the thinning of the cover. Faults can be planar or listric in geometry, are oriented N-NE and NE-SW and have displacements of <500 ms.

The relatively scarcity of reactive diapirs on the Halten Terrace, when compared to other salt-influenced basins such as the Gulf of Mexico suggests either that the rate of extension, or the volume of the salt source was insufficient to generate significant diapirism. Given a thick present-day salt layer (ranging from 50 – 800 ms thick), and an absence of welds between basement and cover, it is suggested that the salt source was not depleted and thus the volume of salt remained sufficient to charge

diapirs. Therefore, the rate of extension is suggested as the dominant factor controlling the relative paucity of diapirs in the region. On the Halten Terrace diapirs are observed, which are points of weakness that localise strain during regional extension, in areas of high net extension adjacent to the most coupled faults in the region. The rate of extension in these areas was most likely high enough to initiate reactive diapirs which then localised strain enabling the development of a few, large displacement coupled faults, e.g. Smørbukk and Trestakk.

4.4.2.2 Cover-dominated (Structural Styles G – I)

Cover-dominated styles are thin-skinned faults typically associated with gravity sliding along a tilted detachment surface. Faults are entirely decoupled from the pre-salt stratigraphy with deformation localised to within the post-salt sequence. They trend oblique to the dominant NE-SW fault trend and always detach on Triassic evaporites. In many cases, the geometry of cover-dominated faults is similar to other partially coupled faults; however it is argued that the mechanism for deformation in each case may be different. In particular, three factors are used to differentiate gravity-driven faults: (i) their orientation perpendicular to the local or regional dip direction; (ii) the absence of basement faults with a similar trend; and (iii) the onset of fault activity, which initiate post-Middle Jurassic, subsequent to activity on thick-skinned faults.

Type G - Gravity sliding

A sedimentary sequence with a basal layer of salt can glide driven by its own weight down a slope of less than 1° (Vendeville, 1987; Mauduit *et al*, 1997) (**Figure 4.5G**). Gravitational sliding induces thin-skinned extensional tectonics above a salt décollement and is characterised by normal growth faults, many examples of which have been imaged in seismic data from the Atlantic margins of Africa (Duval *et al*, 1992; Rouby *et al*, 2002) and Brazil (Cobbold & Szatmari, 1991; Demercian *et al*, 1993; Rouby *et al*, 1993). Existing knowledge of the process of gravity-induced faulting has been greatly improved by the use of experimental models (Vendeville *et al*, 1987; Vendeville & Jackson, 1992a, b; Gaullier *et al*, 1993) which suggest that the geometry and dynamics of gravity-induced faults are controlled by the slope

orientation, with listric growth faults and associated salt structures generally oriented perpendicular to the strike of the slope (Gaullier *et al*, 1993).

The interpretation of gravity-driven faults on the Halten Terrace is based upon their orientation oblique to the trend of basement-involved structural styles (System 3, **Figure 4.4**), and the onset of fault activity relative to basement-involved faults. It is suggested that these thin-skinned faults form due to downslope displacement of the post-salt cover in a system that is decoupled from basement fault activity. The onset of active gravity-driven faulting initiates in the Middle Jurassic (see chapter 3), when basement-involved faults have been active for sufficient time (~20Ma) to tilt the detachment surface and initiate sliding.

The geometry of gravity-induced faults is similar to that of Type E structures but, the main differences between the two are: their orientation in map-view (**Figure 4.13a**); the relative timing of deformation (see Chapter 3); and the inferred mechanism for their formation. Rollers and graben (Type E) form due to extension of the cover during rifting and thus initiate with the onset of extension in the Early Jurassic. In contrast, gravity-driven faults form due to the downslope translation of cover blocks above Triassic evaporites which initiated deformation in the cover from the Middle Jurassic to Early Cretaceous (see 3.4.2.2).

In cross-section structures are geometrically similar to simple graben and rollers or a series of rotated graben that detach on evaporites above an inclined basement surface (**Figure 4.13a, b**). Faults are planar or listric in geometry, with displacements generally <600 ms, although they reach 1000 ms on the Trestakk fault which is influenced by both hard-linkage (i.e. crustal extension) and gravity-sliding (**Figure 4.12a**).

Faults are observed in a wide variety of orientations (E-W, WNW-ESE, NW-SE, ENE-WSW), oblique to the dominant NE-SW trending basement and cover faults (**Figure 4.4**), with lengths between 10-15 km and spacings that are irregular and unpredictable. Faults of this structural style are dominantly in the Halten West Segment, the Sklinna Saddle/Morvin Segment and the Smørbukk-Heidrun Segment where regional dip at Base Salt is to the south-west, perpendicular to the dominant fault strike. Thus, it is suggested that the present-day fault strike can be used to infer the dip on the basement surface synchronous with fault growth.

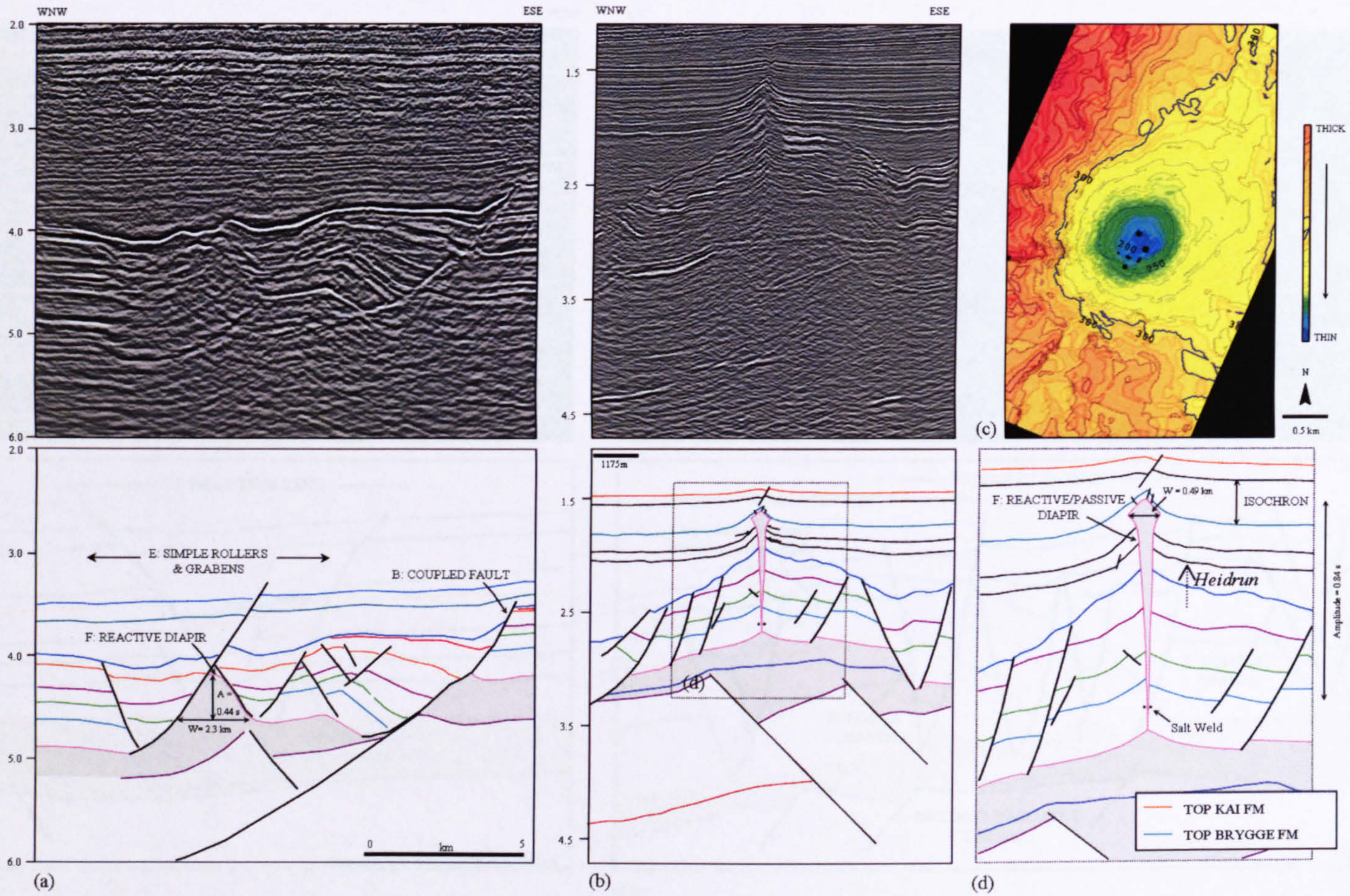

Figure 4.12: Structural style F; (a) a reactive diapir in the footwall of the Smørbukk fault, southern segment (see Figure 4.6a). (b) Cross-section through a salt spine in the Heidrun field, the only structure like it on the Halten Terrace. (c) Isochron illustrating the timing of diapir growth was Miocene in age (Post- Top Brygge), later than other diapirs in the area which are Jurassic-Cretaceous in age. (d) Close up interpreted section through the diapir, highlighting the dimensions of the diapir and the main period of diapir growth. The stratigraphic age of the Kai formation is Upper Miocene – Lower Pliocene, and the Brygge formation is lower to middle Eocene (Eidvin *et al*, 1998). See Figure 2.25 for colour codes used for seismic marker horizons.

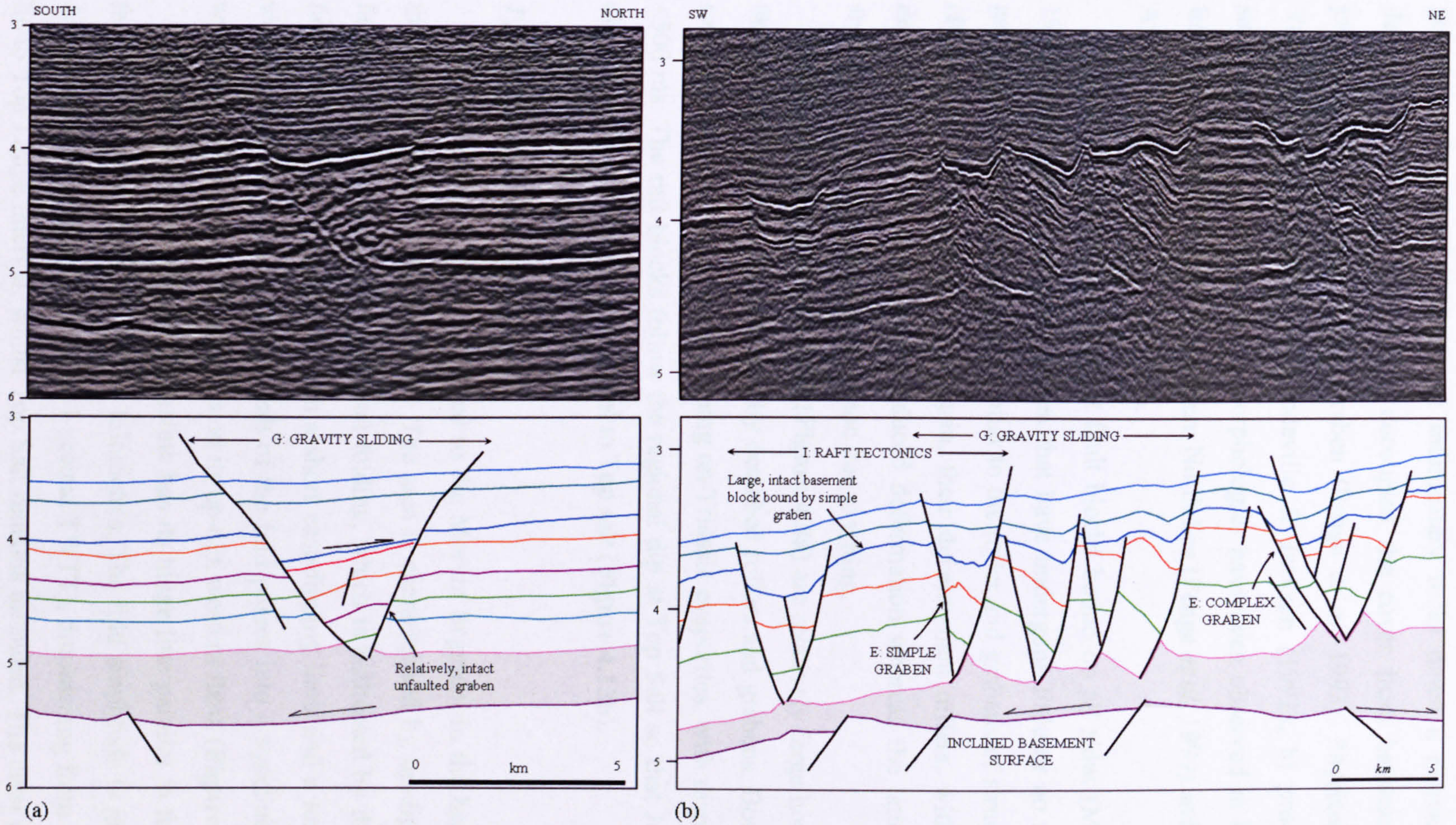

Figure 4.13: Structural styles that form due to gravity-driven deformation above mobile evaporites; (a) A gravity-driven graben (structural style G) in the hangingwall of the Smørbukk fault forms perpendicular to the strike of the fault. (b) A series of rollers, graben and raft blocks trending NW-SE, oblique to the dominant fault trend and normal to the regional dip on the Halten Terrace. See Figure 4.3b for the location of cross-sections. See Figure 2.25 for colour codes used for seismic marker horizons.

Type H - Raft blocks

The concept of rift-raft tectonics was used to describe structures formed by gravitational gliding of blocks of sedimentary rocks down a regional dip on a detachment layer of salt, which decoupled the cover from basement extension processes, in the East Central Graben (Penge *et al*, 1993). Physical models by Vendeville *et al* (1987) and Vendeville & Jackson (1992a, b) produce similar structures and variants of these morphologies have been observed in basins of the Irish Sea, Central North Sea, Southern North Sea (Penge *et al*, 1999) and on the West African margin (Rouby *et al*, 2002).

'Rafts' are defined as coherent fault blocks bound on all sides (Mauduit *et al*, 1997) by simple or complex graben that have undergone little or no rotation. The geometry of rafts is once again similar to the roller and grabens of structural style E (**Figure 4.5H**). However, once again, their development differs, with the former developing due to later gravity-induced deformation whereas the latter (structural style E) forms during earlier extension due to rifting.

Rafts, such as the Kristin field (**Figure 4.8a**) are relatively large horst blocks (c. 8km x 20km in map-view) bound by detached rollers and grabens. Bounding faults can be planar or listric, both detaching on Triassic evaporites, with displacements of <500 ms. The raft blocks follow the regional dip at Top Salt so that Jurassic strata dip and strike parallel or sub-parallel to Top salt (**Figure 4.13b**).

Type I - Compressional folding

Compressional folding is limited to the Morvin Segment in the hangingwall of the Smørbukk fault (**Figure 4.5I**). The area is characterised by up-dip extensional faulting and down-dip compressional folding, which is buttressed by the Smørbukk fault. The fold is asymmetric, with a short east-dipping limb and a longer, steeper west-dipping limb. The western limb of the fold passes into a syncline to the west with shallowly-dipping, listric faults on its up-dip, western flank (**Figure 4.14a**).

The down-dip hangingwall anticline has its hinge line parallel to the Smørbukk fault and a trace length of over 25 kilometres. The fold amplitude is greatest in the Åre Coal to Top Ile interval (up to 1 second TWTT), diminishing from the post-Top Ile to Top Lange interval, whilst Top Salt remains unfolded. The crest of the fold is offset by a series of antithetic and synthetic faults intersecting reflectors from Top

Åre to the BCU. Additionally a number of low displacement faults (< 60 ms) offset the Intra Åre and Åre Coal horizons.

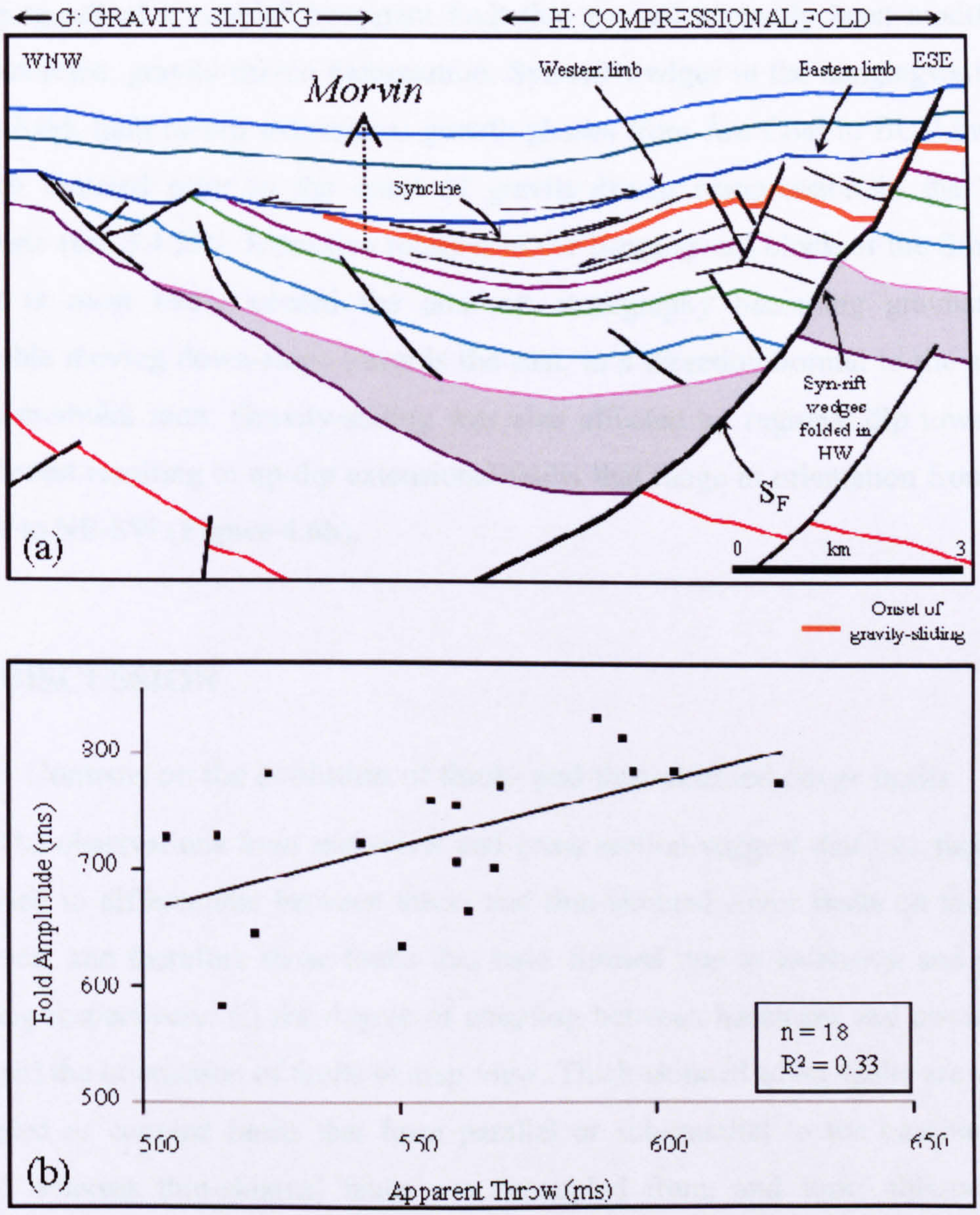

Figure 4.14: (a) A cross-section through a compressional fold (structural style H) in the hangingwall of the Smørbukk fault. The fold, which forms due to gravity-sliding above an inclined basement surface, is defined by up-dip extension and down-dip compression against the Smørbukk fault. (b) A graph of fold amplitude vs. throw on the Smørbukk fault. The regression line shows a positive correlation between fold amplitude and throw supports our interpretation of gravity-sliding above a rotated hangingwall block, where the magnitude of displacement controls the magnitude fold development. See Figure 2.25 for colour codes used for seismic marker horizons.

The magnitude of fold amplitude increases with increasing displacement on the Smørbukk fault (**Figure 4.14b**) and so also with the degree of rotation in the

hangingwall of the fault block. It is suggested that the magnitude of fold amplitude is controlled by the degree of rotation in the hangingwall of the Smørbukk fault block.

This geometry is interpreted as an extensional rollover anticline in the hangingwall of a coupled basement fault that has subsequently been modified by thin-skinned, gravity-driven deformation. Syn-rift wedges in the hangingwall of the Smørbukk fault record extensional growth phases from Åre Coal to BCU intervals, which initiated prior to the onset of gravity-driven compression in the Middle Jurassic (see 3.4.2.2). Extensive rotation in the hangingwall block of the Smørbukk fault is most likely caused the post-salt stratigraphy becoming gravitationally unstable moving down-slope towards the east, in a direction normal to the strike of the Smørbukk fault. Gravity-sliding was also affected by regional dip towards the southwest resulting in up-dip extensional faults that range in orientation from NNE-SSW to NE-SW **(Figure 4.6b)**.

4.5 DISCUSSION

4.5.1 Controls on the evolution of thick- and thin-skinned cover faults

The observations from map-view and cross-section suggest that two factors can be used to differentiate between thick- and thin-skinned cover faults on the Halten Terrace, and therefore those faults that have formed due to extension and gravity-sliding respectively: (i) the degree of coupling between basement and cover faults; and (ii) the orientation of faults in map-view. Thick-skinned cover faults are partially coupled or coupled faults that form parallel or sub-parallel to the basement fault trend whereas thin-skinned faults are decoupled from, and form oblique to the basement fault trend. The mechanisms that control the degree of coupling and the orientation of faults for both thick- and thin-skinned structural styles are considered. Furthermore, the description of the temporal evolution of faults in the area is used to suggest that the mechanisms controlling the evolution of thick- and thin-skinned cover faults differ between those faults that have formed due to extension and gravity-sliding respectively, where thin-skinned faults initiate subsequent to thick-skinned faults when the basement surface has gained sufficient tilt to initiate sliding in the cover.

4.5.1.1 Thick-skinned structural styles

Based on observations presented in this paper, it is suggested that four factors control the degree of coupling between basement and cover faults: the duration of extension; the magnitude of displacement; the rate of extension; and the relative distribution and orientation of faults in the basement and cover.

Observations suggest that the spatial distribution of cover faults, that form in response to basement extension, and the rate of extension on basement faults controls the evolution of coupled and partially coupled faults. In general, the preferential alignment of cover faults over a basement fault and a higher rate of extension initiates more coupled faults (e.g. S_F and T_F, **Figure 4.15B**). Alternatively, where cover faults do not initiate above a basement fault and in areas where the rate of extension is lower, or faults became inactive early in the rift history, it is more difficult for basement and cover faults to couple through an evaporite layer and thus less coupled fault geometries initiate (N_F and NE_{syn}, **Figure 4.15B**). In this study the rate of extension on faults has not been quantified, but existing work suggests that the largest, longest lived faults typically experience the highest rates of extension (Nicol *et al*, 1997) and that faults with apparently lower rates of extension will generate the same geometry as those that simply became inactive sooner and thus have smaller displacements. Consequently in this study, it is not possible to differentiate faults that have undergone high displacement rates from those that were active for longer and thus have larger displacements. Instead the temporal evolution of faults is used to constrain the longest lived faults, which are assume to have undergone the highest rates of extension. Fault activity maps that summarise the temporal evolution of basement and cover faults throughout the Jurassic and into the Early Cretaceous (**Figure 4.15**) are used to address the relationship between the duration of extension, the rate of extension (applying the assumptions discussed above) and the degree of coupling. It is shown that the longest-lived faults are commonly the most coupled, and that the degree of coupling evolves over time from partially coupled (**Figure 4.15A**) to increasingly coupled (**Figures 4.16B**). The introduction of decoupled faults which initiate in the Middle Jurassic and remain active into the Early Cretaceous (**Figure 4.15C**) is also significant. The mechanisms for such decoupled faults are discussed in section 4.5.1.2.

Throughout this paper it is suggested that the magnitude of displacement on both basement *and* cover faults is larger in more coupled systems, such as coupled faults

and breached folds. The opposite is true for partially coupled faults, which become more decoupled as displacement in the basement and cover decreases.

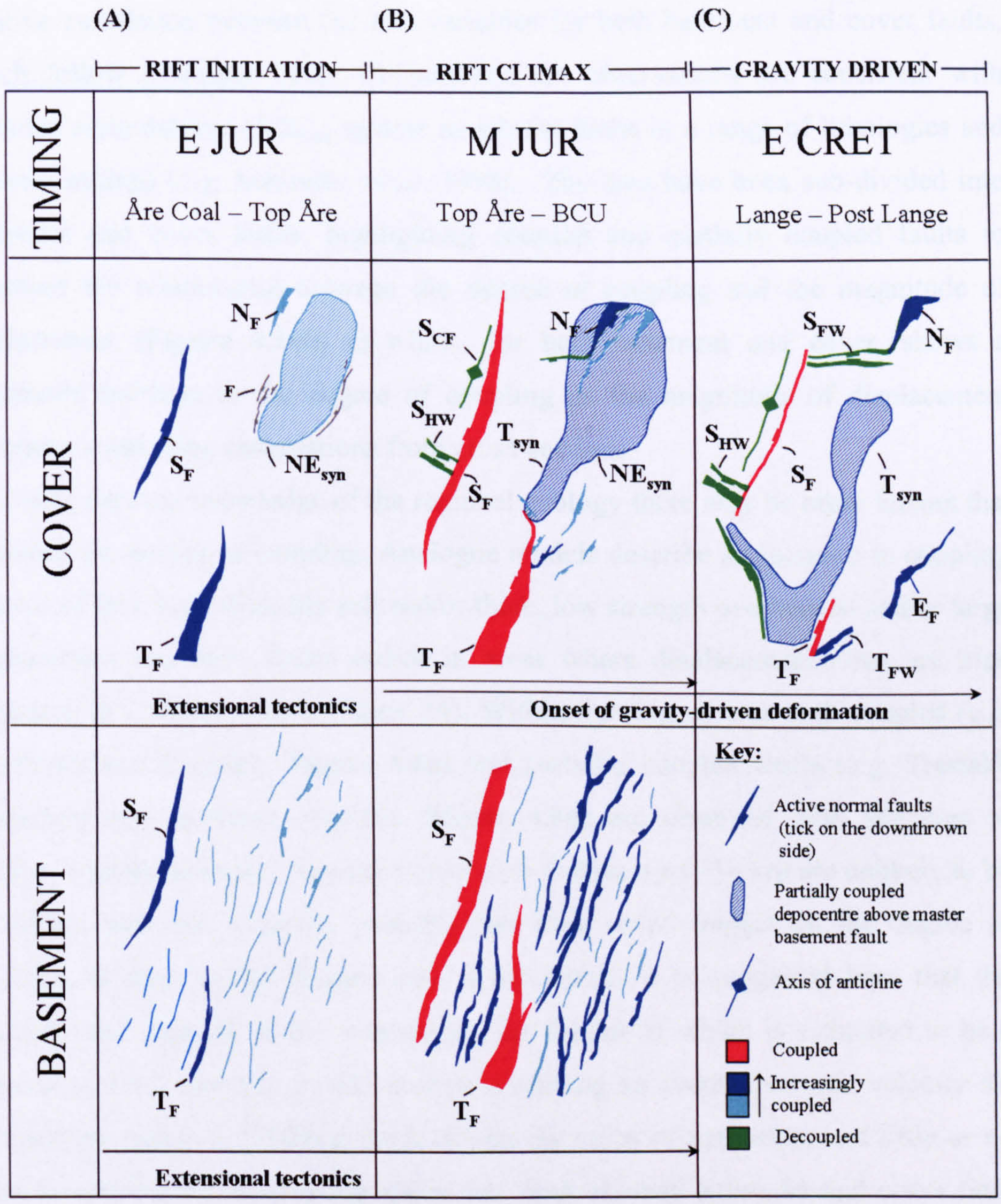

Figure 4.15: Schematic diagram showing the relationship between the duration of extension and the degree of coupling between basement and cover faults from (A) a partially coupled system during the onset of rifting in the Early Jurassic to (B) an increasingly coupled system with coupled and partially coupled faults and the initiation of decoupled faults. (C) The system is dominated by decoupled and partially coupled faults due to gravity-driven deformation

The observations presented can be tested using displacement and length data from faults in the Åsgard area (**Figure 1.4a**). In this approach the magnitude of

displacement using values of displacement maxima (D_{max}) and fault length is quantified, where higher magnitude displacements correspond with larger values of D_{max} and length (**Figure 1.4b**). Plots of D_{max} against length (**Figure 4.16a**) show a positive correlation between the two variables for both basement and cover faults, which follow a similar trend. Collectively, the observations are consistent with previous compilations of D_{max} against length for faults in a range of lithologies and tectonic settings (e.g. Schlische *et al.* 1996). The data have been sub-divided into basement and cover faults, highlighting coupled and partially coupled faults to constrain the relationship between the degree of coupling and the magnitude of displacement (**Figure 4.16b, c**) which, for both basement and cover, shows a systematic increase in the degree of coupling as the magnitude of displacement increases, supporting observations from cross-sections.

Using existing knowledge of the regional geology there may be other factors that influence the degree of coupling. Analogue models describe an increase in coupling in areas of thin, high viscosity salt and/or thick, low strength overburden and/or large displacement basement faults and/or in areas where displacement rates are high (Withjack & Callaway, 2000, figure 14). Within the Åsgard area both coupled (e.g. Smørbukk and Trestakk, **Figure 4.6a**) and partially coupled faults (e.g. Trestakk monocline and northeast syncline, **Figure 4.6a**) are observed with spacings of c.10km. Variations in the viscosity of salt over distances of ~10 km are unlikely to be significant and thus viscosity probably has little or no impact on the degree of coupling, at least in the Åsgard area. Furthermore, it is suggested here that the thickness and strength of the overburden, the former of which is estimated to be a minimum of 0.5 seconds, or 625 metres (assuming an average seismic velocity for sedimentary rocks of 2500m/s) thick during the onset of extension, had little or no effect on the degree of coupling given that thick-skinned basement and cover fault activity initiated synchronously, and thus beneath the same thickness of overburden, in the Early Jurassic (see section 3.4.2). It is reasonable to speculate that the thickness of salt influenced the degree of coupling between basement and cover faults, but the present-day thickness of salt cannot be used to infer its thickness at the time of fault activity. A reconstruction of the depositional thickness of salt is beyond the scope of this study although restoration techniques for areas of salt tectonics could be applied (e.g. Rowan, 1993).

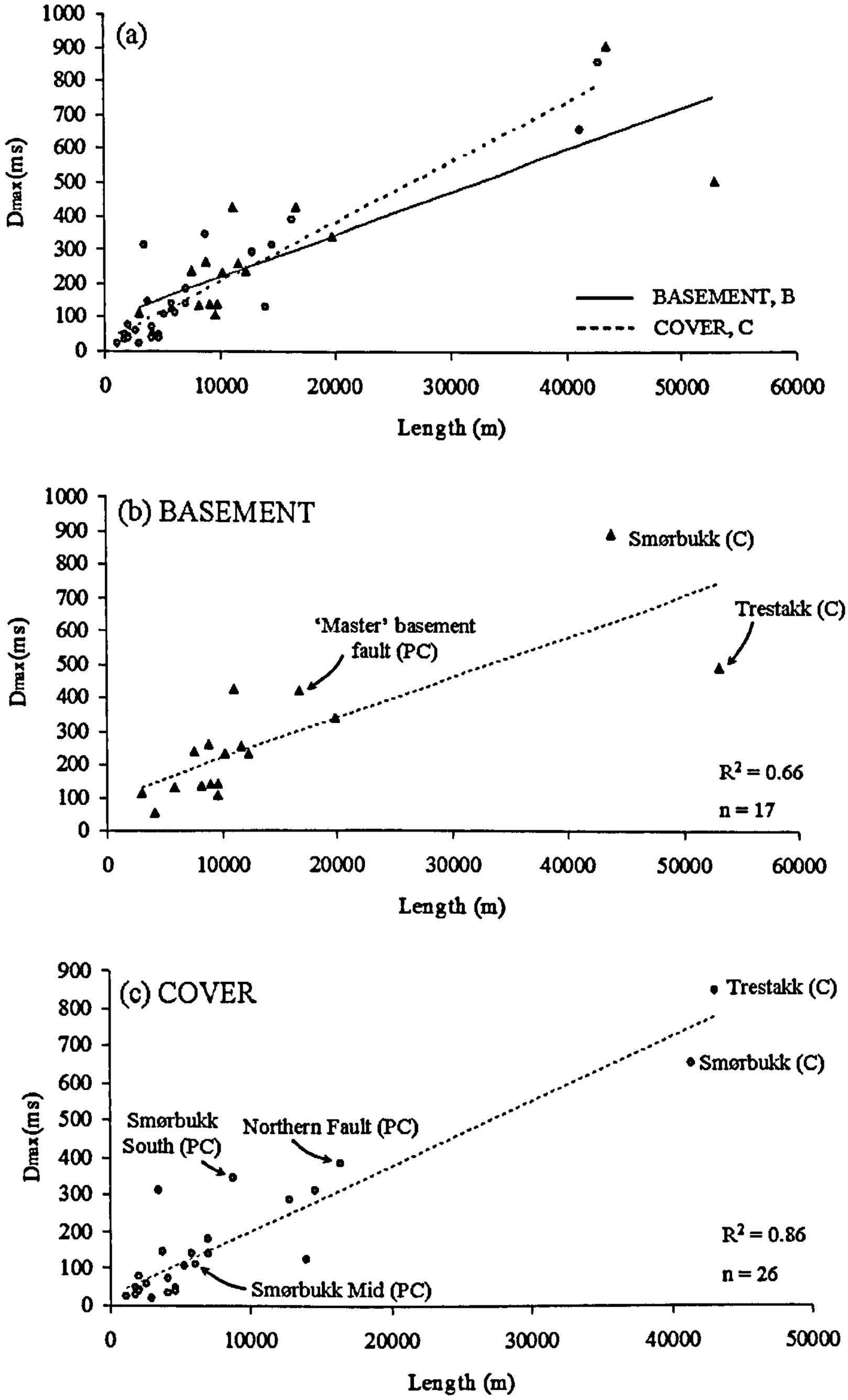

Figure 4.16: D_{max}-length plots for thick-skinned basement and cover faults to illustrate (a) the positive correlation between the magnitude of displacement for both basement and cover faults, suggesting high displacement basement faults are balanced by higher displacement in the cover. (b) and (c) illustrate the relationship between the degree of coupling and the magnitude of displacement, which for both sub- and supra-salt faults increases as the degree of coupling increases, as we might expect. Note, C refers to coupled faults whereas PC refers to those that are partially coupled. Linear regression lines are included on each plot along with values of n (the number of points in the dataset) and R^2 (a statistical measure of how well a regression line approximates real data points, where 1 indicates a perfect fit).

The orientation of thick-skinned faults is, to a first order, likely to be controlled by the regional extension direction resulting in two main sets of faults: (i) those trending perpendicular to the E-W maximum horizontal extension direction of the Jurassic (Mosar *et al*, 2002); and (ii) dominant NNE-NE trending faults whose trend may be explained by the rotation of the maximum horizontal extension direction into NW-SE orientation during the Cretaceous (Mosar *et al*, 2002). The observations from seismic data suggest that the longest-lived, most coupled faults and partially coupled faults are oriented NNE-NE (**Figure 4.15**), whereas more decoupled faults that die out earlier in the rift history follow a more N-NNE fault trend (basement, **Figure 4.15A**). The orientation of NNE-NE trending fold axes, which trend parallel or sub-parallel to master basement faults, is similarly controlled by the maximum horizontal extension direction associated with crustal extension (see Chapter 3).

4.5.1.2 Thin-skinned structural styles

On the Halten Terrace, thin-skinned, gravity-driven faults typically form oblique to the dominant basement fault trend, in the footwalls and hangingwalls of coupled faults and in overlap zones between major faults. The primary control on gravity-driven deformation is the spatial and temporal variation in throw and linkage within basement fault systems. As basement faults increase in displacement, the basement surface gains a sufficient tilt to initiate cover sliding, thus thin-skinned cover faults are spatially related to the largest displacement basement faults. Well-developed thin-skinned faults are observed in the footwall and hangingwall of major coupled faults such as the Smørbukk fault (**Figure 4.6a**).

Thin-skinned faults are observed trending at ~90° to the strike of the underlying basement surface in the footwall and hangingwall of the Smørbukk fault (**Figure 4.4b, c**). Thus the dominant mechanism controlling the evolution of thin-skinned cover faults is the magnitude and direction of dip on the basement surface, which is ultimately controlled by the local fault-controlled tilt, which is associated with the 3D basement fault geometry, e.g. in a relay zones (**Figure 4.2**). An additional component of regional tilt, which was generated in the Early Cretaceous due to uplift associated with the continued northwards propagation of the Central Atlantic Ocean (Torsvik *et al*, 2002), interacts with local fault-controlled tilt. Gravity-driven faults are observed trending perpendicular to the resultant southwest and westerly dip on the Halten Terrace (stage 3, **Figure 4.17c**), e.g. Smørbukk South fault.

4.5.2 Conceptual Model

Our observations can be summarised from map-view and cross-section, along with constraints on the factors controlling the evolution of thick- and thin-skinned structural styles, in a model for the spatial and temporal evolution of thick- and thin-skinned faults in three stages (**Figure 4.17**).

4.5.2.1 Thick-skinned

Internally on the Halten Terrace, fault growth in the basement and cover initiated synchronously in the earliest Jurassic (see section 3.4.2). Deformation in the basement behaves as a purely brittle system initiating with a number of small, low-displacement faults (Stage 1, **Figure 4.17a,** see also Figure 3.14A) which subsequently gain length and displacement linking into large, through-going faults (Stages 2 & 3, **Figure 4.17a**). Faults that form in the cover to accommodate basement extension initiate above a basement fault scarp and similarly grow and link from initially isolated segments (e.g. C_1 & C_2, **Figure 4.17a**). Figure 4.17a summarises the evolution of coupled faults, from initially isolated fault segments in map-view and cross-section (Stage 1), to increasingly coupled (Stage 2) and completely coupled (Stage 3) as the displacement and length of faults increases through segment linkage (Childs *et al*, 1995; Cartwright *et al*, 1996) during continued extension into the Late Jurassic and Early Cretaceous. Cross-sections show the gradual linkage of initially isolated basement and cover faults which progressively displace the salt layer as faults gain displacement, or as the rate of extension increases. Upon gaining sufficient displacement to offset the entire salt layer (Stage 3), basement and cover fault blocks come into contact and behave as one through-going fault. Examples of evolutionary stages 1 – 3 are observed along strike of the Trestakk fault, which is coupled at the point of maximum displacement (Stage 1), becoming increasingly decoupled as the fault loses displacement towards its tips (Stages 2 and 3).

4.5.2.2 Partially Coupled Faults

The same model of strain localisation can be applied to partially coupled faults and folds which similarly trend NNE-NE and have remained active into the Cretaceous. **Figure 4.16b** illustrates the evolution of partially coupled faults and folds which initiate as a decoupled system in which isolated, low-displacement

basement faults, with no overlying cover fault, have little or no impact on deformation in the form of folds in the cover (Stage 1). A relatively low rate of extension or a thick salt layer would limit the degree of coupling between basement and cover deformation.

As displacement localises onto a few, large faults, the master basement fault gains sufficient displacement, or slips at sufficient rate, to initiate folding in the cover and the degree of coupling increases (Stage 2). During this stage, synclinal and anticlinal fold hinges initiate above the master basement fault hangingwall and footwall respectively, and cover faults form to accommodate basement extension and the flexure of the fold (C_1 & C_2). As the master basement fault links to form one through-going fault segment, fold hinge lines, and hence synclinal depocentres (e.g. Anders & Schlische, 1994) similarly link, recorded by fold azimuths that trend sub-parallel to the basement fault trend in map-view (Stage 3). Existing cover faults gain displacement as the master basement fault grows, and new faults (C_3) initiate to accommodate the increased amplitude of the monocline and down-dip translation of cover blocks over the fold hinge.

4.5.2.3 Thin-skinned

Thin-skinned cover faults initiate when strain localises from many, small displacement basement faults (**Figure 4.17A, B**) onto a few, large faults (**Figure 4.17C-E**), which generate sufficient structural relief (tilt) beneath the salt to initiate sliding within the cover in the Middle Jurassic. Early in the evolution of faults in the basement, the basement surface has insufficient dip to initiate gravity-driven deformation in the cover (Stage 1, **Figure 4.17C**). As the basement faults grow and progressively link into larger displacement faults (Stage 2), thin-skinned cover faults initiate where the dip on the basement surface is sufficient for sliding in the cover. With increasing rotation between overlap zones between basement faults, a larger number of higher displacement decoupled faults develop (Stage 3).

The development of significant regional tilt in the Early Cretaceous (Stage 3, **Figure 4.17C**) interacts with local fault-controlled tilt, resulting in the initiation of new faults perpendicular to the regional dip (Fault C_4, **Figure 4.17C**), whilst fault growth above local fault-controlled tilt (Fault C_1, C_2, C_3, **Figure 4.17C**) reaches a maximum at this time.

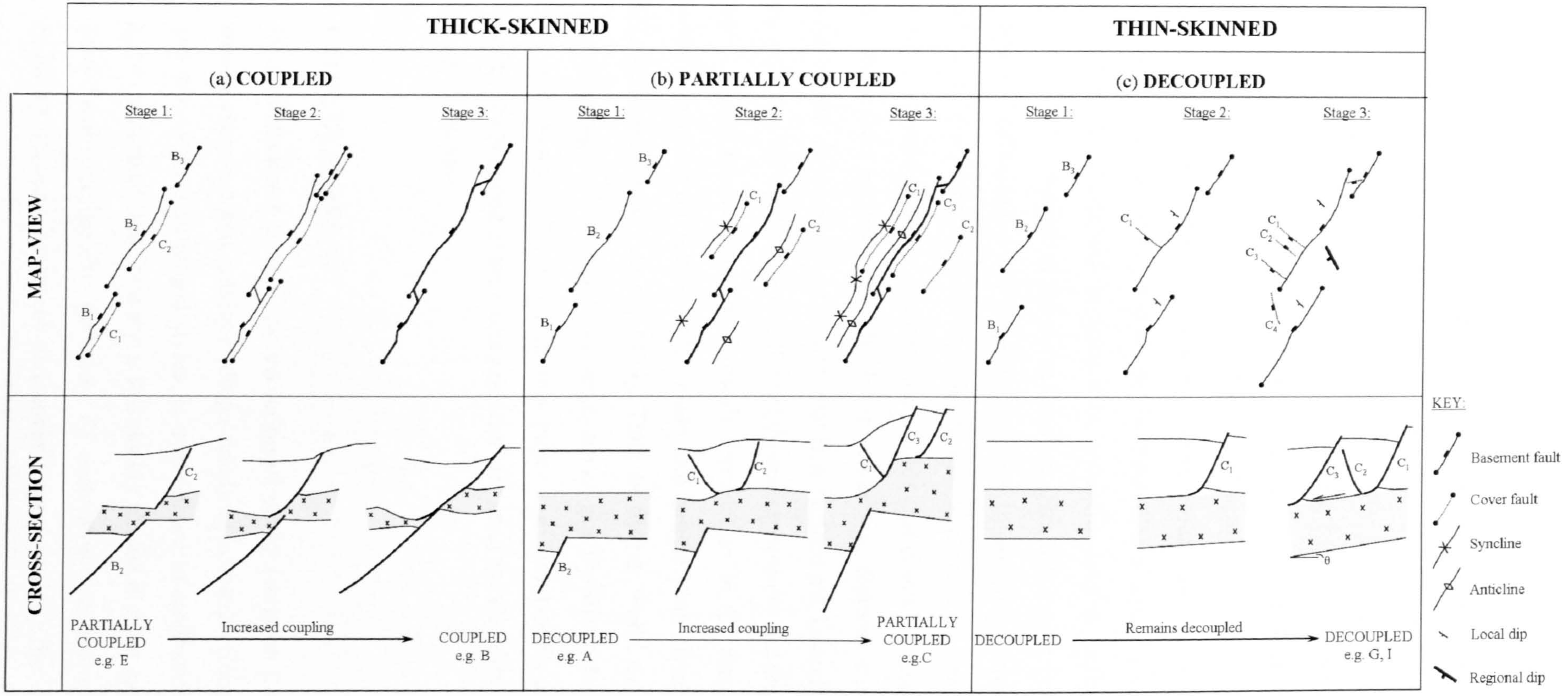

Figure 4.17: The evolution of fault systems that form in the presence of a weak stratigraphy in map-view and cross-section, based on our observations from seismic data for (a) Coupled (structural styles B, E) (b) Partially coupled (structural styles A, C, E) and (c) Decoupled (structural styles G, H, I) basement and cover faults. Faults that initiate in the basement and cover progressively link in both map-view and cross-section as faults gain length and displacement.

4.5.3 Further work

Differentiating between the two components of deformation - tectonic and gravity-driven - is essential when restoring sections influenced by thick- and thin-skinned tectonics, however time constraints have prevented us from balancing the sections presented in this study. The magnitude of displacement on thick-skinned basement and cover faults is expected to balance so that deformation, in the form of normal growth fault and extensional forced folds, above and below an evaporite layer is of broadly the same magnitude. Displacement associated with thin-skinned extension is surplus to this and should be treated as a separate system in which up-dip extensional faults will balance with down-dip reverse faults and folds, in the absence of a free-surface at the toe of the slide (Hesthammer & Fossen, 1999).

Section balancing could provide valuable information about the evolution of thick- and thin-skinned structures in the region. In particular, note the absence of any down-dip reverse faults or compressional folds that could balance the gravity-driven faults described in this paper. Such compressional features may not exist in the region due to the presence of a continual free surface but instead cover fault blocks may have slid off the terrace into the neighbouring basin to the west. A record of this process would be preserved as footwall degradation in the form of gravity-driven footwall scarps on the Klakk fault system and hangingwall slumps (Underhill *et al*, 1997; Hesthammer & Fossen, 1999). Thus as further work, time should be spent interpreting regional seismic lines down-dip of gravity-driven faults, e.g. across the Klakk fault system. Crucially, in this paper the foundations are laid for a later balancing study aimed at separating out the effects of gravity-driven deformation and regional extension.

4.6 CONCLUSIONS

- Two mechanisms control the evolution of cover faults on the Halten Terrace - crustal extension and gravity-sliding - resulting in the development of both thick- and thin-skinned structural styles. It is important to emphasise that the initiation and evolution of these two styles are closely related in most cases.
- Two factors define the geometry of each structural style: (i) the degree of coupling between basement and cover faults; and (ii) the dominant structural

orientation. These can be used to distinguish faults that form directly due to the effects of crustal extension from those that are gravity-driven.

- Gravity-driven faults are identified based upon: (i) their orientation perpendicular to the local or regional dip direction; and (ii) the onset of fault activity, which initiates post-Middle Jurassic, subsequent to activity on thick-skinned faults.
- Furthermore, the main factors controlling the geometry and distribution of thick- and thin- skinned structural styles are;
    - Along-strike changes in the magnitude of displacement on basement *and* cover faults
    - The relative distribution and orientation of faults in the basement and cover
    - The duration of extension
    - The rate of extension
- Consequently, the longest-lived, highest displacement thick-skinned faults and those subject to the highest strain rates, undergo the largest degree of coupling.
- The dominant mechanisms controlling the magnitude of displacement and the distribution of thin-skinned cover faults are the magnitude and direction of dip on the basement surface. The largest displacement thin-skinned faults will form above surfaces with the greatest dip which occurs adjacent to the largest displacement thick-skinned faults, or in areas with the greatest regional dip.
- These results have implications for constraining the distribution and magnitude of displacement on cover faults that offset important reservoir intervals. Time should be spent constraining the spatial and temporal evolution of cover faults and folds in order to predict the magnitude and distribution of structures in prospective hydrocarbon provinces, and thus the degree of reservoir compartmentalisation in new and existing prospects on the Halten Terrace.

CHAPTER 5

5: 3D analysis of faults in the Åsgard area, offshore Mid-Norway: a new model for fault growth in brittle-ductile systems

5.1 INTRODUCTION

Normal fault zones play a fundamental role in the development of sedimentary basins and in the migration and trapping of hydrocarbons. There are now well-established idealised conceptual models to explain displacement variations across isolated post-sedimentary normal faults (Barnett *et al*, 1987, Walsh & Watterson, 1989), and for the process of fault growth and linkage in brittle systems where overlapping segments interact across relay ramps (or zones). Displacement is transferred from one fault segment to the other by ductile strain within the relay ramp. Given sufficient strain, a breaching fault may propagate across the relay ramp, thus linking the two segments (Peacock & Sanderson, 1991; Cartwright *et al*, 1995; Childs *et al*, 1995, 1996b; Huggins et al, 1995). Relay zones often host significant hydrocarbon traps, so that an understanding of the styles and evolution of fault linkages - which may strongly influence both trap location and reservoir compartmentalisation - is vital for any petroleum system.

Existing conceptual models of fault growth and relay zone formation, which describe the structural geometries expected in brittle fault systems, fall into three groups: (i) fault growth by radial propagation (Watterson, 1986; Cowie & Scholz, 1992a, b); (ii) fault growth by segment linkage (Peacock & Sanderson, 1991, Trudgill & Cartwright, 1994); and (iii) the alternative model of fault growth (Walsh *et al*, 2002), where fault lengths are near constant from an early stage and subsequent growth is mostly achieved by an increase in displacement. Assessing the applicability of these models to the dataset requires careful consideration of the 3-D geometry and characteristics of the fault population in the Åsgard area.

A fault growing by radial propagation follows a growth path defined by the scaling law (Watterson, 1986):

$$D = cL^n \qquad (5.1)$$

Where D is displacement, c is a constant relating to the rock properties, L is the fault length and n is some exponent (Schlische *et al*, 1996). Provided that the material

properties are constant throughout the period of deformation, incremental increases in D and L are such that the fault remains on the same growth path throughout its evolution (Cartwright *et al*, 1995) (**Figure 5.1a**). In contrast, faults that grow by segment linkage evolve due to the propagation, interaction and linkage of originally isolated segments (**Figure 5.1b**). Initially faults grow towards each other by radial propagation (stage i, **Figure 5.1b**) and thus follow the growth path defined by the scaling law (equation 5.1) above (Cartwright *et al*, 1995). Faults eventually overlap and interact across relay zones and as stress fields in the tip regions are altered, further propagation is inhibited and D/L ratios for individual segments will increase (Peacock & Sanderson, 1991). At this point, the growth path followed by fault segments may deviate above an idealised growth line. However, the growth path for the fault as a whole will deviate beneath the 'idealised' line, since the sum of the lengths of individual segments will produce a longer trace length for a limited increase in maximum displacement (Cartwright *et al*, 1995) (stage ii, **Figure 5.1b**). In the final stage of the growth cycle, the fault accumulates displacement with little or no increase in length returning it back towards the growth line (**Figure 5.1c**). Thus, fault growth models that describe radial propagation and segment linkage suggest that faults grow by the simultaneous accumulation of both displacement and length (Walsh and Watterson, 1988). In contrast, the alternative model (Walsh *et al*, 2002), which is based upon an analysis of syn-sedimentary growth faults in the Timor Sea, suggests that the displacement to length ratio of faults progressively increases as they grow. In this model, fault growth is divided into two stages. During the first stage, the fault grows predominantly through the rapid lateral propagation of the fault tips until the length of the fault is established (stage i, **Figure 5.1c**). In the second stage, lateral growth is retarded and the fault continues to grow mainly by the accumulation of displacement (stage ii, **Figure 5.1c**).

Crucially, existing models of fault growth do not explicitly consider the driving mechanism for faulting i.e. tectonic extension vs. gravity-driven deformation. This paper demonstrates that a component of gravity-driven deformation can affect the displacement-length history, and hence the displacement-length profile, of a fault. Thus, it is suggested that the tectonic boundary conditions, which are not considered in existing fault growth models, exert control over the growth path followed by faults.

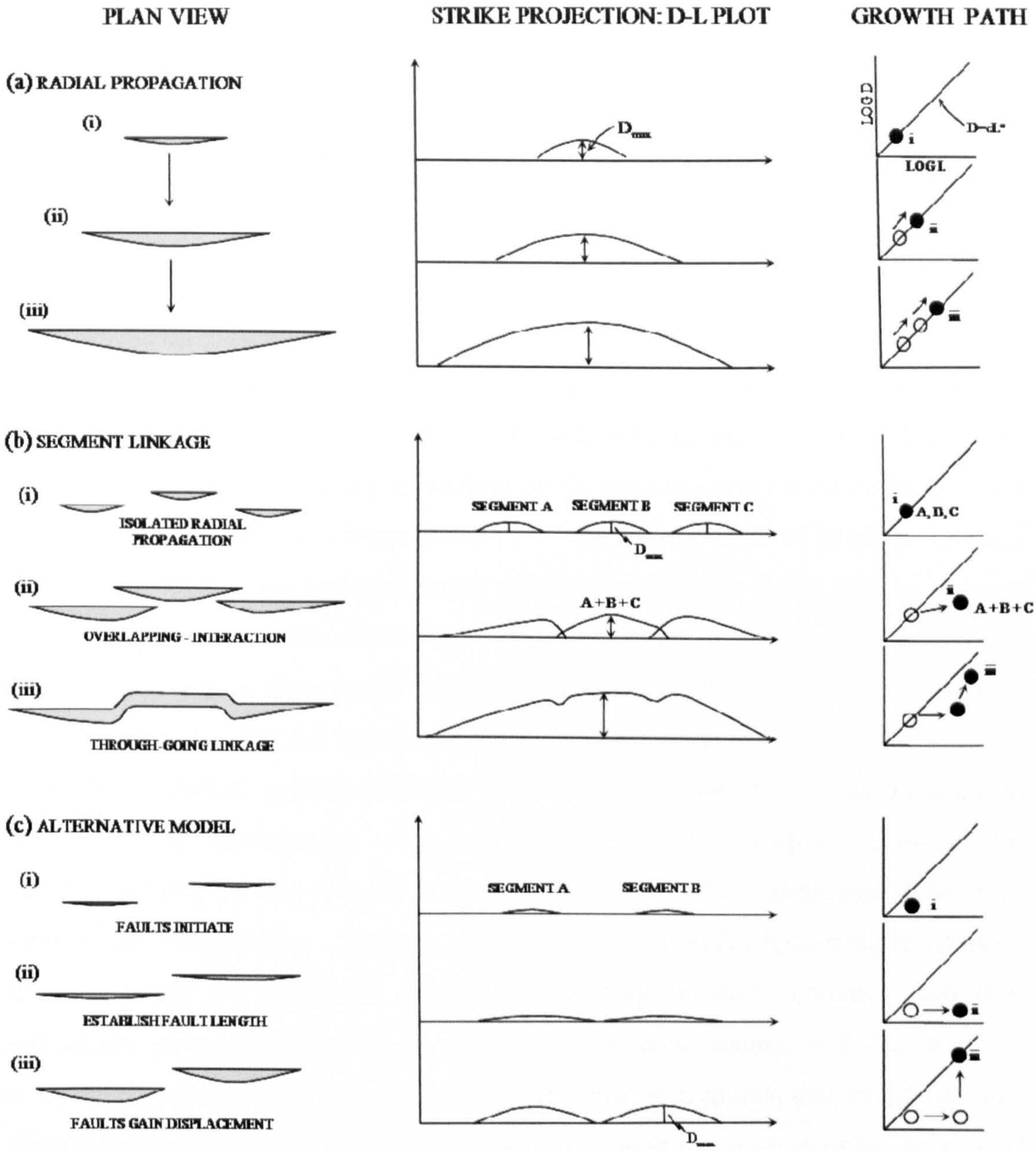

Figure 5.1: A comparison of existing conceptual models of fault growth (a) radial propagation, (b) segment linkage and (c) the alternative model, in both plan view, on a displacement against distance plot and a log maximum displacement versus log trace length plot. Each model follows contrasting pathways on the log L-log D plots, with the radially propagating model following a linear and predictable growth path whereas during segment linkage the model follows a step-wise, more unpredictable path. Individual segments may deviate from the idealised growth line as they begin to interact with neighbouring segments (stage ii, log-log plot in (b)) (Redrawn from Cartwright *et al*, 1995). (c) In the alternative model of fault growth, faults establish their length early in the growth history by rapid lateral propagation of fault tips (stage i and ii). Lateral growth is then retarded and the fault grows by accumulating displacement (stage iii).

Displacement-length (D-L) profiles show the variations in displacement along individual faults. Where fault growth has occurred through segment linkage, the points of linkage are marked by displacement minima (Peacock & Sanderson, 1991). In this case, proflies of *aggregate* displacement for overlapping, initially isolated fault segments display distinct displacement minima, which can be used to sub-divide D-L profiles into first-order segments (e.g. Fig. 5.1b, stage iii). In nature, fault segmentation occurs on a wide variety of scales (Peacock & Sanderson, 1994) and in a variety of tectonic settings (Aydin & Nur, 1985; Morley et al, 1990); however the majority of published studies consider only the growth and linkage of faults that form in purely brittle systems. Patterns of fault growth in brittle-ductile systems have been less studied, which is surprising given their likely importance in evaporite basins from hydrocarbon-producing provinces around the world (e.g. Gulf of Mexico, Caspian Sea, West Africa). This omission likely reflects the inherent difficulties in imaging sub-salt faults which often remain un-interpreted. Even in well-imaged basins, the sub-salt basement is often ignored unless it has hydrocarbon potential and thus an economic drive to carry out interpretations at greater depths.

In brittle-ductile systems faulting occurs in the presence of weak mechanical layers in the stratigraphy, such as evaporites. The unique rheology and incompressibility of salt - which is much weaker than other lithologies under both tension and compression - together with its buoyancy make it inherently unstable under a range of geological conditions, resulting in often complex structural geometries. Evaporites are able to deform in a viscous manner and can therefore accommodate strain by ductile deformation. It is also well known that evaporites may allow the detachment and partitioning of deformation in the pre-evaporite "basement" from that in the post-evaporite cover. Extension of the basement beneath a regionally extensive detachment, such as a salt layer, can lead to two geometrically and kinematically distinct types of structure in the post-salt cover. Thick-skinned cover structures, i.e. those that are coupled or partially coupled to the basement structures (**Figure 5.2a**), evolve during crustal extension to accommodate far-field tectonic stretching (Rowan, 1993; Stewart *et al*, 1997). Basement extension can also lead to the rotation of major basement fault blocks either through footwall uplift,or hangingwall rollover due to reverse drag (e.g. Barnett *et al.* 1987), by rotation of strata in relay zones between overlapping fault segments (e.g. Peacock & Sanderson, 1991) or above a surface with regional tilt. These rotational strains tilt the detachment

layer and may give rise to the development of gravity-driven, thin-skinned faults and folds (Duval *et al*, 1992; Vendeville & Jackson, 1992a; Jackson *et al*, 1994a, b), where 'thin-skinned' refers to decoupled faults that detach on mechanically weak evaporites (**Figure 5.2b**). Previous chapters described thin-skinned, gravity-driven faults that form oblique to the dominant basement fault trend, in the footwalls and hangingwalls of coupled faults and in overlap zones between major faults in the Åsgard area (see Chapter 4). In this example, the dominant mechanism controlling the evolution of thin-skinned cover faults is the magnitude and direction of dip on the basement surface and existing regional tilt which interact to generate decoupled faults trending at high angles to the trend of the underlying basement faults.

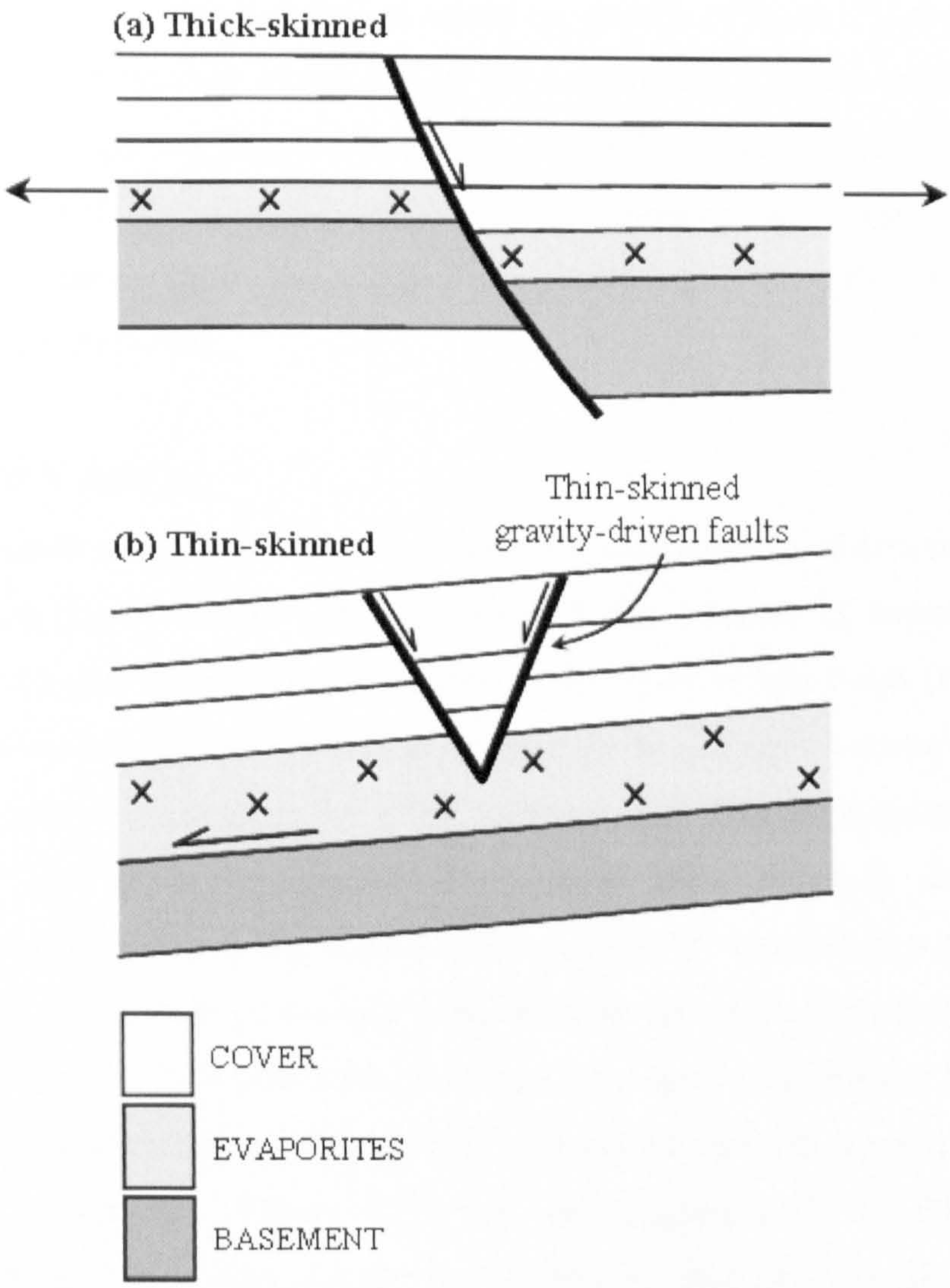

Figure 5.2: (a) A coupled system in which a continuous fault links basement and cover strata by offsetting the entire evaporite sequence. (b) A decoupled system in which cover extension initiates due to gravity-sliding above an inclined basement surface.

In this study, it is suggested that existing models of fault growth may provide only a *partial* explanation for the fault displacement distributions observed where fault growth is influenced by the presence of a detachment surface. Well data is integrated with structural and stratigraphic interpretations of a high-quality 3D seismic dataset, which images faults and horizons within the sub-evaporite basement, from the Åsgard area of the Halten Terrace. The 3-D model is used to describe the evolution of two faults trending parallel to the dominant NE-SW basement fault trend. The unique geometry and displacement-length analyses on the Trestakk fault are then used to propose a new model of fault growth due to both extensional tectonics *and* gravity-driven deformation, and to suggest that not all gravity-related faults form oblique to the dominant basement fault trend.

There are few published studies where the growth of faults that are influenced by thick- and thin-skinned tectonics has been examined in areas with a significant presence of evaporites (e.g. Richardson *et al*, 2005). Given the relative abundance of significant salt deposits in many hydrocarbon-bearing basins, the structural geometries and evolution described in the present study are likely to be applicable elsewhere in the world.

5.2 STUDY AREA

The results presented here are based on the interpretation of data from the Åsgard area of the Halten Terrace (**Figure 1.1a & 5.3b**), a region of approximately 1400 km^2 covering the Smørbukk and Smørbukk Sør hydrocarbon fields (**Figure 5.3b**) in the north-western part of the Halten Terrace. Permo-Triassic basement rocks on the Halten Terrace are overlain by a thick sequence of Triassic evaporites, separating basement and cover stratigraphy. The Åsgard area, which is characterised by dominantly NE-SW trending normal faults that display westerly dips and both planar and listric geometries, is strongly influenced by salt-related extension. Two faults, the Smørbukk and Trestakk faults, dominate the Åsgard area (**Figure 5.3**).

Fault activity within the Permo-Triassic basement and the Jurassic cover initiated in the Early Jurassic (**Figure 5.4a**) and was ongoing until the Early Cretaceous (**Figure 5.4b**) in the Åsgard area (see Chapter 3). Activity was focussed on a few dominant faults in the Early Jurassic until the onset of gravity-driven deformation,

which initiated in Middle Jurassic and continued into the Early Cretaceous, led to the initiation of new faults.

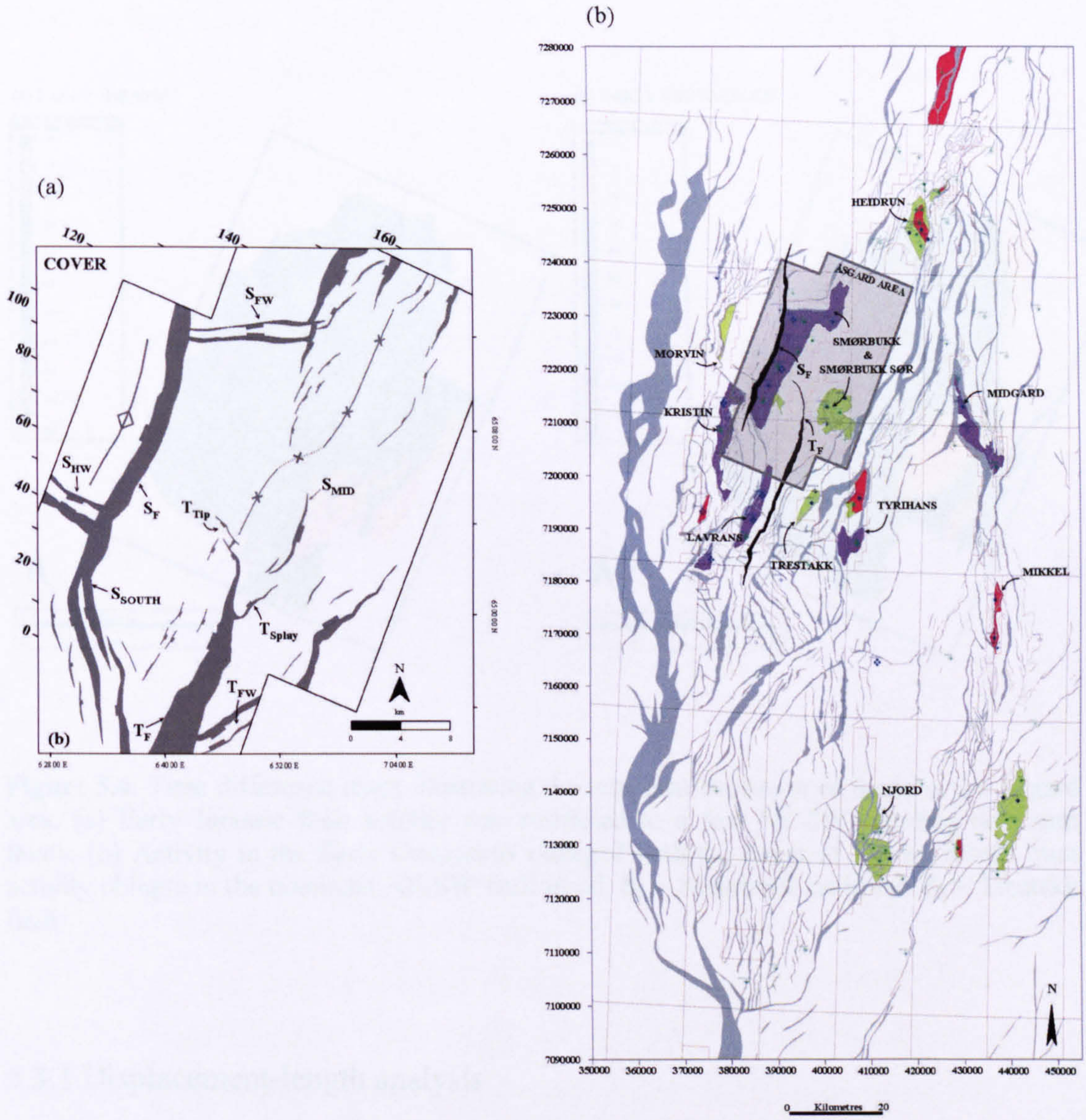

Figure 5.3: (a) Fault polygon map for cover faults from the Åsgard area where S_F = Smørbukk Fault, S_{FW} = Smørbukk Footwall Graben, S_{HW} = Smørbukk Hangingwall Graben, T_F = Trestakk Fault, T_{FW} = Trestakk Footwall Graben, T_{TIP} = Trestakk tip, T_{SPLAY} = Trestakk splay and S_{MID} = Smørbukk Mid Fault. (c) Fault polygon map from the Halten Terrace with the location of hydrocarbon fields (purple = gas/condensate, green = oil/gas and red = gas) and the Åsgard area (grey box). The Smørbukk and Trestakk faults are highlighted.

5.3 DATA & METHODOLOGY

The survey covers an area of 1400 km^2 and has a line spacing of 12.5m. Horizons and faults were interpreted manually every 20 lines across the entire survey and every 10 lines around fault tips. Interpreted fault and horizon data from the Åsgard

survey area were exported to TrapTester's fault analysis software to construct a 3-D structural model for the area. Variations in fault throw were used to generate fault polygons, defined by footwall and hangingwall cut-offs (**Figure 5.5a**).

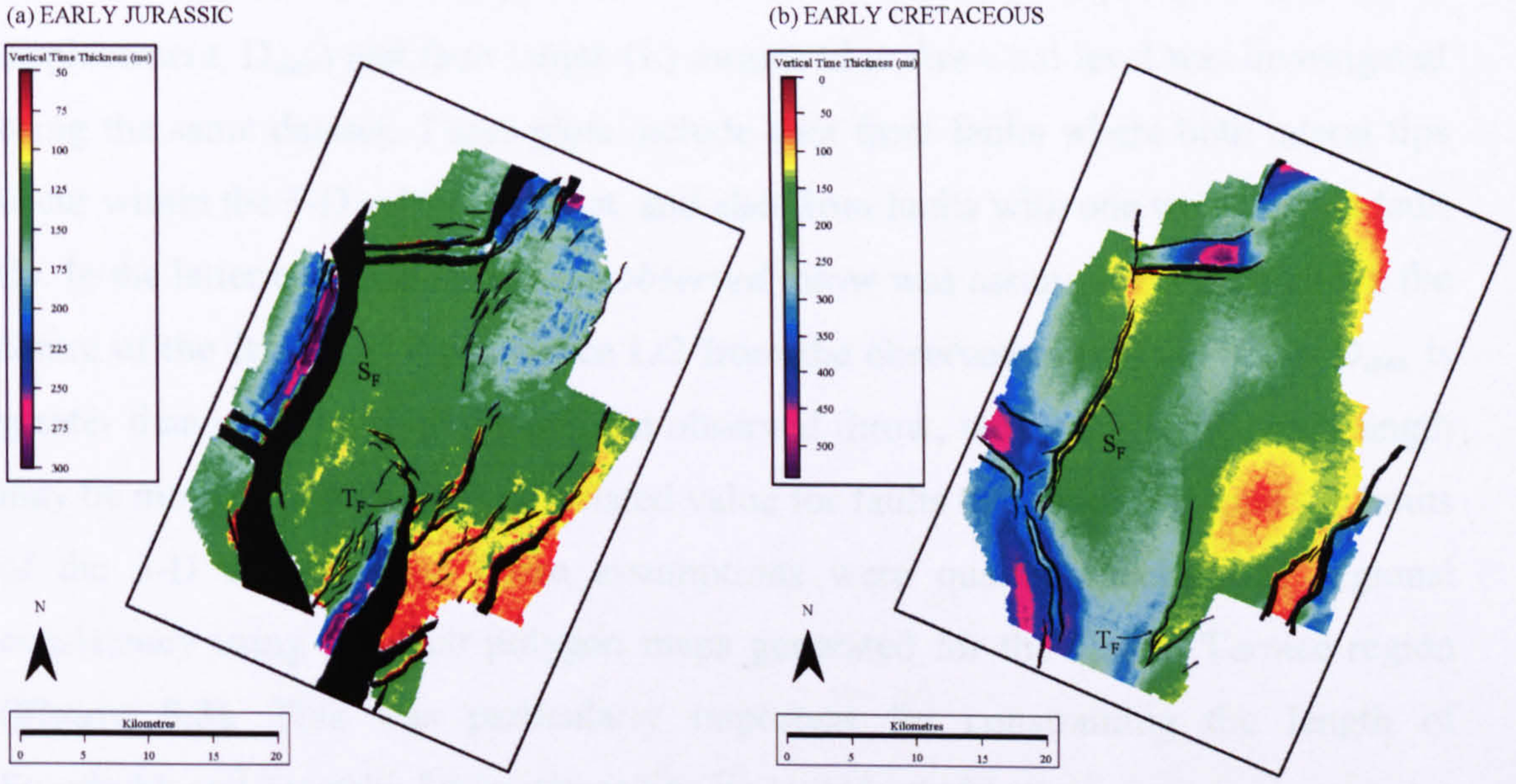

Figure 5.4: Time difference maps illustrating the temporal evolution of faults in the Åsgard area. (a) Early Jurassic fault activity was restricted to a few NE-SW trending dominant faults. (b) Activity in the Early Cretaceous changed with the onset of gravity-driven fault activity oblique to the dominant NE-SW fault trend. S_F = Smørbukk fault and T_F = Trestakk fault.

5.3.1 Displacement-length analysis

In order to generate fault displacement-length profiles, a sampling grid with a spacing of 292m was set up orthogonal to the local strike of each fault. Throw data in milliseconds two-way travel time (TWTT) were exported from TrapTester at each sampling point (i.e. every 292 metres) and plotted against distance along the fault. Such profiles were recorded at the Åre Coal level which is free from the effects of footwall erosion meaning that footwall and hangingwall cut-offs can be determined with a good deal of accuracy (see section 5.3.3). The seismic data have not been depth-converted therefore true displacements cannot be accurately measured because of uncertainties in measuring the dip of the fault. The precise orientation of the slip direction within the fault surface is also unconstrained. Consequently throw, which is

measured along vertical planes perpendicular to the fault, is used as a proxy for displacement. These plots, which show the throw (displacement) distribution along individual faults and interactions between faults, can be used to assess if fault growth has occurred through segment linkage.

In addition, the relationship between maximum throw (as a proxy for maximum displacement, D_{max}) and fault length (L) measured at Åre Coal level was investigated using the same dataset. These plots include data from faults where both lateral tips occur within the 3-D seismic dataset, and also from faults with one well-imaged fault tip. In the latter case, the maximum *observed* throw was assumed to be located in the centre of the fault, i.e. at a distance L/2 from the observed lateral tip. Thus, D_{max} is greater than or equal to the maximum observed throw, whilst the actual fault length may be more or less than the calculated value for faults that extend beyond the limits of the 3-D survey area. These assumptions were quality checked for regional consistency using the fault polygon maps generated for the Halten Terrace region (**Figure 5.3**). This was particularly important for constraining the length of Smørbukk and Trestakk faults whose tips lie outside study area.

5.3.2 Depth conversion

In order to generate logarithmic plots of length against maximum throw, footwall and hangingwall cut-offs were depth converted using a simple two layer model. The model consists of an upper layer of sedimentary rocks and a lower layer of evaporitic rocks, interbedded with mudstones (**Figure 5.5b**). For layer 1 (cover, **Figure 5.5b**) a seismic velocity of 4000m/s (calculated from interval velocities for exploration wells in the Smørbukk area – see Appendix 4) was used. Layer 2 consists of two evaporitic layers, each 400 metres thick, interbedded with a 500 metre thick package of mudstones (Jacobsen & Van Veen, 1984). Here an average seismic velocity of 3920m/s was used, which was calculated taking into account the relative proportions of evaporitic and mudstone layers in the total layer thickness (equation 5.2), using a velocity of 4500m/s and 3000m/s respectively.

Velocity = [(Thickness of both salt layers/Total thickness layer 2) x 4500m/s] +
[(Thickness of mud layer/Total thickness layer 2) x 3000m/s] (5.2)

Footwall and hangingwall cut-offs were depth converted for both the cover and basement faults, and the difference used to calculate throw values in metres. The accuracy of a simple two layer model, in which the velocity of layer 2 was averaged (as in equation 2.2) was tested against a four layer model which honours the seismic velocity of each individual layer. The two layer model produced depth-converted footwall and hangingwall cut-off values up to 100 metres larger than the four-layer model. However, in all cases the throw values (i.e. the *difference* between the footwall and hangingwall cut-offs) output from each model were the same.

Depth-converted fault surfaces, calculated following the assumptions described (eqn 2.2), were used to estimate the magnitude of fault dip.

5.3.3 Uncertainty

3-D seismic data are used to obtain a sample of a fault population in the subsurface, however datasets commonly have a vertical resolution of ~20-30 metres (Yielding *et al*, 1996). Faults with displacements less than 20-30 metres are therefore not visible on the seismic data, which makes imaging the fault tip line, and thus the entire length of the fault impossible. As a result fault lengths interpreted from seismic data are always underestimated (**Figure 5.5c**). The unimaged length of the fault can be estimated by extrapolating displacement-length profiles, (assuming the fault maintains the same displacement gradient) to intersect the horizontal axis i.e. where the displacement is zero. In Figure 5.5c the displacement-length profiles sampled from the Åsgard area dataset, which are typically underestimated by lengths of between 250 and 800 metres, are extrapolated to estimate the unimaged length.

The low magnitude scatter on fault displacement-length profiles can be used to estimate the accuracy of the throw measurements to +/- 60 ms (**Figure 5.5c**); this uncertainty is suggested to be due to the resolution of the dataset e.g. where the seismic expression of a horizon changes (e.g. from peak to trough) due to a lateral change in facies.

5.4 GEOMETRY

A quantitative description of the 3-D geometry of the Smørbukk and Trestakk faults from the Åsgard area (**Figure 5.3b**) is presented which considers:

- the geometry of each fault in plan-view and cross-section;

- the 3-D geometry of the fault surface including the variation in displacement on the fault surface;
- the variation in dip on the fault surface; and
- the relationship between the dimensions and the maximum displacement of each fault.

All the 3-D observations refer to the geometries associated with those parts of each fault that cut the supra-salt cover sequences. Here, the two faults have strikingly different geometries and thus remain the focus of this discussion, unless otherwise stated.

The geometry of the faults is described using the *length* of the fault, defined as the maximum dimension of the surface in a direction normal to the dip direction (which is assumed to be parallel to fault slip), the *displacement*, which refers to the displacement accumulated throughout the active life of the fault (Walsh & Watterson, 1988) and the *average horizontal displacement gradient*, i.e. the rate at which the displacement changes along the length of the fault. Displacement gradients are calculated using the ratio of maximum displacement (D) and the fault radius (R) (**Figure 5.5d**), where higher values describe a greater rate of change in displacement along the length of a fault. Displacement gradients vary with fault size and with mechanical properties of the host rock (Barnett *et al*, 1987).

The Smørbukk and Trestakk faults are thick-skinned faults that bound large rotated fault blocks and have sufficient displacement to offset the entire salt layer, thus coupling deformation of the basement and cover stratigraphies. Coupled faults are generally planar in geometry and follow the same trend, NE-SW or N-S, as the largest displacement underlying basement faults (section 4.4.1.2). Activity on the Smørbukk and Trestakk faults initiated synchronously in the Early Jurassic (following deposition of the Åre Coal horizon) and they remained active into the Early Cretaceous (**Figure 5.4**). The faults have a horizontal separation, measured in a direction approximately perpendicular to fault strike, of ~10 km, overlap by ~14 km and are similar in length (41.5km and 43.15km respectively). However the maximum displacement on the Trestakk fault is 200 ms or 225 metres (using the depth conversion described in 5.3.2) greater than the Smørbukk fault (**Figure 5.6b**).

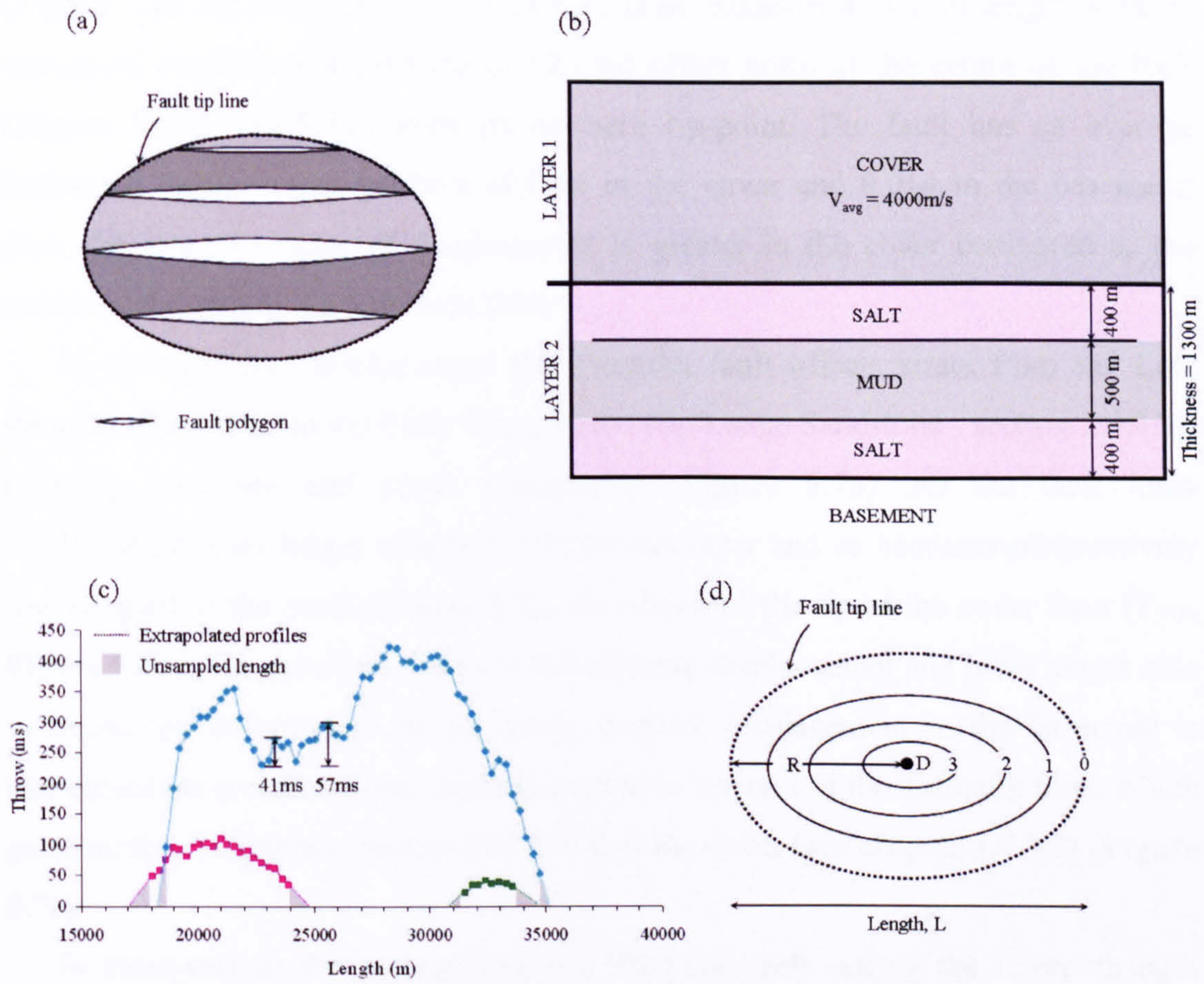

Figure 5.5: (a) Schematic strike projection (i.e. view along normal to fault surface) of an idealised fault plane. Fault polygons, defined by the cut-offs of displaced horizons in the footwall and hangingwall of the mapped surface, are in white. Offset decreases towards the tip line. (b) A simple two-layer model used to depth convert fault polygons in the basement and cover. An average seismic velocity of 4000m/s is used for the cover sequence (layer 1). For the salt layer (layer 2) the seismic velocity was calculated taking into account the presence of a thick mud layer (see text for detail). (c) Displacement-length profile highlighting the uncertainty associated with constraining the length of faults mapped in seismic data. Low magnitude scatter in displacement profiles quantifies the uncertainty in picking footwall and hangingwall cut-offs. (d) Schematic displacement contour diagram for a simple, isolated fault drawn normal to the fault surface (strike-view). Maximum displacement is in the fault centre (D_{max}).

5.4.1 Trestakk Fault

The strike of the Trestakk cover fault is parallel to the dominant NE-SW fault trend along the majority of its length, changing to a N-S to NNW-SSE trend along the northernmost ~6 km of the fault up to its tip-point (**Figure 5.6a**). The fault, which initiated in the south during the Early Jurassic (**Figure 5.4a,** and section 3.4.2.2), propagating north throughout the Jurassic and into the Early Cretaceous

(**Figure 5.4b** and sections 3.4.3.2, 3.4.4.2), is in excess of 43 km in length, with its maximum displacement (848 ms or 925 m) offset north of the centre of the fault (**Figure 5.6b**), ~12.5 km from its northern tip-point. The fault has an average horizontal displacement gradient of 0.06 in the cover and 0.014 in the basement; thus, the rate of change of displacement is greater in the cover compared to the immediately underlying basement fault.

At its maximum displacement the Trestakk fault offsets strata from the Late Permian (Base Salt) to the Early Cretaceous (Top Lange Sandstone - section 3.4.3.2), coupling basement and cover stratigraphy (**Figure 5.7a**). As the fault loses displacement it no longer offsets the entire salt layer and so becomes progressively less coupled to the north (**Figure 5.7c, d**). Ahead of the tip of the cover fault (T_{TIP}, **Figure 5.6a**), the underlying basement fault loses displacement and is no longer able to impact on deformation in the cover. Instead, displacement in the basement is transferred progressively onto fault M located to the east of the Trestakk fault, which gains sufficient displacement to fold and flex the cover (see chapter 4.4.1.3) (**Figure 5.7e**).

In cross-section the geometry of the Trestakk fault cutting the cover changes along strike, from a shallow-dipping, listric fault in the south (**Figure 5.7a, b**) to a progressively steeper-dipping more planar fault further north (**Figure 5.7c, d**). The change in dip along-strike of the fault is apparent from the geometry of the fault surface (**Figure 5.8**) which becomes increasingly rotated towards the horizontal from north to south. A rollover anticline develops in the hangingwall as the fault surface becomes increasingly listric. Contouring the fault surface for dip (**Figure 5.8c**) highlights the change in dip along strike of the fault, from a maximum of 45° in the north to less than 15° at the point of maximum displacement in the south. Thus the change in dip along strike of the Trestakk fault is greater than 30°. The basement continuation of the fault dips at ~30° and is comparable to, or steeper in dip than the cover fault along its length (**Figure 5.7**). The change in geometry along strike of the Trestakk fault is interpreted as the transition between a planar fault dominated by tectonic extension, to a listric fault with a component of gravity-driven deformation.

A number of faults, (T_{TIP} and T_{Splay}, **Figure 5.8a**), intersect the footwall of the fault interacting with the main fault trace in the cover. Displacement transfer between faults occurs at branchlines (B) where the faults intersect (**Figure 5.9a**). The fault polygon at Åre Coal level (**Figure 5.9b**) and the displacement-length profile in

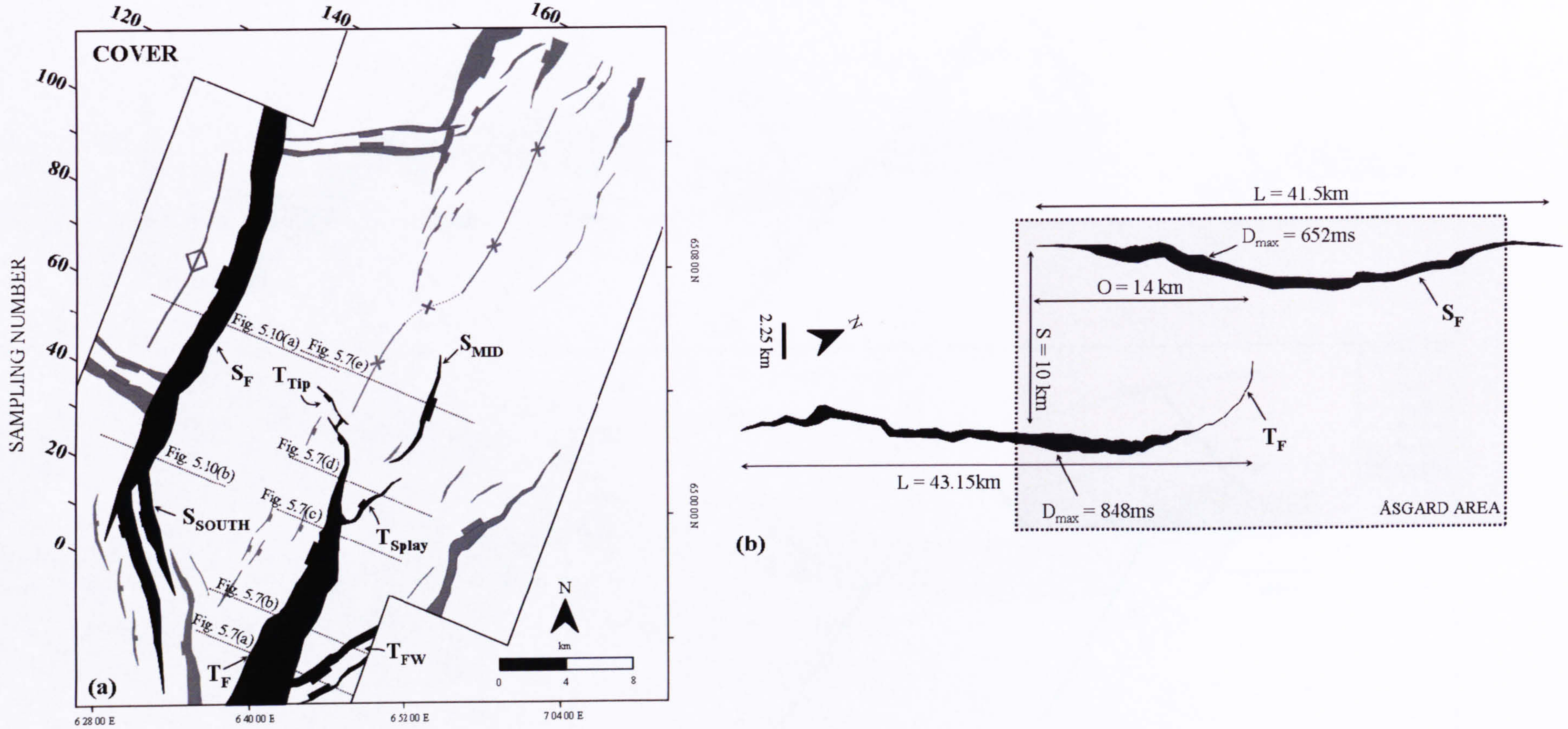

Figure 5.6: (a) Fault polygon map for cover faults from the Åsgard area with the Trestakk fault, the Smørbukk fault and splays highlighted. T_F = Trestakk Fault, T_{FW} = Trestakk Footwall Graben, T_{TIP} = Trestakk tip, T_{SPLAY} = Trestakk splay and S_{MID} = Smørbukk Mid Fault, S_F = Smørbukk Fault, S_{SOUTH} = Smørbukk southern splay. Note, the locations of cross-sections in Figure 5.6 are highlighted. (b) Plan view of the Trestakk and Smørbukk faults interpreted from regional data, highlighting the portion of the fault covered by the Åsgard area dataset, the separation (S) and overlap (O) of the faults. Note, the length of the fault was measured from the regional data and D_{max} is interpreted from the Åsgard area.

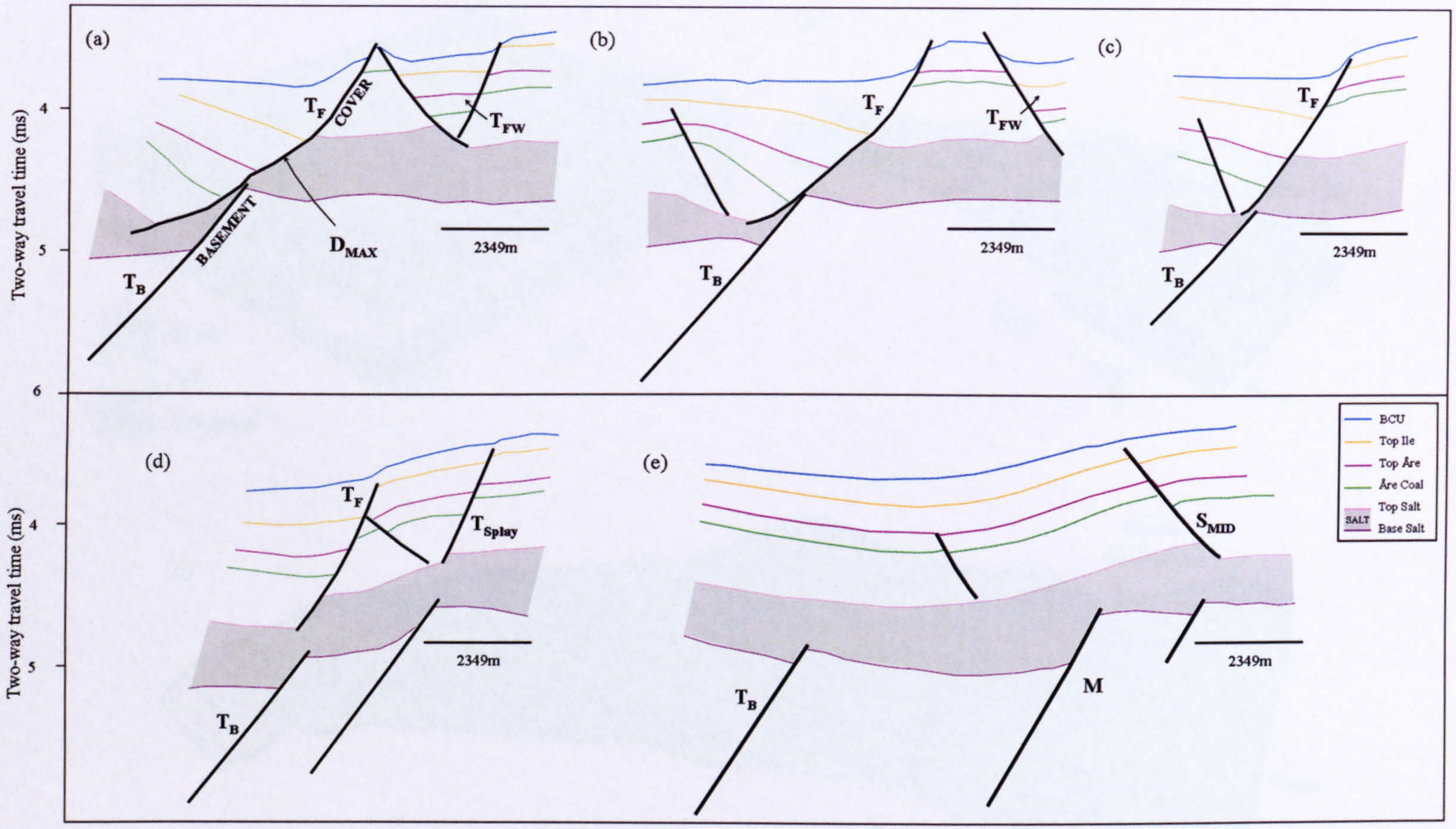

Figure 5.7: Cross sections (a-e) through the Trestakk fault highlighting the change in geometry along strike of the fault from south (a) to north (f). T_F is the cover, and T_B is the basement portion of the fault. Note, the fault becomes increasingly shallow in dip towards the south in (a), where the hangingwall beds are rotated the most. As the Trestakk fault in the basement and cover lose displacement to the north the faults are steeper in dip and have less growth into their rotated hangingwalls (c, d). In (e) the displacement on T_B is insufficient to deform the cover, instead displacement is transferred onto M which folds and flexes the overlying cover forming fault S_{MID}.

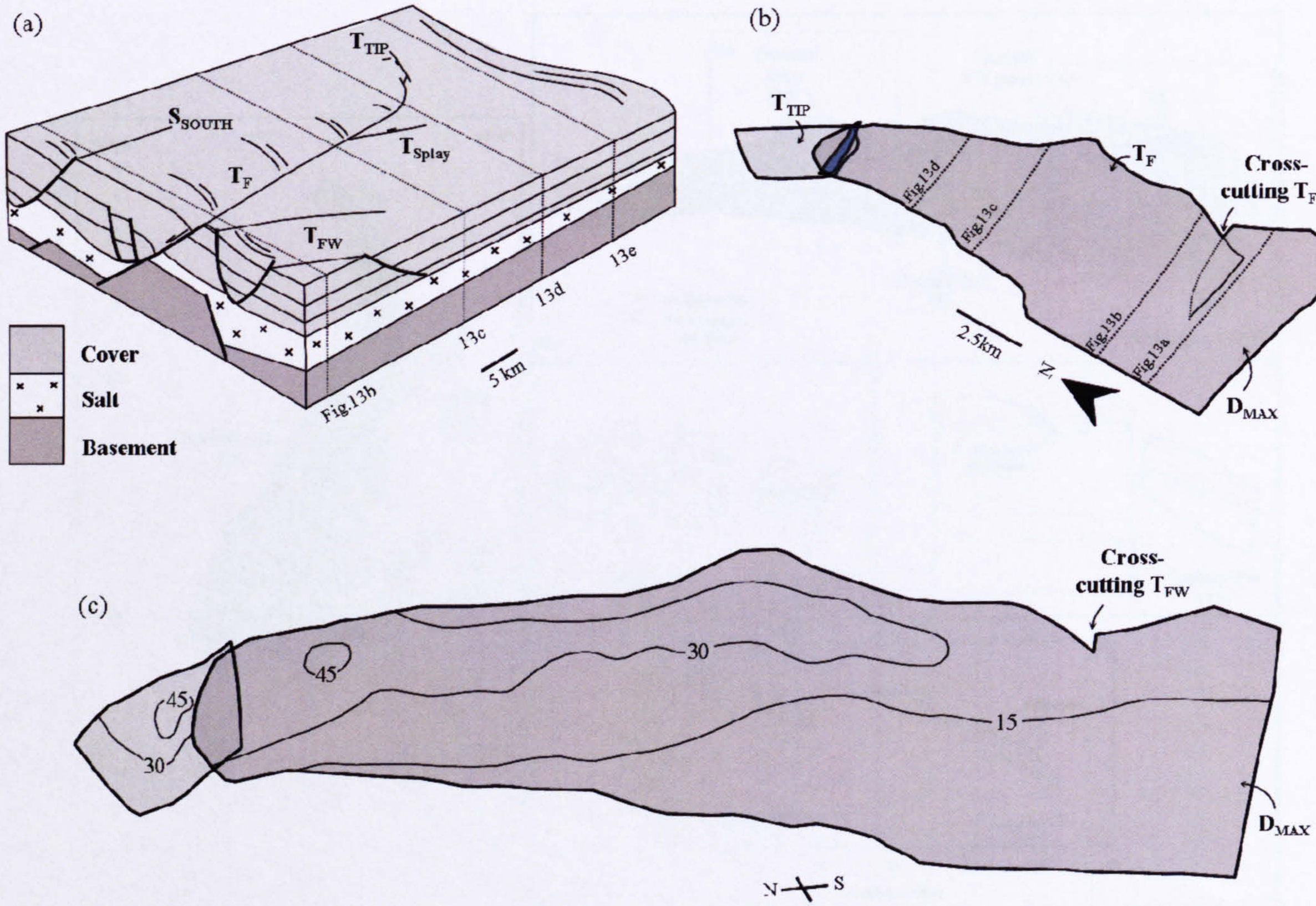

Figure 5.8: The 3D geometry of the Trestakk fault. (a) A schematic block diagram illustrating the geometry of the Trestakk fault and associated footwall splays. (b) The geometry of the Trestakk fault surface which splays at its northern tip (T_{TIP}). Note, the locations of cross-sections in Fig.5.7 are highlighted on the fault surface. (c) A strike-view projection of the Trestakk fault surface contoured for dip, demonstrating the change in dip from relatively steeply dipping in the north (45°) to shallow in the south (15°).

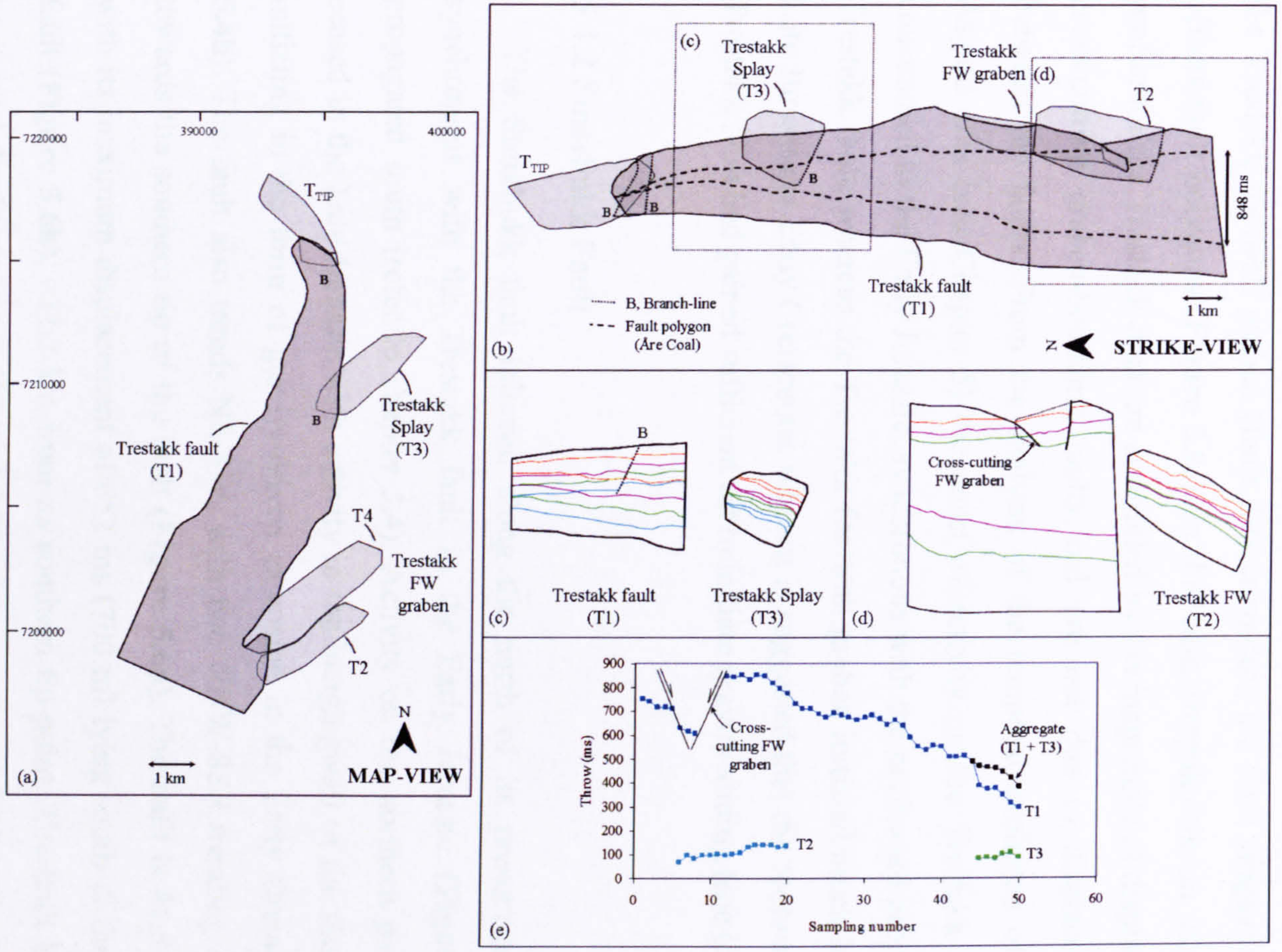

Figure 5.9: 3D geometry of the Trestakk fault, (a) in map-view and (b) in strike view. The Trestakk fault and the location of: (c) the branchline, B, with the Trestakk splay and (d) the Trestakk footwall graben. Fault polygons are included for Intra Åre (light blue), Åre Coal (green), Top Åre (purple) and Top Ile (orange). (e) Displacement-length profile for the Trestakk fault and splays. Aggregate profile for C1 and C3 results in a more regular profile whereas the footwall graben (C2 and C4) cross-cut the Trestakk fault offsetting the profile.

Figure 5.9e highlight the along-strike change in displacement on the Trestakk fault (T1), with a sharp discontinuity at the point of intersection with the Trestakk splay (T3) (Barnett *et al*, 1987; Needham *et al*, 1996) (**Figure 5.9b, c**). Diagrams of the cumulative displacement on the Trestakk (T1) and Trestakk splay faults (T3) have regular displacement profiles (T1 + T3, **Figure 5.9e**).

Further south, towards the point of maximum displacement on the Trestakk fault, the Trestakk footwall graben (fault T4) cross-cuts the fault (**Figure 5.9a, b**), and offsets fault polygons (**Figure 5.9c**). In this case, irregularities in the displacement profile for the Trestakk fault are controlled by the magnitude of displacement on the cross-cutting graben-bounding faults and are not due to displacement transfer between the faults. From the analysis of the temporal evolution of faults in the Åsgard area (see Chapter 3) the onset of activity on the Trestakk Splay fault is constrained to the Early Jurassic, synchronous with the northward propagation of the Trestakk fault, whereas the Trestakk footwall graben initiated much later during the Late Jurassic to Early Cretaceous, when it is suggested that the footwall block of the Trestakk fault had gained sufficient tilt to initiate gravity-sliding (see Chapter 4).

5.4.2 Smørbukk Fault

The Smørbukk fault initiated along the north of its present-day fault trace synchronous with the Trestakk fault in the Early Jurassic (**Figure 5.4a**), and propagated south (refer to chapter 3.4). Activity on the northern part of the fault ceased in the Late Jurassic with activity in the hangingwall of the fault to the south initiating in the form of gravity-driven extension in the Early Cretaceous (**Figure 5.4b**). The fault also trends NE-SW, with two NNW-SSE trending splays located towards the southern tip of the fault (**Figure 5.6a**). The fault is 41.5 km in length, with its maximum displacement of 652 ms (700 m) lying south of the centre of the fault (**Figure 5.6b**), ~11.2 km from its southern tip-point. The fault has an average horizontal displacement gradient of 0.03 in the cover and 0.05 in the basement; thus the rate of change of displacement is greater in the basement than the cover, i.e. the opposite of the gradients along the Trestakk fault.

The geometry of the Smørbukk fault surface, which is representative of a typical coupled fault in the region e.g. Bremstein Fault, is more consistent along-strike compared to the Trestakk fault (**Figure 5.10**). In cross-section the Smørbukk fault is

planar in geometry with dips ranging from 15-30° (**Figure 5.11d**), with the lowest values located at the base of the fault where it detaches onto Triassic evaporites. The magnitude of change in dip along strike of the fault is up to 15°, half that of the Trestakk fault. The basement continuation of the fault similarly dips at ~30° (**Figure 5.10**) and is at no point shallower in dip than the cover fault. At its maximum displacement the Smørbukk fault cuts strata from the Upper Permian (Base Salt) to the Early Cretaceous (Top Lange Sandstone) thus offsetting the entire salt layer, coupling basement and cover stratigraphy (**Figure 5.10a**). As the fault loses displacement it also becomes progressively less coupled (**Figure 5.10b**), and displacement is transferred onto footwall splay faults (**Figure 5.11a**); however the fault maintains it planar geometry.

Two faults intersect the footwall of the Smørbukk fault, interacting with the main fault trace (**Figure 5.11**). Displacement transfer between Smørbukk South and the main fault trace occurs at branchline (B) where the two faults intersect (**Figure 5.11a**). Along-strike changes in the displacement profile on the Smørbukk fault (**Figure 5.11c, e**) are compensated for by the displacement transferred onto the splay fault, which together result in a more regular displacement-length profile (S1 + S2, **Figure 5.11e**). The Smørbukk cover fault also has local sharp discontinuities in displacement due to faults intersecting (S_{FW} and S_{HW}) the main fault trace (**Figure 5.11b**). Both footwall (S_{FW}) and hangingwall faults (S_{HW}) formed due to gravity-sliding in the Early Cretaceous (see Chapter 3).

5.4.3 Summary

Observations of two faults are presented, the Trestakk and Smørbukk faults, which have very different geometries despite sharing many similarities including: structural setting; duration of activity; and fault length. There are three key differences between the faults: (i) the horizontal displacement gradient; (ii) the fault dip and dip variations; and (iii) the magnitude of the maximum displacements. In each case, the Trestakk fault has higher values than the Smørbukk fault.

There are also two types of splays developed in the footwalls of both faults: (i) *interacting* splays; and (ii) *intersecting* splays. In the latter cases, the analysis suggests that gravity-driven deformation controls the evolution of faults which offset the main fault trace and the displacement-length profiles in each case.

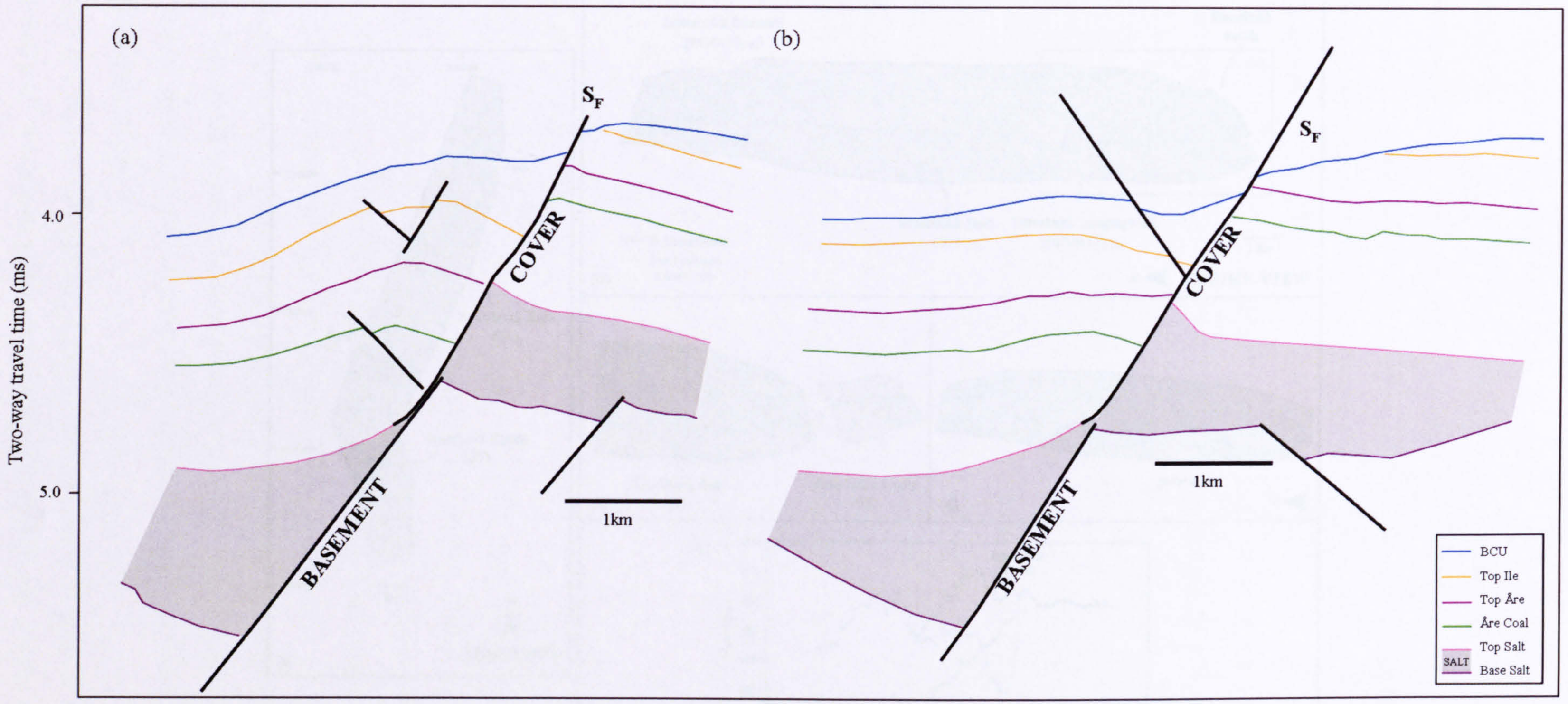

Figure 5.10: Cross sections through the Smørbukk fault highlighting the geometry of the fault at D_{max} (a) and further south where the fault loses displacement (b). The basement and cover portions of the fault are highlighted. The geometry of the fault surface is similar along strike of the fault, with little variation dip compared to the Trestakk fault (see Figure 5.11).

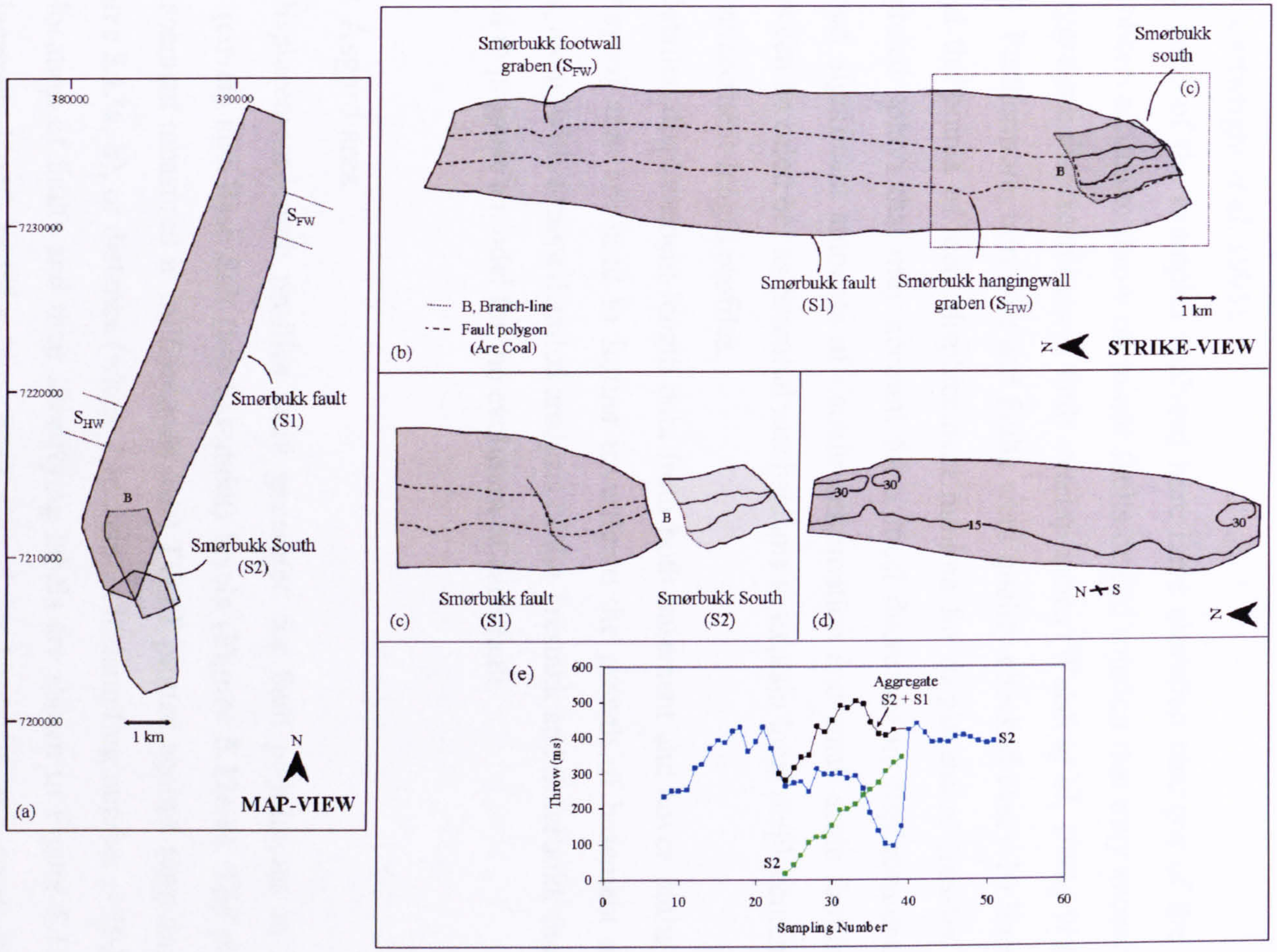

Figure 5.11: The 3D geometry of the Smørbukk fault in map-view (a) and strike view (b). Note, the locations of the Smørbukk footwall and hangingwall grabens are highlighted in (a). (c) The branchline, B, between the Smørbukk Fault and Smørbukk south with the polygon for Åre Coal level highlighted on the fault. (d) Dip contours on the Smørbukk fault surface (e) Displacement-length profile for the Smørbukk fault, southern splay and the aggregate profile for S1 and S3 which results in a more regular profile.

5.5 DISPLACEMENT-LENGTH ANALYSES

The transient nature of fault overlap zones has been demonstrated for syn-sedimentary normal faults in which the formation and breaching of fault overlaps occurs throughout the development of the fault system (Childs *et al*, 1995). In many cases, the sites of previously intact relay zones are preserved as displacement minima on displacement-length profiles (Peacock & Sanderson, 1991, Trudgill & Cartwright, 1994; Cartwright *et al*, 1995).

In none of the examples analysed here have elevation changes of the horizons been observed due to throw on minor faults or bed rotation that may account for the low aggregate displacements in fault overlap zones (Walsh *et al*, 1996; Walsh *et al*, 2003). Furthermore, horizons and faults were quality checked every 10 lines (125m) around the points of local displacement minima for displacement transfer onto un-interpreted splays that may account for a local decreases in displacement. In their absence, significant amounts of ductile deformation and small-scale faulting and/or splays can be ruled out as potential mechanisms to explain local displacement minima on displacement-length profiles.

Detailed displacement-length data from both basement and cover faults arrays in the Åsgard area are used to further investigate the growth of basement and cover faults, along with a more detailed analysis of the Trestakk and Smørbukk faults which is used to propose a model for the evolution of each fault.

5.5.1 Åsgard area

Displacement-length profiles were generated for fault populations at both Åre Coal (cover) and Base Salt (top basement) levels (**Figure 5.12c-e**). The plots show displacement measured in milliseconds (ms) TWTT plotted against sampling number (**Figure 5.13a, b**), or distance (where 1 increment in sampling number = 292 metres). The location of faults and their identifying labels are shown in Figure 5.12a and b. Displacement-length profiles have been plotted for basement and cover faults with varying degrees of coupling and different geometries (**Figure 5.12**). Data from those faults whose geometry and displacement variations are best constrained from the available data are used.

Basement fault profiles (**Figure 5.13a**) include faults ranging in length from 5 to 20 km and with maximum displacements of 130 to 430 ms. Faults have an average

horizontal displacement gradient of 0.042, with the highest value of 0.09 on fault B10. Cover fault profiles (**Figure 5.13b**) are significantly different, with lengths ranging from 1 to 18 km and maximum displacements of 22 to 852 ms. Here the majority of strain is localised onto the Trestakk fault (C1), which has the highest displacement gradient of all faults in the cover (0.06), whilst deformation on relatively low displacement (<400ms) faults is distributed widely across the area (**Figure 5.13b, d**). A similar pattern might be expected in the basement, with the majority of displacement on the Trestakk basement fault (B1), but this is not the case. Instead a much more evenly distributed displacement profile is observed with the largest displacements (>400 ms) on a number of faults: B1, B2, B7 and B10 (**Figure 5.13a**).

The longest length basement fault profiles, B1, B2 and B8, have segmented irregular profiles with clear displacement minima and local displacement maxima (**Figure 5.13c**). First-order segments range from 3 to 11 km in length with additional lower magnitude scatter superimposed on some faults (e.g. B1, segment 4 and B2, **Figure 5.13c**). A similar but less pronounced segmentation is observed on the cover faults where much smaller fault lengths restrict the amount of overlap and interaction that may lead to irregular displacement profiles associated with segment linkage. A low magnitude scatter is observed on the cover sections of the Trestakk fault (C1), which has local displacement minima (**Figure 5.13b**), and fault C12 (**Figure 5.13d**). In both cases, first order segments in the cover have a maximum length of 4km. These observations are in agreement with other workers who have observed that faults which are continuous on one scale of observation are segmented when examined in more detail (Cartwright et al. 1996; Childs et al. 1995, 1996a,b; Peacock & Sanderson 1991, 1994; Walsh & Watterson 1987, 1990, 1991). Segmentation occurs on a wide variety of scales (Peacock & Sanderson, 1994; Peacock, 2003), and thus the shortest faults (lengths <6 km) may be segmented at a scale below the resolution of the dataset.

It is suggested that segmented displacement-length profiles in the basement and on the longest cover faults record fault growth by radial propagation and the coincidental overlap, interaction and linkage of fault segments (Peacock & Sanderson, 1991, Trudgill & Cartwright, 1994; Cartwright *et al*, 1995). The alternative model of fault growth (Walsh *et al*, 2002) is ruled out based on the interpretation of the temporal evolution of faults in the area (see Chapter 3), in which

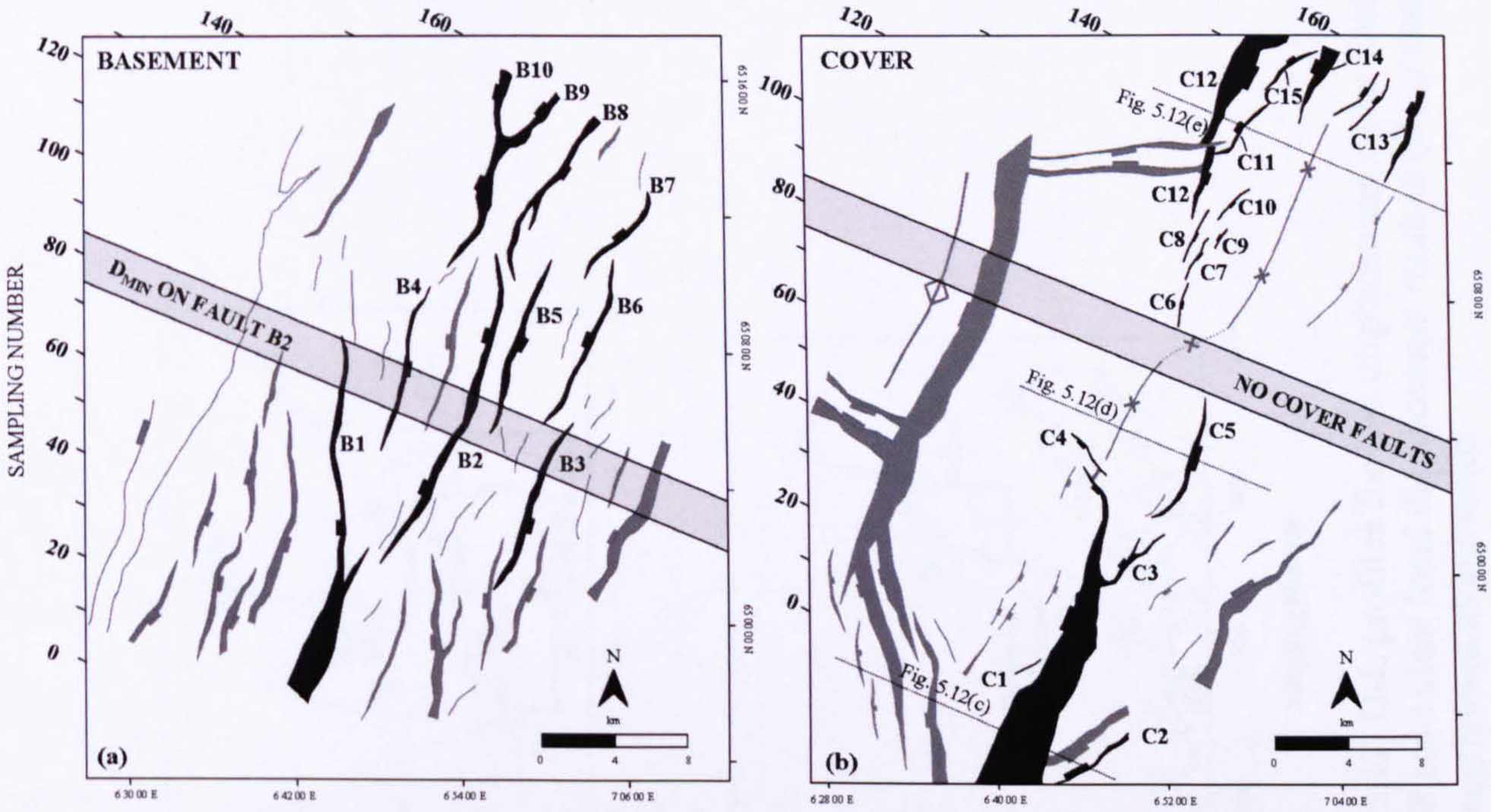

(c)

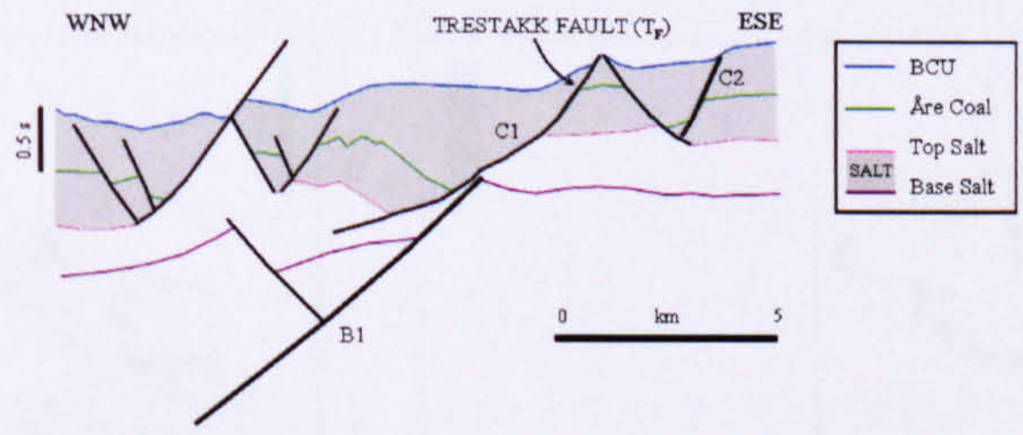

(d)

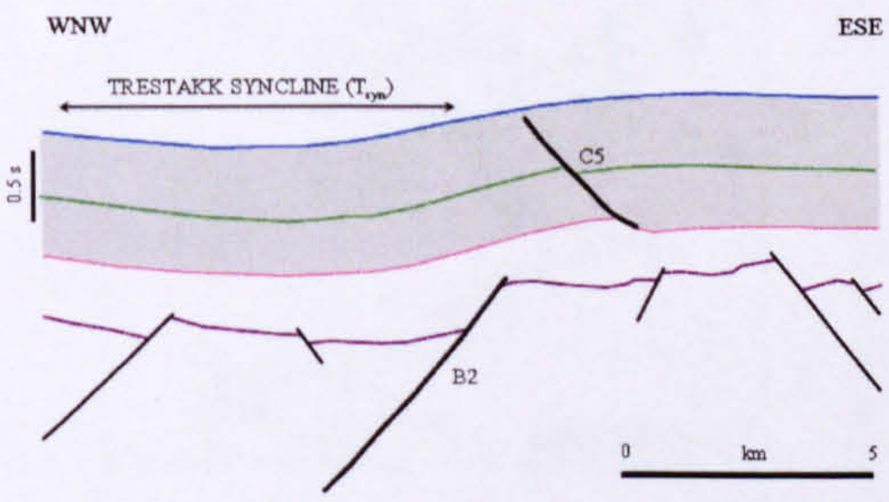

(e)

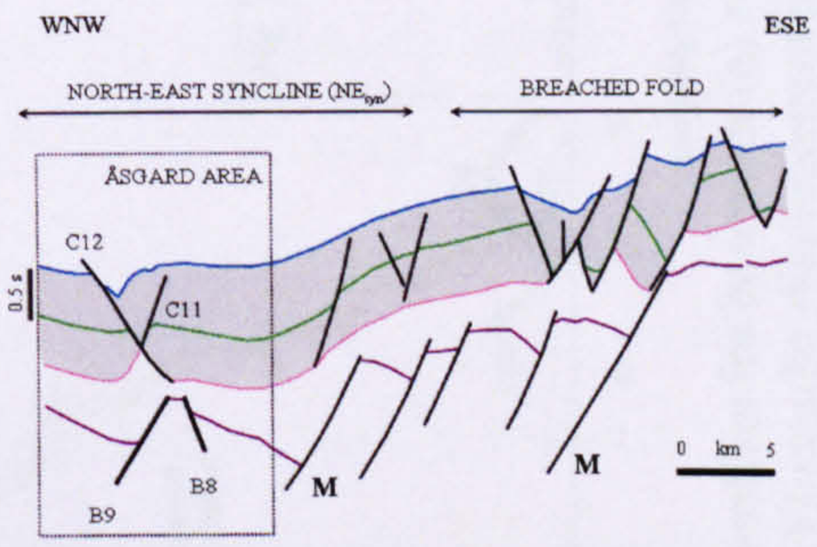

Figure 5.12: Fault polygons in the basement (a) and cover (b) from the Åsgard area. Displacement-length profiles for faults highlighted in black have been plotted in Fig. 5.13. Cross-sections (c-e) illustrate the geometry of main faults used in displacement analyses.

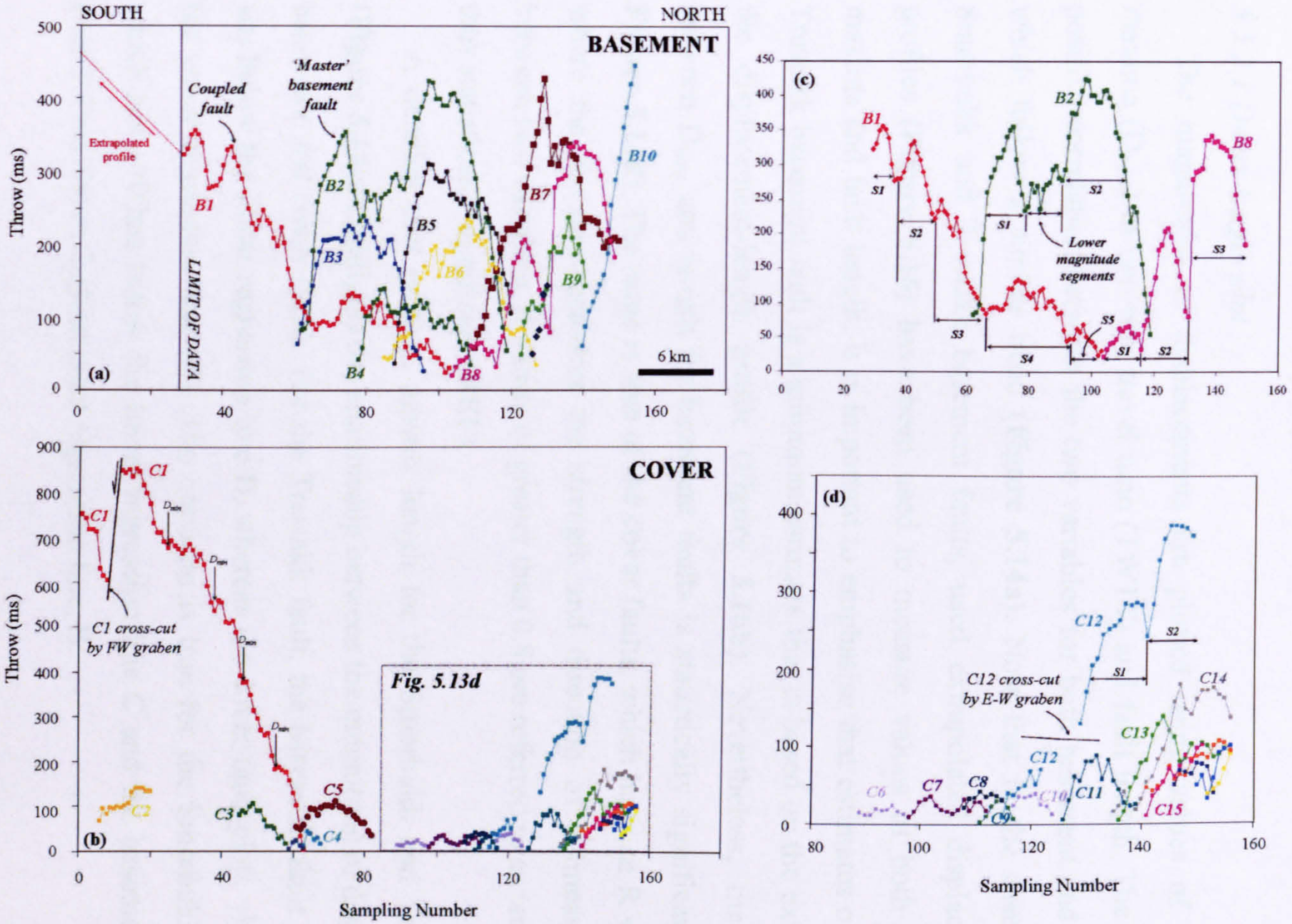

Figure 5.13: Displacement-length profiles for basement (a) and cover faults (b) highlighted in Figure 5.12. D-L profiles for low displacement cover faults (inset in b) are highlighted in (d). (c) Irregular displacement profiles for basement faults B1, B2 and B8 have clear local displacement minima (D_{min}) and local displacement maxima defining segments (S) along each fault which suggests that faults were initially segmented along strike.

it is demonstrated that the Smørbukk and Trestakk faults gained length by step-wise lateral propagating from the Early Jurassic to Early Cretaceous and thus did not rapidly establish their length as suggested by the model.

5.5.2 Trestakk & Smørbukk faults

5.5.2.1 Dmax-length plot

The magnitudes of displacements are plotted using values of displacement maxima (D_{max}) in two-way travel time (TWTT) and fault length. The plots show a positive correlation between the two variables for both basement and cover faults, which follow a similar trend (**Figure 5.14a**). Note that in the case of both the Smørbukk and Trestakk basement faults, used extrapolated displacement-length profiles (**Figure 5.16**) have been used to measure values of both displacement maxima and fault length. It is important to emphasise that estimates of D_{max} on the Trestakk basement fault is a minimum estimate that is based on the extrapolation of the displacement-length profile (**Figure 5.16b**). Nevertheless, the relationship between D_{max} and length for basement faults is statistically significant ($R = 0.81$, **Figure 5.14d**). The same is true of the cover faults, which have an R value of 0.93, where the R-value measures the strength and direction of a linear relationship between two variables. R values of greater than 0.8 are referred to as 'strong' and are thus statistically significant (**REF**).

A detailed plot of D_{max} against length for the Smørbukk and Trestakk faults (**Figure 5.14b**) highlights the relationship between the magnitude of displacement on basement and cover faults. For the Trestakk fault, the basement fault displacement sits below the linear regression line B, whereas the cover fault plots ~100 ms above the cover regression line (C). The opposite is true for the Smørbukk cover fault which sits ~100ms below the linear regression line C and the basement is located over 300ms above the basement regression line, B.

5.5.2.2 Logarithmic displacement-length plot

The data was depth-converted to check that the measurements of basement and cover fault displacement, taken in two-way travel-time, are representative of depth measurements, and that the relationship between D_{max} and length is still applicable taking into account the velocity of the overburden, in particular the salt layer.

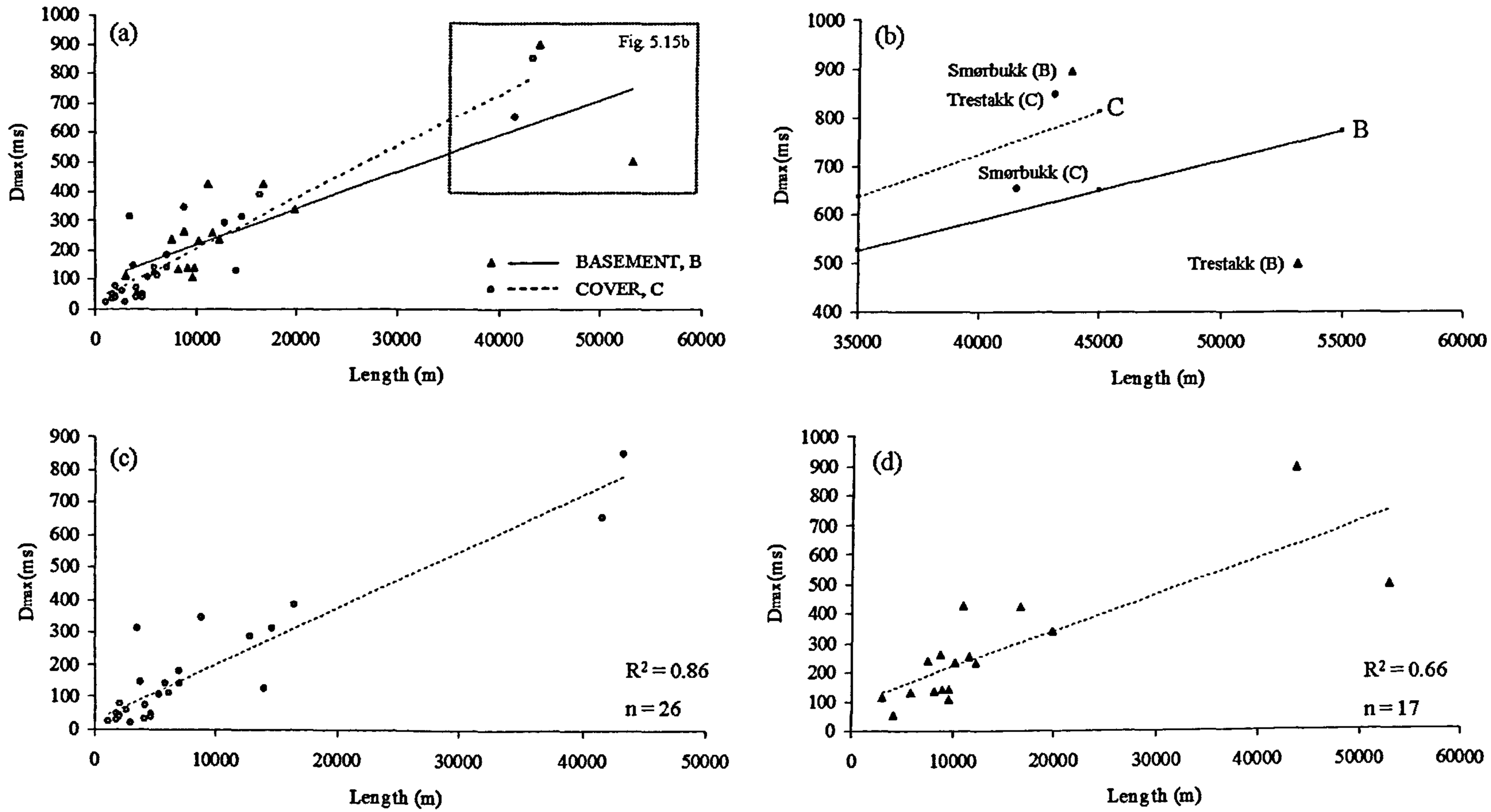

Figure 5.14: (a) Displacement maxima-length plots for basement and cover faults from the Åsgard area. (b) The Trestakk cover fault is much larger displacement than its basement continuation whereas the opposite is true for the Smørbukk fault. Individual plots of (c) cover and (d) basement faults highlighting R^2 and n values for each. In each case (a-d), a linear regression line is included for basement data, cover data or both.

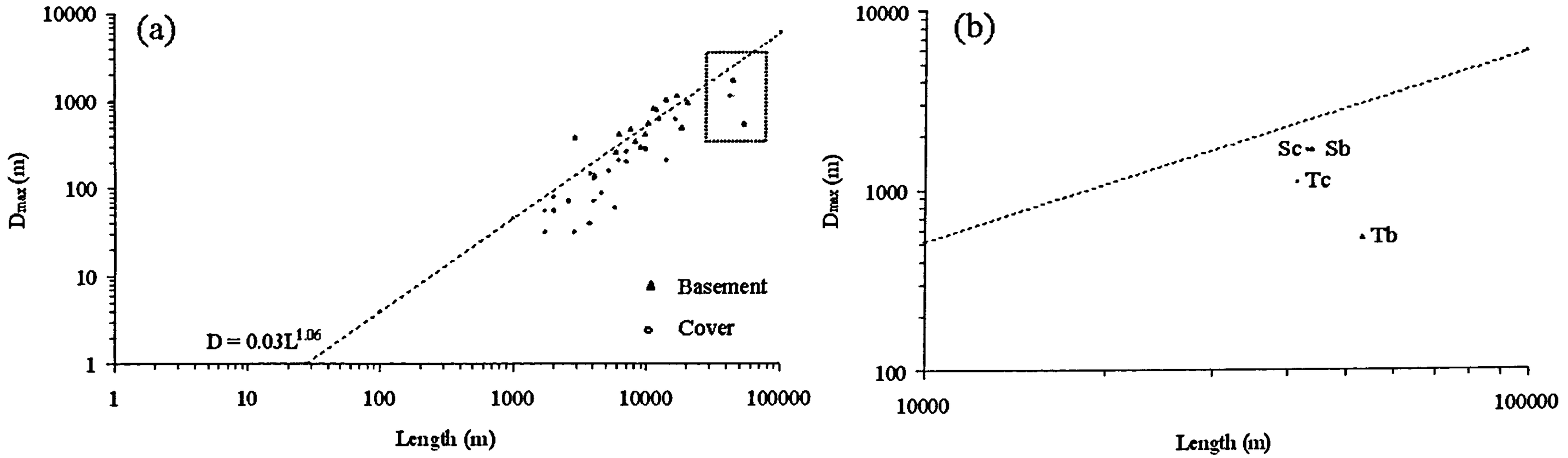

Figure 5.15: (a) A log-log plot of displacement vs. length for basement and cover faults, the box in (a) outlines the area shown in (b). The dashed diagonal line represents the average scaling relation of faults documented in Schlische *et al* (1996) where $D_{max} = 0.03L^{1.06}$. Note Sb = Smørbukk basement fault, Tb = Trestakk basement fault, Sc = Smørbukk cover fault and Tc = Trestakk cover fault.

The depth-converted data fall onto the best-fit trend line established for normal faults in a variety of lithologies and at different scales (Schlische *et al*, 1996), indicating a linear relationship between D and L, and therefore an n value close to 1 **(Figure 5.15a)**. Scatter in the data may relate to inaccuracies in measuring maximum fault length and maximum displacement (Gillespie *et al*, 1992), uncertainties associated with depth conversion and/or the effects of fault linkage (Cartwright *et al*, 1995).

The basement fault data falls closer to the trend line compared to the cover faults, supporting the observation that basement fault displacements are generally greater than those in the cover. Figure 5.15b shows that the Smørbukk basement fault falls closest to the best-fit trendline, with the Trestakk basement fault located furthest away. The magnitude of maximum displacement on the Trestakk cover fault is larger (by 568 metres, see Appendix 3) than the basement part of the fault (**Figure 5.15b**), despite the depth conversion, supporting the suggestion that the Trestakk fault is anomalous compared to other faults in the dataset, including the Smørbukk fault.

5.5.2.3 Displacement-length profiles

The Smørbukk cover fault has local sharp discontinuities in displacement due to faults interacting (S_{SOUTH} fault) or intersecting (S_{FW} and S_{HW}) the main fault trace **(Figure 5.16a)**. The sum of displacement on the Smørbukk and Smørbukk South faults creates a more regular displacement profile **(Figure 5.16c)** whereas the cross-cutting Smørbukk hangingwall fault offsets the hangingwall polygon creating a local high in the values of displacement on the Smørbukk fault **(Figure 5.16c)**. Such sharp discontinuities in displacement-length profiles due to cross-cutting faults do not reflect displacement transfer between faults or true changes in displacement along the main fault trace.

The Smørbukk cover fault has a flat-topped profile with low magnitude displacement minima. Similarly, the Smørbukk basement fault has an irregular profile with local displacement minima **(Figure 5.16a)**, thus both basement and cover profiles support the model of fault growth due to segment linkage. Low magnitude displacement minima, as observed on the Smørbukk fault, may suggest early interaction and segment linkage during fault growth.

Displacements in the basement, which have higher displacement gradients than the cover, are 150 to 300 ms higher than in the cover **(Figure 5.16a)**. Extrapolating

the basement fault profile to the north gives a higher maximum displacement (~ 900 ms) compared to the cover (650 ms), and a basement fault ~43 km in length, assuming the maximum displacement is located in the centre of the fault, i.e. at a distance L/2 from the observed lateral tip. From regional studies of structural geometries in the basement and cover, other coupled faults, like the Smørbukk fault, also have the largest displacements in the basement and lower displacements in the cover, e.g. the coupled fault east of the Midgard field (Figure 4.10, Chapter 4).

In contrast to the Smørbukk fault, the basement continuation of the Trestakk fault has a lower maximum displacement, which is predicted (using an extrapolated profile) to be a minimum of 500 ms, compared to the cover fault (**Figure 5.16b**). Displacement on the Trestakk cover fault, which has a well-defined northern tip-point and a much higher horizontal displacement gradient compared to the basement fault, exceeds that of the basement fault at a point X, where the displacement-length profiles overlap (**Figure 5.16b**). At the point of maximum displacement, the cover fault exceeds the basement fault displacement by 350 ms. It is acknowledged that the estimation of D_{max} on the Trestakk basement fault is a minimum estimate based on the extrapolation of the displacement-length profile (**Figure 5.16b**), and that the true value of D_{max} may be located further south and have a higher value than the current estimate. However this would not affect the observation of diverging basement and cover displacement profiles on the Trestakk fault (**Figure 5.16b**). Thus, the relationship between the basement and cover fault displacements on the Trestakk fault differs markedly compared to the observations from the Smørbukk fault and other regionally recognised structures in the Halten Terrace area.

An additional mechanism, in addition to regional tectonic extension, is proposed to control the evolution of the Trestakk fault. West- and south-westerly-directed gravity sliding is observed in the footwall and hangingwall of the Smørbukk and Trestakk faults (4.4.2.2, Chapter 4). Furthermore raft blocks, such as the Kristin field immediately west of the Trestakk fault, likely formed due to gravity-sliding above a locally and regionally inclined basement surface overlain by salt (4.4.2.2, Chapter 4). It is therefore suggested that the cover segment of the Trestakk fault, which lies up-dip of the Kristin field, has also undergone a degree of west- to southwesterly-directed gravity-driven extension. Along-strike variations in the magnitude and direction of dip on the basement surface, due to both local and regional tilting, are suggested to control the degree of gravity-driven deformation, and thus the

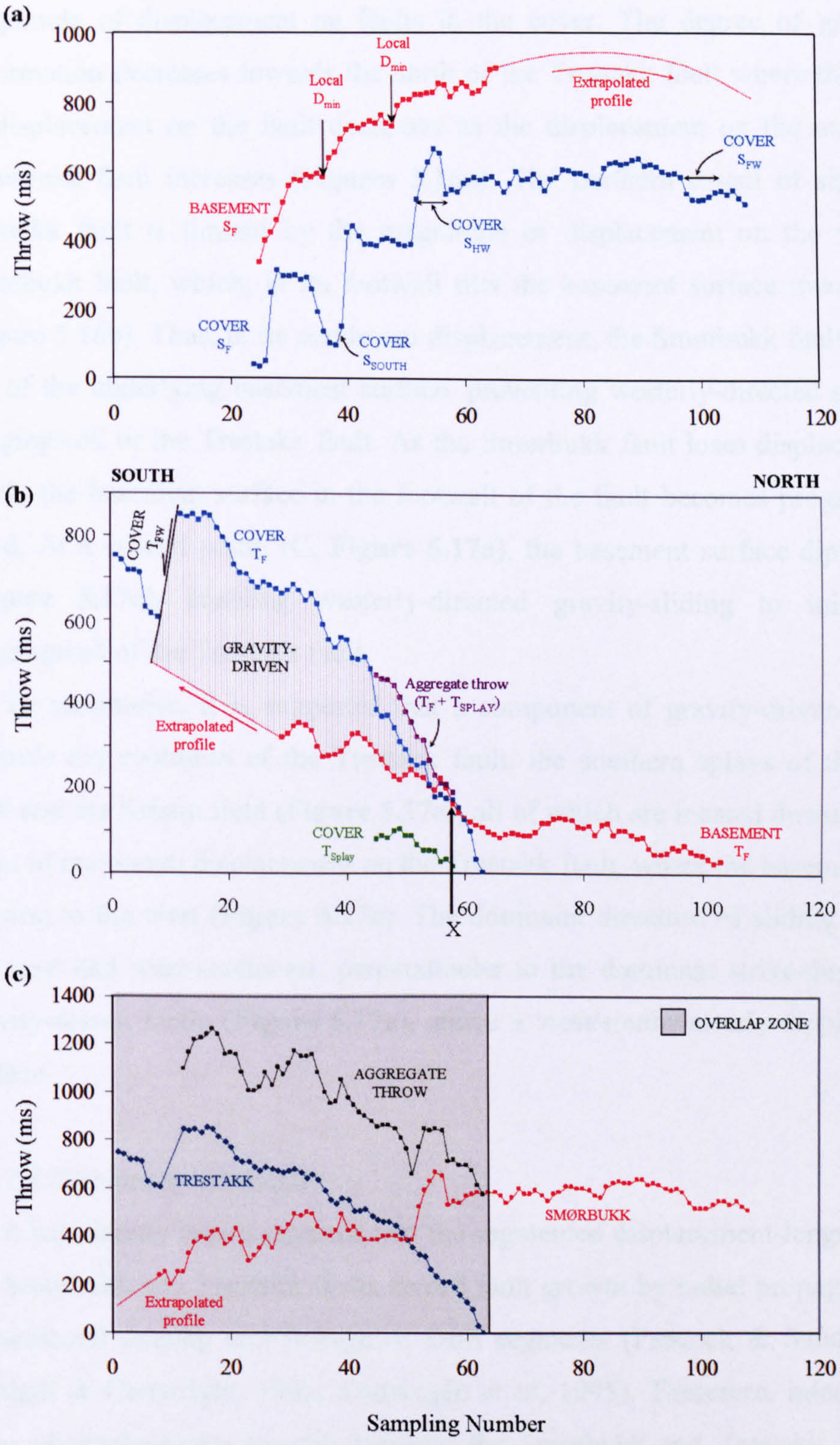

Figure 5.16: Displacement-length profiles for basement and cover portions of (a) the Smørbukk and (b) the Trestakk faults. (a) Displacement-length profiles for the Smørbukk fault show the basement fault displacement is larger than the cover displacement along the entire imaged and extrapolated length of the fault. The average displacement gradient in the basement is greater (0.05) than the cover (0.03). (b) The cover portion of the Trestakk fault has a much higher displacement gradient (0.06) and a larger D_{max} than the basement fault (0.014). The cover displacement profile crosses over becoming higher magnitude than the basement fault displacement profile at X. (c) The cumulative displacement profile for the Smørbukk and Trestakk faults has an irregular profile.

magnitude of displacement on faults in the cover. The degree of gravity-driven deformation decreases towards the north of the Trestakk fault where the magnitude of displacement on the fault decreases as the displacement on the more westerly Smørbukk fault increases (**Figures 5.16a**). The northern extent of sliding on the Trestakk fault is limited by the magnitude of displacement on the west-dipping Smørbukk fault, which, in its footwall tilts the basement surface towards the east (Figure 5.16b). Thus, at its maximum displacement, the Smørbukk fault controls the dip of the underlying basement surface, preventing westerly-directed sliding in the hangingwall of the Trestakk fault. As the Smørbukk fault loses displacement to the south, the basement surface in the footwall of the fault becomes progressively less tilted. At a critical point, (C, **Figure 5.17a**), the basement surface dips to the west (**Figure 5.17c**), enabling westerly-directed gravity-sliding to initiate in the hangingwall of the Trestakk fault.

To summarise, it is suggested that a component of gravity-driven deformation controls the evolution of the Trestakk fault, the southern splays of the Smørbukk fault and the Kristin field (**Figure 5.17a**), all of which are located down-dip from the point of maximum displacement on the Trestakk fault, where the basement surface is dipping to the west (**Figure 5.17c**). The dominant direction of sliding was towards the west and west-southwest, perpendicular to the dominant strike-direction of the gravity-driven faults (**Figure 5.17a**), above a west/southwesterly-dipping basement surface.

5.5.2.4 Displacement transfer

It has already been suggested that the segmented displacement-length profiles on the Smørbukk and Trestakk faults record fault growth by radial propagation and the coincidental overlap and linkage of fault segments (Peacock & Sanderson, 1991, Trudgill & Cartwright, 1994; Cartwright *et al*, 1995). Therefore, interaction in the form of displacement transfer between the Smørbukk and Trestakk faults, which overlap by ~14 km, may be expected. Corfield and Sharp (2000) describe the overlap zone between the two faults as the 'Smørbukk south relay zone' and suggest that displacements on the south of the Smørbukk fault are transferred to the Trestakk fault across this relay zone.

Displacement transfer between two faults which overlap is typically identified by a decrease in displacement on both faults and high displacement gradients in the

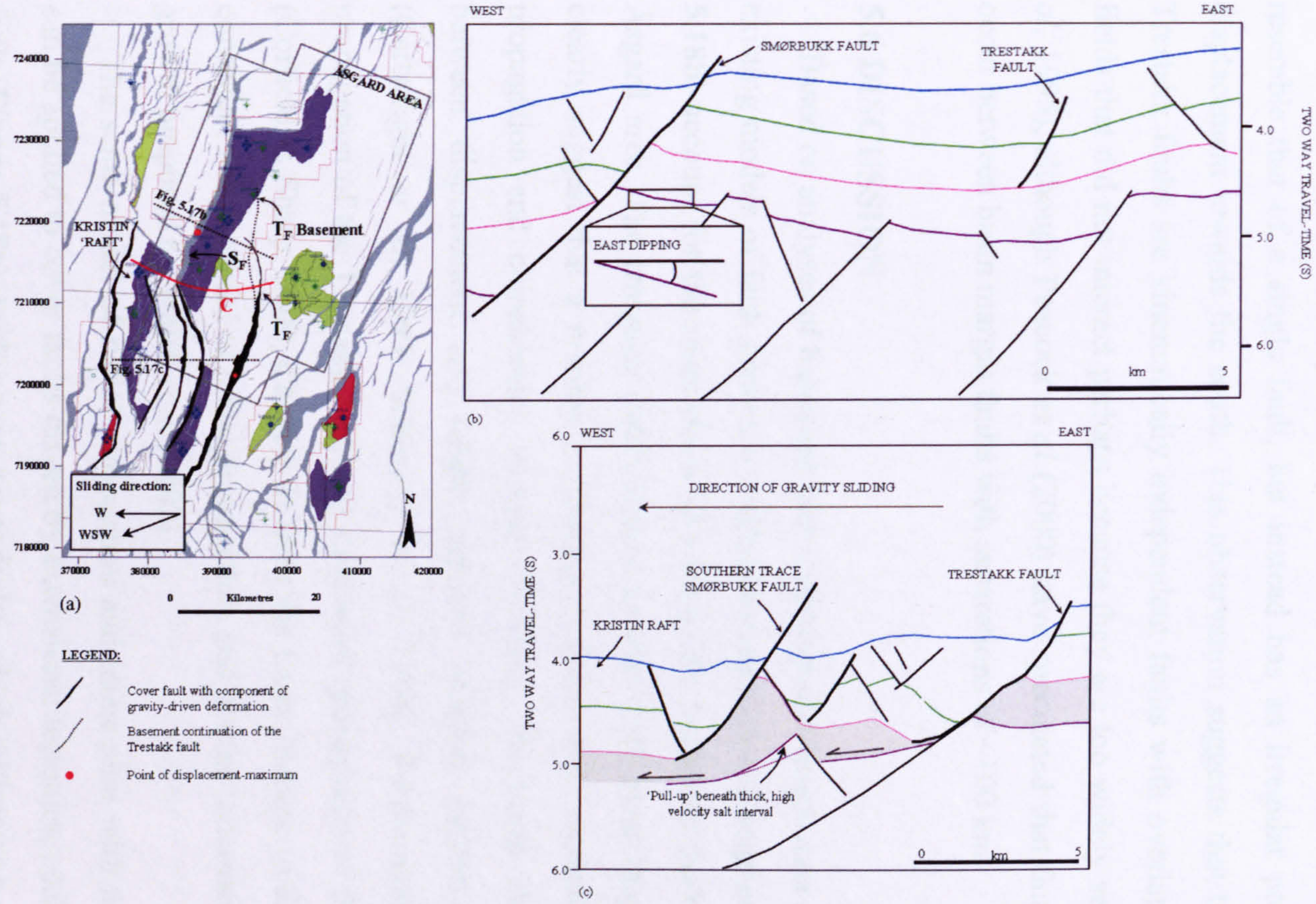

Figure 5.17: Faults that have undergone a component of gravity-driven deformation. (a) A zone of westerly-directed gravity-related deformation in the hangingwall of the Trestakk fault. The dominant direction of gravity-sliding is highlighted on the map, along with the location of cross-sections in (b) and (c) (dotted lines) and the critical point, C (red line), south of which gravity-sliding initiated. (b) Cross-section through the Smørbukk fault demonstrating the east-dipping basement surface beneath the footwall of the fault close to its displacement maximum. (c) Cross-section through the gravity-related faults taken approximately parallel to the direction of sliding. The faults shown in map-view in (a) are highlighted in bold. The average dip of the basement surface is towards the west, enabling westerly directed gravity-sliding to take place.

overlap zone (Childs *et al*, 1995). Displacements on the individual fault surfaces may be aggregated to produce a displacement distribution which resembles that of a single fault (Walsh & Watterson, 1991; Peacock & Sanderson, 1991). Displacement-length profiles for the Smørbukk and Trestakk faults, which include displacements transferred onto interacting footwall splays in both cases, have been summed in the overlap zone. The resulting aggregate displacement profile (**Figure 5.16c**) does *not* resemble that of a single fault, but instead has an irregular profile which gains displacement towards the south. This observation suggests that the Smørbukk and Trestakk faults are kinematically independent faults with overlapping deformation fields that did not interact perhaps because they are too widely separated (Childs *et al*, 1995), although Peacock *et al* (2000) have speculated that fault interactions can occur between basin margin faults with separations of ~100 km.

5.6 DISCUSSION

Based on analyses of basement fault displacement-length data it is suggested that existing models of fault growth by radial propagation and segment linkage (**Figure 5.18b**) account for the main characteristics of the basement fault population in the Åsgard area. The irregular displacement profiles with clear displacement minima clearly suggest that a number of initially isolated fault segments grew by radial propagation and coincidental overlap. Similarly, the linear scaling relationship between displacement and length supports existing models of fault growth (Cartwright *et al*, 1995; Schlische *et al*, 1996). Furthermore, the northward propagation of the Trestakk fault and southward propagation of the Smørbukk fault (Corfield & Sharp, 2000; Chapter 3) from the Early Jurassic to Early Cretaceous is consistent with a model of radial propagation, and not the 'alternative' model of fault growth proposed by Walsh *et al* (2002).

The same model of radial propagation and interaction with neighbouring faults can be applied to cover faults driven by extensional tectonics, such as the Smørbukk fault (**Figure 5.18a**). In this case, cover faults, which initiate as a number of isolated segments (**Figure 5.18a**, stage i) have lower values of maximum displacement and lower horizontal displacement gradients than their basement counterparts (D-L plot, **Figure 5.18a**). This relationship is maintained throughout the growth history of tectonic faults as they interact with neighbouring faults (**Figure 5.18a**, stage ii)

eventually forming one through-going fault trace (**Figure 5.18a**, stage iii). Basement and cover faults follow the idealised growth path of Cartwright *et al* (1995) in which a linear scaling relationship between displacement and length is maintained (**Figure 5.18a**) despite the step-wise growth path during linkage cycles. Faults driven by extensional tectonics, such as the Smørbukk fault, are generally planar in cross-section, undergo less rotation and are more consistent in geometry along strike (**Figure 5.10 & 5.11**). The basement and cover faults in such cases are suggested to initiate in-line with one another (stage 1, **Figure 5.19A**), as the two faults gain displacement they link to form one through-going fault (stage 2, **Figure 5.19A**) which continues to gain displacement until the dip on the basement surface is sufficient to initiate gravity-sliding and compressional folding in the hangingwall of the cover fault (stage 3, **Figure 5.19A**).

To account for structures such as the Trestakk fault, the growth of faults in such cases is suggested to be influenced by extensional tectonics *and* gravity-driven deformation. A model that describes the evolution of cover faults that form above a detachment layer, such as salt is proposed and it is suggested that such faults follow a different model of fault growth. Initially, the faults form as a number of isolated segments (**Figure 5.18b,** stage i), but as the area becomes progressively tilted, due to both local and regional tilting, during ongoing tectonic activity (see chapter 4), the dip on the basement surface becomes sufficient to initiate gravity-driven deformation. Gravity-driven deformation provides an additional component of displacement which gives rise to cover faults with a larger than expected displacements for a given length (**Figure 5.18b**, stage ii). With this additional displacement, cover faults are able to 'catch-up' with the displacement profile of underlying basement faults, eventually exceeding the value of D_{max} in the basement in cases where large amounts of gravity-driven deformation occur (**Figure 5.18b**, stage iii). Hence the growth profile of faults with a component of gravity-driven deformation will differ due to the additional component of cover fault displacement. Thus, faults that undergo a component of gravity-driven deformation on the Halten Terrace are predicted to initiate later in the overall growth history of the area (Late Jurassic and Early Cretaceous), and to follow a steeper growth path than tectonic faults, in which the extent of deflection above the idealised growth path of Cartwright *et al* (1995) is controlled by the magnitude of displacement due to gravity-driven deformation.

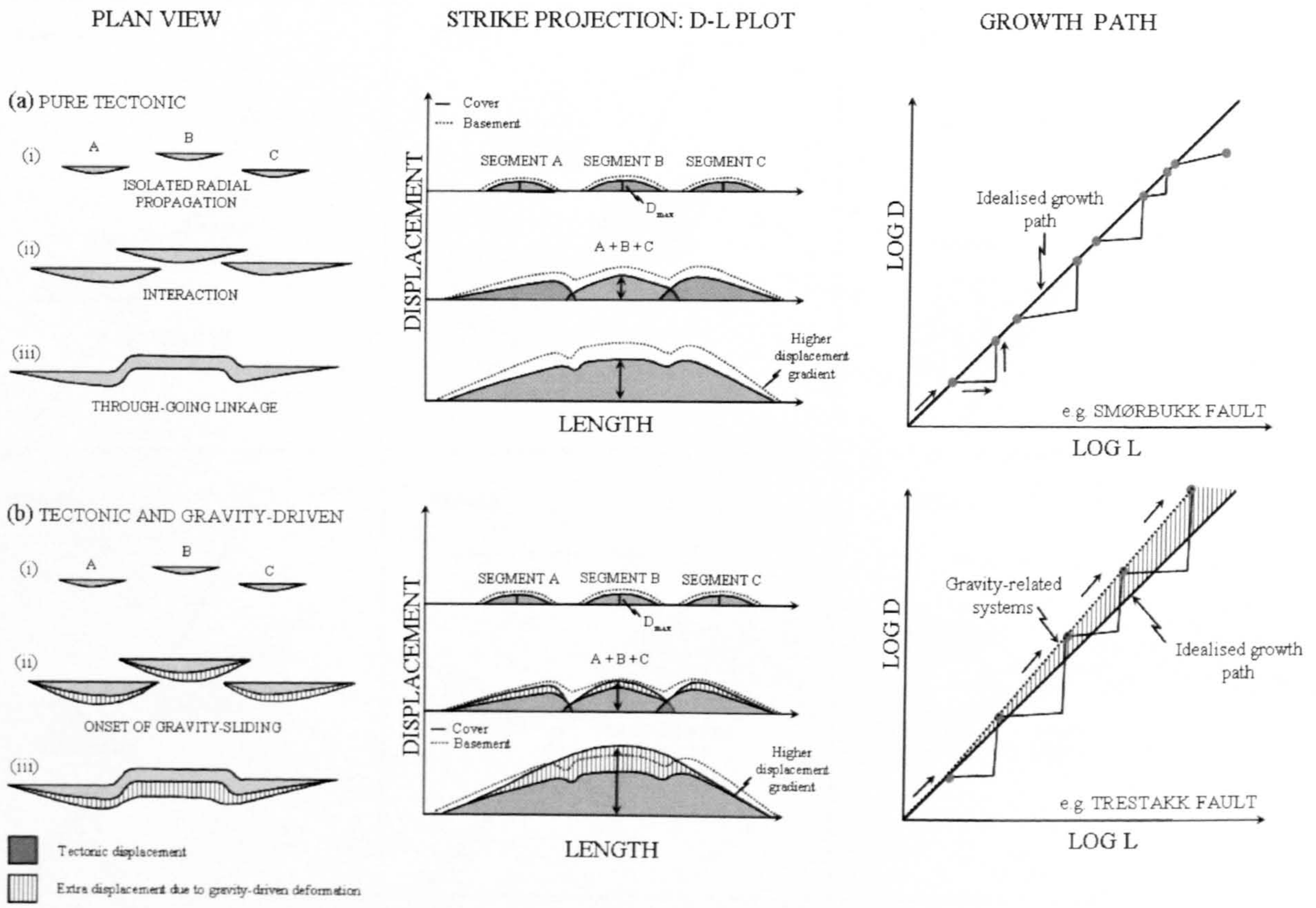

Figure 5.18: A new model of fault growth for cover faults that form due to (a) tectonic deformation and (b) tectonic and gravity-driven deformation. During tectonic deformation, segment linkage dominates the model which follows a step-wise growth path as predicted by Cartwright *et al*, 1995 (Modified from Cartwright *et al*, 1995). Note, in this model both basement and cover faults form due to segment linkage however basement faults have a larger D_{max} than in the cover. In (b) additional displacement due to gravity-driven deformation leads to cover faults, which have a larger D_{max} than the basement faults and higher displacement gradients. Faults follow the same step-wise pattern of linkage however due to a component of gravity-sliding faults gain more displacement and fall above the idealised growth line thus deflecting the trend to a steeper profile.

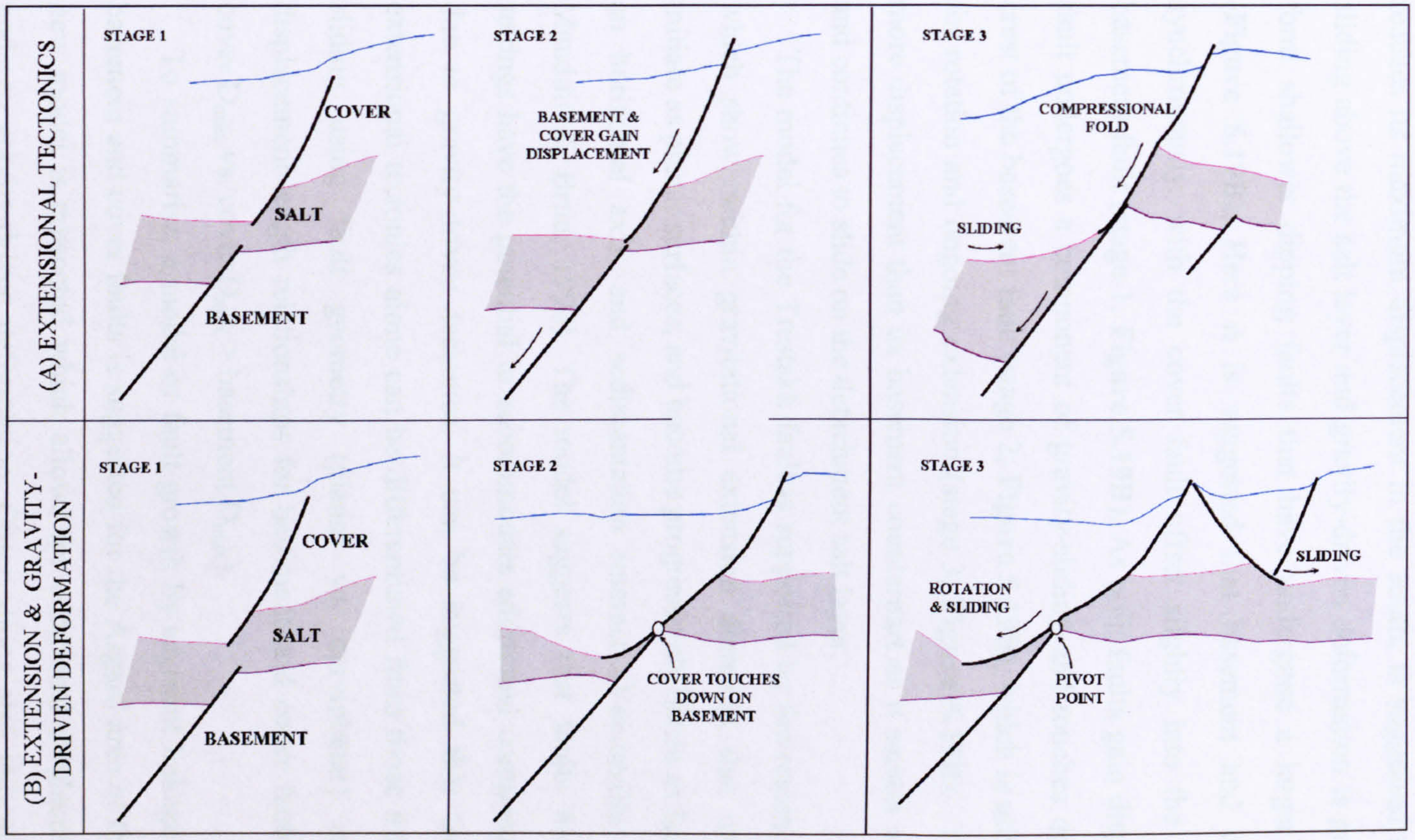

Figure 5.19: A model of fault growth for (A) extensional faults and (B) faults driven by extension and gravity-driven deformation, used to account for the differences in geometry between the two faults. In (A) the basement and cover faults initiate aligned with one another (stage 1), as the two faults gain displacement they link to one through-going fault (stage 2) which continues to gain displacement until the dip on the basement surface is sufficient to initiate gravity-sliding and compressional folding in the hangingwall of the cover fault (stage 3). (B) In contrast the Trestakk basement and cover faults initiate with the cover fault offset slightly into the hangingwall of the basement fault (stage 1). As the faults gain displacement, the cover fault touches down on the footwall crest of the basement fault (stage 2), which is then utilised as a pivot point for ongoing displacement in the cover due to both extension and gravity-driven sliding (stage 3).

The geometry of faults influenced by gravity-driven deformation, such as the Trestakk fault which changes in geometry from planar in the north to shallow-dipping and listric in geometry to the south, also differs from that of normal faults formed due to tectonic extension. The geometry of the Trestakk fault, where the fault reaches its maximum displacement in the south, is suggested to be influenced by sliding above the salt layer and gravity-driven deformation is proposed to generally form shallower dipping faults that have undergone a larger degree of rotation (**Figure 5.19B**). Here it is suggested that basement and cover faults initiate synchronously, with the cover fault offset slightly into the hangingwall of the basement fault (stage 1, **Figure 5.19B**). As both faults gain displacement, the cover fault undergoes a component of gravity-sliding and touches down on the footwall crest of the basement fault (stage 2, **Figure 5.19B**), which is utilised as a pivot point for rotation and ongoing extension (stage 3, **Figure 5.19B**). The cover fault gains more displacement than its basement counterpart as it rotates about the pivot point and continues to slide on the detachment salt layer.

The model for the Trestakk fault is supported by the results of analogue models which show, within gravitational extension domains, that normal faults usually initiate as planar surfaces, and become progressively listric as faulting, rotation about an horizontal axis, and sedimentation interact (Vendeville & Cobbold, 1988; Mauduit & Brun, 1998). The model suggests that faults formed in salt-related settings have the potential to accommodate additional components of displacement due to gravity-driven tectonics. It can be suggested that faults formed due to extensional tectonics alone can be differentiated from those influenced by gravity-sliding using fault geometry (planar vs. curviplanar) and comparing the displacement-length relationships for basement and cover faults (basement D_{max} > cover D_{max} vs. cover D_{max} > basement D_{max}).

To summarise, a model of fault growth by segment linkage that applies to both basement and cover faults is suggested for the Åsgard area of the Halten Terrace. A new model is presented which allows for additional displacements on faults that undergo gravity-driven deformation. Observations also indicate that the model of fault growth applies only to faults with separations of less than 10 km. Displacement transfers only occurs between faults with smaller separations where displacements on the individual fault surfaces may be aggregated to produce a displacement distribution which resembles that of a single fault e.g. Trestakk and Trestakk splay

(Walsh & Watterson, 1991; Peacock & Sanderson, 1991). Faults that intersect the footwall of the Smørbukk and Trestakk faults are also observed that are proposed to form due to gravity-driven deformation above the detachment salt layer. These faults form oblique to the trend of the main fault trace, intersect displacement-length profiles, offset the main fault surface and form later in the growth history than the main fault trace (**Figure 5.4**). Such obliquely-oriented gravity-driven faults intersect faults driven both by extensional tectonics (e.g. Smørbukk fault) as well as those affected by extensional tectonics and gravity-sliding (e.g. Trestakk fault).

The observations presented provide new insights into the evolution of faults that form above a detachment layer, such as salt. The process of fault segment growth, interaction and linkage is more complex than existing models suggest as fault growth can be influenced by both gravity-driven deformation *and* extensional tectonics. The observations presented are used to propose a new model for the evolution of syn-rift depocentres in response to fault array development in a salt-related system. In the new model, the onset of deformation in both the basement and cover is defined by diffuse deformation characterised by the nucleation of numerous isolated small segments, similar to that of Cowie *et al* (2000). During this stage, numerous small, isolated depocentres develop adjacent to small fault segments. As basement faults increase in length, isolated depocentres begin to interact and coalesce to form larger through-going depocentres. In addition, as the basement surface becomes progressively tilted, cover faults start to slide above the detachment layer, faults become more rotated, shallower in dip and their hangingwalls subside at a faster rate. Consequently deeper depocentres open up in the hangingwalls of the largest fault segments. It is speculated that the deepening of depocentres is followed by an abrupt increase in fault length as neighbouring faults continue to interact; however faults remain over-displaced for a given length due to the effects of gravity-sliding (**Figure 5.18c**). Thus, for normal faults where there is an additional component of gravity-driven deformation, such as the Trestakk fault, depocentres will be deeper and will subside at a faster rate than expected for faults formed due to extensional tectonics alone.

5.7 CONCLUSIONS

- Normal faults influenced by extensional tectonics *and* gravity-driven deformation have higher average horizontal displacement gradients, higher maximum displacements and shallower dips compared to faults formed by extensional tectonics alone.
- Displacement-length profiles suggest that basement *and* cover faults in the Åsgard area record fault growth by radial propagation and the coincidental overlap and linkage of fault segments.
- Displacement transfer is limited to faults with separations of less than 10 km
- A new model of growth for faults influenced by extensional tectonics *and* gravity-driven deformation is proposed, in which gravity-driven deformation accounts for the additional components of displacement observed on faults of a given length.
- Faults that accommodate additional components of gravity-sliding have higher displacements, higher subsidence rates and thus deeper depocentres compared to faults formed by tectonic extension alone.

CHAPTER 6

6: DISCUSSION & CONCLUSIONS

6.1 DISCUSSION

The results presented highlight the complexities of fault system evolution in basins where extensional faulting in the basement and cover is decoupled by the presence of a regionally extensive ductile salt layer. It has been demonstrated that the spatial and temporal evolution of basement faults, the passive movement of evaporites and the growth of faults and folds in the cover are intimately linked (Chapters 3 & 4). These processes fundamentally control the surface morphology and thus have a direct impact on the development of accommodation space and on sediment pathways across the area during the deposition of economically important reservoir intervals (Figure 3.14). The aim of this discussion, and one of the main outcomes of this thesis, is to emphasise the importance of a holistic approach to fault interpretation in salt-related settings. In particular, such an approach emphasises the importance of understanding the evolution of both *basement* and *cover* faults, in order to produce a robust structural model, which accounts for the unique mechanical properties of evaporites.

The impact of the results on understanding fault growth in basins influenced by salt is considered through a comparison with a well-established conceptual model of faulting in the presence of salt (Stewart, 1999). Thereafter the implications of the results for future exploration and production on the Halten Terrace, offshore Mid-Norway are discussed.

6.1.1 Fault growth in salt-related basins

In the analysis of fault growth in salt-related basins three aspects of basin evolution have been considered: (i) the timing of fault growth (Chapter 3); (ii) the geometry of structural styles, as observed mainly in cross-section views (e.g. on seismic dip-lines) (Chapter 4); and (iii) the 3D geometry of faults and the impact of salt on fault displacement-length scaling (Chapter 5).

Two mechanisms - crustal extension and gravity-sliding - control the evolution of post-evaporite cover faults on the Halten Terrace resulting in the development of both thick-skinned, basement-rooted faults and thin-skinned, decoupled faults that

detach on mechanically weak evaporites. It has been demonstrated that links exist between: the timing of fault activity (early onset vs. late onset); the orientation and geometry of structural styles; the growth path of faults in salt-related systems (crustal extension vs. crustal extension *and* gravity-driven deformation); and the mechanism of faulting (thick vs. thin-skinned) (**Figure 6.1**). It is shown that thick-skinned faults are typically N-S or NE-SW oriented (section 4.4.2.1), are generally more planar in geometry (e.g. Smørbukk fault, section 5.4.2), can link through the entire salt layer, initiate early in the growth history of the area (section 3.4.2), and follow existing models of fault growth through the interaction and linkage of initially isolated fault segments (section 5.5.1) (**Figure 6.1a**). In contrast, thin-skinned (gravity-driven) faults are generally oriented perpendicular to the dominant thick-skinned fault trend (i.e. perpendicular to the local or regional surface dip) (section 3.4.4 & 4.4.2.2), and form later in the growth history (post middle Jurassic, section 3.4.3 & 3.4.4) (**Figure 6.1b**). The onset of gravity-driven, thin-skinned faulting initiated after a period of crustal extension (~25Ma, Hettangian to Bajocian, on the Halten Terrace) which is sufficient to tilt the basement surface and initiate sliding in the cover. The period of lag between the onset of crustal extension and the onset of gravity-driven deformation will vary between salt-related basins depending on the magnitude, rate and duration of extension, which are the dominant factors controlling the basement surface morphology (section 4.5.1). The thickness of the evaporite layer will also be an important factor as this controls the extent and duration of decoupling during basement-cover faulting.

Examples of fault systems which undergo a degree of thick- and thin-skinned deformation on the Halten Terrace are also recognised (Chapter 5), e.g. Trestakk fault (**Figure 6.1c**). In these cases, the dominant fault strike and the initiation of fault growth will follow that of a typical thick-skinned fault, which controls the early evolution of such structures. Following the onset of a component of gravity-driven deformation (i.e. after ~25Ma), the geometry of the fault is altered due to sliding above the salt layer, and the fault follows a newly proposed and distinct growth path (section 5.6) to thick-skinned faults due to the additional component of displacement during gravity-sliding (**Figure 6.1c**). Faults that undergo the combined affect of thick- and thin-skinned faulting (hereafter referred to as 'hybrid' faults) are generally the longest-lived faults in the area, e.g. Trestakk fault.

	(a) THICK-SKINNED	(b) THIN-SKINNED	(c) HYBRID MODEL
Timing	EARLY ONSET (Early Jurassic – Late Jurassic/Early Cretaceous)	LATE ONSET (during or following rift climax)	EARLY ONSET CONTINUING POST-RIFT*
Structural trend	NE-SW N-S 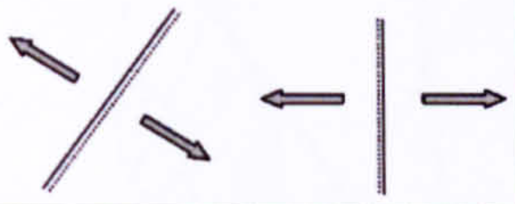	NW-SE E-W 	NW-SE N-S NW-SE 
Structural geometry	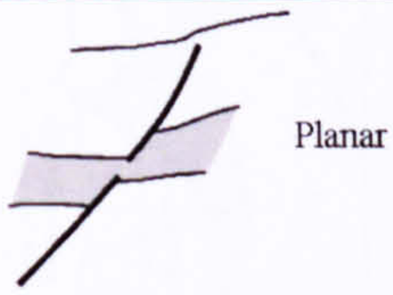 Planar	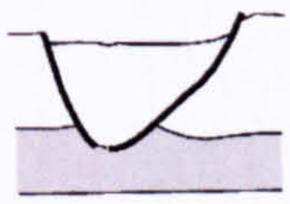 Planar/ listric	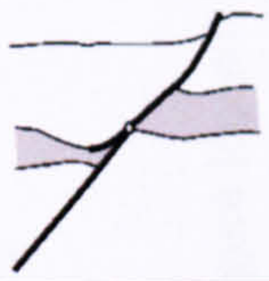 Planar/ listric
Degree of linkage	Coupled → Partially coupled 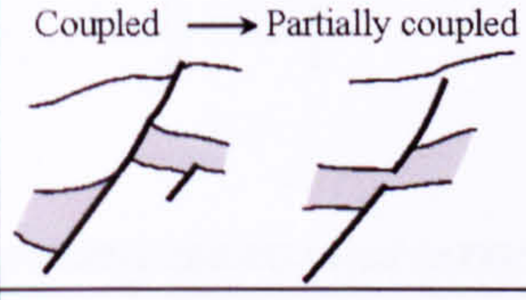	Decoupled 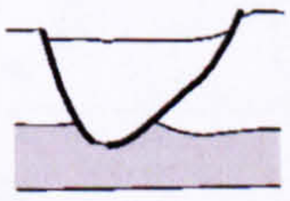	Coupled → Decoupled 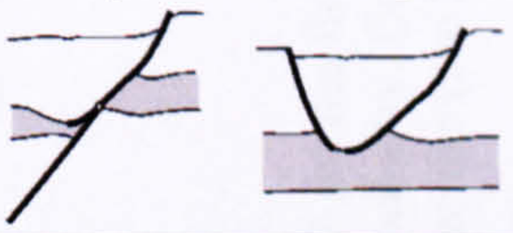
Growth path	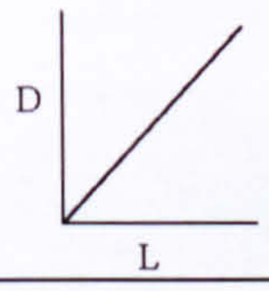 D L Idealised growth path		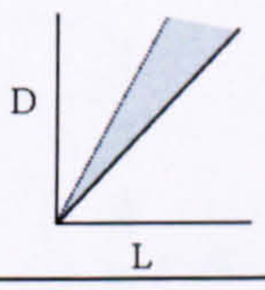 D L New growth path
Mechanism	CRUSTAL EXTENSION	GRAVITY SLIDING	CRUSTAL EXTENSION & GRAVITY SLIDING

KEY

 Extension direction

 Fault (basement)

 Fault (cover)

* Longest lived faults

 Evaporites

Figure 6.1: Table of fault characteristics and the mechanism of faulting summarised from chapter's 3, 4 and 5. A link exists between: the timing of fault activity; the orientation and geometry of structural styles; the degree of linkage through the salt layer; and the growth path of faults in salt-related systems. We can use the relationships established between characteristics to predict the mechanism of faulting, and thus the impact of faults on reservoir development (see section 6.1.2).

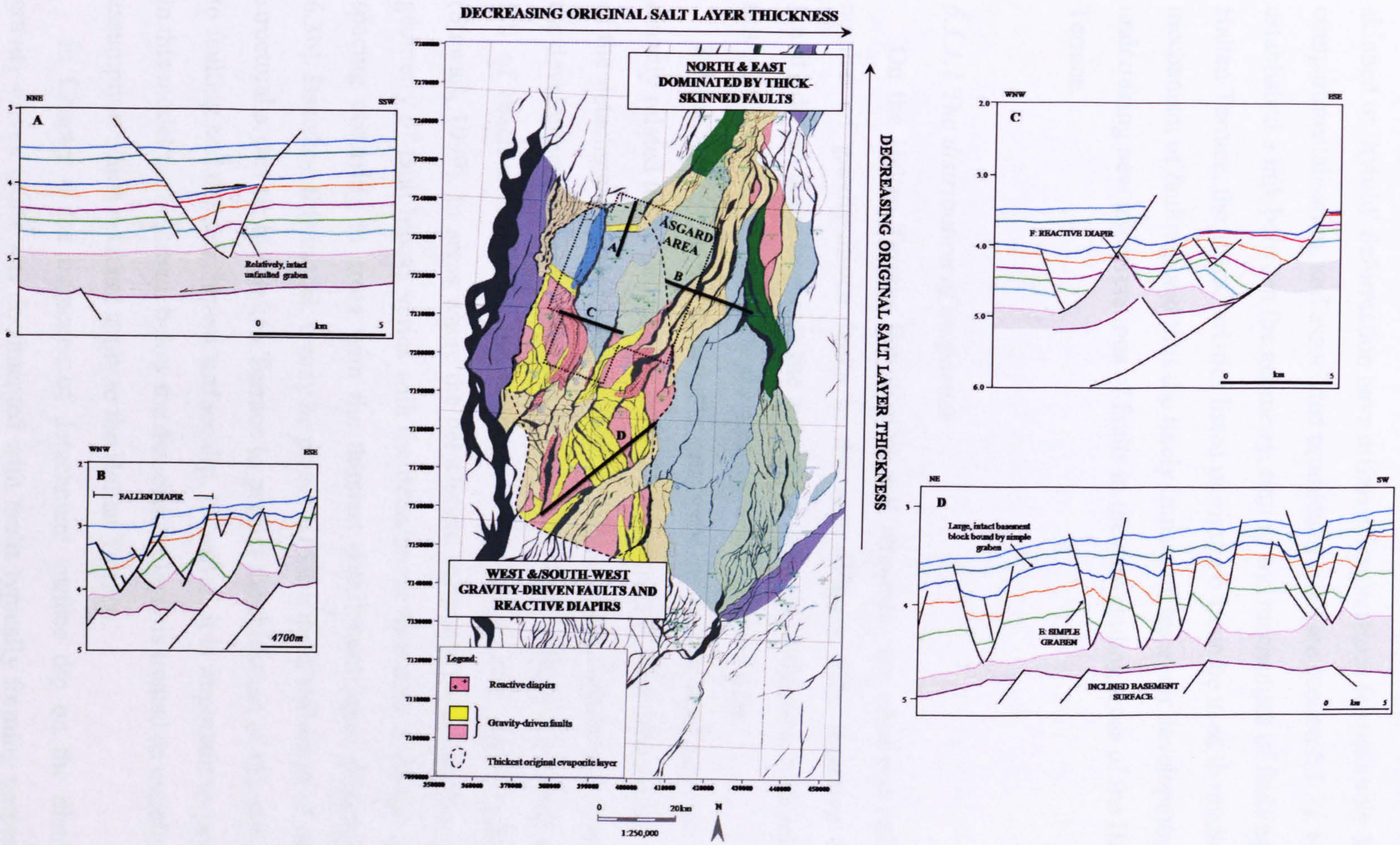

Figure 6.2: The original thickness of the evaporite layer on the Halten Terrace, (see Figure 4.7 for the full figure legend) based on regional knowledge, (see Chapter 4) and Stewart's (1999) model of detachment layer thickness and thin-skinned fault geometry. Cross-sections A-D highlight the change in structural geometry in the cover from north to south, which we relate to salt layer thickness and detachment dip (see Figure 6.3).

These observations suggest that fault geometry and orientation, the timing of fault initiation, and the duration of fault activity can be used to infer the mechanism of fault growth on the Halten Terrace. Faults that form due to thick-skinned, thin-skinned or 'hybrid' deformation have different implications for reservoir distribution, compartmentalisation, and associated production risk (see section 6.1.2). Having established a link between the geometry, timing and mechanism of faulting on the Halten Terrace, the characteristics listed in Figure 6.1 can be used to predict the mechanism of faulting, and thus the likely impact on reservoir development, when undertaking new interpretations of faults in the surrounding areas of the Halten Terrace.

6.1.1.1 The distribution of evaporites

On the Halten Terrace few diapiric salt structures are observed relative to the number of gravity-driven faults in the area (**Figure 6.2**). Reactive diapirs and gravity-driven faults dominate the west and southwest of the area, with relatively few salt/gravity-related structures to the east and north (**Figure 6.2**).

Stewart (1999) suggests that the geometry of thin-skinned tectonic systems is directly related to the detachment layer thickness, in this case evaporites, and the dip of the detachment surface (**Figure 6.3**). A thin, low dip detachment layer results in the development of narrow grabens separated by wide rafts, in contrast to the rise and fall of reactive diapirs in the presence of a thicker, low dip detachment layer (Stewart, 1999). In areas where the detachment surface is high dip, the spacing and geometry of fault blocks varies with the detachment thickness, with the lowest fault spacing occurring in areas with the thinnest detachment layer thickness (**Figure 6.3b**). Based on this model, it may be possible to use the distribution of thin-skinned structural styles on the Halten Terrace to predict the thickness of the salt layer prior to faulting and the detachment surface dip. However, it is important to point out that in this model the basement below the detachment layer is treated as undeformable, an assumption which does not apply to the Halten Terrace.

In Chapter 4 the influence of detachment surface dip on the distribution of gravity-driven faults was documented with faults typically forming perpendicular to surfaces with sufficient dip to initiate sliding (see section 4.4.2.2). Whilst it is likely that the thickness of salt influenced the degree of coupling between basement and

cover faults, there is some uncertainty as to whether the *present-day* thickness of salt can be used to infer its thickness at the time of fault activity. An alternative approach, based on Stewart's (1999) observations from the UK North Sea, could be to use the geometry and distribution of structural styles (gravity-driven faults & reactive diapirs) to predict the thickness of the evaporite layer across the area *immediately prior to* the onset of gravity-sliding. Using this approach it can be suggested that, prior to gravity-sliding, the evaporite layer was thickest in the southwest and west of the Halten Terrace, south of the Åsgard area (**Figure 6.2 C, D**), where the rise and fall of reactive diapirs and the dominance of gravity-driven faults is observed (see Chapter 4). The presence of domino fault arrays with thin high horsts (**Figure 6.2D**) suggests a high dip detachment surface and a thick detachment layer was present in the southwest of the area (**Figure 6.3b**). Further north and west, reactive diapirs are preserved between broad synclines (**Figure 6.2C**), suggesting a thick detachment layer exists above a lower dipping surface (**Figure 6.3a**). In the east and north of the terrace, only one fallen diapir, in the Gimsan Basin (**Figure 6.2B**), is observed and fewer gravity-driven faults are present suggesting that overall the salt layer was thinner, and thus the basement and cover were more coupled, and the detachment dip was lower (**Figure 6.3a**).

At the onset of gravity-driven deformation, crustal extension had been ongoing for ~25Ma. Crustal extension loads and unloads the salt layer and tilts the detachment surface, causing evaporites to move (see Chapter 4). The interaction between basement faulting, salt movement and gravity-driven deformation is therefore more complex than suggested by Stewart's (1999) model, which treats the basement below the detachment layer as undeformable. This model can be used to reconstruct the regional salt layer thickness prior to gravity-driven deformation, and to recognise that crustal extension most likely redistributed evaporites during the ~25Ma prior to gravity-sliding, thus some uncertainty regarding the pre-rift salt layer thickness remains. However, it is difficult to precisely restore the original salt thickness and predictions that aim to do so without taking into account all aspects of the fault system, such as the strain rate, duration and extent of faulting in the basement *and* cover should be treated with caution.

An incorrect interpretation of the original depositional thickness of a salt layer or of the significance of present-day changes in salt layer thicknesses can lead to mis-information on both the basement and cover fault growth histories. An example of

this is given in Figure 6.4, where the present-day structural geometry (**Figure 6.4a**) is described by a series of basement faults separated from the cover by a layer of evaporites. The sequence of evaporites is associated with a package of divergent reflectors indicating stratal thickening into the hangingwall of the fault. Two alternative interpretations of the salt geometry are presented. In the first, the present-day geometry of the evaporite layer is interpreted to represent a period of fault activity synchronous with evaporite deposition, resulting in divergent internal reflectors and thickening into the fault (**Figure 6.4b**). In the second interpretation (**Figure 6.4c**), the geometries of the basement interval immediately underlying, and the cover interval overlying the evaporite package are interpreted to represent a pre-rift package (i.e. parallel reflectors, no thickness change across the fault) suggesting that the present-day geometry of the evaporite layer is a consequence of salt flow *after* deposition rather than a syn-rift geometry. This example highlights the importance of understanding the evolution of both *basement* and *cover* faults, in order to produce a robust structural model, which accounts for the unique mechanical properties of evaporites.

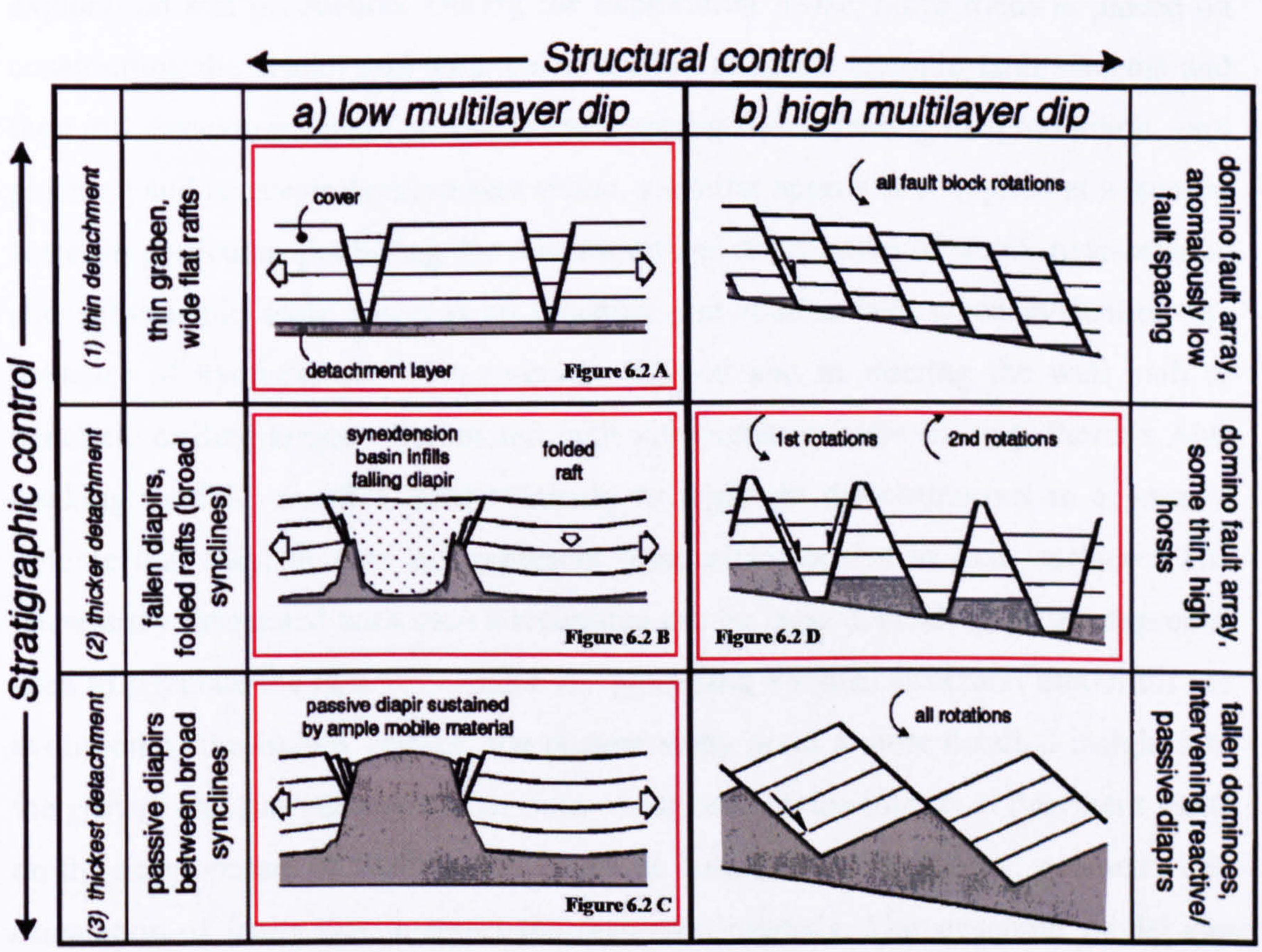

Figure 6.3: Figure caption on following page.

Figure 6.3 (previous page): The impact of detachment layer thickness on thin-skinned extensional fault geometry, divided into low and high multilayer dip cases (modified from Stewart, 1999). (a) Low multilayer dip: (1) For a thin detachment layer, conjugate fault pairs intersect at the top detachment surface defining narrow graben and wide, relatively undeformed rafts. (2) For a thicker detachment, more complex symmetrical graben occur, underlain by a reactive diapir. Where no more detachment material is available to feed the diapir, the diapir collapses giving a new deep basin between the rafts (Vendeville & Jackson, 1992a, b). (3) For the thickest detachment layer, sufficient supply of detachment material delays diapir fall. (b) High multilayer dip, where high refers to sufficient regional dip to promote domino-faults that dip in the same direction as the dip of the detachment. (1) Domino faults of consistent, down-dip facing polarity and faults that are relatively closely spaced. (2) For a thicker detachment, back rotation of fault blocks is sufficient to allow a second, antithetic generation of faults to develop. Fault array characterised by thin, high horsts. (3) For the thickest detachment, keels of fault blocks, defined by first generation faults, never touch down.

6.1.2 Implications for Exploration and Production

6.1.2.1 The spatial distribution, geometry and density of faults

Constraining the spatial distribution, magnitude and frequency of faults that offset economically important reservoir intervals has implications for both exploration and production. During the exploration phase, more focus is placed on constraining the spatial and temporal evolution of major tectonic fault systems and their influence on potential prospects and trapping styles. During the production, well planning and reservoir development phase, a similar approach is applied at a smaller scale. In particular, predicting the orientation and distribution of small, near-seismic and sub-seismic scale faults is an essential and routine task when evaluating the presence of hydrocarbons in a reservoir interval and in steering the well path to penetrate drilling targets. Automated fault interpretation software (e.g. Petrel's Ant-tracking module) is often used routinely to highlight discontinuities in a seismic volume that may, or may not represent discontinuities due to fault surfaces. The uncertainty associated with such a technique can be large depending on the approach used to populate the data with faults. By producing a robust structural model for the evolution of the Halten Terrace, the present study gives a more detailed insight into the growth and evolution of faults, from understanding the impact of basement faults on the development of faults in the cover, to constraining the timing, geometry and orientation of faults that intersect the reservoir intervals. The structural model can therefore be used as a predictive tool for identifying areas of low and high strain (i.e.

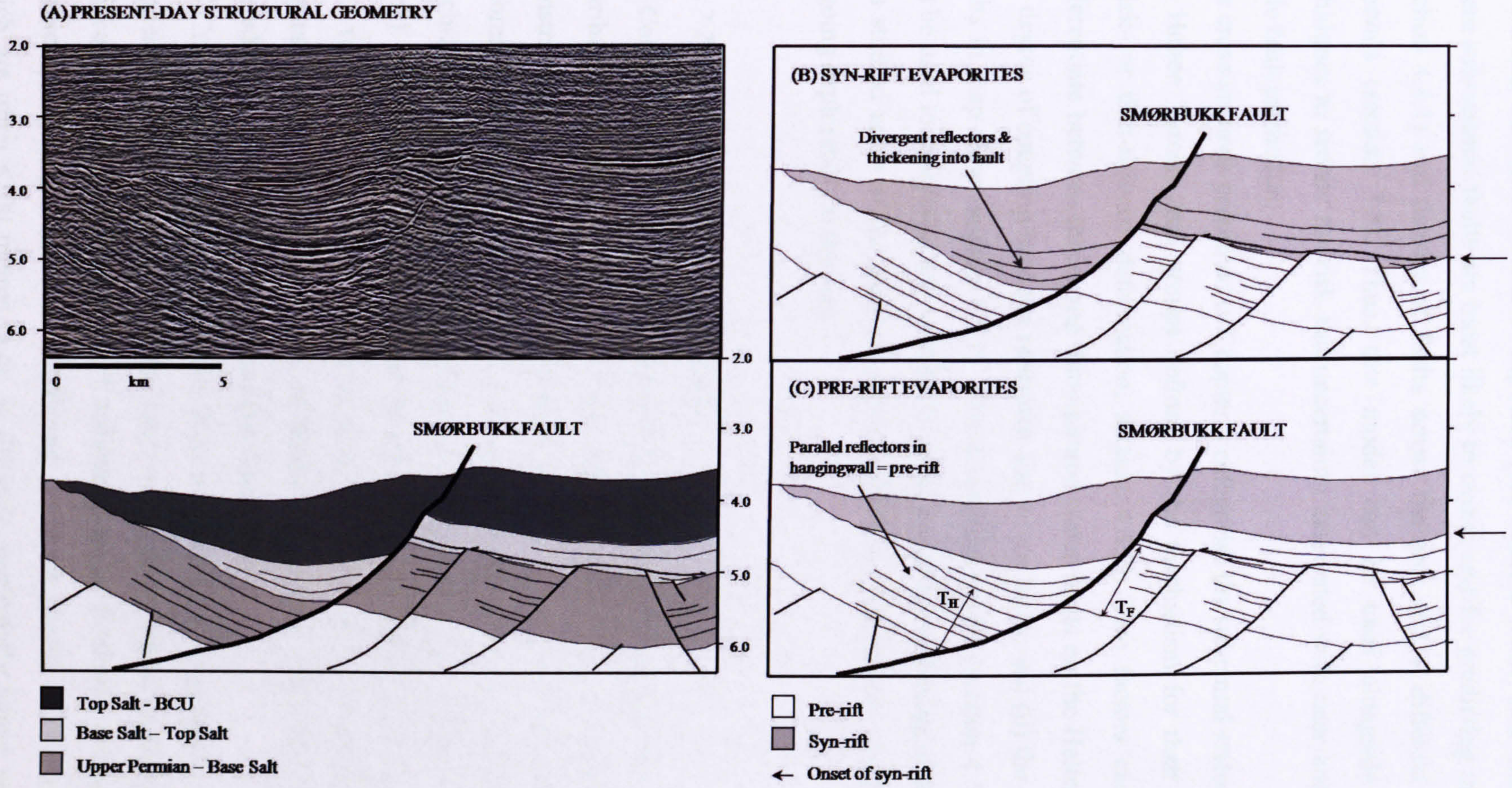

Figure 6.4: Contrasting interpretations of the present-day thickness of a salt layer from the same seismic section (A). (B) A package of divergent reflectors are interpreted to indicate stratal thickening into the hangingwall of the fault during a period of fault activity synchronous with evaporite deposition. (C) A more holistic approach, in which basement and cover fault geometries are interpreted, interprets the evaporites as a pre-rift package.

areas above the largest displacement basement faults, or where gravity-sliding above an inclined basement surface is expected (see section 4.4.2), and thus those areas where sub-seismic faults are most likely to occur, and for predicting the orientation (section 4.4.1) and density of faults across the area and at different stratigraphic intervals (section 3.3). Thus, this model can be used alongside geophysical techniques to reduce the risk and uncertainty associated with near and sub-seismic scale fault prediction.

The cross-sections presented in Chapter 4 categorise the structural styles observed on the Halten Terrace into groups defined by the mechanism for their development (thick- or thin-skinned deformation, section 4.4.2). Two factors can be used to differentiate between thick- and thin-skinned cover faults on the Halten Terrace: (i) the degree of coupling between basement and cover faults; and (ii) the orientation of faults in map-view (section 4.5.1). The conceptual model (section 4.5.2) presented can be used to categorise and predict the style, intensity and timing of deformation in less studied areas of the Halten Terrace, which is of particular importance during ongoing exploration in the area.

6.1.2.2 The temporal evolution of faults

Constraining the temporal evolution of faults has implications for predicting the distribution of depocentres that form synchronous with reservoir deposition. Constraining the timing and distribution of active faults and the development of accommodation space throughout the Jurassic and Early Cretaceous provides a much-improved method of predicting reservoir distribution (see sections 3.4.3 & 3.4.4). The interpretation shows that the distribution of Early Cretaceous depocentres does not follow the same pattern as those in the Jurassic, with the distribution, orientation and overall geometry of faults being more variable and thus more unpredictable in the Early Cretaceous (section 3.4.4).

Crucially, the evolution of faults from many isolated segments to a few, linked segments over time (section 5.5.1 & Figure 4.19) has an impact on the areal extent of depocentres and thus the ability of sediments to be funnelled through connected depocentres during deposition. Predicting the areal extent of reservoir intervals, which are often <100 metres thick, is difficult, particularly where well control is limited. It is possible, however, to use the timing of fault activity, which controls the

distribution and connectivity of depocentres during reservoir deposition, to predict the lateral extent of deposition during a particular interval (see Chapter 3.5.2).

Furthermore, the results have implications for constraining the distribution of cover faults that offset important reservoir intervals and the magnitude of their displacement. Crucially, if the duration of extension and the magnitude and rate of displacement are the dominant controls over the distribution of faults in the cover sequence (see section 4.5.1), the spatial and temporal evolution of faults and folds can be used to predict the magnitude and distribution of structures in prospective hydrocarbon provinces, allowing better assessment of the degree of reservoir compartmentalisation in new and existing prospects on the Halten Terrace.

6.1.2.3 Field-scale complexity & structural uncertainty

An improved knowledge of the structural history of the area and the structural complexity of individual fields can be used to highlight some of the challenges faced during the production of each field. Two categories of structural styles can be defined on the Halten Terrace, thick- and thin-skinned, which can be used to categorise the fields in the area according to the mechanism dominant in their development, i.e. thick- skinned vs. thin-skinned vs. 'hybrid' extension.

Each category has its own set of implications for hydrocarbon prospectivity and thus each field can be ranked according to its development risk. Each field has been risked according to the degree of fault complexity and structural uncertainty, whilst also accounting for the data available to constrain uncertainty. Thus many of the early-phase projects are high risk due to a lack of data.

THICK-SKINNED	THIN-SKINNED	HYBRID
Smørbukk* L	Kristin* M	Smørbukk Sør* M
Heidrun* M	Morvin^ H	Lavrans^ H
Midgard* M		Trestakk^ M
Mikkel^ M		Tyrihans^ M
		Njord* H/M
LOW/MEDIUM	**MEDIUM/HIGH**	**MEDIUM/HIGH**

Table 1: StatoilHydro operated fields on the Halten Terrace sub-divided into categories associated with the dominant mechanism controlling their structural evolution. Each field is ranked according to its reservoir development risk, and each category given an overall ranking (in bold). Note, * = established fields in production, ^ = early phase development projects, H, M, L = High, Medium and Low risk respectively, which is defined based on the structural complexity and or uncertainty of each field.

Thick-skinned

Thick-skinned fields are defined by classic rotated fault blocks that have undergone little gravity-related deformation. Although often complex structural settings (i.e. compartmentalised by many seismic and sub-seismic scale faults), these are the most-tested traps that have been proven to be successful for production to date, e.g. Smørbukk and Heidrun. Based on the examples studied in this thesis, the key production challenges associated with thick-skinned faults are likely to be that:

- Such fields are characterised by the longest lived faults, which are thus likely to impact upon depositional patterns for all reservoir intervals (section 3.5.2, figures 3.14 & 4.16).
- The degree of reservoir compartmentalisation varies between thick-skinned fields depending on their structural history i.e. coupled fault vs. breached folds (figures 4.10 & 4.11).
- The highest displacement faults (section 4.4.2.1, Type B) have undergone extensive footwall erosion, which removes reservoir intervals from footwalls (section 3.5.2.2) and therefore potentially reworks and redistributes good quality sands elsewhere. Predicting the pathways for redistributed sands is difficult without constraint on the active fault history.
- Reservoir quality decreases with increasing burial (section 3.5.2.2), i.e. in the hangingwalls of the largest displacement, thick-skinned faults.

Thick-skinned faults which develop from a fault-propagation fold to a linked, breached fold, for example, those seen in the Heidrun and Mikkel fields, have the most complex and uncertain fault patterns placing them in a higher risk category than a simple rotated fault block with few internal faults, e.g. Smørbukk field. The Smørbukk field is ranked as the lowest risk because it is relatively unfaulted

compared to Heidrun, Midgard and Mikkel. It also has a well constrained structural history, with wells penetrating both the footwall and hangingwall of the fault constraining growth from the Early Jurassic (Åre formation). It is also a well developed field with much production data.

Thin-skinned

Thin-skinned faults which do not link to the basement are smaller displacement structures which have undergone less footwall uplift and erosion (section 4.4.2.2) than basement-linking faults. Thin-skinned faults were typically active for a shorter period of time relative to thick-skinned faults (sections 3.5.1, 4.5.1 & Figure 4.16) and thus have little/no impact on the development of depocentres during Åre, Tilje and Ile deposition.

That said, intra-reservoir faulting in these fields is complex, difficult to predict from seismic data and the faults are often sealing, resulting in many individual pressure compartments within one field, e.g. Kristin (Figure 4.9a). As a result, the Kristin and Morvin fields are higher risk due to:

- High risks associated with predicting reservoir compartmentalisation, and thus planning well-paths, due to uncertainties with fault seal analysis.
- The orientation of faults is more difficult to predict without constraint on the dip of the basement surface, which is often difficult to map (e.g. Figure 4.13a).
- Many near- or sub-seismic scale faults are indicated from production pressure data; however, seismic-scale faults appear to only offset the pre-reservoir stratigraphy (e.g. Åre Coal level) and are difficult to trace between seismic sections (Figure 4.15).

Many early phase developments reside in structurally complex fault blocks which are relatively understudied and hence poorly understood, e.g. Morvin. The Morvin field sits up-dip of the compressional fold in hangingwall of Smørbukk fault in an area of up-dip extension and most-likely complex fault interactions (Figure 4.15). From seismic data the field is a relatively simple, unfaulted glide-block with few, internal faults. However, given its development in a decoupled, gravity-driven system (section 4.4.2.2), similar to that of the Kristin field, it is predicted that many

sub-seismic scale faults will likely fracture the reservoir. Using the Kristin field as an analogue for Morvin may be the best approach during field development.

Hybrid

Fields that undergo a component of both thick- and thin-skinned extension are likely to be the most structurally complex, and thus highest risk fields to develop, e.g. Lavrans field (Figure 4.9a). The Lavrans field is located in the hangingwall of the Trestakk fault, which changes in geometry along-strike as the fault undergoes an increasing degree of gravity-sliding (sections 5.4.1 & 5.5.2), and on the flanks of a reactive diapir. The field is segmented by many small displacement faults associated with the rollover into the listric trace of the Trestakk fault (section 5.4.1). There is much uncertainty regarding the orientation, magnitude and density of faults above the salt diapir adjacent to the field. Furthermore, the lateral extent of the salt diapir and hence the volume of salt within the reservoir interval is difficult to constrain from the seismic data, which has implications for the volume of potentially hydrocarbon-bearing reservoir in the Lavrans field, and thus controls the economic viability of the field.

Hybrid fields are affected by the production challenges already listed for thick-skinned and thin-skinned faults, as well as additional risks which include:

- Hybrid faults have higher maximum displacements (section 5.5.2) - and are thus likely to experience more extensive footwall erosion - and have shallower dips (section 5.4.1) than thick-skinned faults.
- Faulted rollover anticlines may develop in the hangingwalls of listric hybrid faults, potentially compartmentalising reservoir intervals.
- Hybrid faults have higher displacements, higher subsidence rates and thus deeper depocentres (section 5.6) compared to thick- or thin-skinned faults, thus reservoir quality is likely to be poor due to deep burial (section 3.5.2.2)

To summarise, the conceptual models presented in this thesis have implications for both exploration and ongoing production on the Halten Terrace, in particular:

- Predicting the size, location and intensity of faults that offset reservoir intervals is essential when steering wells across faults to reach drilling targets.

- Constraining the timing of fault growth is essential for predicting the distribution of depocentres that form synchronous with reservoir deposition (see section 6.1.2.2).
- A conceptual model of fault growth by segment linkage, based on detailed displacement-length analysis (see Chapter 5), can be used to constrain the evolution of depocentres over time (i.e. from a number of isolated to one through-going depocentre).

As a direct result of the results presented in this thesis, many seismic interpreters in-house in StatoilHydro recognise the value-added from interpreting both basement and cover faults to gain a better understanding of the structural history of each field, in particular, these results are being applied in the development of new geo-models for Smørbukk, Smørbukk Sør and the Njord fields.

6.2 SUGGESTIONS FOR FURTHER WORK

The research presented in this thesis has highlighted areas which are of interest for future study. In particular studies which would further improve the current understanding of fault growth in salt-related settings include:

(i) Section balancing could provide valuable information about the evolution of thick- and thin-skinned structures in the region. Time should be spent interpreting regional seismic lines down-dip of gravity-driven faults, e.g. across the Klakk fault system. Crucially, this thesis lays the foundations for a later balancing study aimed at separating out the effects of gravity-driven deformation and regional extension. The magnitude of displacement on thick-skinned basement and cover faults should ultimately balance so that deformation, in the form of normal growth fault and extensional forced folds, above and below an evaporite layer is of broadly the same magnitude. Displacement associated with thin-skinned extension is surplus to this and may occur in a different direction to the regional extension vector. The gravity-driven deformation should be treated as a separate system in which up-dip extensional faults will balance with down-dip reverse faults and folds, in the absence of a free-surface at the toe of the slide (Hesthammer & Fossen, 1999).

(ii) The use of biostratigraphy to constrain the strain rate on faults of different structural styles during rifting. Results could be used to support the suggestion made

in this thesis that the duration and rate of extension controls the geometry and distribution of thick- and thin- skinned faults.

(iii) Perform more seismic interpretation to constrain fault growth within the seismic packages presented in this study, i.e. constrain fault growth, and thus the impact of fault activity during each interval of reservoir deposition. The following seismic horizons would be beneficially studied in greater depth and detail: Top Tilje, Top Tofte and Top Garn.

(iv) Produce a regional scale 3-D fault model across other fields/prospects, to test the results presented in Chapter 5. A key objective should be to investigate whether there other examples of 'hybrid' faults on the Halten Terrace, which, like the Trestakk fault, have undergone both thick- and thin-skinned extension. If such faults exist, it may be possible to test the wider application of the fault growth model presented in Chapter 5. The characteristics of 'hybrid' faults and those that have undergone thin-skinned extension could be used to further constrain the variables controlling the distribution of gravity-driven faults and the thickness of evaporites.

(v) Integrate the current seismic study with an analogue field study to understand: (i) the spatial distribution of sub-seismic scale faults and deformation bands; (ii) the size and extent of the fault zones; and (iii) the properties of the fault rocks, e.g. variations in shale gouge along the length of the fault. Such a study would be beneficial to production well-planning when the location and properties of a fault zone are crucial to defining pressure compartments and to successfully steering a well into the correct target zone.

The Moab fault, Utah, where fault growth is influenced by the presence of salt, may provide a good analogue for the Trestakk fault. The Moab fault is similar in plan view, splays towards the tip of the fault and changes in trend along-strike of the fault, similar to the Trestakk fault. Similarly, it should be possible to use this study of the Trestakk fault, in which the sub- and supra-salt faults have been imaged, to better understand the development of the Moab fault.

6.3 THESIS CONCLUSIONS

I. Two mechanisms control the evolution of faults on the Halten Terrace: Thick-skinned extensional tectonics; and thin-skinned gravity-driven

deformation. Three factors define the geometry of the structural styles associated with each mechanism:

(i) The **degree of coupling** between basement and cover faults

(ii) The **dominant structural orientation** of faults.

(iii) The **timing of fault growth.**

II. Fault growth in salt-related basins is recorded by the development of thick- and thin-skinned faults and extensional fault propagation folds. Growth of sediments into fault-propagation folds records the early onset of sub-salt basement fault activity during the Early Jurassic.

III. Thick-skinned basement and cover fault activity on the Halten Terrace initiated synchronously in the Early Jurassic, without the need to invoke basement fault reactivation. However, basement reactivation cannot be ruled-out from the currently available seismic and well data. Faults remained active throughout the Jurassic and into the Early Cretaceous, during which time strain progressively localised onto a few large basement and cover faults.

IV. The main factors controlling the geometry and distribution of thick- and thin-skinned faults are:

(i) Along-strike changes in the magnitude of displacement on basement *and* cover faults.

(ii) The relative distribution and orientation of faults in the basement and cover.

(iii) The duration of extension.

(iv) The rate of extension.

V. Thin-skinned, gravity-driven faults are identified based upon: (i) their orientation perpendicular to the local or regional dip direction; and (ii) the onset of fault activity, which initiated post-Middle Jurassic, following the initiation of activity on thick-skinned faults. The majority of thin-skinned fault growth initiated in the Early Cretaceous due to gravity-driven deformation above a locally *or* regionally tilted basement surface. Gravity-driven faults are oriented perpendicular to the local or regional dip direction and have no basement faults with a similar trend.

VI. Thus, the dominant mechanisms controlling the magnitude of displacement and the distribution of thin-skinned cover faults are the magnitude and direction of dip on the basement surface (controlled by the factors listed in

point (IV)). The largest displacement thin-skinned faults will form above surfaces with the greatest dip which occurs adjacent to the largest displacement thick-skinned faults, or in areas with the greatest regional dip.

VII. Displacement-length profiles suggest that basement *and* cover faults in the Åsgard area record fault growth by radial propagation and the coincidental overlap and linkage of fault segments.

VIII. Normal faults influenced by extensional tectonics *and* gravity-driven deformation, e.g. Trestakk fault, have higher average horizontal displacement gradients, higher maximum displacements and shallower dips compared to faults formed by extensional tectonics alone. Thus, a new model of growth for faults influenced by extensional tectonics *and* gravity-driven deformation is proposed, in which gravity-driven deformation accounts for the additional components of displacement observed on faults of a given length.

IX. By constraining the timing, distribution and geometry of active faults and the development of accommodation space throughout the Jurassic and Early Cretaceous it is possible to provide a much-improved method of predicting reservoir distribution and the magnitude of fault displacements at important reservoir target intervals on the Halten Terrace.

X. Fault growth in brittle-ductile systems is more complex that in a pure brittle system as reflected by the timing of basement and cover fault activity, the structural styles and the model of fault growth presented here. Crucial to all the observations made here is the presence of a weak, ductile stratigraphy, which controls the behaviour of faults above and below the interval. Thus, it is suggested that time should be spent constraining the spatial and temporal evolution of basement *and* cover faults and folds in order to predict the magnitude and distribution of structures in prospective hydrocarbon provinces, and also the degree of reservoir compartmentalisation in new and existing prospects on the Halten Terrace and other salt-related basins worldwide.

REFERENCES

REFERENCES

Ackermann, R. V., Schlische, R. W. & Withjack, M. O. 2001. The geometric and statistical evolution of normal fault systems: an experimental study of the effects of mechanical layer thickness on scaling laws. *Journal of Structural Geology*, **23**, 1803-1809.

Anders, M. H. & Schlische, R. W. 1994. Overlapping Faults, Intrabasin Highs and the Growth of Normal Faults. *The Journal of Geology*, **102**, 165-180.

Baldwin, B. & Butler, C. O. 1985. Compaction curves. *American Association of Petroleum Geologists Bulletin*, **69**, 622-626.

Barnett, J.A.M., Mortimer, J., Rippon, J., Walsh, J.J., Waterson, J., 1987. Displacement geometry in the volume containing a single normal fault. *American Association of Petroleum Geologists Bulletin,* **71**, 925–937.

Blystad, H., Brekke, H., Færseth, R. B., Larsen, B. T., Skogseid, J. & Tørudbakken, B. 1995. Structural elements of the Norwegian continental shelf. Part II: The Norwegian Sea Region. *NPD Bulletin*, 8.

Brekke, H. 2000. The tectonic evolution of the Norwegian Sea Continental Margin with emphasis on the Vøring and Møre Basins. *In:* Nøttvedt, A. *et al.* (eds) *Dynamics of the Norwegian Margin.* Geological Society, London, Special Publication, **167**, 327-378.

Brekke, H. and Riis, F. 1987. Tectonics and basin evolution of the Norwegian shelf between 62°N and 72°N. Nor. Geol. Tidsskr., **67**, 295–322

Brockbank, P. & Hanssen, O. K. 2004. Haltenbanken Tectonics and Stratigraphy: a semi-regional project with emphasis on Middle Jurassic reservoir development. Internal StatoilHydro report.

Bukovics, C., Shaw, N. D., Cartier, E. G. & Ziegler, P. A. 1983. Structure and development of the Mid-Norway continental margin. *In:* Spencer, A. M. *et al.* (eds) *Petroleum Geology of the North European Margin.* Graham & Trotman, London, 271-284.

Butler, R. W. H., Holdsworth, R. E. H. & Lloyd, G. E. 1997. The role of basement reactivation in continental deformation. *Journal of the Geological Society of London,* **154**, 69-71.

Cartwright, J., Mansfield, C. & Trudgill, B. 1995. The growth of faults by segment linkage: evidence from the Canyonlands grabens of S. E. Utah. *Journal of Structural Geology*, **17**, 1319-1326.

Caselli, F. 1987. Oblique-slip tectonics Mid-Norway Shelf. *In:* Brooks, J & Glennie, K (*eds*) *Petroleum Geology of North West Europe,* 1049-1063.

Childs, C., Easton, S. J., Vendeville, B. C., Jackson, M. P. A., Lin, S. T., Walsh, J. J., Watterson, J. 1993. Kinematic analysis of faults in a physical model of growth faulting above a viscous salt analog. *Tectonophysics*, **228** (3-4), 313-329.

Childs, C., Watterson, J., & Walsh, J. J. 1995. Fault overlap zones within developing normal fault systems. *Journal of the Geological Society,* **152**, 535-549.

Childs, C., Nicol, A., Walsh, J. J. & Watterson, J. 2003. The growth and propagation of syn-sedimentary faults. *Journal of Structural Geology*, **25** (4), 633-648

Cobbold, P. R. & Szatmari, P. 1991. Radial gravitational gliding on passive margins. *Tectonophysics*, **187**, 249-289.

Contreras, J., Scholtz, C. H. & King, G. C. P. 1997. A model of rift basin evolution constrained by first-order stratigraphic observations. *Journal of Geophysical Research*, **102**, 7673-7690.

Corfield, S., Sharp, I., Häger, K-O., Dreyer, T. and Underhill, J. 2001. An integrated study of the Garn and Melke formations (Middle to Upper Jurassic) of the Smørbukk area, Halten Terrace, mid-Norway. *In*: Martinsen, O. J., Dreyer, T. (eds.) *Sedimentary Environments Offshore Norway-Palaeozoic to Recent.* NPF Special Publication 10, 199-210.

Corfield, S. & Sharp, I. R. 2000. Structural style and stratigraphic architecture of fault propagation folding in extensional settings: a seismic example from the Smørbukk area, Halten Terrace, Mid-Norway. Basin Research, **12**, 329-341.

Cowie, P. A., & Scholz, C. H. 1992a. Physical explanation of the displacement-length relationship of faults using a post yield fracture-mechanics model. *Journal of Structural Geology*, **14** (10), 1133 – 1148.

Cowie, P. A., & Scholz, C. H. 1992b. Displacement-length scaling relationships for faults – data synthesis and discussion. *Journal of Structural Geology*, **14** (10), 1149 – 1156.

Cowie, P. A. 1998. A healing-reloading feedback control on the growth rate of seismogenic faults. *Journal of Structural Geology*, **20**, 1075-1087.

Coward, M.P., Dewey, J., Hempton, M. & Holroyd, J. 2003. Tectonic Evolution. *In:* Evans, D, Graham, C, Armour, A. & Bathhurst, P. (eds.) *The Millenium Atlas: Petroleum Geology of the Central and Northern North Sea.* Geological Society, London.

Dalland, A., Worsley, D. & Ofstad, K. 1988. Lithostratigraphic scheme for the Mesozoic and Cenozoic succession offshore Mid and Northern Norway. Oljedirektoratet.

Dam, G., Larsen, B.T., Stemmerik, L. & Monstad, S. 2002. The Norwegian Sea area, as seen from offshore andonshore Greenland – a comparative regional review. *In*: Hurst, A. (ed.) *Offshore-onshore relationships on the North Atlantic margin: NGF abstracts and Proceedings*, **2**, 44-46.

Demercian, S., Szatmari, P. & Cobbold, P. R. 1993. Style and pattern of salt diapirs due to thin-skinned gravitational gliding, Campos and Santos basins, offshore Brazil. *Tectonophysics*, **228**, 393-433.

Doré, A. G. 1992. Synoptic paleogeography of the Northeast Atlantic seaway; late Permian to Cretaceous. *In: Basins on the Atlantic Seaboard: Petroleum Geology, Sedimentology and Basin Evolution.* Geological Society Special Publication, **62**, 191 – 202.

Doré, A. G., Lundin, E.R., Fichler, C., Olesen, I. 1997. Patterns of basement structure and reactivation along the NE Atlantic margin. *Journal of the Geological Society, London,* **154**, 85-92.

Doré, A.G., Lundin, E.R., Jensen, L.N., Birkeland, Ø, Eliassen, P.E. & Fichler, C., 1999. Principle tectonic events in the evolution of the northwest European Atlantic margin. *In*: Fleet, A.J. & Boldy, S.A.R. (eds.) *Petroleum Geology of Northwest Europe: Proceedings of the 5th Conference*, 41-61.

Edgell, H.S. 1996. Salt tectonism in the Persian Gulf Basin. *In:* Alsop, G.I., Blundell, D.J. and Davison, I (*eds*), *Salt Tectonics*, Geological Society Special Publication, **100**, 129-151.

Ehrenberg, S. N., Gjerstad, H. M., Hadler-Jacobsen, F. 1992. Smørbukk Field. A Gas Condensate Fault Trap in the Haltenbanken Province, Offshore Mid-Norway. *In*: Halbouty, M. T. *(eds) Giant oil and gas fields of the decade 1978 – 1988.* American Association of Petroleum Geologists Memoir, **54**, 471-481.

Ehrlich, R. 2003. The structural deformation in hanging-walls of extensional ramp-flat-ramp faults. *PhD thesis*. University of Bergen.

Eidvin, T., Brekke, H., Riis, F., & Renshaw, D.K. 1998. Cenozoic stratigraphy of the Norwegian Sea continental shelf, 64°N-68°N. *Norsk Geologisk Tidsskrift,* **78**, 125-151.

Finch, E., Hardy, S. & Gawthorpe, R. 2004. Discrete-element modelling of extensional fault-propagation folding above rigid basement fault blocks. *Basin Research*, **16**, 489-506.

Færseth, R. B & Lien, T. 2002. Cretaceous evolution in the Norwegian Sea – a period characterised by tectonic quiescence. *Marine and Petroleum Geology,* **19** (8): 1005-1027.

Gabrielsen R.H. & Robinson C., 1984. Tectonic Inhomogeneities of the Kristiansand-Bodø Fault Complex, offshore mid-Norway. *In*: Spencer. A.M. (ed.) *Petroleum Geology of the North European Margin*. Norwegian Petroleum Society, 397-406

Gabrielsen, R. H., Færseth, R., Hamar, G. & Rønnevik, H. 1984. Nomenclature of the main structural features on the Norwegian Continental Shelf north of the 62nd parallel. In: Spencer. A. M. (ed) *Petroleum Geology of the North European Margin.* Norwegian Petroleum Society, 41-60.

Gabrielsen, R. H. & Doré, A. G. 1995. History of tectonic models on the Norwegian Continental Shelf. *In:* Hanslien, S (*ed*) Petroleum Exploration and Exploitation in Norway. NPF Special Publication **4**, 333-368.

Gaullier, V., Brun, J. P., Guérin, G. & Lecanu, H. 1993. Raft tectonics : the effects of residual topography below a salt décollement. *Tectonophysics*, **228**: 363-382.

Gawthorpe, R. L., Sharp, I., Underhill, J. R, Gupta, S. 1997. Linked stratigraphic and structural evolution of propagating normal faults. *Geology*, **25** (9), 795 – 798.

Gibbs, A. D. 1984. Structural evolution of extensional basin margins. *Journal of the Geological Society*, **141**, 609-620.

Gómez, M., Verges, J., Fernàndez, Torne, M., Ayala, C., Wheeler, W & Karpuz, R. 2004. Extensional geometry of the Mid-Norwegian Margin before Early Tertiary continental break-up. Marine and Petroleum Geology, **24** (2), 177-194.

Gowers, M. B. & Lunde, G. 1984. The geological history of Trænabanken. *Petroleum Geology of the North European Margin.* Norwegian Petroleum Society, Graham & Trotman, London, 237-251.

Guardado, L. R., Gamboa, L. A. P. & Lucchesi, C. F. 1990. Petroleum Geology of the Campos Basin, Brazil, a model for a producing Atlantic Type Basin. *In*: Edwards, J. D. & Santogrossi, P. A. (*eds*) Divergent/Passive Margin Basins. *American Association of Petroleum Geologists Memoir*, **48**, 3-80.

Gupta, S., Cowie, P.A., Dawers, N.H. & Underhill, J.R. 1998. Mechanism to explain rift basin subsidence and stratigraphic patterns through fault array evolution. *Geology* **26**, 595-598.

Hesthammer, J. & Fossen, H., 1999. Evolution and geometries of gravitational collapse structures with examples from the Statfjord Field, northern North Sea. *Marine & Petroleum Geology*, **16**, 259-281.

Holdsworth, R.E., Butler, C.A. & Roberts, A.M. 1997. The recognition of reactivation during continental deformation. *Journal of the Geological Society, London*, **154**, 73-78.

Hudec, M.R. & Jackson, M.P.A. 2007. Terra infirma: Understanding salt tectonics. *Earth-Science Reviews*, **82**, 1 – 28.

Jackson, C. A. L., Gawthorpe, R. L. & Sharp, I. R. 2006. Style and sequence of deformation during extensional fault-propagation folding: examples from the Hammam Faraun and El-Qaa fault blocks, Suez Rift, Egypt. *Journal of Structural Geology*, **28**, 519-535.

Jackson, J. S. & Hastings, D. S. 1986. The role of salt movement in the tectonic history of Haltenbanken and Trænabanken and its relationship to structural style. In: *Habitat of hydrocarbons on the Norwegian Continental Shelf.* Norwegian Petroleum Society, Graham and Trotman, London, 241-257.

Jackson, M. P. A. & Talbot, C. J. 1986. External shapes, strain rates and dynamics of salt structures. *Geological Society of America Bulletin*, **97**, 305-323.

Jackson, M. P. A. & Talbot, C. J. 1991. A glossary of salt tectonics. Geological Circular, vol. 91-4. The University of Texas at Austin, Bureau of Economic Geology.

Jackson, M. P. A & Vendeville, B. C. 1994. Regional extension as a geologic trigger for diapirism. *Geological Society of America Bulletin*, **106**, 57 – 73.

Jackson, M. P. A. 1995. Retrospective salt tectonics. *In*: Jackson, M. P. A., Roberts, D. G., Snelson, S. (*eds*). Salt Tectonics: a global perspective. *American Association of Petroleum Geologists Memoir*, **65**, 1-28.

Jackson, M. P. A., Vendeville, B. C. & Schultz-Ela, D. D. 1994a. Structural dynamics of salt systems. *Annual Review of Earth and Planetary Sciences*, **22**, 93-117.

Jackson, M. P. A, Vendeville, B. C. & Schultz-Ela, D. D. 1994b. Salt-related structures in the Gulf of Mexico ; a field guide for geophysicists. *The Leading Edge*, **13**, 837-842.

Jackson, M. P. A, Vendeville, B. C. 1994. Regional extension as a geologic trigger for diapirism. *Geological Society of America Bulletin*, **106**, 57-73.

Jacobsen, V. W., van Veen, P. 1984. The Triassic North of 62°N. . *In:* Spencer, A. M. *et al.* (eds) *Petroleum Geology of the North European Margin.* Graham & Trotman, London, 317 - 329.

Jenyon, M. K. 1986. Salt tectonics. Elsevier, London, p. 5.

Khalil, S. M. & McClay, K. R. 2002. Extensional fault-related folding, north western Red Sea, Egypt. *Journal of Structural Geology*, **24**, 743-762.

Koch, J. O., Heum, O. R. 1995. Exploration trends of the Halten Terrace. *In:* Hanslien, S. (eds) *Petroleum exploration and exploitation in Norway*. NPF Special Publication, **4**, 235-251.

Koyi, H., Jenyon, M. K. & Petersen, K. 1993. The effect of basement faulting on diapirism. *Journal of Petroleum Geology*, **16**, 285-312.

Lundin, E.R. & Doré, A.G. 1997. A tectonic model for the Norwegian passive margin with implications for the NE Atlantic: Early Cretaceous to break-up. *Journal of the Geological Society, London*, **154**, 545-550

Lundin, E. & Doré, A. G. 2002. Mid-Cenozoic post-breakup deformation in the 'passive' margin bordering the Norwegian-Greenland Sea. *Marine and Petroleum Geology*, **19**, 79-93.

Mansfied, C. & Cartwright, J. 2001. Fault growth by linkage: observations and implications from analogue models. *Journal of Structural Geology*, **23**, 745-763.

Martinius, A. W., Ringrose, P. S., Brostrøm, C., Elfenbein, C., Næss, A., Ringås, J. E. 2005. Reservoir challenges of heterolithic tidal sandstone reservoirs in the Halten Terrace, mid-Norway. *Petroleum Geoscience,* **11**, 3 – 16.

Mauduit, T., Guerin, G., Brun, J. P. & Lecanu, H. 1997. Raft tectonics: the effects of basal slope angle and sedimentation rate on progressive extension. *Journal of Structural Geology*, **19**, 1219-1230

Mauduit, T., & Brun, J. P. 1998. Growth fault/rollover systems: birth, growth and decay. *Journal of Geophysical Research*, **103**, 18119-18136.

Mosar, J., Eide, E. A., Osmundsen, P. T., Sommaruga, A. & Torsvik, T. H. 2002. Greenland-Norway separation: A geodynamic model for the North Atlantic. *Norwegian Journal of Geology*, **82**, 281 -198.

Müller, R., Nystuen, J.P, Eide, F. & Lie, H. 2005. Late Permian to Triassic basin infill history and palaeogeography of the Mid-Norwegian shelf – East Greenland region. *In*: Hurst, A. (ed.) *Offshore-onshore relationships on the North Atlantic margin: NGF abstracts and Proceedings,* **2**, 140-142.

Nettleton, L. L. 1934. Fluid mechanics of salt domes. American Association of Petroleum Geologists Bulletin, **18**, 1175-1204.

Nicol, A., Watterson, J., Walsh, J.J., Childs, C., 1996. The shapes, major axis orientations and displacement patterns of fault surfaces. *Journal of Structural Geology,* **18**, 235–248.

Nicol, A., Walsh, J.J., Watterson, J., Underhill, J.R., 1997. Displacement rates of normal faults. *Nature,* **390**, 157-159.

Norwegian Petroleum Directorate, 2007. FACTS, The Norwegian Petroleum Sector, 2007.

Osmundsen, P.T., Sommaruga, A., Skilbrei, J.R., Olesen, O., 2002., Deep structure of the Mid-Norway rifted margin. *Norwegian Journal of Geology,* **82**, 205-224.

Osmundsen, P. T., Eide, E. A., Haabesland, N. E., Roberts, D., Andersen, T. B., Kendrick, M., Bingen, B., Braathen, A. & Redfield, T. F. 2006. Kinematics of the Høybakken detachment zone and the More-Trøndelag Fault Complex, central Norway. *Journal of the Geological Society, London,* **163**, 303-318.

Pascoe, R., Hooper, R., Storhaug, K., Harper, H. 1999. Evolution of extensional styles at the southern termination of the Nordland Ridge, mid-Norway: a response to variations in coupling above Triassic Salt. *In*: Fleet, A. J. and Boldy, S. A. R (*eds*) *Petroleum Geology of Northwest Europe: Proceedings of the 5th Conference,* 83 – 90.

Patton, T. L., Nelson, R. A., Moustafa, A. R. & Abdine, S. A. 1994. Tectonic evolution and structural setting of the Suez rift. *In*: Landon, S. M. (*ed*) Interior rift basins. *American Association of Petroleum Geologists Memoir*, **59**, 9-55.

Peaock, D.C.P. & Sanderson, D, 1991. Displacements, segment linkage and relay ramps in normal fault zones. *Journal of Structural Geology,* **13**, 721-733.

Penge, J., Taylor, B., Huckerby, J. A. & Munns, J. W. 1993. Extension and salt tectonics in the east Central Graben. *In:* Parker, J. R. (*eds*) *Petroleum geology of Northwest Europe: Proceedings of the 4th Conference*. Geological Society, London, 1197-1209.

Penge, J., Munns, J. W, Taylor, B. & Windle, T. M. F. 1999. Rift-raft tectonics: examples of gravitational tectonics from the Zechstein basins of northwest Eurpoe. *In:* Fleet, A. J & Boldy, S. A. R (*eds*) *Petroleum Geology of Northwest Europe: Proceedings of the 5th Conference*, 201-213.

Prosser. S. 1993. Rift-related linked depositional systems and their seismic expressions. *In:* Williams, G. & Dobb, A. (*eds*) *Tectonics and seismic sequence stratigraphy. Geological Society of London Special Publication,* **71**, 35-66.

Ramberg, H. 1967. Gravity, deformation and the Earth's crust as studied by centrifuge models. London, Academic Press, p. 214.

Ramberg, H. 1981. Gravity, deformation and the Earth's crust in theory, experiments and geological application. London, Academic Press, p. 452.

Rattey, R. P. & Hayward, A. B. 1993. Sequence stratigraphy of a failed rift system: the middle Jurassic to early Cretaceous basin evolution of the central and northern North Sea. In: Parker, J. R. (ed), *Petroleum Geology of Northwest Europe: Proceedings of the Fourth Conference*. Geological Society of London, p. 215-249.

Richardson, N. J., Underhill, J. R. & Lewis, G. 2005. The role of evaporite mobility in modifying subsidence patterns during normal fault growth and linkage, Halten Terrace, Mid-Norway. *Basin Research*, **17** (2), 203-223.

Roberts, D.G, Thompson, M., Mitchener, B. Hossack, J., Carmichael, S. & Bjørnseth, H.M. 1999. Palaeozoic to Tertiary rift and basin dynamics: mid-Norway to the Bay of Biscay – a new context for hydrocarbon prospectivity in the deep water frontier. *In*: Fleet, A.J. & Boldy, S.A.R. (eds.) *Petroleum Geology of Northwest Europe: Proceedings of the 5th Conference*, p7-40.

Rouby, D., Cobbold, P. R., Szatmari, P., Demercian, S., Coelho, D. & Rici, J. A. 1993. Restoration in plan-view of faulted Upper Cretaceous and Oligocene horizons and its bearing on the history of salt tectonics in the Campos Basin (Brazil). *Tectonophysics*, **228**, 435-445.

Rouby, D., Raillard, S. Guillocheau, F., Bouroullec, R. & Naplas, T. 2002. Kinematics of a growth fault/raft system on the West African margin using 3-D restoration. *Journal of Structural Geology*, **24**, 783-796.

Rowan, M. & Kligfield, R. 1989. Cross section restoration and balancing as aid to seismic interpretation in extensional terranes. *American Association of Petroleum Geologists Bulletin*, **73**, 955-966.

Rowan, M. 2006. Practical Salt tectonics, kursmanual. Statoil internal course.

Scheck, M., Bayer, U. & Lewerenz, B. 2002. Salt redistribution during extension and inversion inferred from 3D backstripping. *Tectonophysics*, **373**, 55-73.

Schlische, R. W. 1995. Geometry and Origin of Fault-Related Folds in Extensional Settings. *American Association of Petroleum Geologists Bulletin*, **79** (11), 11661-1678.

Schlische, R.W., Young, S.S., Ackermann, R.V. & Gupta, A. 1996. Geometry and scaling reations of a population of very small rift-related normal faults. *Geology* **24**, 683-686.

Schmidt, W.J., 1992. Structure of the Mid-Norway Heidrun Field and its regional implications. *In*: Larsen, R.M., Brekke, H., Larsen, B.T. & Talleraas, E., (eds.)

Structural and Tectonic Modelling and its application to Petroleum Geology. NPF Special Publication, **1**, 381-395

Sherlock, S. C., Watts, L. M., Holdsworth, R. E. and Roberts, D. 2004. Dating fault reactivation by Ar/Ar laserprobe: an alternative view of apparently cogenetic mylonite-pseudotachylite assemblages. *Journal of the Geological Society*, **161**, 335-338.

Skilbrei, J.R., Olesen, O. 2005. Deep structure of the Mid-Norwegian shelf and onshore-offshore correlations: Insight from potential field data. *In:* Wandas, B. *et al* (eds) *Onshore-Offshore relationships on the North Atlantic Margin.* NPF Special Publication, **12**, 43-68.

Skogseid, J., Planke, S., Faleide, J. I., Pedersen, T., Eldholm, O. & Neverdal, F. 2000. NE Atlantic continental rifting and volcanic margin formation. From Nøttvedt, A. *et al (eds) Dynamics of the Norwegian Margin.* Geological Society, London, Special Publications, **167**, 295-326.

Smart, K. J., Morris, A. P. & Ferrill, D. A. 2007. Kinematic analyses and geomechanical modelling of an extensional fault-propagation fold. Abstract, GSA Annual Meeting (28-31 October 2007).

Stewart, S. A., Ruffell, A. H. & Harvey, M. J. 1997. Relationship between basement-linked and gravity-driven fault systems in the UKCS salt basins. *Marine and Petroleum Geology*, **14**, p.581-604

Stewart, S.A. & Clark, J.A., 1999. Impact of salt on the structure of the Central North sea hydrocarbon fairways. *In*: Fleet, A.J. & Boldy, S.A.R. (eds.) *Petroleum Geology of Northwest Europe: Proceedings of the 5th Conference*, 179-200

Stewart, S.A. 1999. Geometry of thin-skinned tetonic systems in relation to detachment layer thickness in sedimentary basins. *Tectonics*, **18** (4), 719-732.

Suppe, J. 1985. Principles in Structural Geology. Prentice-Hall, Englewood Cliffs, New Jersey, p. 537.

Surlyk, F., 1990. Timing, style and sedimentary evolution of late Palæozoic-Mesozoic extensional basins of East Greenland. *In*: Hardman, R.F.P. & Brooks, J. (eds.) *Tectonic events responsible for Britain's Oil and Gas Reserves*. Geological Society Special Publication, **55**, 107-155.

Talbot, C. J. & Aftabi, P. 2004. Geology and models of salt extrusion at Qum Kuh, central Iran. Geological Society London Journal, **161**, p. 321-334.

Torsvik, T. H., Carlos, D., Mosar, J., Robin, L., Cocks, M. & Malme, T. N. 2002. Global reconstructions and North Atlantic palaeogeography 440 Ma to recent. *In*: Eide, E. A. (*eds*) BATLAS: Mid Norway plate reconstruction atlas with global and Atlantic perspectives, p. 18-47.

Torsvik, T. H., Sturt, B. A., Swensson, E., Anderson, T. B. & Dewey, J. F. 1992. Paleomagnetic dating of fault rocks: evidence for Permian and Mesozoic movements and brittle deformation along the extensional Dalsfjord Fault, western Norway. *Geophysical Journal International,* **109** (3), 565–580.

Trudgill, B. & Cartwright, J. 1994. Relay ramp forms and normal fault linkages, Canyonlands National Park, Utah. *Geological Society American Bulletin*, **106**, 1143-1157.

Vendeville, B. & Cobbold, P. R. 1988. How normal faults and sedimentation interact to produce listric fault profiles and stratigraphic wedges. *Journal of structural geology*, **10**, 649-659.

Vendeville, B., Cobbold, P. R., Davy, P., Brun, J. P. & Choukrone, P. 1987. Physical models of extensional tectonics at various scales. *In:* Coward, M. P., Dewey, J. F. & Hancock, P. L. (*eds*) *Continental Extensional Tectonics*. Geological Society, London, Special Publications, **28**, 95-107.

Vendeville, B.C. & Jackson, M.P.A. 1992a. The rise of diapirs during thin-skinned extension. *Marine and Petroleum Geology*, Vol. 9, p.331 - 353

Vendeville, B. C. & Jackson, M. P. A. 1992*b*. The fall of diapirs during thin-skinned extension. *Marine and Petroleum Geology*, **9**, 354-371.

Vendeville, B. C., and Jackson, M. P. A. 1993. Rates of extension and deposition determine whether growth faults or salt diapirs form. *In*: Armentrout, M., Bloch, R., Olson, H. C. & Perkins, B. F. (eds), Rates of Geological Processes: Fourteenth Annual Research Conference, Gulf Coast Section, SEPM Foundation, Program with papers, p. 263-268.

Vendeville, B. C. & Jackson, M. P. A. 1995. Scale models of salt tectonics during basement-involved extension. *Petroleum Geoscience*, **1**, 179-183.

Ville, L. 1856. Notice géologique sur les salines des Zahrez et les gites de sel gemme de Rang el Melah et d'Ain Hadjera (Algerie). *Annales des Mines*, **15**, 351-410.

Warren, J., 1999. Evaporites: Their evolution and economics. Blackwell Science, Oxford, p. 438.

Walsh, J.J., Watterson, J., 1988. Analysis of the relationship between displacements and dimensions of faults. *Journal of structural geology*, **10**, 239-247.

Walsh, J.J., Watterson, J., 1989. Displacement gradients on fault surfaces. *Journal of Structural Geology*, **11**, 307–316.

Walsh, J.J., Watterson, J., 1991. Geometric and kinematic coherence and scale effects in normal fault systems. In: Roberts, A.M., Yielding, G., Freeman, B. (Eds.), The Geometry of Normal Faults. *Geological Society, London, Special Publication,* **56**, 193-203.

Walsh, J.J., Watterson, J., Yielding, G. 1991. The importance of small-scale faulting in regional extension. *Nature*, **351**, 391-393.

Walsh, J.J., Nicol, A., Childs, C., 2002. An alternative model for the growth of faults. *Journal of Structural Geology,* **24**, 1669–1675.

Walsh, J.J., Childs, C., Imber, J., Manzocchi, T., Watterson, J., Nell, P.A.R., 2003. Strain localisation and population changes during fault system growth within the Inner Moray Firth, Northern North Sea. *Journal of Structural Geology,* **25**, 307-315.

Watterson, J., 1986. Fault dimensions, displacements and growth. *Pure and Applied Geophysics,* **124**, 365–373.

Weijermars, R., Jackson, M. P. A. & Vendeville, B. 1993. Rheological and tectonic modelling of salt provinces. *Tectonophysics*, **217**, 143-174.

White, I. R., & Crider, J. G. 2006. Extensional fault-propagation folds: mechanical models and observations from the Modoc Plateau, northeastern California. *Journal of Structural Geology*, **28**, 1352 – 1370.

Willsey, S.P., Umhoefer, P.J. & Hilley, G.E, 2002. Early evolution of an extensional monocline by a propagating normal fault: 3D analysis from combined field study and numerical analysis. *Journal of Structural Geology*, **24**, 651-669.

Withjack, M., Meisling, K., Russell, L. 1989. Forced folding and basement-detached normal faulting in the Haltenbanken area, offshore Norway. *In:* A. J. Tankard and H. R. Balkwill (*eds*) Extensional tectonics and stratigraphy of the North Atlantic margins: *American Association of Petroleum Geologists Memoir*, **46**, 567 – 575.

Withjack, M. Olson, J. & Peterson, E. 1990. Experimental models of extensional forced folds. *American Association of Petroleum Geologists Bulletin*, **74**, 1038-1054

Withjack, M., Callaway, S. 2000. Active normal faulting beneath a salt layer: An experimental study of deformation patterns in the cover sequence. *American Association of Petroleum Geologists Bulletin*, **84** (5), 627- 651.

Worrall, D. M. & Snelson, S. 1989. Evolution of the northern Gulf of Mexico, with emphasis on Cenozoic growth faulting and the role of salt. *In*: Bally, A. & Palmer, A. (*eds*), *The Geology of North America – An Overview*. Geological Society of America, Boulder, Colorado, p. 97-138.

Yielding, G., Needham, T. & Jones, H. 1996. Sampling of fault populations using sub-surface data: a review. *Journal of Structural Geology*, **18**, 135-146.

Ziegler, W. H. 1975. Outline of the geological history of the North Sea. In: A. W. Woodland (*ed*) *Petroleum Geology on the Continental Shelf of North-West Europe*, Vol 1. Geology. British Institute of Petroleum, Applied Science Publishers, London, p. 131-149 & 165-190.

Ziegler, W. H., Doery, R., & Scott, J. 1986. Tectonic habitat of Norwegian oil and gas. In: A. M. Spencer *et al.* (eds) *Habitat of Hydrocarbons on the Norwegian Continental Shelf.* Graham and Trotman, London, p. 3-19.

APPENDICIES

1.1 The structural evolution of the Halten Terrace, offshore Mid-Norway: new insights into fault growth in a brittle-ductile system and implications for hydrocarbon prospectivity

N.Marsh[1], J.Imber[1], R.E.Holdsworth[1], P.Brockbank[2] & P.Ringrose[3]

[1]*Reactivation Research Group, Dept of Earth Sciences, University of Durham, Durham, DH1 3LE*
[2]*StatoilHydro UK, 11a Regent Street, London, SW1Y 4ST*
[3]*StatoilHydro Research Centre, N-7005, Trondheim, Norway.*

ABSTRACT

The Halten Terrace is a prolific hydrocarbon province situated on the Norwegian Margin. It is rapidly becoming mature and future exploration will likely focus on previously under-developed plays within both Jurassic and Cretaceous strata. Better constraints on the Mesozoic structural and stratigraphic evolution of the Halten Terrace are therefore of critical importance. Disagreement exists concerning the spatial and temporal evolution of the region, with different authors emphasising the role of normal faulting with basement fault reactivation, salt tectonics and fault-propagation folding, or even strike-slip tectonics. We have analysed high quality 3D seismic data, regional 2D lines and well data to establish a regionally-consistent structural and stratigraphic framework for the Permo-Triassic to Early Cretaceous interval in the northwestern part of the Halten Terrace.

Here, Permo-Triassic rocks are overlain by a thick sequence of Triassic evaporites, separating "basement" and "cover" stratigraphy. We demonstrate that the mapped basement faults were likely *not* active immediately prior to evaporite deposition. Instead, the formation of broad monoclinal flexures in the post-evaporite cover records the onset of growth above these blind basement faults during the earliest Jurassic. Fault activity in the cover also initiated at this time - which is earlier than previously recognised - and continued into the Early Cretaceous when new faults formed oblique to existing structures. We suggest that most Early Cretaceous fault growth was related to salt withdrawal and gravity-sliding. Despite the approximately synchronous onset of extension in basement and cover, the distinctly different fault patterns above and below the regional evaporite units highlight the role of such rocks in decoupling strain between basement and cover structures during extension. Our results are summarised in a series of fault activity maps which we use to constrain the likely evolution of accommodation space synchronous with deposition of commercially significant Early and Middle Jurassic reservoir intervals.

(Chapter 3 was submitted as a paper to Basin Research, has been reviewed, corrected and re-submitted for publication. The relative contributions of each author to the paper are: Nicola Marsh: 85%; Jonathan Imber & Robert. E. Holdsworth: 5% each in their roles as supervisors to the PhD; Paul Brockbank & Philip Ringrose: 5% in their roles as company supervisors, and for the provision of data and resources from StatoilHydro)

1.2: The evolution of structural styles in a brittle-ductile system: examples from the Halten Terrace, offshore mid-Norway

N.Marsh[1], P.Brockbank[2], J.Imber[1] & R.E.Holdsworth[1]

[1]*Reactivation Research Group, Dept of Earth Sciences, University of Durham, Durham, DH1 3LE*
[2]*Statoil UK, 11a Regent Street, London, SW1Y 4ST*

ABSTRACT

Two mechanisms control the evolution of post-evaporite cover faults on the Halten Terrace - crustal extension and gravity-sliding - resulting in the development of both thick-skinned, basement-rooted faults and thin-skinned decoupled faults that detach on mechanically weak evaporites. The distribution and geometry of both thick- and thin-skinned structural styles is described in map-view and cross-section. The observations presented suggest that two factors define the geometry of each structural style, namely: (i) the degree of coupling between basement and cover faults; and (ii) the dominant structural orientation, can be used to distinguish faults that form due to crustal extension from those that are gravity-driven. In particular, gravity-driven faults are identified based upon: (i) their orientation perpendicular to the local or regional dip direction; (ii) the lack of basement faults with a similar trend; and (iii) the onset of fault activity, which initiates post-Middle Jurassic, subsequent to activity on thick-skinned faults.

These observations, supported by existing knowledge from analogue models, are used to suggest the dominant mechanisms controlling the degree of coupling between basement and cover faults, where coupling refers to the degree of interaction (or linkage) between faults that offset basement and cover strata. The results suggest that the relative distribution and orientation of faults in the basement and cover, along-strike changes in the magnitude of displacement on basement *and* cover faults and the rate of extension affect the degree of coupling between structural styles in pre- and post-salt strata. Knowledge of the temporal evolution of faults and folds in the area is used to suggest a link between the duration of extension and the degree of coupling between basement and cover faults, where the longest-lived faults generally exhibit the largest degree of coupling.

The results have implications for constraining the distribution and magnitude of displacement on cover faults that offset important reservoir intervals. Crucially, if the duration of extension and the magnitude and rate of displacement are the dominant controls over the distribution of faults in the cover sequence, the spatial and temporal evolution of faults and folds can be used to predict the magnitude and distribution of structures in prospective hydrocarbon provinces. It also allows better assessment of the degree of reservoir compartmentalisation in new and existing prospects on the Halten Terrace.

1.3: 3D analysis of faults in the Åsgard area, offshore Mid-Norway: a new model for fault growth in brittle-ductile systems

N.Marsh[1], J.Imber[1] & R.E.Holdsworth[1].

[1]*Reactivation Research Group, Dept of Earth Sciences, University of Durham, Durham, DH1 3LE*

ABSTRACT

Permo-Triassic basement rocks on the Halten Terrace, offshore Mid-Norway, are overlain by a thick sequence of Triassic evaporites, separating basement and cover stratigraphy. The presence of evaporites decouples deformation in much of the supra-salt cover strata from the underlying basement, causing the development of two separate fault systems, one in the cover and the other confined to the pre-salt basement.

The 3D geometry of two structures on the west of the Halten Terrace, the Smørbukk and Trestakk faults, is described and detailed displacement-length analyses used to propose a model of growth for each fault. Both faults formed due to thick-skinned extensional tectonics, where thick-skinned faults are those that are coupled or partially coupled to the basement structures, and were active from the Early Jurassic to Early Cretaceous. Despite their similarities in structural setting, fault length and duration of activity, the geometry and displacement-length data from the Trestakk fault are significantly different to that of the Smørbukk fault, and other thick-skinned faults in the region.

A new model of fault growth is presented which accounts for the geometry and displacement-length profile of the Trestakk fault. It is suggested that this new model is applicable to those situations in which faults, which form above a detachment layer such as salt, are subject to both crustal extension and gravity-sliding.

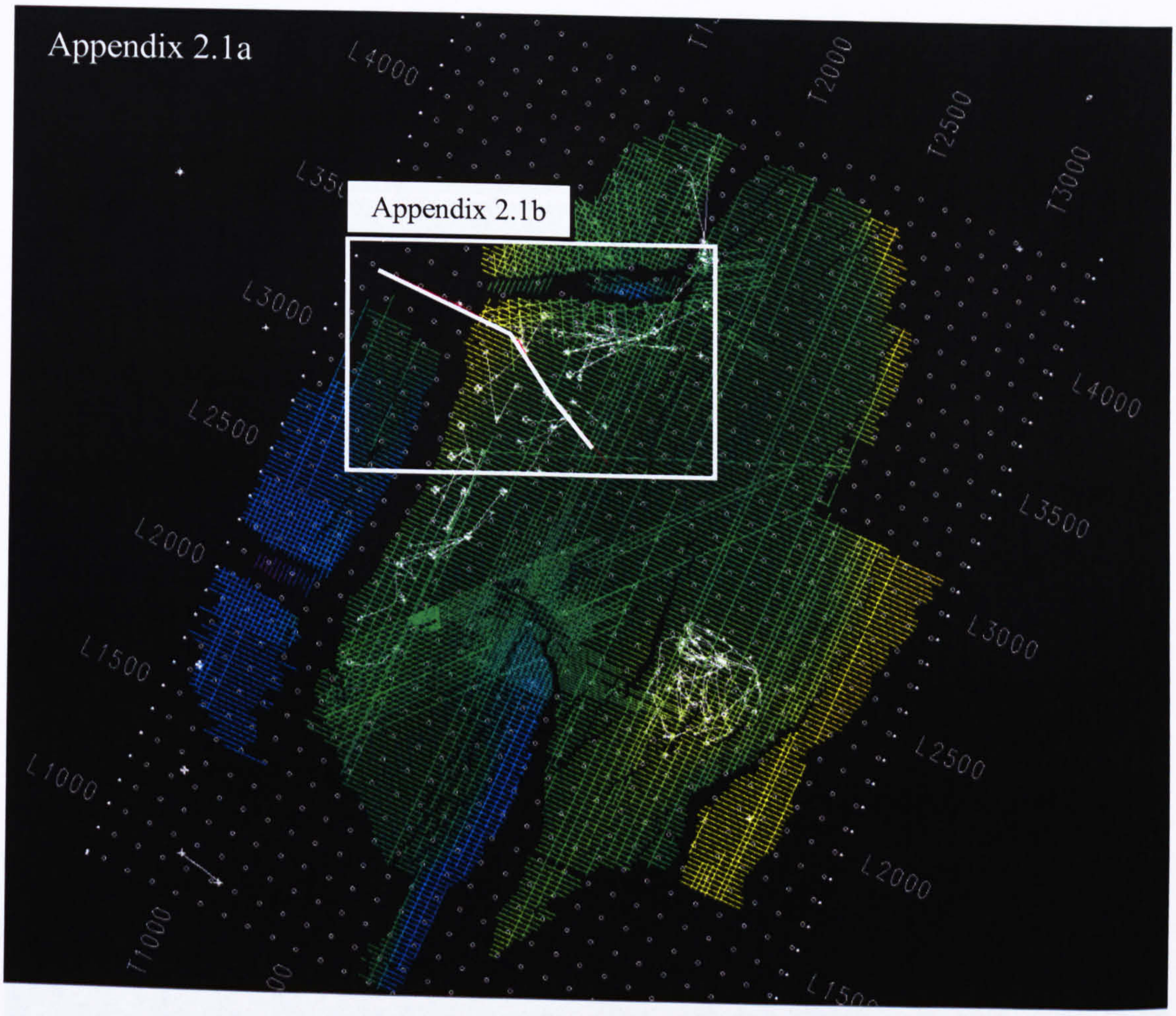
Appendix 2.1a
L4000
T2000
T2500
T3000
L3500
L3000
L2500
L2000
L1500
L1000
T1000
Appendix 2.1b

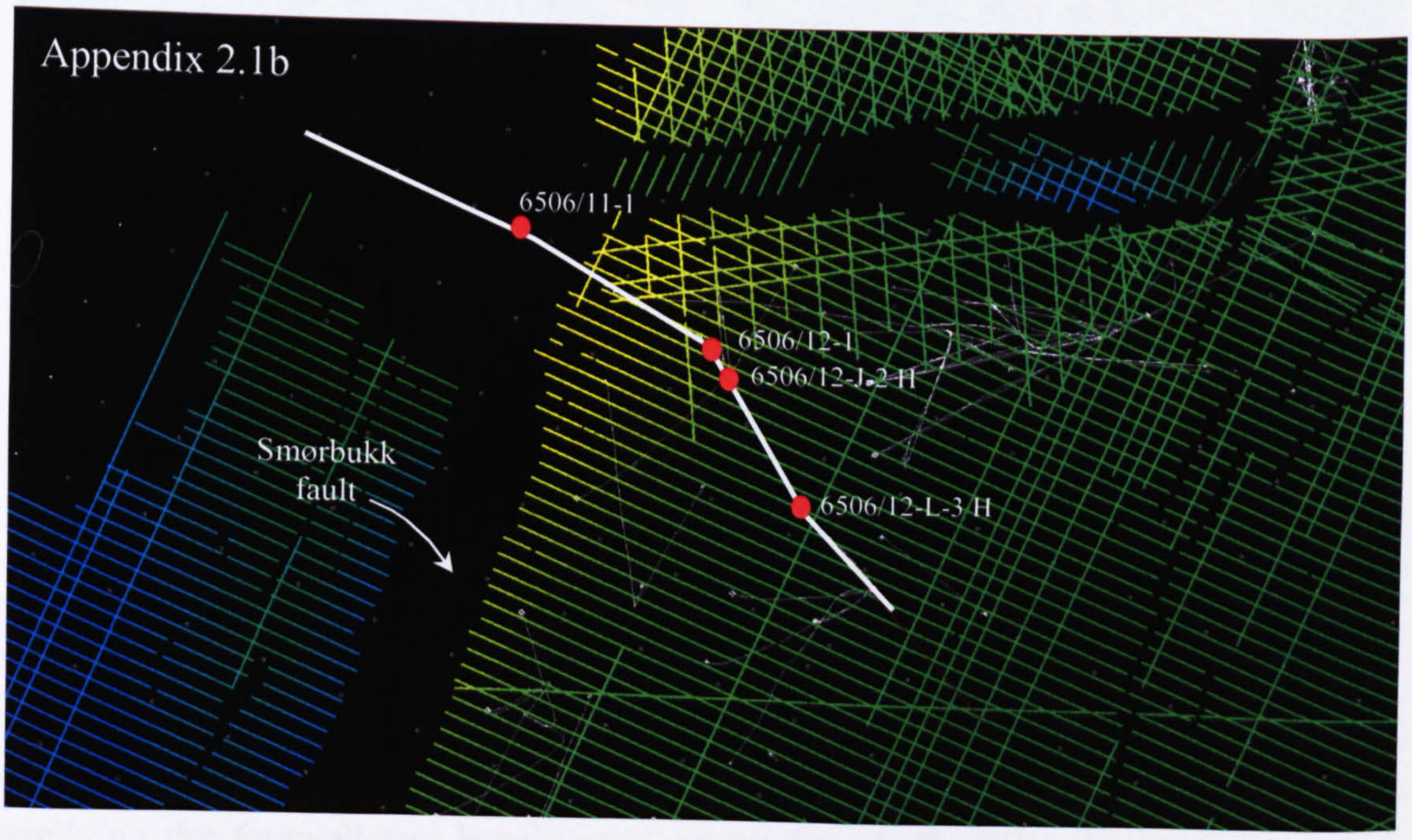
Appendix 2.1b
6506/11-1
6506/12-1
6506/12-1-2 H
6506/12-L-3 H
Smørbukk
fault

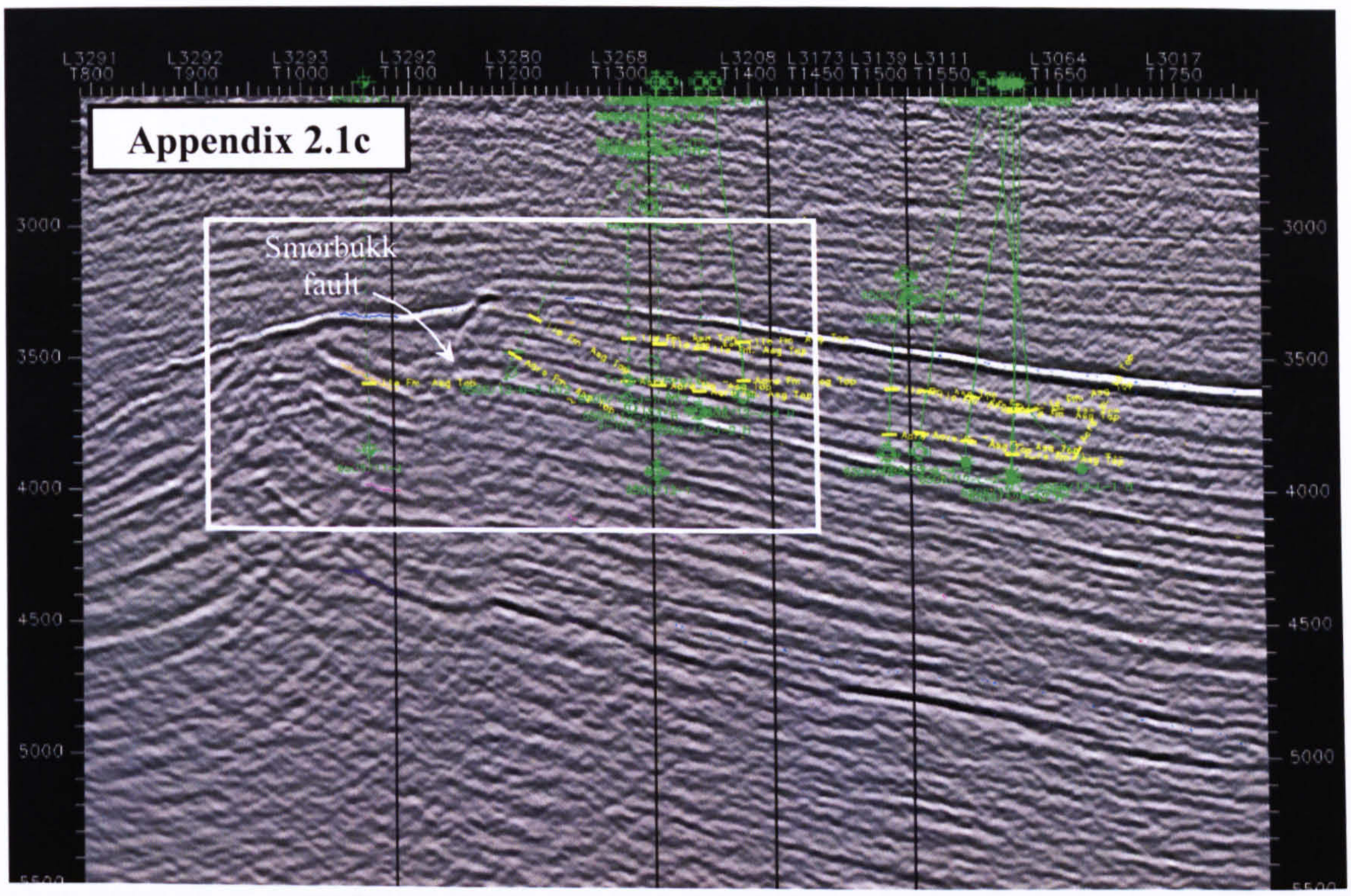

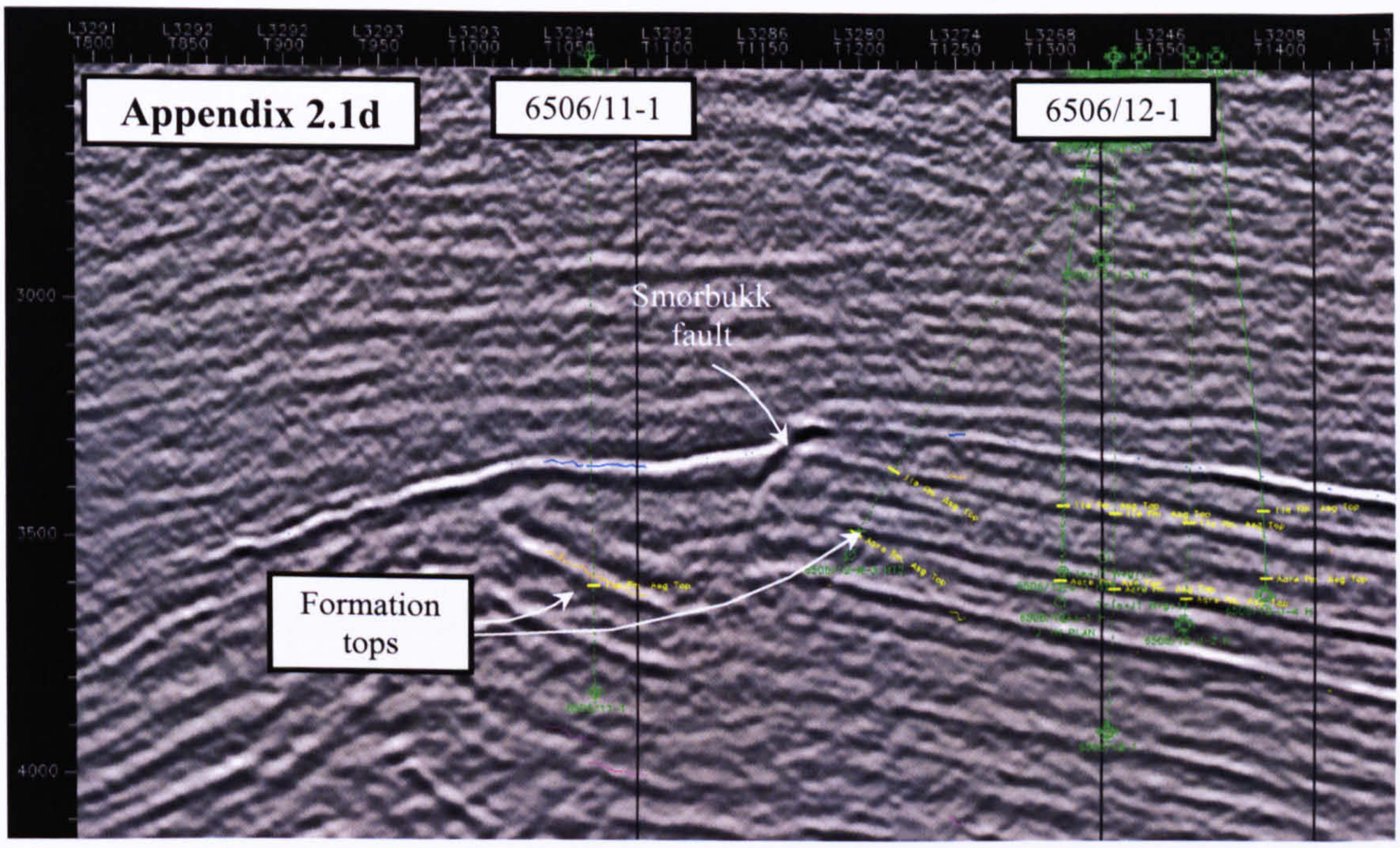

Appendix 2.1: (a) Map-view of the Åsgard area. Location of well-correlation panel highlighted in inset. (b) Location of cross section taken through 4 wells, from footwall to hangingwall of the Smørbukk fault. (c) Cross-section illustrating the location of wells on the footwall and hangingwall of the Smørbukk fault, that can be used to illustrate the change in thickness of formation across the fault (App. 7.2). (d)

	HANGINGWALL	FOOTWALL	
Formation Name	TVT (m) 6506/11-1	TVT (m) 6506/12-1	Δ TVT (m)
Garn	74.00	38.33	35.67
Not	45.26	33.91	11.35
Ile	102.87	60.13	42.74
Ror	115.86	59.84	56.02
Tofte	95.95	52.87	43.08

Formation Name	TVT (m) 6506/11-1	TVT (m) 6506/12-J-2 H	Δ TVT (m)
Garn	74.00	33.67	40.33
Not	45.26	39.48	5.78
Ile	102.87	60.24	42.63
Ror	115.86	60.15	55.71
Tofte	95.95	59.91	36.04

Appendix 2.2: True vertical thicknesses (TVT) taken from well 6506/11-1 (hangingwall of Smørbukk fault) and two wells in the footwall of the fault. Changes in thickness across the fault (Δ TVT) clearly show thickening of all successions on the hangingwall side of the fault, supporting our interpretation of syn-rift fault activity during deposition of these interval.

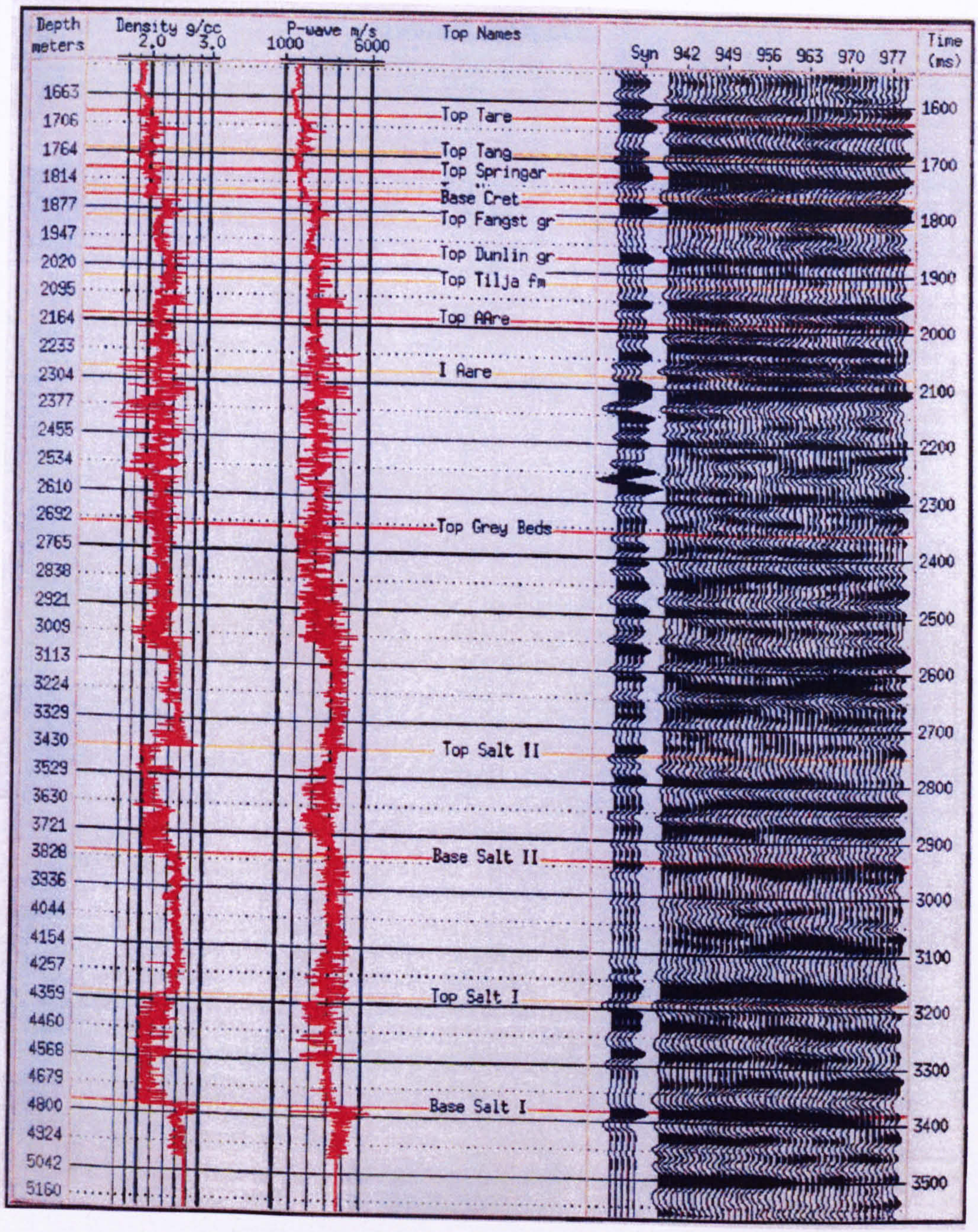

Appendix 2.3: Calibration of well 6507/12-2 to seismic